



**UNIVERSIDADE FEDERAL DO CEARÁ**  
**CENTRO DE TECNOLOGIA**  
**DEPARTMENO DE ENGENHARIA DE TELEINFORMÁTICA**  
**PROGRAMA DE PÓS-GRADUAÇÃO EM ENGENHARIA DE TELEINFORMÁTICA**

**DANILO SOUSA ROCHA**

**NESTED TENSOR DECOMPOSITION APPLIED TO COOPERATIVE MIMO  
COMMUNICATION SYSTEMS**

**FORTALEZA**

**2019**

DANILO SOUSA ROCHA

NESTED TENSOR DECOMPOSITION APPLIED TO COOPERATIVE MIMO  
COMMUNICATION SYSTEMS

Tese apresentada ao Programa de Pós-graduação em Engenharia de Teleinformática do Centro de Tecnologia da Universidade Federal do Ceará, como requisito parcial à obtenção do título de doutor em Engenharia de Teleinformática. Área de Concentração: Sinais e sistemas.

Orientador: Dr. Carlos Alexandre Rolim Fernandes

Coorientador: Dr. Gérard Favier

FORTALEZA

2019

Dados Internacionais de Catalogação na Publicação  
Universidade Federal do Ceará  
Biblioteca Universitária  
Gerada automaticamente pelo módulo Catalog, mediante os dados fornecidos pelo(a) autor(a)

---

R572n Rocha, Danilo Sousa.

Nested tensor decomposition applied to cooperative MIMO communication systems / Danilo Sousa  
Rocha. – 2019.

146 f. : il. color.

Tese (doutorado) – Universidade Federal do Ceará, Centro de Tecnologia, Programa de Pós-Graduação  
em Engenharia de Teleinformática, Fortaleza, 2019.

Orientação: Prof. Dr. Carlos Alexandre Rolim Fernandes.

Coorientação: Prof. Dr. Gérard Favier.

1. Decomposição tensorial. 2. Decomposição Tucker. 3. Receptor semi-cego. 4. Sistemas cooperativos. 5.  
Sistemas MIMO. I. Título.

CDD 621.38

---

DANILO SOUSA ROCHA

NESTED TENSOR DECOMPOSITION APPLIED TO COOPERATIVE MIMO  
COMMUNICATION SYSTEMS

PhD thesis presented to the Postgraduate Program in Teleinformatics Engineering of Federal University of Ceará, in partial fulfilment of the requirements for the degree of Doctor in Teleinformatics Engineering. Concentration area: Signals and Systems.

This document has been approved on January 22th, 2019.

EXAMINING COMMITTEE

---

Dr. Carlos Alexandre Rolim Fernandes (Advisor)  
Universidade Federal do Ceará (UFC)

---

Dr. Gérard Favier (Coadvisor)  
Université Côte d'Azur (UCA)

---

Dr. André Lima Férrer de Almeida  
Universidade Federal do Ceará (UFC)

---

Dr. João César Moura Mota  
Universidade Federal do Ceará (UFC)

---

Dr. João Paulo Carvalho Lustosa da Costa  
Universidade de Brasília (UnB)

---

Dr. Leandro Ronchini Ximenes  
Universidade de Campinas (UNICAMP)

To my wife Dani

## ACKNOWLEDGMENTS

This study was financed in part by the Coordenação de Aperfeiçoamento de Pessoal de Nível Superior - Brasil (CAPES) - Finance Code 001.

Getting to the end of a doctorate is not an easy task. It would be even harder without the help of wonderful people who have lived with me over these 5 years. I ask permission to use my native language so that I can express my thanks and everyone can be fully recognized.

Primeiramente à Deus (seja Ele quem for, independente de crenças e religiões) que, através de meus pais, me concedeu a vida. É esta força sobrenatural que me permite acordar e levantar todos os dias.

À minha esposa Danielle, pela inesgotabilidade do seu amor e paciência. Sua companhia foi a grande responsável por manter minha sanidade durante este período. Você constituiu todo o alicerce sobre o qual eu me apoiei para chegar até o fim desta jornada.

Ao Prof. Dr. Carlos Alexandre, pela orientação, dedicação, incentivo, paciência (sei que demande bastante) e puxões de orelha (reconheço que foram necessários). Eu o considero uma pessoa de um coração enorme, com a qual ficarei feliz de manter a parceria no trabalho, nas pesquisas, na amizade, nas cervejas... na vida.

Ao Prof. Dr. Gérard Favier, pela maravilhosa recepção e orientação que recebi durante o estágio de doutorado sanduíche no Laboratório I3S da Universidade Côte d'Azur, Nice, França. Também aprendi a admirá-lo além da sua brilhante carreira de pesquisador. Sua gentileza e cordialidade nos inspira e engrandece seu trabalho.

Através dos professores André de Almeida e Walter Freitas Jr, meus sinceros agradecimentos à todos os professores do PPGETI, que fazem com brilhantismo um programa de pós-graduação de destaque e referência na área.

Aos professores João César, João Paulo e Leandro Ximenes pela disponibilidade em avaliar este manuscrito, contribuindo de forma valiosa para conclusão deste trabalho.

À Universidade Federal do Ceará (UFC), por toda a formação acadêmica que obtive em minha vida. Chego ao fim de um ciclo (graduação, mestrado e doutorado) de mais de 10 anos, do qual guardo com carinho as melhores lembranças e amizades que a convivência no campus me proporcionou.

Ao Instituto Federal do Ceará (IFCE), em particular ao curso de Licenciatura em Física do campus Sobral (do qual faço parte do corpo docente), pela anuência nas atividades ligadas ao doutorado.

Através dos professores Guilherme de Morais e Wilton Fraga, meus sinceros agradecimentos aos colegas professores, pelo apoio e compreensão nos momentos difíceis. Agradeço também ao professor Glendo de Freitas. Não poderia deixar de mencionar aqui a importância de seu incentivo à realização deste doutorado.

À CAPES, FUNCAP, CNPq e COFECUB pelo apoio financeiro às pesquisas.

Se o curso de doutorado nos leva à pessoas e instituições que contribuem ao nosso engrandecimento acadêmico e profissional, família e amigos compõem o outro lado da balança, nos trazendo momentos majestosos que permitem o engrandecimento enquanto ser humano. Dedico então meus últimos agradecimentos à essas pessoas que participam diariamente da minha vida e contribuíram direta ou indiretamente para a conclusão deste trabalho.

O meu mais profundo agradecimento aos meus pais, por me fazerem quem eu sou. Cada um, na sua forma peculiar de ser, me ensinou a ter educação, honestidade, humildade, ombridade, bem como a saber dar valor às coisas que mais importam na vida. Ao longo da vida tenho tentado absorver o que há de melhor em cada um. Espero que de alguma forma sintam-se orgulhosos de mim, pois busco ser a melhor proporção de vocês dois.

Um agradecimento especial aos amigos e companheiros de vida Anderson, Amanda, Camila, Carina, Felipe Anderson, Felipe Teixeira, Ícaro, Marcus Jr., Gabi, Rafael, Walber e mais alguém que eu possa lembrar posteriormente (me perdoem pela falha nesse momento). Vocês fazem parte da minha vida e também são de extrema importância para a minha sanidade mental, mesmo quando são tão ou mais loucos do que eu.

Aos amigos Pedro, Henrique, Luana, Pablo, Kallyna, Jean Marie e Miguel, companheiros de intercâmbio e parceiros em Nice. Na ausência da família vocês supriram com honraria esta lacuna, tornando ainda mais especial essa maravilhosa experiência que foi viver em Nice. Espero que o destino cruze nossos caminhos mais vezes.

“Words alone can’t provide the essential insights.  
Equations can. They have been a prime mover  
in human civilization for thousands of years.”

(Ian Stewart)

## RESUMO

Sistemas MIMO (do inglês *multiple-input multiple-output*) são frequentemente utilizados para aumentar os ganhos de diversidade e/ou multiplexação através da transmissão de múltiplas versões do mesmo sinal ou de dados independentes através de diferentes canais de comunicação. Como outra forma de explorar diversidade espacial, as comunicações cooperativas vêm surgindo como uma técnica promissora para as novas gerações de sistemas de comunicação sem fio, melhorando significativamente o desempenho e a confiabilidade desses sistemas. Neste contexto, nas últimas décadas, decomposições tensoriais vêm sendo exploradas no processamento de sinais multidimensionais em sistemas MIMO e, mais recentemente, em redes cooperativas, permitindo o design de receptores eficazes para a estimação dos parâmetros de transmissão. Em particular, decomposições aninhadas (*nested decomposition*) têm permitido a modelagem de sinais em sistemas que se beneficiam de múltiplas diversidades, rendendo tensores de alta ordem representados em uma forma compacta. Esta tese apresenta desenvolvimentos realizados no âmbito de novas decomposições tensoriais aninhadas aplicadas à sistemas de comunicação sem fio cooperativos com múltiplas antenas. Mais especificamente, as contribuições teóricas desta tese estão ligadas à proposição de novas decomposições tensoriais aninhadas, bem como à análise de suas propriedades de unicidade, juntamente com a proposição de novos sistemas MIMO cooperativos que são modelados através das decomposições apresentadas. Na primeira parte desta tese, dois novos modelos tensoriais, baseados no modelo NTD (do inglês *nested Tucker decomposition*), são introduzidos. O primeiro modelo é chamado *high-order nested Tucker decomposition* (HONTD), o qual estende o modelo NTD ao considerar tensores de ordem mais alta que resultam da contração de diversas decomposições Tucker em formato de trem. O segundo modelo, chamado *coupled nested Tucker decomposition* (CNTD), pode ser visto como um acoplamento de múltiplos NTDs que compartilham um fator comum, associando os conceitos de aninhamento e acoplamento inicialmente definidos para modelos PARAFAC, estendendo-os para modelos baseados em decomposição Tucker. Nas partes subsequentes desta tese, estes modelos tensoriais são usados na modelagem de três novos sistemas MIMO cooperativos. Dois deles consideram casos com múltiplos relays (com retransmissão sequencial e paralela, respectivamente) enquanto o outro considera um sistema com múltiplas portadoras e relay único. Todos os sistemas propostos consideram codificações tensoriais nos nós de transmissão. Para cada sistema proposto, os modelos tensoriais são explorados para obtenção de algoritmos de estimação semi-cega, permitindo o desenvolvimento de receptores que estimam

conjuntamente os canais e símbolos transmitidos. Condições relacionadas à unicidade das decomposições tensoriais e identificabilidade dos algoritmos propostos também são discutidas. Por fim, resultados de simulações computacionais são apresentados no intuito de avaliar o comportamento do sistema/receptor proposto, ilustrando a eficácia do processamento de sinais baseado em decomposições tensoriais aninhadas.

**Palavras-chave:** Decomposição tensorial. Decomposição Tucker. Receptor semi-cego. Sistemas cooperativos. Sistemas MIMO.

## ABSTRACT

Multiple-input multiple-output (MIMO) systems are often used to increase the diversity and/or multiplexing gains, by transmitting multiple versions of the same signal or independent data onto the communication channels. As another way to exploit spatial diversity, cooperative communications have emerged as a promising technique for the new generations of wireless communication systems, yielding significant improvements in the performance and reliability of these systems. In this context, in the last decades, tensor decompositions have been exploited in the processing of multidimensional signals in MIMO systems and, more recently, cooperative networks, allowing the design of effective receivers for estimation of the transmission parameters. In particular, nested decompositions have allowed the modeling of signals from systems that benefit from multiple diversities, yielding high-order tensors represented in a compact way. This thesis presents developments carried out within the framework of new nested tensor decompositions applied to cooperative wireless communication systems with multiple antennas. Indeed, the theoretical contributions of the present thesis rely on the proposition of new nested tensor decompositions, along with the corresponding uniqueness analysis, as well as the proposition of new cooperative MIMO communication systems that are modeled using the presented nested tensor models. In the first part of this thesis, two new tensor models based on nested Tucker decompositions (NTD) are introduced. The first model, called high-order nested Tucker decomposition (HONTD), extends NTD by considering higher order tensors resulting from the contraction of several Tucker models in a train format. The second model, called coupled nested Tucker decomposition (CNTD), can be viewed as a coupling of multiple NTDs that share a common factor, associating the nesting and coupling concepts initially defined for PARAFAC models, extending them to Tucker-based ones. In the subsequent parts of the thesis, these tensor decompositions are used in the modeling of three new cooperative MIMO systems. Two of them consider multiple relay cases (with sequential and parallel relaying, respectively) and the other one considers a single-relay multicarrier network. All the proposed systems consider tensor codings in the transmit nodes. For each proposed system, the tensor models are exploited to obtain semi-blind estimation algorithms, allowing to design receivers that jointly estimate the channels and transmitted symbols. Necessary conditions required to the uniqueness of the tensor decompositions and identifiability of the proposed algorithms are also discussed. Finally, computational simulation results are presented in order to evaluate the

behavior of the proposed systems/receivers, illustrating the effectiveness of signal processing based on nested tensor decompositions.

**Keywords:** Cooperative systems. MIMO systems. Tensor decomposition. Tucker decomposition. Semi-blind receiver.

## RÉSUMÉ

Les systèmes MIMO (*multiple-input multiple-output*) sont souvent utilisés pour augmenter les gains de diversité et/ou multiplexage en transmettant plusieurs versions d'un même signal ou des données indépendantes sur différents canaux de communication. Un autre moyen d'exploiter la diversité spatiale sont les communications coopératives. Elles sont devenues une technique prometteuse pour les nouvelles générations de systèmes de communication sans fil, qui ont permis d'améliorer considérablement les performances et la fiabilité de ces systèmes. Dans ce contexte, au cours des dernières décennies, les décompositions tensorielles ont été exploitées dans le traitement de signaux multidimensionnels dans les systèmes MIMO et, plus récemment, dans les réseaux coopératifs, permettant la conception de récepteurs efficaces pour l'estimation des paramètres de transmission. En particulier, les décompositions imbriquées (*nested decomposition*) permettent de modéliser les signaux dans les systèmes bénéficiant de multiples diversités, ce qui entraîne des tenseurs d'ordre élevé qui sont représentés de manière compacte. Cette thèse présente des développements réalisés dans le contexte de nouvelles décompositions tensorielles imbriquées appliquées aux systèmes de communication sans fil coopératifs avec plusieurs antennes. En effet, les contributions théoriques de la présente thèse reposent sur la proposition de nouvelles décompositions tensorielles imbriquées, ainsi que sur l'analyse de leurs propriétés d'unicité, ainsi que sur la proposition de nouveaux systèmes MIMO coopératifs modélisés à l'aide des décompositions présentées. Dans la première partie de cette thèse, deux nouveaux modèles tensoriels, basés sur le modèle NTD (*nested Tucker decomposition*), sont introduits. Le premier, appelé *high-order nested Tucker decomposition* (HONTD), étend le modèle NTD en prenant en compte les tenseurs d'ordre supérieur résultant de la contraction de plusieurs décompositions Tucker dans un format de train. Le deuxième, appelé *coupled nested Tucker decomposition* (CNTD), peut être vue comme un couplage de plusieurs NTDs qui partagent un facteur commun, associant les concepts d'imbrication et de couplage définis initialement pour les modèles PARAFAC, en les étendant à des modèles basés sur décomposition Tucker. Dans les parties suivantes, ces décompositions tensorielles sont utilisées dans la modélisation de trois nouveaux systèmes MIMO coopératifs. Deux d'entre eux considèrent des cas avec plusieurs relais (avec retransmission séquentielle et parallèle, respectivement), tandis que l'autre considère un réseau avec plusieurs porteuses et un seul relais. Tous les systèmes proposés prennent en compte les codages tensoriels dans les nœuds de transmission. Pour chaque système proposé, les modèles tensoriels sont exploités pour

obtenir des algorithmes d'estimation semi-aveugles, permettant de développer des récepteurs qui estiment conjointement les canaux et les symboles transmis. Les conditions liées à l'unicité des décompositions tensorielles et à l'identifiabilité des algorithmes proposés sont également discutées. Enfin, les résultats des simulations sont présentés afin d'évaluer le comportement des systèmes/récepteurs proposés, illustrant l'efficacité du traitement du signal basé sur les décompositions de tenseur imbriquées.

**Mots-clés:** Décomposition tensorielle. Décomposition Tucker. Récepteur semi-aveugle. Systèmes coopératifs. Systèmes MIMO.

## LIST OF FIGURES

Figura 1 – MIMO wireless system with $M_T$ transmit and $M_R$ receive antennas . . . . .	25
Figura 2 – Cooperative communication system . . . . .	27
Figura 3 – Tridimensional visualization of the received signal in a MIMO system with TSTC . . . . .	31
Figura 4 – (i) Column fiber; (ii) row fiber; (iii) tube fiber . . . . .	40
Figura 5 – (i) Frontal slice; (ii) vertical slice; (iii) horizontal slice . . . . .	41
Figura 6 – Matrix representation for third-order tensor . . . . .	42
Figura 7 – Block-diagram of a Tucker decomposition for a third-order tensor . . . . .	47
Figura 8 – Block-diagram of a nested Tucker decomposition for a fourth-order tensor . . . . .	51
Figura 9 – Block-diagram of a PARAFAC decomposition for a third-order tensor (i) as a special case of the Tucker decomposition and (ii) as a sum of triads. . . . .	53
Figura 10 – Block-diagram of a coupled PARAFAC decomposition for a fourth-order tensor . . . . .	56
Figura 11 – Block-diagram of a HONTD for a $(N + 3)$ -order tensor . . . . .	62
Figura 12 – Block-diagram of a CNTD for a fifth-order tensor . . . . .	67
Figura 13 – Block-diagram of the alternative CNTD model . . . . .	71
Figura 14 – Multi-hop MIMO relaying system with $K$ relays . . . . .	73
Figura 15 – ZF receiver performance for different numbers of data stream . . . . .	84
Figura 16 – ZF receiver performance for different values of $P_0$ , $P_1$ and $P_2$ . . . . .	85
Figura 17 – ZF receiver performance for different numbers of antennas . . . . .	85
Figura 18 – ZF receiver performance for different numbers of relays . . . . .	86
Figura 19 – SER performance for the proposed ALS receiver . . . . .	87
Figura 20 – Convergence of the proposed ALS receiver . . . . .	88
Figura 21 – Channel NMSE for the proposed ALS receiver . . . . .	88
Figura 22 – SER performance comparison with LSKP receiver for $K = 2$ . . . . .	89
Figura 23 – SER performance with the LSKP receiver for different numbers of relays . . . . .	90
Figura 24 – SER performance with the LSKP receiver for different values of $R$ and $P_0$ . . . . .	91
Figura 25 – NMSE of the individual channel estimates with LSKP receiver for $K = 2$ . . . . .	91
Figura 26 – SER performance comparison for $K = 2$ . . . . .	93
Figura 27 – NMSE of the individual channel estimates for $K = 2$ . . . . .	93
Figura 28 – Two-hop MIMO relaying system with $K$ relays . . . . .	96
Figura 29 – Tensor model of noiseless received signals . . . . .	99

Figura 30 – ZF receiver performance for different numbers of relays . . . . .	103
Figura 31 – ZF receiver performance for different time-spreading lengths $P$ and $J$ . . .	104
Figura 32 – Trade-off for the time-spreading lengths $P$ and $J$ . . . . .	104
Figura 33 – ZF receiver performance for different numbers of data streams . . . . .	105
Figura 34 – ZF receiver performance for different numbers of antennas . . . . .	105
Figura 35 – ZF receiver performance for $K M_R$ constant . . . . .	106
Figura 36 – ZF receiver performance for $K M_D$ constant . . . . .	107
Figura 37 – Impact of the number of relays on the SER performance . . . . .	107
Figura 38 – Impact of the time-spreading length on the SER performance . . . . .	108
Figura 39 – SER performance for the LSKP receiver with $JK = 8$ . . . . .	108
Figura 40 – SER performance for the LSKP receiver with $JK = 12$ . . . . .	109
Figura 41 – SER performance comparison for several receivers . . . . .	110
Figura 42 – NMSE of $\mathcal{H}^{(SR)}$ for the LSKP receiver with (a) $JK = 8$ and (b) $JK = 12$ .	110
Figura 43 – NMSE of $\mathcal{H}^{(RD)}$ for the LSKP receiver with (a) $JK = 8$ and (b) $JK = 12$ .	111
Figura 44 – Channel NMSE comparison for several receivers . . . . .	111
Figura 45 – Two-hop OFDM MIMO relaying system . . . . .	114
Figura 46 – Block diagram for the CNTD-based signal model . . . . .	116
Figura 47 – SER performance for different numbers of subcarriers . . . . .	120
Figura 48 – Influence of the number of subcarriers on the SER performance . . . . .	120
Figura 49 – Performance comparison with ZF receiver for different values of $P$ and $J$ .	120
Figura 50 – NMSE of $\mathbf{H}^{(SR)}$ for coupled and non-coupled estimation . . . . .	121
Figura 51 – NMSE of $\mathbf{H}^{(RD)}$ for coupled and non-coupled estimation . . . . .	121
Figura 52 – Impact of the number of subcarriers on the channel NMSE . . . . .	122
Figura 53 – SER performance for CNTD-based systems . . . . .	123
Figura 54 – NMSE of $\mathbf{H}^{(SR)}$ for CNTD-based systems . . . . .	123
Figura 55 – NMSE of $\mathbf{H}^{(RD)}$ for CNTD-based systems . . . . .	123
Figura 56 – Block-diagram for a doubly coupled nested Tucker decomposition . . . . .	132

## LIST OF TABLES

Tabela 1 – ALS receiver for multi-hop MIMO relay system . . . . .	79
Tabela 2 – LSKP receiver for multi-hop MIMO relay system . . . . .	82
Tabela 3 – Condition number of the LSKP and ZF receivers with different codings . . .	90
Tabela 4 – LSKP receiver for two-hop MIMO multirelay system . . . . .	101
Tabela 5 – LSKP receiver for two-hop OFDM MIMO relay system . . . . .	118

## LIST OF ACRONYMS

<b>AF</b>	Amplify-and-forward
<b>ALS</b>	Alternating least square
<b>AWGN</b>	Additive white Gaussian noise
<b>BSS</b>	Blind source separation
<b>CANDECOMP</b>	Canonical decomposition
<b>CF</b>	Compress-and-forward
<b>CNTD</b>	Coupled nested Tucker decomposition
<b>CP</b>	Canonical polyadic
<b>CSI</b>	Channel State Information
<b>DF</b>	Decode-and-forward
<b>DFT</b>	Discrete Fourier transform
<b>DS-CDMA</b>	Direct-sequence code division multiple access
<b>HONTD</b>	High-order nested Tucker decomposition
<b>KP</b>	Kronecker product
<b>KRST</b>	Khatri-Rao space-time
<b>LM</b>	Levenberg-Marquardt
<b>LS</b>	Least square
<b>LSKP</b>	Least square of Kronecker product
<b>MC</b>	Monte Carlo
<b>MIMO</b>	Multiple input multiple output
<b>MMSE</b>	Minimum mean-squared error
<b>NMSE</b>	Normalized mean square error
<b>NTD</b>	Nested Tucker decomposition
<b>OFDM</b>	Orthogonal frequency-division multiplexing

<b>PCA</b>	Principal component analysis
<b>PARAFAC</b>	Parallel factor analysis
<b>QAM</b>	Quadrature amplitude modulation
<b>SER</b>	Symbol-error-rate
<b>SISO</b>	Single input single output
<b>SNR</b>	Signal-to-noise ratio
<b>ST</b>	Space-time
<b>STF</b>	Space-time-frequency
<b>SVD</b>	Singular value decomposition
<b>TST</b>	Tensor space-time
<b>TSTF</b>	Tensor space-time-frequency
<b>TSTC</b>	Tensor space-time coding
<b>WLAN</b>	Wireless local area network
<b>ZF</b>	Zero-forcing

## LIST OF SYMBOLS

$\mathbb{R}$	Field of real numbers
$\mathbb{C}$	Field of complex numbers
$a$	Scalar
$\mathbf{a}$	Column vector
$\mathbf{e}_n^{(N)}$	$n$ -th canonical vector in Euclidean space $\mathbb{R}^N$
$\mathbf{A}$	Matrix
$\mathbf{A}^T$	Transpose matrix
$\mathbf{A}^*$	Complex conjugate
$\mathbf{A}^H$	Hermitian
$\mathbf{A}^\dagger$	Moore-Penrose pseudo-inverse
$\mathbf{a}_i, (\mathbf{a}_j)$	$i$ -th ( $j$ -th) row (column) of $\mathbf{A}$
$\mathcal{A}$	$N$ -order tensor – array of order higher than two
$[\mathcal{A}]_{i_1, \dots, i_N, a_{i_1, \dots, i_N}}$	$(i_1, \dots, i_N)$ -th element of tensor $\mathcal{A} \in \mathbb{C}^{I_1 \times \dots \times I_N}$
$[\mathcal{A}]_{(i_n), \mathcal{A}_{(i_n)}}$	Tensor with the $n$ -th mode fixed
$vec(\cdot)$	Vectorization operator
$vec_b(\cdot)$	Block-vectorization operator
$diag(\cdot)$	Diagonal matrix formed from the elements of the argument vector
$diag_n(\cdot)$	Diagonal matrix formed from the elements of the $n$ -th column vector of the argument matrix
$bdiag(\cdot)$	Block-diagonal operator
$r_{\mathbf{A}}$	Rank of $\mathbf{A}$
$\langle \cdot, \cdot \rangle$	Inner product

$\cdot \circ \cdot$	Outer product
$\cdot \otimes \cdot$	Kronecker product
$\cdot \boxtimes \cdot$	Block-Kronecker product
$\cdot \diamond \cdot$	Khatri-Rao product
$\cdot \times_n \cdot$	Mode- $n$ product
$\cdot *_m^n \cdot$	Contraction operation over $m$ -th mode of the first factor and $n$ -th mode of the second factor
$\cdot \sqcup_n \cdot$	Concatenation operation
$\  \cdot \ _F$	Frobenius norm

## SUMMARY

<b>1</b>	<b>INTRODUCTION</b> . . . . .	<b>23</b>
<b>1.1</b>	<b>MIMO communication systems</b> . . . . .	<b>25</b>
<b>1.2</b>	<b>Cooperative communication systems</b> . . . . .	<b>26</b>
<b>1.3</b>	<b>Signal processing based on tensor models</b> . . . . .	<b>29</b>
<b>1.4</b>	<b>Thesis content</b> . . . . .	<b>32</b>
<b>2</b>	<b>TENSOR REQUISITES</b> . . . . .	<b>38</b>
<b>2.1</b>	<b>Notations, definitions and basic matrix and tensor operations</b> . . . . .	<b>38</b>
<b>2.2</b>	<b>Background on tensor decompositions</b> . . . . .	<b>45</b>
<b>2.2.1</b>	<i>Tucker decomposition</i> . . . . .	<b>46</b>
<b>2.2.2</b>	<i>Generalized Tucker decomposition</i> . . . . .	<b>48</b>
<b>2.2.3</b>	<i>Nested Tucker decomposition</i> . . . . .	<b>50</b>
<b>2.2.4</b>	<i>PARAFAC decomposition</i> . . . . .	<b>52</b>
<b>2.2.5</b>	<i>Coupled PARAFAC decomposition</i> . . . . .	<b>55</b>
<b>2.3</b>	<b>Bibliographic review on tensor decompositions applied to wireless communication systems</b> . . . . .	<b>56</b>
<b>3</b>	<b>ORIGINAL CONTRIBUTIONS ON TENSOR DECOMPOSITIONS</b> .	<b>61</b>
<b>3.1</b>	<b>High-order nested Tucker decomposition – HONTD</b> . . . . .	<b>61</b>
<b>3.1.1</b>	<i>Uniqueness analysis</i> . . . . .	<b>63</b>
<b>3.2</b>	<b>Coupled nested Tucker decomposition – CNTD</b> . . . . .	<b>65</b>
<b>3.2.1</b>	<i>Uniqueness analysis</i> . . . . .	<b>68</b>
<b>3.2.2</b>	<i>Alternative structure for the CNTD model</i> . . . . .	<b>69</b>
<b>4</b>	<b>MULTI-HOP MIMO RELAY SYSTEM WITH TSTC BASED ON HONTD</b>	<b>72</b>
<b>4.1</b>	<b>System model</b> . . . . .	<b>72</b>
<b>4.1.1</b>	<i>Case with two relays</i> . . . . .	<b>73</b>
<b>4.1.2</b>	<i>General case – <math>K</math> relays</i> . . . . .	<b>75</b>
<b>4.2</b>	<b>Semi-blind receivers</b> . . . . .	<b>76</b>
<b>4.2.1</b>	<i>ALS Receiver</i> . . . . .	<b>76</b>
<b>4.2.2</b>	<i>LSKP Receiver</i> . . . . .	<b>80</b>
<b>4.3</b>	<b>Simulation results</b> . . . . .	<b>83</b>
<b>4.3.1</b>	<i>Zero-forcing receiver with perfect channel knowledge</i> . . . . .	<b>84</b>

4.3.2	<i>ALS receiver performance</i>	86
4.3.3	<i>LSKP receiver performance</i>	88
4.3.4	<i>Performance comparison of the proposed receivers</i>	92
4.4	Summary	93
5	<b>TWO-HOP MIMO MULTIRELAY SYSTEM WITH TSTC BASED ON</b>	
	<b>CNTD</b>	95
5.1	System model	95
5.2	Semi-blind receiver	98
5.3	Simulation results	102
5.3.1	<i>ZF performance with perfect channel knowledge</i>	103
5.3.2	<i>LSKP receiver performance</i>	107
5.4	Summary	112
6	<b>TWO-HOP OFDM MIMO RELAY SYSTEM WITH TSTC BASED ON</b>	
	<b>CNTD</b>	113
6.1	System Model	113
6.2	Semi-blind receiver	116
6.3	Simulation Results	118
6.3.1	<i>ZF and LSKP performance</i>	119
6.3.2	<i>Performance comparison of CNTD-based systems</i>	122
6.4	Summary	124
7	<b>CONCLUSION</b>	126
8	<b>FUTURE WORKS</b>	130
8.1	<b>Two-hop OFDM MIMO multi-relay system and doubly coupled tensor decomposition</b>	130
8.2	<b>Perspectives</b>	133
	<b>REFERENCES</b>	134
	<b>APPENDICES</b>	141
	<b>APPENDIX A – Uniqueness properties of tensor models</b>	141
	<b>APPENDIX B – Matrix representation of a generalized Tucker decomposition</b>	142
	<b>APPENDIX C – LS estimation of Kronecker product factors</b>	144

## 1 INTRODUCTION

Wireless communication between mobile stations, held for the first time in the nineteenth century, has experienced from the beginning of 1990s a great growth in the number of users. The consolidation of cellphones as a toll of personal communication led to a large increasing in the industry of wireless communication devices. Cellphone systems can be considered the most successful application of wireless networking [1]. Since the first voice transmission between New York and San Francisco in 1915, these systems have been gaining more and more industrial/commercial interest, leading to the insertion of innumerable resources, as is the case of the most recent generations that integrate voice, data and images.

In this scenario, the demand for high data transmission rate and broader coverage required to provide services such as online games, streaming TV, among other multimedia applications, grows asymptotically. However, high-speed wireless transmission has fundamental physical limitations such as interference from different sources, attenuation of signal power with distance, and other signal fading effects connected to the wireless communication channel. In order to increase the capacity of communication systems, new technologies using strategies that aim to improve the spectral efficiency, ensuring quality and reliability in the transmission and reception of information, are required.

The transmitted signals in wireless communication systems have a very irregular behavior due to attenuation and distortion usually caused by noise and interference in the communication channel. Roughly, the signal power is dropped due to effects that can be divided in two classes [1–3]: large-scale (macroscopic) fading and small-scale (microscopic) fading. The first one results from the combination of effects such as the inverse square law power loss, absorption, ground reflection and shadowing (caused by blocking effects due to buildings and natural features). The second one, also known as small-scale fading, comes from the constructive and destructive interference between the multiple signal paths. Therefore, it is clear that the understanding of how these fading occur is of extreme importance for the design of wireless communication systems.

The study on channel behavior is a fundamental problem, since it allows to translate the physical phenomena of the propagation in a model that synthesizes the modifications of the environment on the transmitted signals. Mathematical models that aim to describe the behavior of the communication channels and, consequently, the influence of these distortions in the transmitted information are constantly exploited by the scientific community in order to develop

equalizers and receivers adapted to each situation. In practice, these channels follow statistical models characterized by means of time-varying random variables.

Besides the study of the channel behavior, the development of techniques that avoid the deep fading of the signal before reaching its destination is needed. An alternative to deal with these undesired effects present on wireless channels is to exploit the so called signal diversities, such as space, time, frequency, coding, and cooperation diversities.

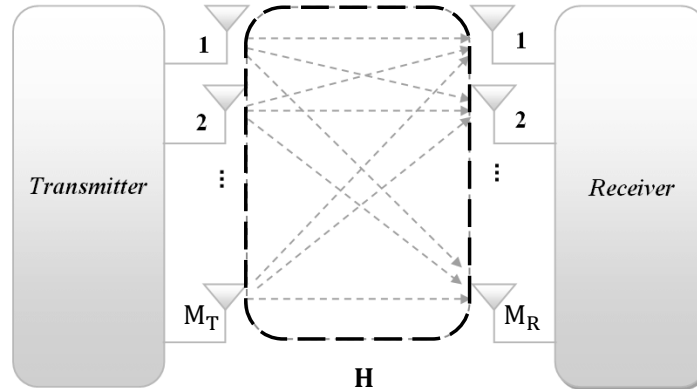
By diversity we mean a set of techniques that aims to enhance the quality of received signals in communication systems, providing a wireless link improvement at a relatively low cost [3, 4]. The main idea in diversity is create redundancies of the signal by exploiting the random nature of the radio propagation in such a way that different and independent versions of the same signal reach the destination. The probability of all these copies being simultaneously in a deep fading is small.

There are many ways to obtain diversity. For instance, time diversity can be obtained via coding: information is coded and the coded symbols are dispersed across time domain in different periods so that different parts of the codewords experience roughly uncorrelated fadings. On the other hand, when the channel is frequency-selective, one can exploit frequency diversity replaying the signals across multiple subcarriers. Since diversity is such an important resource, a wireless system can use several types of diversity simultaneously.

Spatial diversity can be found in multiple-input multiple-output (MIMO) systems, which have multiple antennas at the transmit and receive nodes, allowing to improve the quality of signal by exploiting diversity [5–7]. The benefit from spatial diversity with MIMO systems comes from the redundancies in the transmitted signal, leading the receive antennas to possibly obtain uncorrelated faded versions of the same signal. In this way, the probability of effective reception of the transmitted information is increased.

MIMO systems are also useful to increase the transmission rate by multiplexing data across the multiple antennas [1]. In this case, the channel structure is exploited to obtain independent signaling paths that can be used to send independent data. Due to the importance of MIMO systems in the development of new wireless communication generations, as well as in the research addressed in this thesis, we highlight an overview of some features of MIMO channels in the following section.

Figure 1 – MIMO wireless system with  $M_T$  transmit and  $M_R$  receive antennas



### 1.1 MIMO communication systems

The increasing interest in MIMO systems began with the promising spectral efficiency obtained with wireless systems that have multiple transmit and receive antennas. In [8–10], one can find some pioneering works that address the architecture and capacity of MIMO channels. A simple wireless communication system with  $M_T$  transmit and  $M_R$  receive antennas is shown in Figure 1. The signals received at the receiver in this system can be represented as  $\mathbf{y} = \mathbf{H}\mathbf{x} + \mathbf{n}$ , where  $\mathbf{x}$  and  $\mathbf{y}$  are the vectors whose the entries represent the transmitted and received symbols, respectively. The vector  $\mathbf{n}$  represents the additive noise at each receive antenna and  $\mathbf{H}$  is the  $M_R \times M_T$  matrix of channel gains, whose the entries are the impulse responses. It was deduced that, under certain conditions, antennas separated by a distance of order of half wavelength would have approximately uncorrelated channels [1]. This feature can be exploited to provide diversity and multiplexing gains.

The diversity order in MIMO systems is equal to the product of the number of antennas at the transmit and receive nodes, if the corresponding channels are independently faded. For effective exploitation of this diversity, it is needed the knowledge of the matrix  $\mathbf{H}$ , which can be obtained by sending pilot sequences. Many studies assume a model where the entries of  $\mathbf{H}$  are independent and identically distributed (i.i.d.) zero mean, unit variance, complex circularly symmetric Gaussian random variables. In general, different assumptions about the channel state information (CSI) and its random nature lead to different channel capacities.

MIMO systems are also used to increase the multiplexing gain, by transmitting independent data onto the independent channels. This multiplexing gain leads to an increasing in data rate when compared to single-input single-output (SISO) systems, which have only

one antenna at the transmit and receive nodes. However, the properties of  $\mathbf{H}$  also determines how much spatial multiplexing it can support. It is worth mentioning that the possibility of these two mechanisms of MIMO system exploitation raises the question on which is the best way to exploit multiple antennas (either through diversity gain, multiplex gain or both). Many references [1, 11–13] that addressed this question show that there is a tradeoff between diversity and multiplexing gains. In practice, it is possible to adapt the diversity and multiplexing gains relative to channel conditions. In adverse scenarios, with deeper faded channels, more antennas can be used for diversity gain, improving the quality of the signal, whereas in better scenarios, more antennas can be used for multiplexing to obtain data rate gains. Adaptive techniques to exploiting the diversity/multiplexing tradeoff based on channel conditions can find in [14, 15].

Another way to provide spatial diversity is through the concept of cooperative communication. In the sequel, we discuss the characterization of communication channels in cooperative systems, providing a motivation of their use.

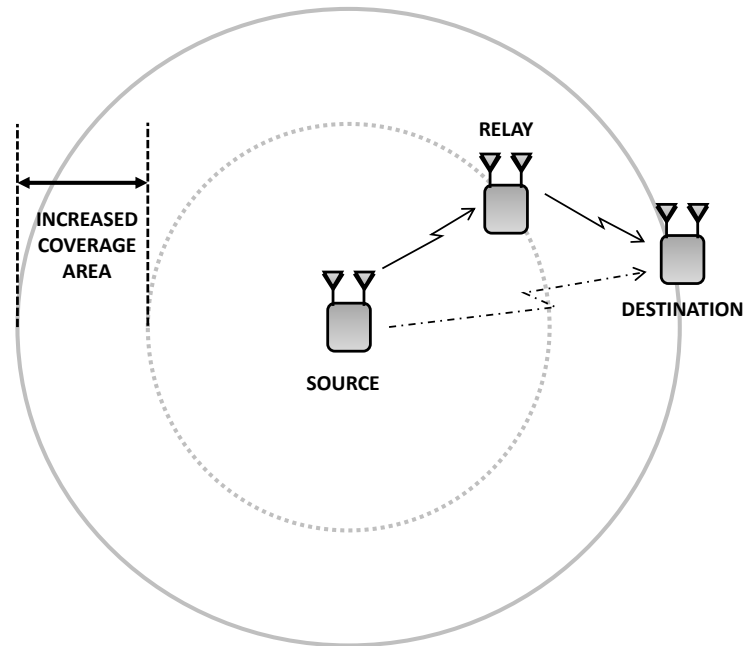
## 1.2 Cooperative communication systems

Cooperative communication was proposed for the first time in 1971 in a work that used a cooperative channel as a way to make easier to transmit information from the source to the destination [16]. The cooperative diversity has been shown to be applicable in several types of communication systems, such as cellphone networks, wireless local area networks (WLAN), sensor arrays, among others [17], emerging as a promising technique in the development of current and future generations of wireless communication systems.

Cooperative systems are based on the exploitation of users or fixed stations as retransmitters (relays) of the signal coming from other users. In other words, all the involved nodes can be used as relays of the signal transmitted by the source. The repetition of the signal sent by the source through the relay allows the extension of the coverage area, amplifying the signal power that reaches the destination, yielding significant gains in the capacity and performance of the system. Due to the resounding growth in the number of mobile stations in the last decades, cooperative communications have emerged as a technique that can significantly improve the quality of wireless communications systems, being prominent in the development of new signal processing techniques for 5G communication systems.

Figure 2 shows a simple example of a wireless system that utilizes cooperative communication. Cooperative systems are composed of a transmitter (source), one or more relays

Figure 2 – Cooperative communication system



and one or more receivers (destination). In this scenario, a user can act as a relay for another user, forwarding the information by using established relaying protocols. Thus, the signal that the destination will receive is a combination at different times of the direct and cooperative links. According to Figure 2, the source-relay-destination link enlarges the coverage area, intensifying the signal that arrives at the destination node. The literature has shown significant gains in the capacity and performance of these systems, being similar to the gains obtained with MIMO systems.

Systems such as represented in Figure 2 are said single-relay systems. These systems improve the quality of the received signal, raising SNR levels by providing a signal power gain before forwarding to the destination. However, when the direct (source-destination) link, also called line-of-sight (LOS), is not available (corresponding to the case when the signals are deeply faded), the single-relay system does not provide diversity, since there are no independent copies of the signal. In order to effectively exploit the cooperative diversity, recent works [18–21] have been addressed cooperative systems with multiple relays (multi-relay systems) in two cooperation scheme, namely sequential and parallel relaying.

The use of cooperative channels can be roughly classified into two categories: fixed and adaptive cooperation. The first one is characterized by the cooperative link being always used, regardless of channel status and intensity levels of the forwarded signal. This type has a simpler implementation, but requires constant relaying, even in unnecessary situations or in

unfavorable scenario. On the other hand, adaptive cooperation uses the cooperative link in a smart way, being required only when necessary. The cost of this cooperation kind is a more complex implementation, requiring a higher processing cost.

Relaying (or cooperation) protocols are techniques that define the manner by which the relays process the signal to be re-transmitted. It is possible to find in the literature many relaying protocols. However, the main applications address some classes of protocols, namely: AF (amplify-and-forward), DF (decode-and-forward), and CF (compress-and-forward). The use of CF relays usually requires that the direct link is always available, which is not the case of other protocols. However, by transmitting a smaller amount of information, the CF relays save signal bandwidth, increasing the spectral efficiency of the system. In cases where the destination is close to the source, CF relays are more efficient than DF relays.

These cooperation protocols can also be classified with respect to how the relays deal with the signal to be re-transmitted. Protocols are said to be non-regenerative when the relay just amplifies the received signal (e.g. AF protocol), and said to be regenerative when the relay performs a treatment on the received signal before forwarding (e.g. DF or CF protocol). For the last kind of protocols, the transmitted symbols can be modified during the demodulation process at the relay node.

Yet on the operating scheme of the relays, they can be full-duplex or half-duplex. In the full-duplex configuration [22, 23], the relays can transmit and receive the signals at the same time. Although the spectral efficiency is improved, the cost of implementation is high and the transmitted signals may cause strong interference to incoming relatively weak received signals. The most common configuration is half-duplex [24, 25], where the relays receive and transmit at different channels, being easier to implement. However, they cause a degradation in spectral efficiency. This led to the development of bidirectional (or two-way) half-duplex relay systems [26].

In general, cooperative communication brings advantages in terms of improving system performance, quality of service, cost and structure reduction (since it uses mobile stations already connected to the network). The main limitations are related to the increase in processing load, relay selection (in adaptive protocols) and the need to estimate a larger amount of channels.

An efficient way to mitigate the undesirable effects in wireless communication links is associate multiple types of diversity. Next generations of wireless communication systems will be structurally provided with multiple diversity techniques in order to establish reliable

transmission schemes and to compensate for the effects of signal fading and shadowing. In the last years, cooperative MIMO systems have become one of the hot topics in the wireless communications and have attracted much research interest [18, 20, 21, 24, 27–34].

When nodes in the cooperative system are installed with multiple antennas, frequently called MIMO relay communication system, we can obtain an optimal exploitation of the diversity/multiplexing trade-off of the spatially-distributed antennas. Indeed, the cooperation between the nodes can provide diversity by using multiple nodes to aid in forwarding different versions of the signal to destination, while the nodes transmit independent data across the multiple antennas. In this way, MIMO relay systems can extend the network coverage, increase the spatial diversity and multiplexing gains and improve the effectiveness and reliability of communication systems.

Other systems that combine multiple diversities can be found in the literature. For instance, in [35–38] we can find MIMO systems with codings that provides space-time (ST) diversity. In [39–41], space-time-frequency (STF) codings are applied to orthogonal frequency division multiplexing (OFDM) MIMO systems. ST MIMO relay [18, 30, 31, 34, 42] and STF relay systems [43] were also addressed. In [44], we can also find cooperative MIMO systems applied to wireless sensor networks (WSN). Works on the exploitation of OFDM MIMO systems with cooperative diversity is still scarce.

Concerning the signal processing in systems that benefit from multiple diversities, such as ST MIMO relay systems, the use of techniques based on tensor decompositions has attracted considerable attention. In the sequel, we introduce the main features and motivations to use tensor-based approaches to improve signal processing efficiency.

### 1.3 Signal processing based on tensor models

High order tensors (i.e., multiway arrays) and tensor decompositions (also called tensor factorization) can be seen as useful tools for representing multidimensional data in a compact way. Recent developments in multilinear algebra have made it possible to apply tensor analysis to several areas [45–51].

In some applications, tensor decompositions can be viewed as generalizations of matrix decompositions such as singular value decomposition (SVD) to higher order arrays. The reading of a tensor by its decomposition factors is useful in analysis where different contributions must be identified from measured data. In addition to enabling multidimensional data processing,

tensor analysis has uniqueness properties that becomes possible to solve undetermined solution problems under conditions more relaxed than conventional matrix approaches [6, 34, 45–48, 52].

In particular, tensor approaches have gained considerable space in signal processing. The proposition of new factorizations of tensors, as well the study of uniqueness and identifiability conditions, have a great potential to provide remarkable improvements in several areas as biomedical engineering, machine learning and computer vision. In the literature, one can find several applications of tensor approaches aiming to increase the capacity of wireless networks. In [53, 54], for instance, one can find tensor completion techniques applied to internet traffic data to solve missing data problems. The recent studies show that it is more accurate to interpolate the missing data with a 3-D tensor as compared with the interpolation methods based on a 2-D matrix. In [55], a tensor approach is used to obtain a more accurate algorithm for data anomaly detection. On the other hand, in [51, 56–58], tensor-based techniques are applied to solve the blind source separation (BSS) of a mixture of signals received by an antenna array.

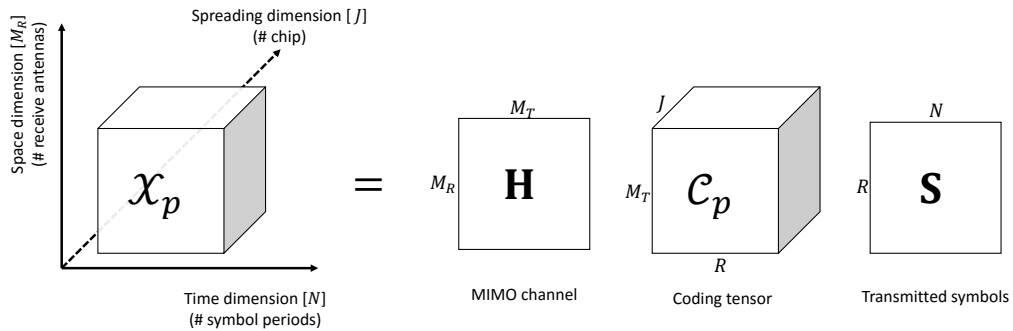
In wireless communications, the fact that the signals received at destination may accumulate different systematic variations of the system suggests that they can be viewed as multidimensional arrays (tensors) where each index may be linked to some particular form of diversity, benefiting simultaneously all of them [6, 34, 47]. Its multilinear nature means that each signal sample corresponds to an element of a multidimensional space, where each index is associated with variations of a specific system parameter. This fact is one of the main reasons for using tensor modeling in wireless communication.

Tensor models allow the benefit from multiple (more than two) forms of signal diversity to perform jointly and blindly signal separation/equalization, information recovery and channel estimation under mild conditions. Indeed, the identifiability of the parameters with a tensor approach is ensured under less restrictive conditions when compared to conventional approaches.

Tensor-based approaches also include the possibility of using tensor coding, with simultaneous spatial multiplexing, spreading spectrum, time spreading and multicarrier modulation, yielding diversity and spectral efficiency gains. In [59], a block coding scheme based on the Khatri-Rao matrix product was proposed. We can find in [18, 30, 39, 42] examples of applications of this coding scheme to different systems based on different tensor decompositions.

In [35], a tensor space-time coding (TSTC) was proposed aiming to increase the diversity and multiplexing gain by introducing two extra time dimensions (chips and blocks), in

Figure 3 – Tridimensional visualization of the received signal in a MIMO system with TSTC



addition to common space and time (symbol period) dimensions, via a third-order coding tensor and two allocation matrices in a MIMO system. A block-diagram interpretation of multimodal data is illustrated Figure 3, where we can see the tensor of signals received at destination during the  $p$ -th time-block. At each block  $p$ , a different set of data streams can be sent using a different resources (transmit antennas), depending on the allocation matrices embedded in the coding tensor. Globally, the received signals form a fourth-order tensor. The TSTC was also applied to a two-hop MIMO relay systems in [34].

Among the most popular tensor decompositions, Tucker [60] and parallel factors analysis (PARAFAC) [61], as well as their derivations (PARATUCK [35], nested PARAFAC [41], coupled PARAFAC [62], generalized PARATUCK [40] and nested Tucker [34]), are commonly used in signal processing for wireless communications. PARAFAC models have the important property of being essentially unique. Tucker models are not essentially unique, except under certain conditions like a priori knowledge of the core tensor. Despite this, Tucker models have been emerged as one of the most flexible tensor decompositions [57].

For this thesis, in particular, nested and coupled decompositions are crucial. For the nested decompositions based on PARAFAC and Tucker models found in the literature, the nesting operation results from the fact that two successive tensors arranged in a train format have a matrix factor in common. On the other hand, a set of tensor decompositions is said to be coupled when at least one of the involved factors is shared by all the decompositions. To our knowledge, the recent concept of coupled decompositions has been applied only to PARAFAC-based models and have not yet been applied in the context of telecommunications. In this thesis, we extend the concepts of nesting and coupling to higher-order tensors and/or to Tucker-based models. In Subsection 2.2, we bring a more detailed overview of the main tensor decompositions found in the literature.

In this context, tensor decompositions have been widely exploited in the design of algorithms for the blind estimation of transmission parameters, without require the use of training sequences or previous knowledge of CSI. Different algorithms for parameter estimation applied to cooperative MIMO systems, with different configurations, different relaying protocols and different codings can be found in the literature [18, 21, 24, 27, 34, 39, 42, 48]. In Subsection 2.3, we make a deeper bibliographic survey.

For cooperative networks, the reliability of signal detection depends on the accuracy of CSI for all the links involved in the communication scheme [27]. The knowledge of individual channels plays an important role for optimizing MIMO relay systems in terms of power allocation, decoding and adaptive relaying protocols that must decide when a cooperation is feasible and select a suitable relay [63, 64]. However, in most of real applications, CSI for all the links is not available at the destination node and needs to be estimated.

The semi-blind estimation of symbols and channels has become a powerful tool for the development of the next generations of wireless communication systems. Many papers that propose receivers based on matrix and tensor models admit the use of training sequences for channel estimation [20, 21, 65, 66] or assume the perfect knowledge of the CSI at the receivers [29, 67–69]. The semi-blind receivers provide spectral efficiency gains by using fewer pilot symbols. In this scenario, tensor-based receivers seem to be a promising solution.

Finally, the study of tensor models applied to more complex cooperative MIMO systems is still scarce. Such researches are important so that the scientific community can effectively test and understand the behavior, advantages and limitations of each case, being therefore a topic of interest for new communication strategies that enable a scientific-technological development capable of following the demands of the new generations of wireless systems.

#### **1.4 Thesis content**

In this thesis, we address nested tensor decompositions applied to cooperative MIMO communication systems. In particular, the main contributions of the this thesis rely on the proposition of two new tensor decompositions applied to high-order tensors and of new cooperative MIMO communication systems, which are modeled by the presented nested tensor models. In the first part of this thesis, two new tensor models, called high-order nested Tucker decomposition (HONTD) and coupled nested Tucker decomposition (CNTD), are introduced. A detailed discussion on the uniqueness properties of these new models is made. In the subsequent parts,

the new proposed tensor models are used to modeling signals received at destination in three new cooperative MIMO relay systems. By exploiting the tensor-based modeling, we derive semi-blind receiver algorithms to jointly estimate the transmitted symbols and communication channels of the proposed systems. Extensive Monte Carlo simulations to illustrate the behavior and the effectiveness of the proposed schemes were performed.

### *Thesis organization*

In addition to the global overview on wireless communication in this introduction, the Chapter 2 brings a background on tensor models, operations and applications. The notations, and main matrix and tensor operations that will be necessary along of this work are presented. We also discuss some useful properties used throughout the thesis. An overview of the most known tensor decomposition is introduced. At the end of this chapter, we summarize some recent and important applications of tensor models to design wireless communication systems.

Chapter 3 presents the first original contributions of this work, by presenting the tensor decompositions proposed in this thesis. Based on a nested Tucker decomposition (NTD) proposed in [34], we derive to new tensor decompositions that generalize the NTD model to higher-order tensors. The first one is called high-order nested Tucker decomposition (HONTD), which is characterized by a train of Tucker models that share common decomposition factors. The second one is called a coupled nested Tucker decomposition (CNTD). This model can be seen as a combination of the concepts of coupled and nested decompositions that were originally introduced separately. Coupled decomposition was initially introduced to PARAFAC-based models and CNTD extends this concept to Tucker-based models. Details on the properties of the proposed models are discussed and uniqueness theorems are provided.

In the following chapters, the proposed new tensor models are applied to three different cooperative MIMO systems, whose relays operate in AF protocol and half-duplex configuration. In Chapter 4, we propose a multi-hop MIMO relay system that uses a TSTC to encode the signals to be transmitted at the source and the relays. The transmission scheme is composed by  $K + 1$  steps, where  $K$  is the number of relays available on the cooperative network. The multi-hop scenario yields high-order tensor signals that satisfy a HONTD model, which is exploited to derive semi-blind receiver algorithms for symbols and channels joint estimation. The performance of the system is improved with this system due to the smaller path-loss and the

multiple coding provided by the new TSTC at each transmit node. Although the system proposed in this chapter exploits cooperative communications, it does not exploit the cooperative diversity.

Chapter 5 introduces a new two-hop MIMO multi-relay system with TSTC at the source and the relays. Unlike the system presented in Chapter 4, the multi-relay system proposed here takes into account a parallel cooperation scheme, which provide an exploitation of the cooperative diversity. The multiple relays use orthogonal channels (parallel relaying) to increase the diversity order, assuming that all the relays can communicate directly with the destination, resulting in a combination of independent versions of the same information sent from the source and forwarded by the relays. This system can be viewed as a generalization of recently proposed systems [24, 30, 34, 35], aiming to exploit the cooperative diversity provided by the multiple relays in a MIMO system with TSTC. Indeed, the presented system extends previous works in different ways, either by proposing a more general tensor decomposition, by using a more general relay coding, by extending these works to the multi-relay case and/or by using a different estimation algorithm. The signals at destination are described as a fifth-order tensor that satisfies a CNTD model. The coupling of this decomposition is given in the sense that coded symbols sent by the source are common to all the relays, playing a role of coupling factor of multiple NTDs. The use of the CNTD model in this chapter is the first application of coupled tensor models in the context of wireless communications. CNTD-based system is exploited to derive a closed-form semi-blind receiver that jointly estimates the symbols and individual channels. Performance gains on the parameter estimation show the effectiveness of globally process coupled data.

In Chapter 6, a new two-hop OFDM MIMO relay system with TSTC at the source and the relay is presented. This system is another application of the CNTD model. In this case, the transmitter sends a data tensor using a TSTC with multiplexing of the symbols across space (antennas), time (blocks) and frequency (subcarriers) domains and the relay forwards the received data tensor to the destination by using a new TSTC. The subcarriers used by the source are assumed neighbors in such a way that the channel coefficients are invariant across the subcarriers. The signals received at the destination form a fifth-order tensor that satisfies a CNTD, which have a different structure when compared to the one exploited in Chapter 5. Indeed, in the tensor model exploited in this chapter, the channel matrices perform the coupling factor, being common to all the subcarriers. The tensor modeling is exploited to derive a closed-form semi-blind receiver for jointly estimating the symbols and channels. Simulation results corroborate the advantages of exploiting approaches based on coupled tensor decompositions.

In Chapter 7, a raising of the main conclusions on the contributions of this work is made. Some advantages and limitations of the addressed methods and systems are highlighted. Finally, in Chapter 8, some perspectives for future researches are drawn.

### *Main original contributions*

Briefly, the main contributions of this thesis can be summarized as follows:

#### Chapter 3

- Presentation of the new tensor model called HONTD, which generalizes the existing NTD proposed in [34] to higher order tensors, by considering successive Tucker models in a train format;
- Presentation of the new tensor model called CNTD, which generalizes the existing NTD proposed in [34] to higher order tensors and extends the coupling concept, introduced for PARAFAC models, to Tucker-based decompositions, by considering the coupling of multiple NTDs that share a common factor;
- Demonstration of the uniqueness of new tensor models under certain conditions, filling a lack in the literature on the uniqueness of NTD models.

#### Chapter 4

- Presentation of a new multi-hop MIMO relaying system with TSTC at all the nodes, generalizing recently proposed systems [18, 24, 34, 42]. It is shown that the signals at destination satisfy a HONTD model;
- Exploitation of proposed HONTD to develop semi-blind receivers, based on iterative and non-iterative (closed-form) methods, for jointly estimating the symbol matrix and the individual channels;
- Discussion on identifiability conditions of the proposed algorithms;
- Presentation of extensive Monte Carlo simulation results for illustrating the effectiveness of the proposed systems and evaluating the receiver performance.

#### Chapter 5

- Presentation of a new two-hop MIMO multi-relay system with TSTC at the source and the relays, generalizing systems proposed in previous works. It is shown that the signals at destination satisfy a fifth-order CNTD model;

- Exploitation of proposed CNTD to develop a semi-blind receiver, based on closed-form solution, for jointly estimating the symbol matrix and the individual channels;
- Discussion on identifiability conditions of the proposed algorithms;
- Presentation of extensive Monte Carlo simulation results for illustrating the effectiveness of the proposed systems and evaluating the receiver performance.

## Chapter 6

- Presentation of a new two-hop OFDM MIMO relay system with TSTC at the source and the relay with tensor data multiplexing symbols across the subcarriers, generalizing systems proposed in previous works. It is shown that the signals at destination satisfy a fifth-order CNTD model;
- Exploitation of proposed CNTD to develop a semi-blind receiver, based on closed-form solution, for jointly estimating the symbol matrix and the individual channels;
- Discussion on identifiability conditions of the proposed algorithms;
- Presentation of extensive Monte Carlo simulation results for illustrating the effectiveness of the proposed systems and evaluating the receiver performance.

## *Scientific production*

The studies addressed in this thesis yielded five full papers (two for international conferences and three for international journals), which the results are presented along this manuscript. Below, one can find the references of the related papers.

## Conference papers

ROCHA, D.S.; FAVIER, G.; FERNANDES, C.A.R. Tensor coding for three-hop MIMO relay systems. In: **IEEE Symposium on Computers and Communication (ISCC2018)**, Natal, Brazil, June 2018.

ROCHA, D.S.; FERNANDES, C.A.R.; FAVIER, G. Space-Time-Frequency (STF) MIMO Relaying System with Receiver Based on Coupled Tensor Decompositions. In: **Asilomar Conference on Signals, Systems, and Computers**, Pacific Grove, USA, October 2018.

Journal papers

ROCHA, D.S.; FAVIER, G.; FERNANDES, C.A.R. Closed-Form Receiver for Multi-Hop MIMO Relay Systems with Tensor Space-Time Coding. Accepted to publication in **Journal of Communication and Information Systems (JCIS)**, December 2018.

ROCHA, D.S.; FERNANDES, C.A.R.; FAVIER, G. MIMO multi-relay systems with tensor space-time coding based on coupled nested Tucker decomposition. Accepted to publication in **Digital Signal Processing – Elsevier**, March 2019.

ROCHA, D.S.; FERNANDES, C.A.R.; FAVIER, G. Doubly coupled nested Tucker decomposition (D-CNTD) for cooperative OFDM-MIMO systems with multiple relays. Under construction, 2019.

## 2 TENSOR REQUISITES

The theory of tensors is a branch of linear algebra called multilinear algebra. A tensor can be interpreted in many ways depending on its application. For the interests of this thesis, in a simple way, tensors are multimodal arrays with order higher than two. System modeling based on tensor approaches plays an increasing role in many areas such as chemometrics, psychometrics, numerical analysis, telecommunications and signal and image processing [6, 34, 45, 46, 49, 70]. In particular, tensor models have been extensively used for designing different types of signal processing techniques for wireless communication systems during the last decades.

In this chapter, we introduce the mathematical background necessary for the development of this work. In Section 2.1, we define the notations, the main concepts of multilinear algebra and some basic operations involving matrices and tensors, which are used throughout this thesis. In Section 2.2, we recall the main tensor decompositions exploited in the literature. In Section 2.3, we bring up an overview of tensor decompositions applied to communication systems.

### 2.1 Notations, definitions and basic matrix and tensor operations

Scalars, column vectors, matrices and tensors of order higher than two are denoted by lowercase  $(a, b, \dots)$ , boldface lower case  $(\mathbf{a}, \mathbf{b}, \dots)$ , boldface uppercase  $(\mathbf{A}, \mathbf{B}, \dots)$  and uppercase calligraphic  $(\mathcal{A}, \mathcal{B}, \dots)$  letters, respectively. Given a matrix  $\mathbf{A} \in \mathbb{C}^{I \times J}$ , the transpose, conjugate, Hermitian transpose, Moore-Penrose pseudo-inverse and rank are denoted respectively by  $\mathbf{A}^T$ ,  $\mathbf{A}^*$ ,  $\mathbf{A}^H$ ,  $\mathbf{A}^\dagger$  and  $r_{\mathbf{A}}$ . The  $i$ -th element of  $\mathbf{a}$  is denoted by  $[\mathbf{a}]_i$  or  $a_i$ , the  $(i, j)$ -th element of  $\mathbf{A}$  is denoted by  $[\mathbf{A}]_{i,j}$  or  $a_{i,j}$ , and the  $(i_1, \dots, i_N)$ -th element of the  $N$ -th order tensor  $\mathcal{A}$  is given by  $[\mathcal{A}]_{i_1, \dots, i_N}$  or  $a_{i_1, \dots, i_N}$ . Moreover, the  $i$ -th row and the  $j$ -th column of the matrix  $\mathbf{A}$  are respectively denoted by the vectors  $\mathbf{a}_{i \cdot}$  and  $\mathbf{a}_{\cdot j}$ .

The vector  $\mathbf{e}_n^{(N)} \in \mathbb{R}^N$  represents the  $n$ -th vector of the canonical base of the Euclidean space  $\mathbb{R}^N$  (i.e., vector containing an element equal to 1 in its  $n$ -th position and zeros elsewhere). The operator  $\text{vec}(\cdot)$  transforms a matrix into a column vector by stacking the columns of its matrix argument. The operator  $\text{diag}(\mathbf{a})$  forms a diagonal matrix from its vector argument while  $\text{diag}_n(\mathbf{A})$  forms a diagonal matrix from the  $n$ -th row of the matrix  $\mathbf{A}$ . Similarly, the operator  $\text{bdiag}(\mathbf{A}_k) \triangleq \text{bdiag}(\mathbf{A}_1, \dots, \mathbf{A}_K)$  forms a block-diagonal matrix composed of the  $K$  matrices  $\mathbf{A}_k$ , with  $k = 1, \dots, K$ . In the sequel, we present some matrix operations widely used

in the context of tensor algebra.

**Definition 1.** (Kronecker product) *The Kronecker product of two matrices  $\mathbf{A} \in \mathbb{C}^{I \times J}$  and  $\mathbf{B} \in \mathbb{C}^{M \times N}$  is defined as*

$$\mathbf{A} \otimes \mathbf{B} = \begin{bmatrix} a_{1,1}\mathbf{B} & a_{1,2}\mathbf{B} & \cdots & a_{1,J}\mathbf{B} \\ a_{2,1}\mathbf{B} & a_{2,2}\mathbf{B} & \cdots & a_{2,J}\mathbf{B} \\ \vdots & \vdots & \ddots & \vdots \\ a_{I,1}\mathbf{B} & a_{I,2}\mathbf{B} & \cdots & a_{I,J}\mathbf{B} \end{bmatrix} \in \mathbb{C}^{IM \times JN}. \quad (2.1)$$

Note that the matrix defined by  $\mathbf{A} \otimes \mathbf{B}$  has all possible combinations of products of the elements of  $\mathbf{A}$  and  $\mathbf{B}$ . Given a set  $\mathbb{S} = \{1, \dots, N\}$  and the matrices  $\mathbf{A}^{(n)} \in \mathbb{C}^{I_n \times J_n}$ , we represent a multiple Kronecker product as  $\bigotimes_{n \in \mathbb{S}} \mathbf{A}^{(n)} = \mathbf{A}^{(1)} \otimes \mathbf{A}^{(2)} \otimes \cdots \otimes \mathbf{A}^{(N)} \in \mathbb{C}^{I_1 \cdots I_N \times J_1 \cdots J_N}$ . A generalization of the Kronecker product for partitioned matrices was introduced by Tracy and Singh [71], and it is called block Kronecker product or  $\pi$ -product [72, 73]. Intuitively, a partitioned matrix can be viewed as a matrix that has a concatenation of vertical and/or horizontal sections called blocks or submatrices. If  $\mathbf{A}$  is a partitioned matrix with  $I$  vertical blocks and  $J$  horizontal blocks,  $I, J > 1$ , then we can write  $\mathbf{A} = [\mathbf{A}_{i,j}] \in \mathbb{C}^{IM \times JN}$ , with blocks  $\mathbf{A}_{i,j} \in \mathbb{C}^{M \times N}$ , for  $i = 1, \dots, I$  and  $j = 1, \dots, J$ . In particular, in this thesis, it will be useful the case where the matrices are equally partitioned. In this case, the block Kronecker product is said to be balanced [72].

**Definition 2.** (Balanced block Kronecker product) *Let  $\mathbf{A} = [\mathbf{A}_k] \in \mathbb{C}^{I \times KJ}$  and  $\mathbf{B} = [\mathbf{B}_k] \in \mathbb{C}^{M \times KN}$  be partitioned matrices composed of  $K$  horizontal blocks  $\mathbf{A}_k \in \mathbb{C}^{I \times J}$  and  $\mathbf{B}_k \in \mathbb{C}^{M \times N}$ , respectively. The balanced block Kronecker product is defined as*

$$\mathbf{A} \bowtie \mathbf{B} = \begin{bmatrix} \mathbf{A}_1 \otimes \mathbf{B}_1 & \mathbf{A}_2 \otimes \mathbf{B}_2 & \cdots & \mathbf{A}_K \otimes \mathbf{B}_K \end{bmatrix} \in \mathbb{C}^{IM \times KJN}. \quad (2.2)$$

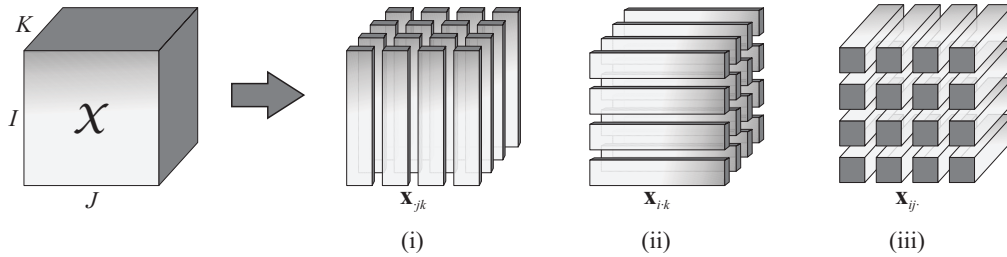
**Definition 3.** (Khatri-Rao product) *The Khatri-Rao product of two matrices  $\mathbf{A} \in \mathbb{C}^{I \times J}$  and  $\mathbf{C} \in \mathbb{B}^{M \times J}$  is equivalent to a column-wise Kronecker product and is defined as*

$$\mathbf{A} \diamond \mathbf{B} = \begin{bmatrix} \mathbf{A}_{\cdot 1} \otimes \mathbf{B}_{\cdot 1} & \mathbf{A}_{\cdot 2} \otimes \mathbf{B}_{\cdot 2} & \cdots & \mathbf{A}_{\cdot J} \otimes \mathbf{B}_{\cdot J} \end{bmatrix} \in \mathbb{C}^{IM \times J}. \quad (2.3)$$

The Khatri-Rao product of two matrices only exists if they have the same number of columns. Another way to compute the Khatri-Rao product is given by

$$\mathbf{A} \diamond \mathbf{B} = \begin{bmatrix} \mathbf{B} \text{diag}_1(\mathbf{A}) \\ \vdots \\ \mathbf{B} \text{diag}_I(\mathbf{A}) \end{bmatrix}. \quad (2.4)$$

Figure 4 – (i) Column fiber; (ii) row fiber; (iii) tube fiber



Let us define some useful matrix properties that involve the presented operations. For this, we consider the matrices  $\mathbf{A} \in \mathbb{C}^{I \times P}$ ,  $\mathbf{B} \in \mathbb{C}^{P \times M}$ ,  $\mathbf{C} \in \mathbb{C}^{J \times M}$ ,  $\mathbf{D} \in \mathbb{C}^{M \times N}$ .

**Property 1.**

$$\text{vec}(\mathbf{A}\mathbf{B}\mathbf{C}^T) = (\mathbf{C} \otimes \mathbf{A})\text{vec}(\mathbf{B}) \in \mathbb{C}^{JI}. \quad (2.5)$$

**Property 2.**

$$(\mathbf{A} \otimes \mathbf{C})(\mathbf{B} \otimes \mathbf{D}) = (\mathbf{A}\mathbf{B}) \otimes (\mathbf{C}\mathbf{D}) \in \mathbb{C}^{IJ \otimes MN}. \quad (2.6)$$

**Property 3.** Let  $\mathbf{A}$  be a full column rank matrix, then  $r_{\mathbf{A}\mathbf{B}} = r_{\mathbf{B}}$ . This implies that  $\mathbf{A}\mathbf{B}$  is full column rank if and only if  $\mathbf{A}$  and  $\mathbf{B}$  are full column rank.

**Property 4.** Given  $\mathbf{M} = \mathbf{A} \otimes \mathbf{C}$ , then  $r_{\mathbf{M}} = r_{\mathbf{A}}r_{\mathbf{C}}$ . This implies that  $\mathbf{M}$  is full column rank if and only if  $\mathbf{A}$  and  $\mathbf{C}$  are full column rank.

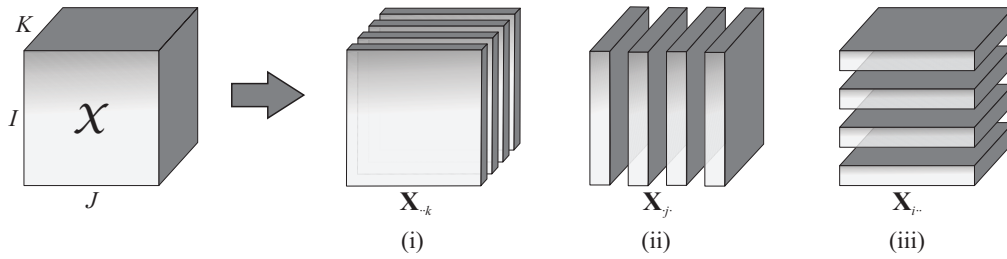
For demonstrations and discussions on these properties, see [45, 73]. For the next definitions presented in this section, unless otherwise stated, we consider the following tensors:

- a  $N$ -th order tensor  $\mathcal{A} \in \mathbb{C}^{I_1 \times \dots \times I_N}$ ;
- a  $M$ -th order tensor  $\mathcal{B} \in \mathbb{C}^{J_1 \times \dots \times J_M}$ ;
- a third-order tensor  $\mathcal{X} \in \mathbb{C}^{I \times J \times K}$ .

**Definition 4.** (Fiber) *Fibers are vectors obtained by fixing the indices of all modes of a tensor, except for one. For example, the third-order tensor  $\mathcal{X}$  has three kinds of fibers: (i) column fibers ( $\mathbf{x}_{.jk} \in \mathbb{C}^I$ ) obtained by fixing the indices  $j$  and  $k$ ; (ii) row fibers ( $\mathbf{x}_{i.k} \in \mathbb{C}^J$ ) obtained by fixing the indices  $i$  and  $k$ ; (iii) tube fibers ( $\mathbf{x}_{ij.} \in \mathbb{C}^K$ ) obtained by fixing the indices  $i$  and  $j$ . Figure 4 illustrates the fibers for this case.*

**Definition 5.** (Matrix slice) *Matrix slices are matrices obtained by varying the indices of two modes and fixing all the others. For a  $N$ -th order tensor, there are  $\binom{N}{2}$  ways to slice it, where*

Figure 5 – (i) Frontal slice; (ii) vertical slice; (iii) horizontal slice



$\binom{N}{2}$  denotes the binomial coefficient, i.e., the number of possibilities to choose 2 elements from a set of  $N$  elements. For the third-order tensor  $\mathcal{X}$ , the three kinds of slices are: (i) frontal slices ( $\mathbf{X}_{..k} \in \mathbb{C}^{I \times J}$ ); (ii) vertical slices ( $\mathbf{X}_{.j} \in \mathbb{C}^{I \times K}$ ); (iii) horizontal slices ( $\mathbf{X}_{i..} \in \mathbb{C}^{J \times K}$ ). Figure 5 illustrates the three kinds of slices of a third-order tensor.

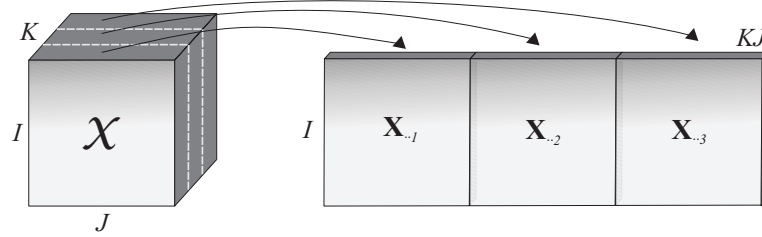
Commonly, slices are defined as matrices obtained by varying two indices of the tensor, as above defined. In this thesis, we propose a generalization of this concept for tensor slices, which are obtained by varying  $N_1$  indices of a  $N$ -th order tensor, with  $3 \leq N_1 \leq N$ , while the others  $N - N_1$  indices remain fixed, resulting in a  $N_1$ -th order tensor slice. Note that if we assume  $N_1 = 1$ , we get fibers, and if we assume  $N_1 = 2$ , we get matrix slices. By fixing the index  $i_n$  of  $\mathcal{A}$ , for instance, we define a  $(N - 1)$ -th order tensor, which will be denoted by  $[\mathcal{A}]_{(i_n)}$  or  $\mathcal{A}_{(i_n)} \in \mathbb{C}^{I_1 \times \dots \times I_{n-1} \times I_{n+1} \times \dots \times I_N}$ .

**Definition 6.** (Unfolded matrix) *Matrix unfolding is a matrix representation (or matricization) of a high-order tensor. The tall (or flat) mode- $n$  unfolding of  $\mathcal{A}$  is obtained by mappings its elements into a matrix  $\mathbf{A}_{P_1 \dots P_{N-1} \times P_N}$  (or  $\mathbf{A}_{P_N \times P_1 \dots P_{N-1}}$ ), where  $\{P_1, \dots, P_N\}$  is any permutation of  $\{I_1, \dots, I_N\}$ , whose the entries are  $a_{p_1, \dots, p_N} = [\mathbf{A}_{P_1 \dots P_{N-1} \times P_N}]_{\bar{p}, p_N}$ , with*

$$\bar{p} = (p_1 - 1)P_2 \cdots P_{N-1} + (p_2 - 1)P_3 \cdots P_{N-1} + \cdots + (p_{N-2} - 1)P_{N-1} + p_{N-1}. \quad (2.7)$$

From Definition 6, we can see a mode- $n$  unfolding as a rearrangement of the elements of  $\mathcal{A}$  obtained by varying a index  $i_n$  and keeping the other indices fixed, in such a way that the fibers of the  $n$ -th mode are placed along the rows (tall unfolding) or columns (flat unfolding). For example, let us consider the third-order tensor  $\mathcal{X}$ . There are two flat mode-1 unfoldings,  $\mathbf{X}_{I \times KJ}$  and  $\mathbf{X}_{I \times JK}$ , which consist of column fibers placed side by side, according to the order of combination of the modes. The order of appearance of the modes forms different unfoldings and may vary from one definition to another. Here, we consider that the indices that vary faster are the ones appearing in the right, i.e.,  $[\mathbf{X}_{I \times KJ}]_{i, (k-1)J+j} = [\mathcal{X}]_{i,j,k}$  and  $[\mathbf{X}_{I \times JK}]_{i, (j-1)K+k} = [\mathcal{X}]_{i,j,k}$ .

Figure 6 – Matrix representation for third-order tensor



Equivalently, an unfolded matrix can be obtained by stacking the slices of a given mode, as shown in Figure 6. Note that, in our notation, the subscript characters in the unfolded matrix explicit the order in which the modes are combined and, consequently, the size of the unfolded matrix.

Unlike the mode- $n$  unfolding, which combines all modes of a tensor in rows (or columns) excepting for the  $n$ -th mode, it is possible to define a generalized unfolding where multiple modes are combined in rows and columns of the resulting unfolded matrix. For this generalized unfolding, let us define the set  $\mathbb{S} = \{1, \dots, N\}$  and the representations  $I_{\mathbb{S}}$ ,  $\bar{I}_{\mathbb{S}}$  and  $i_{\mathbb{S}}$ , which denote, respectively, short forms for the dimension, product of the dimensions and the set of indices associated to the modes of the set  $\mathbb{S}$ . For instance, for  $N = 3$ , we have  $I_{\mathbb{S}} = I_1 \times I_2 \times I_3$ ,  $\bar{I}_{\mathbb{S}} = I_1 I_2 I_3$  and  $i_{\mathbb{S}} = \{i_1, i_2, i_3\}$ . Thus, defining  $\mathbb{S}_1$  and  $\mathbb{S}_2$  as ordered subsets of the set  $\mathbb{S}$ , such that  $\mathbb{S}_1 \cup \mathbb{S}_2 = \mathbb{S}$ , we can make the matricization of  $\mathcal{A} \in \mathbb{C}^{I_{\mathbb{S}}}$  as

$$\mathbf{A}_{\bar{I}_{\mathbb{S}_1} \times \bar{I}_{\mathbb{S}_2}} = \sum_{i_1=1}^{I_1} \cdots \sum_{i_N=1}^{I_N} a_{i_1, \dots, i_N} \left( \bigotimes_{n \in \mathbb{S}_1} \mathbf{e}_{i_n}^{(I_n)} \right) \left( \bigotimes_{n \in \mathbb{S}_2} \mathbf{e}_{i_n}^{(I_n)} \right)^T, \quad (2.8)$$

with  $\bar{I}_{\mathbb{S}_1}$  and  $\bar{I}_{\mathbb{S}_2}$  being any ordered combination of the dimensions of the tensor  $\mathcal{A}$ .

**Definition 7.** (Inner product) *Let us consider a tensor  $\mathcal{T} \in \mathbb{C}^{I_1 \times \dots \times I_N}$  of same order of  $\mathcal{A}$ . The inner product between  $\mathcal{A}$  and  $\mathcal{T}$  is defined as*

$$\langle \mathcal{A}, \mathcal{T} \rangle = \sum_{i_1=1}^{I_1} \cdots \sum_{i_N=1}^{I_N} a_{i_1, \dots, i_N} t_{i_1, \dots, i_N}^*. \quad (2.9)$$

**Definition 8.** (Outer product) *The outer product between the  $N$ -th order tensor  $\mathcal{A}$  and the  $M$ -th order tensor  $\mathcal{B}$  yields a new tensor, whose the entries are defined as*

$$[\mathcal{A} \circ \mathcal{B}]_{i_1, \dots, i_N, j_1, \dots, j_M} = a_{i_1, \dots, i_N} b_{j_1, \dots, j_M}. \quad (2.10)$$

Equation (2.10) defines a  $(N + M)$ -th order tensor with dimension  $I_1 \times \dots \times I_N \times J_1 \times \dots \times J_M$  and can be interpreted as a generalization of the concept of outer product of two vectors.

**Definition 9.** (Rank-one tensor) *The tensor  $\mathcal{A}$  is said to be a rank-one tensor if it can be written as the outer product of  $N$  vectors  $\mathbf{u}^{(n)} \in \mathbb{C}^{I_n}$ , with  $n \in [1, N]$ , as follows*

$$\mathcal{A} = \mathbf{u}^{(1)} \circ \dots \circ \mathbf{u}^{(N)}, \quad (2.11)$$

whose the entries are  $a_{i_1, \dots, i_N} = u_{i_1}^{(1)} \dots u_{i_N}^{(N)}$ .

Note that this definition is a generalization of the concept of rank-one matrix, where a matrix  $\mathbf{A} \in \mathbb{C}^{I_1 \times I_2}$  has rank equal to one if there are two vectors  $\mathbf{u}^{(1)} \in \mathbb{C}^{I_1}$  and  $\mathbf{u}^{(2)} \in \mathbb{C}^{I_2}$  such that  $\mathbf{A} = \mathbf{u}^{(1)} \circ \mathbf{u}^{(2)} = \mathbf{u}^{(1)} \mathbf{u}^{(2)T}$ . As will be discussed later, some tensor decompositions express the tensor as linear combinations of rank-one tensors.

**Definition 10.** (Tensor rank) *The rank of a tensor is the smallest number of rank-one tensors needed to write this tensor in a linear combination.*

The above definition implies that any arbitrary tensor of rank  $R \geq 1$  can be written as a sum of  $R$  rank-one tensors, i.e., if  $\mathcal{A}$  has rank  $R$ , we can write

$$\mathcal{A} = \sum_{r=1}^R \mathbf{u}_r^{(1)} \circ \dots \circ \mathbf{u}_r^{(N)}. \quad (2.12)$$

Hitchcock [74] was the first to introduce the idea of writing a tensor as a sum of rank-one tensors.

**Definition 11.** (Kruskal rank) *The Kruskal-rank, or simply  $k$ -rank, of a matrix  $\mathbf{A} \in \mathbb{C}^{M \times N}$  is the maximum number  $k_{\mathbf{A}}$  such that any set of  $k_{\mathbf{A}}$  columns of  $\mathbf{A}$  is linearly independent. Note that the  $k$ -rank is always less than or equal to the rank of a matrix:  $k_{\mathbf{A}} \leq r_{\mathbf{A}} \leq \min(M, N)$ .*

**Definition 12.** (Identity tensor) *A identity tensor of order  $N$ , denoted by  $\mathcal{I}_R^{(N)} \in \mathbb{C}^{R \times R \times \dots \times R}$ , is a superdiagonal tensor containing elements equal to 1 in the positions where all indices are the same, and equal to zero elsewhere.*

**Definition 13.** (Frobenius norm) *Frobenius norm of the tensor  $\mathcal{A}$  is defined by*

$$\|\mathcal{A}\|_F = \sqrt{\langle \mathcal{A}, \mathcal{A} \rangle} = \left( \sum_{i_1=1}^{I_1} \dots \sum_{i_N=1}^{I_N} |a_{i_1, \dots, i_N}|^2 \right)^{1/2}. \quad (2.13)$$

Frobenius norm can be viewed as a measure of the square root of the energy of a tensor and it is useful to compute the angle between two tensors. For the tensors  $\mathcal{A}$  and  $\mathcal{T}$ , the angle can be obtained as

$$\theta = \arccos \frac{\langle \mathcal{A}, \mathcal{T} \rangle}{\|\mathcal{A}\|_F \|\mathcal{T}\|_F}. \quad (2.14)$$

**Definition 14.** (Tensor-matrix mode- $n$  product) *Let us consider a matrix  $\mathbf{U} \in \mathbb{C}^{R_n \times I_n}$ , whose number of columns is equal to the dimension of the  $n$ -th mode of  $\mathcal{A}$ . The mode- $n$  product between the tensor  $\mathcal{A}$  and the matrix  $\mathbf{U}$  yields a  $N$ -th order tensor  $\mathcal{C} = \mathcal{A} \times_n \mathbf{U} \in \mathbb{C}^{I_1 \times \dots \times I_{n-1} \times R_n \times I_{n+1} \times \dots \times I_N}$  defined as*

$$c_{i_1, \dots, i_{n-1}, r_n, i_{n+1}, \dots, i_N} = \sum_{i_n=1}^{I_n} a_{i_1, \dots, i_{n-1}, i_n, i_{n+1}, \dots, i_N} u_{r_n, i_n}. \quad (2.15)$$

**Definition 15.** (Tensor-tensor mode- $n$  product) *Given a set  $\mathbb{S} = \{1, \dots, N\}$ , let  $\mathbb{S}_t$  be an ordered subset of  $\mathbb{S} - \{n\}$ , with  $1 \leq n \leq N$ . Let us consider a  $N_t$ -th order tensor  $\mathcal{T} \in \mathbb{C}^{R_n \times I_n \times I_{\mathbb{S}_t}}$ , with  $3 \leq N_t \leq N + 1$ . The mode- $n$  product between the tensors  $\mathcal{A}$  and  $\mathcal{T}$ , denoted by  $\mathcal{A} \times_n \mathcal{T}$ , gives a tensor  $\mathcal{C} \in \mathbb{C}^{I_1 \times \dots \times I_{n-1} \times R_n \times I_{n+1} \times \dots \times I_N}$  defined as*

$$c_{i_1, \dots, i_{n-1}, r_n, i_{n+1}, \dots, i_N} = \sum_{i_n=1}^{I_n} a_{i_1, \dots, i_{n-1}, i_n, i_{n+1}, \dots, i_N} t_{r_n, i_n, i_{\mathbb{S}_t}}. \quad (2.16)$$

Note that, by convention, in Definitions 14 and 15, we assume that the second mode of  $\mathbf{U}$  (or  $\mathcal{T}$ ) is equal to the  $n$ -th mode of  $\mathcal{A}$ . In both cases, the mode- $n$  product does not change the size of the resulting tensor, but provides a linear transformation on the  $n$ -th mode of  $\mathcal{A}$ .

**Property 5.** *Considering the tensors  $\mathcal{A}, \mathcal{T}^{(1)} \in \mathbb{C}^{R_n, I_n, I_{\mathbb{S}_1}}$  and  $\mathcal{T}^{(2)} \in \mathbb{C}^{P_n, R_n, I_{\mathbb{S}_2}}$  of orders  $N, N_1$  and  $N_2$ , respectively, let us define  $\mathbb{S}_1$  and  $\mathbb{S}_2$  as two ordered subsets of  $\mathbb{S} - \{n\}$ , with  $N_1 - 2$  and  $N_2 - 2$  elements, respectively, such that  $\mathbb{S}_1 \subseteq \mathbb{S}_2$ . We have*

$$(\mathcal{A} \times_n \mathcal{T}^{(1)}) \times_n \mathcal{T}^{(2)} = \mathcal{A} \times_n (\mathcal{T}^{(1)} \times_n \mathcal{T}^{(2)}) \in \mathbb{C}^{I_1 \times \dots \times I_{n-1} \times P_n \times I_{n+1} \times \dots \times I_N}. \quad (2.17)$$

*Proof.*

$$\begin{aligned} (\mathcal{A} \times_n \mathcal{T}^{(1)}) \times_n \mathcal{T}^{(2)} &= \sum_{r_n=1}^{R_n} \sum_{i_n=1}^{I_n} a_{i_1, \dots, i_{n-1}, i_n, i_{n+1}, \dots, i_N} t_{r_n, i_n, i_{\mathbb{S}_1}}^{(1)} t_{p_n, r_n, i_{\mathbb{S}_2}}^{(2)} \\ &= \sum_{i_n=1}^{I_n} a_{i_1, \dots, i_{n-1}, i_n, i_{n+1}, \dots, i_N} \left( \sum_{r_n=1}^{R_n} t_{r_n, i_n, i_{\mathbb{S}_1}}^{(1)} t_{p_n, r_n, i_{\mathbb{S}_2}}^{(2)} \right) \\ &= \mathcal{A} \times_n (\mathcal{T}^{(1)} \times_n \mathcal{T}^{(2)}), \end{aligned} \quad (2.18)$$

which is the desired result.  $\square$

**Definition 16.** (Contraction operation) *Let us consider the tensors  $\mathcal{A}$  and  $\mathcal{B}$  sharing a common dimension ( $I_p = J_q = K$ , with  $1 \leq p \leq N$  and  $1 \leq q \leq M$ ). The contraction of  $\mathcal{A}$  with  $\mathcal{B}$ , denoted by  $\mathcal{A} *_{p,q}^{\mathcal{B}}$ , is defined as the following sum over the common mode ( $i_p = j_q = k$ ) [75]*

$$c_{i_1, \dots, i_{p-1}, j_1, \dots, j_{q-1}, j_{q+1}, \dots, j_M, i_{p+1}, \dots, i_N} = \sum_{k=1}^K a_{i_1, \dots, i_{p-1}, k, i_{p+1}, \dots, i_N} b_{j_1, \dots, j_{q-1}, k, j_{q+1}, \dots, j_M}, \quad (2.19)$$

which results in a  $(N+M-2)$ -th order tensor  $\mathcal{C} \in \mathbb{C}^{I_1 \times \dots \times I_{p-1} \times J_1 \times \dots \times J_{q-1} \times J_{q+1} \times \dots \times J_M \times I_{p+1} \times \dots \times I_N}$ .

Note that the contraction operation, unlike mode- $n$  product, accumulates all the modes of both involved tensors, except for the common mode. However, it can be rewritten as the following tensor-matrix mode- $k$  products by combining some modes of  $\mathcal{A}$  or  $\mathcal{B}$

$$\mathcal{C}_{I_1 \times \dots \times I_{p-1} \times J_1 \dots J_{q-1} J_{q+1} \dots J_M \times I_{p+1} \times \dots \times I_N} = \mathcal{A} \times_k \mathbf{B}_{J_1 \dots J_{q-1} J_{q+1} \dots J_M \times K}, \quad (2.20)$$

$$\mathcal{C}_{J_1 \times \dots \times J_{q-1} \times I_1 \dots I_{p-1} I_{p+1} \dots I_N \times J_{q+1} \times \dots \times J_M} = \mathcal{B} \times_k \mathbf{A}_{I_1 \dots I_{p-1} I_{p+1} \dots I_N \times K}, \quad (2.21)$$

where  $\mathbf{B}_{J_1 \dots J_{q-1} J_{q+1} \dots J_M \times K}$  and  $\mathbf{A}_{I_1 \dots I_{p-1} I_{p+1} \dots I_N \times K}$  are tall unfoldings of  $\mathcal{B}$  and  $\mathcal{A}$ , respectively, and  $\mathcal{C}_{I_1 \times \dots \times I_{p-1} \times J_1 \dots J_{q-1} J_{q+1} \dots J_M \times I_{p+1} \times \dots \times I_N}$  and  $\mathcal{C}_{J_1 \times \dots \times J_{q-1} \times I_1 \dots I_{p-1} I_{p+1} \dots I_N \times J_{q+1} \times \dots \times J_M}$  are contracted forms of the tensor  $\mathcal{C}$ , whose the sizes are explicit in the subscript characters.

**Definition 17.** (Concatenation operation) *Let us consider the  $N$ -th order tensors  $\mathcal{A}^{(r)} \in \mathbb{C}^{I_1 \times \dots \times I_N}$ , with  $r = 1, \dots, R$ . The concatenation of the  $R$  tensors  $\mathcal{A}^{(r)}$  along the  $(N+1)$ -th mode yields the  $(N+1)$ -th order tensor  $\mathcal{G} \in \mathbb{C}^{I_1 \times \dots \times I_N \times R}$  as follows*

$$\mathcal{G} = \mathcal{A}^{(1)} \sqcup_{N+1} \mathcal{A}^{(2)} \dots \sqcup_{N+1} \mathcal{A}^{(R)} \iff g_{i_1, \dots, i_N, r} = a_{i_1, \dots, i_N}^{(r)}. \quad (2.22)$$

The matrix representation presented in Definition 6 can be viewed as a concatenation operation. The stacking of the slices represented in Figure 6 is obtained by concatenating the frontal slices of the tensor  $\mathcal{X}$  ( $\mathbf{X}_{..k}$ ) along the second mode as follows

$$\mathbf{X}_{I \times K \times J} = \mathbf{X}_{..1} \sqcup_2 \mathbf{X}_{..2} \dots \sqcup_2 \mathbf{X}_{..K} \iff [\mathbf{X}_{I \times K \times J}]_{i, (k-1)J+j} = x_{i,j,k}. \quad (2.23)$$

## 2.2 Background on tensor decompositions

In this section, we present the most important decompositions of high-order tensors. Tensor decomposition, also referred as multi-way factor analysis, is a tool that allows recovering information of multivariate datasets by decomposing tensors into elementary factors. The analysis of a tensor in terms of its decomposed factors is useful in problems where a given parameter is subject to different influences that must be separately identified. In several signal processing problems, tensor decomposition applications are related to the separation of signals transmitted by different sources.

In some cases, tensor decompositions can be viewed as generalizations of PCA or SVD to orders higher than two. For example, a third-order Tucker decomposition can also

be viewed as a generalization of the higher-order singular value decomposition (HOSVD) [45, 70], since it replaces the singular vectors by matrix factors. The main motivation for using tensor-based approaches is related to their natural capability to model multimodal data, with useful uniqueness properties under more relaxed conditions, in contrast to conventional matrix approaches, such as SVD, where the pair of singular matrices is unique due to the imposition of orthogonality. When convenient, we recall the uniqueness properties and conditions for the presented tensor models. Demonstrations of the theorems of uniqueness are given in the Appendix A.

Tucker [60] and PARAFAC [61] models, as well as their derivations, are the most commonly used tensor decompositions in signal processing for wireless communications. PARAFAC models have the important property of being essentially unique, which is not the case of the Tucker models, except under certain conditions, like the a priori knowledge of the core tensor. Essential uniqueness means that the decompositions are unique up to arbitrary scaling and permutation of columns of the factor matrices. However, Tucker models are one of the most important and flexible tensor decompositions [57]. From these main models, several tensor decompositions are derived for specific cases. A combination of the structures of the PARAFAC and Tucker decompositions was proposed in [76], yielding a model named PARATUCK, which considers an iteration between its matrix factors. Other derivations as nested PARAFAC [41], generalized PARATUCK [40] and nested Tucker [34] decompositions were proposed with application in signal processing problems.

### 2.2.1 Tucker decomposition

The Tucker decomposition was introduced by L. Tucker in 1966 [60]. This model consists on the decomposition of a tensor into a core tensor of the same order that interacts with factor matrices. For a  $N$ -th order tensor  $\mathcal{X} \in \mathbb{C}^{I_1 \times \dots \times I_N}$ , the Tucker decomposition is defined as

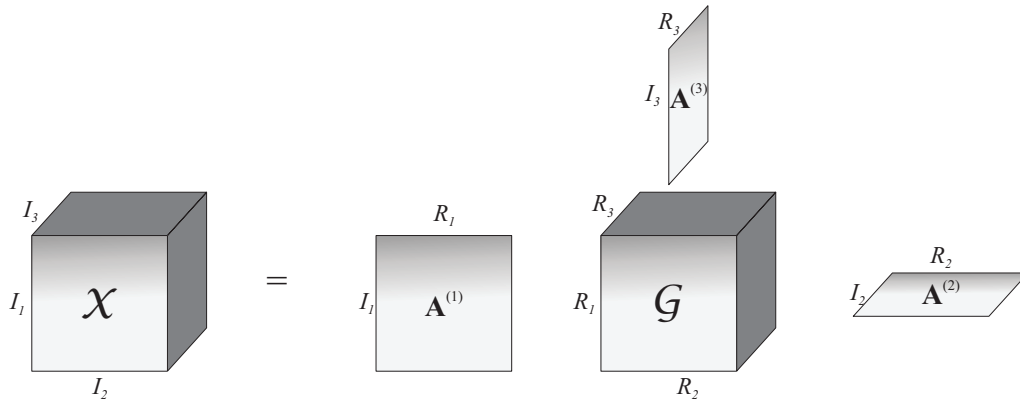
$$\mathcal{X} = \mathcal{G} \times_1 \mathbf{A}^{(1)} \times_2 \mathbf{A}^{(2)} \dots \times_N \mathbf{A}^{(N)}, \quad (2.24)$$

where  $\mathcal{G} \in \mathbb{C}^{R_1 \times \dots \times R_N}$  is the core tensor and  $\mathbf{A}^{(n)} \in \mathbb{C}^{I_n \times R_n}$ , with  $n = 1, \dots, N$ , are the factor matrices. It can be written in scalar form as

$$x_{i_1, \dots, i_N} = \sum_{r_1=1}^{R_1} \dots \sum_{r_N=1}^{R_N} g_{r_1, \dots, r_N} \prod_{n=1}^N a_{i_n, r_n}^{(n)}. \quad (2.25)$$

The Tucker decomposition defined in (2.24) has the following matrix representation,

Figure 7 – Block-diagram of a Tucker decomposition for a third-order tensor



which corresponds to a generic formulation for a tall mode- $n$  unfolding

$$\mathbf{X}_{I_{n+1} \cdots I_N I_1 \cdots I_{n-1} \times I_n} = (\mathbf{A}^{(n+1)} \otimes \cdots \otimes \mathbf{A}^{(N)} \otimes \mathbf{A}^{(1)} \otimes \cdots \otimes \mathbf{A}^{(n-1)}) \mathbf{G}_n \mathbf{A}^{(n)T}, \quad (2.26)$$

where  $\mathbf{G}_n \in \mathbb{C}^{R_{n+1} \cdots R_N R_1 \cdots R_{n-1} \times R_n}$  is the corresponding tall mode- $n$  unfolding of  $\mathcal{G}$ . A corresponding generic flat mode- $n$  unfolding is obtained by transposing (2.26). Commonly, the mode- $n$  unfolding  $\mathbf{X}_{I_{n+1} \cdots I_N I_1 \cdots I_{n-1} \times I_n}$  is denoted simply by  $\mathbf{X}_n$ .

Special cases of the Tucker model consider the decomposition of a  $N$ -th order tensor that has  $N_1$  factor matrices, with  $N > N_1$ . That is,  $N - N_1$  decomposition factors are equal to identity matrices. Considering  $\mathbf{A}^{(n)} = \mathbf{I}_{I_n}$  for  $n = N_1 + 1, \dots, N$ , which implies  $R_n = I_n$ , the Tucker- $(N_1, N)$  model [77] corresponds to

$$\mathcal{X} = \mathcal{G} \times_1 \mathbf{A}^{(1)} \times_2 \mathbf{A}^{(2)} \cdots \times_{N_1} \mathbf{A}^{(N_1)} \times_{N_1+1} \mathbf{I}_{I_{N_1+1}} \cdots \times_N \mathbf{I}_{I_N}, \quad (2.27)$$

or simply

$$\mathcal{X} = \mathcal{G} \times_1 \mathbf{A}^{(1)} \times_2 \mathbf{A}^{(2)} \cdots \times_{N_1} \mathbf{A}^{(N_1)} = \mathcal{G} \times_{n=1}^{N_1} \mathbf{A}^{(n)}, \quad (2.28)$$

with  $\mathcal{G} \in \mathbb{C}^{R_1 \times \cdots \times R_{N_1} \times I_{N_1+1} \times \cdots \times I_N}$ . For the case  $\mathcal{X} \in \mathbb{C}^{I_1 \times I_2 \times I_3}$ , with the core tensor  $\mathcal{G} \in \mathbb{C}^{R_1 \times R_2 \times R_3}$  and the factors  $\mathbf{A}^{(1)} \in \mathbb{C}^{I_1 \times R_1}$ ,  $\mathbf{A}^{(2)} \in \mathbb{C}^{I_2 \times R_2}$  and  $\mathbf{A}^{(3)} \in \mathbb{C}^{I_3 \times R_3}$ , the third-order Tucker decomposition  $\mathcal{X} = \mathcal{G} \times_1 \mathbf{A}^{(1)} \times_2 \mathbf{A}^{(2)} \times_3 \mathbf{A}^{(3)}$  is illustrated in Figure 7. This model can also be represented in a compact form as  $(\mathcal{G}, \mathbf{A}^{(1)}, \mathbf{A}^{(2)}, \mathbf{A}^{(3)})$ .

Some authors use the nomenclature Tucker-3 to the third-order Tucker decomposition above represented. When one of the matrix factors of this decomposition is equal to the identity matrix, for example  $\mathbf{A}^{(1)} = \mathbf{I}$ , we say that we have a Tucker-2 given by  $\mathcal{X} = \mathcal{G} \times_2 \mathbf{A}^{(2)} \times_3 \mathbf{A}^{(3)}$ , which is equivalent to a Tucker-(2, 3) decomposition. Similarly, when two of the matrix factors are equal to identity matrices, for example  $\mathbf{A}^{(1)} = \mathbf{A}^{(2)} = \mathbf{I}$ , we define a Tucker-1, or Tucker-(1, 3) decomposition, and  $\mathcal{X}$  becomes  $\mathcal{X} = \mathcal{G} \times_3 \mathbf{A}^{(3)}$ .

### Uniqueness

The Tucker model is not essentially unique, since the factor matrices  $\mathbf{A}^{(n)}$  and the core tensor  $\mathcal{G}$  are not identifiable in a unique way, i.e., they can be replaced by  $\bar{\mathbf{A}}^{(n)} = \mathbf{A}^{(n)} \Delta_n$  with  $\Delta_n \in \mathbb{C}^{R_n \times R_n}$  nonsingular, and the core tensor  $\mathcal{G}$  replaced by  $\bar{\mathcal{G}} = \mathcal{G} \times_{n=1}^N (\Delta_n)^{-1}$ , without changing the tensor  $\mathcal{X}$ . Indeed, from (2.24), we have

$$\begin{aligned}
 \mathcal{X} &= \bar{\mathcal{G}} \times_{n=1}^N \bar{\mathbf{A}}^{(n)} \\
 &= \mathcal{G} \times_{n=1}^N (\Delta_n)^{-1} \times_{n=1}^N \mathbf{A}^{(n)} \Delta_n \\
 &= \mathcal{G} \times_{n=1}^N \mathbf{A}^{(n)} \Delta_n (\Delta_n)^{-1} \\
 &= \mathcal{G} \times_{n=1}^N \mathbf{A}^{(n)}.
 \end{aligned} \tag{2.29}$$

This result means that there are alternatives for the matrix factors and core tensor that satisfy the same decomposition model. However, if we consider the core tensor  $\mathcal{G}$  known, the following uniqueness theorem is valid for Tucker models.

**Theorem 1.** *Consider a  $N$ -order tensor  $\mathcal{X} \in \mathbb{C}^{I_1 \times \dots \times I_N}$  that satisfies a Tucker decomposition. When the core tensor  $\mathcal{G} \in \mathbb{C}^{R_1 \times \dots \times R_N}$  is known, the matrix factors  $\mathbf{A}^{(n)} \in \mathbb{C}^{I_n \times R_n}$ , for  $n = 1, \dots, N$ , are unique up to the scalar ambiguities  $\bar{\mathbf{A}}^{(n)} = \mathbf{A}^{(n)} \Delta_n$ , such that  $\Delta_n = \delta_n \mathbf{I}_{R_n}$ , with  $\prod_{n=1}^N \delta_n = 1$ .*

*Proof.* See Appendix A.

### 2.2.2 Generalized Tucker decomposition

The generalized Tucker decomposition corresponds to a Tucker decomposition where some (or all) matrix factors are replaced by tensors, i.e.,  $\mathbf{A}^{(n)}$  in (2.24) is replaced by  $\mathcal{A}^{(n)}$ , resulting in tensor-tensor mode- $n$  products. Similarly to the Tucker model, a special case of the generalized Tucker model was introduced in [40] for cases where some factors are equal to identity matrices. For a given  $N$ -th order tensor  $\mathcal{X} \in \mathbb{C}^{I_1 \times \dots \times I_N}$ , the generalized Tucker- $(N_1, N)$  model can be written as

$$\mathcal{X} = \mathcal{G} \times_1 \mathcal{A}^{(1)} \times_2 \mathcal{A}^{(2)} \dots \times_{N_1} \mathcal{A}^{(N_1)} = \mathcal{G} \times_{n=1}^{N_1} \mathcal{A}^{(n)}, \tag{2.30}$$

with core tensor  $\mathcal{G} \in \mathbb{C}^{R_1 \times \dots \times R_{N_1} \times I_{N_1+1} \times \dots \times I_N}$  and tensor factors  $\mathcal{A}^{(n)} \in \mathbb{C}^{I_n \times R_n \times I_{\mathbb{S}_n}}$ , where  $\mathbb{S}_n$  is an ordered subset of the set  $\mathbb{S} = \{N_1 + 1, \dots, N\}$ . The tensor factor  $\mathcal{A}^{(n)}$  is a  $N_n$ -th order tensor, with  $3 \leq N_n \leq N - N_1 + 2$ .

The matricization of a generalized Tucker model depends on the number of matrix and tensor factors, as well as on the set  $\mathbb{S}_n$ . Therefore, it is not possible to define a generic formulation to its unfolding, as defined in (2.26) for Tucker models. However, it is possible to define the unfolding matrices of some particular cases of generalized Tucker models. In the sequel, we take a generalized Tucker-(2, 4) model as example, which will be useful to the problems addressed in this thesis. Let us consider a fourth-order tensor  $\mathcal{X} \in \mathbb{C}^{I_1 \times I_2 \times I_3 \times I_4}$  and the tensor factors  $\mathcal{A}^{(1)} \in \mathbb{C}^{I_1 \times R_1 \times I_4}$  and  $\mathcal{A}^{(3)} \in \mathbb{C}^{I_3 \times R_3 \times I_4}$ . A possible generalized Tucker-(2, 4) decomposition of  $\mathcal{X}$  is given by  $\mathcal{X} = \mathcal{G} \times_1 \mathcal{A}^{(1)} \times_3 \mathcal{A}^{(3)}$ , where  $\mathcal{G} \in \mathbb{C}^{R_1 \times I_2 \times R_3 \times I_4}$  is the core tensor, and it can be written in a scalar form as

$$x_{i_1, i_2, i_3, i_4} = \sum_{r_1=1}^{R_1} \sum_{r_3=1}^{R_3} g_{r_1, i_2, r_3, i_4} a_{i_1, r_1, i_4}^{(1)} a_{i_3, r_3, i_4}^{(3)}. \quad (2.31)$$

In the model (2.31), there are two factors, over the first and the third modes, in such a way that  $\mathbb{S} = \{2, 4\}$  and  $\mathbb{S}_1 = \mathbb{S}_2 = \{4\}$ . Let us define two useful unfoldings of this tensor model. The first one, a tall mode-3 unfolding, is given by

$$\mathbf{X}_{I_2 I_4 I_1 \times I_3} = \left[ \mathbf{I}_{I_2} \otimes \text{bdiag} \left( \mathbf{A}_{\cdot \cdot i_4}^{(1)} \right) \right] \mathbf{G}_{I_2 I_4 R_1 \times I_4 R_3} \mathbf{A}_{I_4 R_3 \times I_3}^{(3)}, \quad (2.32)$$

where  $\mathbf{A}_{I_4 R_3 \times I_3}^{(3)}$  is a tall mode-1 unfolding of  $\mathcal{A}^{(3)}$ ,  $\text{bdiag} \left( \mathbf{A}_{\cdot \cdot i_4}^{(1)} \right)$  results in a matrix of size  $I_4 I_1 \times I_4 R_1$  and  $\mathbf{G}_{I_2 I_4 R_1 \times I_4 R_3} = \left[ \text{bdiag} \left( \mathbf{G}_{\cdot 1 \cdot i_4} \right)^T \cdots \text{bdiag} \left( \mathbf{G}_{\cdot I_2 \cdot i_4} \right)^T \right]^T$ . The second useful unfolding of  $\mathcal{X}$  is obtained by combining the first and third modes as rows and the second and fourth modes as columns of the unfolded matrix, as follows

$$\mathbf{X}_{I_1 I_3 \times I_4 I_2} = \left[ \mathbf{A}_{I_1 \times I_4 R_1}^{(1)} \bowtie \mathbf{A}_{I_3 \times I_4 R_3}^{(3)} \right] \mathbf{G}_{I_4 R_1 R_3 \times I_4 I_2}, \quad (2.33)$$

where the unfoldings  $\mathbf{A}_{I_1 \times I_4 R_1}^{(1)}$  and  $\mathbf{A}_{I_3 \times I_4 R_3}^{(3)}$  can be seen as block matrices with  $I_4$  column blocks and the balanced block Kronecker product, as defined in (2.2), is  $\mathbf{A}_{I_1 \times I_4 R_1}^{(1)} \bowtie \mathbf{A}_{I_3 \times I_4 R_3}^{(3)} = \left[ \mathbf{A}_{\cdot \cdot 1}^{(1)} \otimes \mathbf{A}_{\cdot \cdot 1}^{(3)} \cdots \mathbf{A}_{\cdot \cdot I_4}^{(1)} \otimes \mathbf{A}_{\cdot \cdot I_4}^{(3)} \right]$ . The demonstrations of these two unfoldings are given in Appendix B.

### Uniqueness

The generalized Tucker decomposition, like the Tucker one, is also not essentially unique when the core tensor is unknown, since its factors are unique up to nonsingular transformations. To discuss the uniqueness properties of this decomposition, let us consider the generalized Tucker-(2, 4) model in (2.31). By fixing the index  $i_4$ , the tensor  $\mathcal{X}$  becomes a Tucker-(2, 3) model, denoted by  $\mathcal{X}_{(i_4)} \in \mathbb{C}^{I_1 \times I_2 \times I_3}$ , and its unfolding given in (2.33) simplifies as

$$[\mathbf{X}_{I_1 I_3 \times I_2}]_{(i_4)} = \left( \mathbf{A}_{\cdot \cdot i_4}^{(1)} \otimes \mathbf{A}_{\cdot \cdot i_4}^{(3)} \right) [\mathbf{G}_{R_1 R_3 \times I_2}]_{(i_4)}, \quad (2.34)$$

for  $i_4 = 1, \dots, I_4$ .

Let us consider an alternative solution for (2.34) given by  $\bar{\mathbf{A}}_{\cdot \cdot i_4}^{(1)} = \mathbf{A}_{\cdot \cdot i_4}^{(1)} \mathbf{\Delta}_{\cdot \cdot i_4}^{(1)}$ ,  $\bar{\mathbf{A}}_{\cdot \cdot i_4}^{(3)} = \mathbf{A}_{\cdot \cdot i_4}^{(3)} \mathbf{\Delta}_{\cdot \cdot i_4}^{(3)}$  and  $\bar{\mathcal{G}} = \mathcal{G} \times_1 \mathcal{F}^{(1)} \times_3 \mathcal{F}^{(3)}$ , with nonsingular matrices  $\mathbf{\Delta}_{\cdot \cdot i_4}^{(n)} \in \mathbb{C}^{R_n \times R_n}$  and  $\mathcal{F}^{(n)} \in \mathbb{C}^{R_n \times R_n \times I_4}$  being a tensor with mode-3 slices given by  $(\mathbf{\Delta}_{\cdot \cdot i_4}^{(n)})^{-1}$ , for  $n = 1, 3$ . The triplet  $(\bar{\mathcal{G}}, \bar{\mathbf{A}}_{\cdot \cdot i_4}^{(1)}, \bar{\mathbf{A}}_{\cdot \cdot i_4}^{(3)})$  lead to the same unfolding  $[\mathbf{X}_{I_1 I_3 \times I_2}]_{(i_4)}$  given in (2.34). The demonstration is obtained by considering  $[\bar{\mathcal{G}}]_{(i_4)} = [\mathcal{G}]_{(i_4)} \times_1 \left( \mathbf{\Delta}_{\cdot \cdot i_4}^{(1)} \right)^{-1} \times_3 \left( \mathbf{\Delta}_{\cdot \cdot i_4}^{(3)} \right)^{-1}$  for any value of  $i_4$ , such that (2.34) becomes

$$[\bar{\mathbf{X}}_{I_1 I_3 \times I_2}]_{(i_4)} = \left( \bar{\mathbf{A}}_{\cdot \cdot i_4}^{(1)} \otimes \bar{\mathbf{A}}_{\cdot \cdot i_4}^{(3)} \right) [\bar{\mathbf{G}}_{R_1 R_3 \times I_2}]_{(i_4)}. \quad (2.35)$$

Being (2.35) a Tucker decomposition, we can easily get  $[\bar{\mathbf{X}}_{I_1 I_3 \times I_2}]_{(i_4)} = [\mathbf{X}_{I_1 I_3 \times I_2}]_{(i_4)}$ , which shows that the generalized Tucker-(2, 4) is not unique. However, if we consider the core tensor  $\mathcal{G}$  known, the following uniqueness theorem is valid.

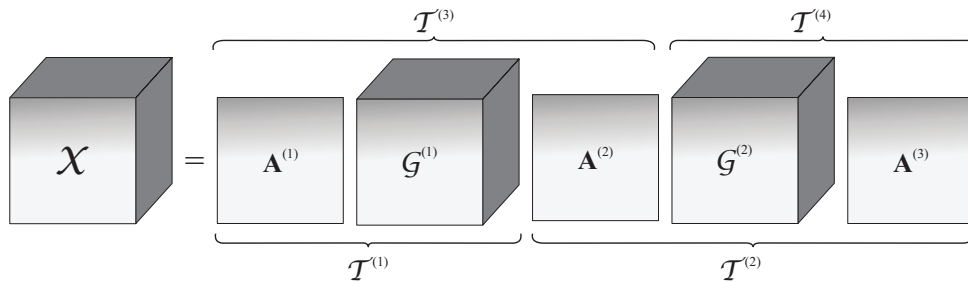
**Theorem 2.** *Consider a fourth-order tensor  $\mathcal{X} \in \mathbb{C}^{I_1 \times I_2 \times I_3 \times I_4}$  that satisfies a generalized Tucker-(2, 4) decomposition as defined in (2.31). When the core tensor  $\mathcal{G} \in \mathbb{C}^{R_1 \times I_2 \times R_3 \times I_4}$  is known, the tensor factors  $\mathcal{A}^{(1)} \in \mathbb{C}^{I_1 \times R_1 \times I_4}$  and  $\mathcal{A}^{(3)} \in \mathbb{C}^{I_3 \times R_3 \times I_4}$  are unique up to the ambiguities  $\bar{\mathbf{A}}_{\cdot \cdot i_4}^{(1)} = \delta_{i_4}^{(1)} \mathbf{A}_{\cdot \cdot i_4}^{(1)}$  and  $\bar{\mathbf{A}}_{\cdot \cdot i_4}^{(3)} = \delta_{i_4}^{(3)} \mathbf{A}_{\cdot \cdot i_4}^{(3)}$ , with  $\delta_{i_4}^{(1)} \delta_{i_4}^{(3)} = 1$ ,  $\forall i_4 \in [1, I_4]$ .*

*Proof.* See Appendix A.

### 2.2.3 Nested Tucker decomposition

The nested Tucker decomposition (NTD) was recently introduced in [34] as a special case of the tensor train (TT) decomposition [78, 79]. This model can be viewed as a nesting of two Tucker-(2, 3) models which share a matrix factor. Considering the core tensors  $\mathcal{G}^{(1)} \in \mathbb{C}^{R_1 \times I_2 \times R_2}$  and  $\mathcal{G}^{(2)} \in \mathbb{C}^{R_3 \times I_3 \times I_4}$  and the factors  $\mathbf{A}^{(1)} \in \mathbb{C}^{I_1 \times R_1}$ ,  $\mathbf{A}^{(2)} \in \mathbb{C}^{R_2 \times R_3}$  and  $\mathbf{A}^{(3)} \in \mathbb{C}^{I_4 \times R_4}$ , let

Figure 8 – Block-diagram of a nested Tucker decomposition for a fourth-order tensor



us define two Tucker-(2, 3) models  $(\mathcal{G}^{(1)}, \mathbf{A}^{(1)}, \mathbf{A}^{(2)T})$  and  $(\mathcal{G}^{(2)}, \mathbf{A}^{(2)}, \mathbf{A}^{(3)})$ , with  $\mathbf{A}^{(2)}$  being the common factor. The nesting of these two models by the common matrix factor yields a fourth-order NTD, denoted by NTD(4), which is defined as

$$x_{i_1, i_2, i_3, i_4} = \sum_{r_1=1}^{R_1} \sum_{r_2=1}^{R_2} \sum_{r_3=1}^{R_3} \sum_{r_4=1}^{R_4} a_{i_1, r_1}^{(1)} g_{r_1, i_2, r_2}^{(1)} a_{r_2, r_3}^{(2)} g_{r_3, i_3, r_4}^{(2)} a_{i_4, r_4}^{(3)}. \quad (2.36)$$

Figure 8 illustrates a block-diagram for this NTD.

Since the matrix  $\mathbf{A}^{(2)}$  can be associated with both the core tensors  $\mathcal{G}^{(1)}$  and  $\mathcal{G}^{(2)}$ , (2.36) can be decomposed into two different forms (also illustrated in Figure 8). For instance, let us consider the following Tucker-(1, 3) and Tucker-(2, 3) models, representing the tensors  $\mathcal{T}^{(1)} \in \mathbb{C}^{I_1 \times I_2 \times R_2}$  and  $\mathcal{T}^{(2)} \in \mathbb{C}^{R_2 \times I_3 \times I_4}$ ,

$$t_{i_1, i_2, r_2}^{(1)} = \sum_{r_1=1}^{R_1} g_{r_1, i_2, r_2}^{(1)} a_{i_1, r_1}^{(1)}, \quad (2.37)$$

$$t_{r_2, i_3, i_4}^{(2)} = \sum_{r_3=1}^{R_3} \sum_{r_4=1}^{R_4} g_{r_3, i_3, r_4}^{(2)} a_{r_2, r_3}^{(2)} a_{i_4, r_4}^{(3)}. \quad (2.38)$$

Note that the dimensions of  $\mathcal{X}$  accumulates the dimensions of  $\mathcal{T}^{(1)}$  and  $\mathcal{T}^{(2)}$ , except for the common dimension ( $R_2$ ). Therefore, we can write  $\mathcal{X}$  as the following summation

$$x_{i_1, i_2, i_3, i_4} = \sum_{r_2=1}^{R_2} t_{i_1, i_2, r_2}^{(1)} t_{r_2, i_3, i_4}^{(2)}, \quad (2.39)$$

which represents a contraction operation (Definition 16). Thus, the tensor  $\mathcal{X}$  is obtained by contracting the tensors  $\mathcal{T}^{(1)}$  and  $\mathcal{T}^{(2)}$  along their common mode  $r_2$ , in such a way that the NTD(4)  $(\mathbf{A}^{(1)}, \mathcal{G}^{(1)}, \mathbf{A}^{(2)}, \mathcal{G}^{(2)}, \mathbf{A}^{(3)})$  is defined as

$$\mathcal{X} = \mathcal{T}^{(1)} *_3^1 \mathcal{T}^{(2)}. \quad (2.40)$$

We say that the tensors  $\mathcal{T}^{(1)}$  and  $\mathcal{T}^{(2)}$  are components of the NTD, while  $\mathbf{A}^{(1)}$ ,  $\mathbf{A}^{(2)}$  and  $\mathbf{A}^{(3)}$  are the decomposition factors, and  $\mathcal{G}^{(1)}$  and  $\mathcal{G}^{(2)}$  are the core tensors. Similarly, we can define the NTD(4) as a contraction of the tensors  $\mathcal{T}^{(3)}$  and  $\mathcal{T}^{(4)}$  (see Figure 8), by associating the factor  $\mathbf{A}^{(2)}$  with the core tensor  $\mathcal{G}^{(1)}$ .

The NTD, as a Tucker-based model, is not essentially unique. Let us consider that the contraction in (2.40) can be written as a mode-1 product deduced from (2.21)

$$\mathcal{X}_{I_2 I_1 \times I_3 \times I_4} = \mathcal{T}^{(2)} \times_1 \mathbf{T}_{I_2 I_1 \times R_2}^{(1)}, \quad (2.41)$$

where  $\mathbf{T}_{I_2 I_1 \times R_2}^{(1)}$  is a tall mode-3 unfolding of  $\mathcal{T}^{(1)}$  and  $\mathcal{X}_{I_2 I_1 \times I_3 \times I_4}$  is a third-order contracted form of  $\mathcal{X}$  obtained by combining the first and second modes. Assuming  $\bar{\mathcal{T}}^{(2)} = \mathcal{T}^{(2)} \times_1 \Delta^{-1}$  and  $\bar{\mathbf{T}}_{I_2 I_1 \times R_3}^{(1)} = \mathbf{T}_{I_2 I_1 \times R_3}^{(1)} \Delta$  as alternative solutions for (2.41), where  $\Delta \in \mathbb{C}^{R_3 \times R_3}$  is a nonsingular ambiguity matrix, the tensor  $\mathcal{X}_{I_2 I_1 \times I_3 \times I_4}$  becomes

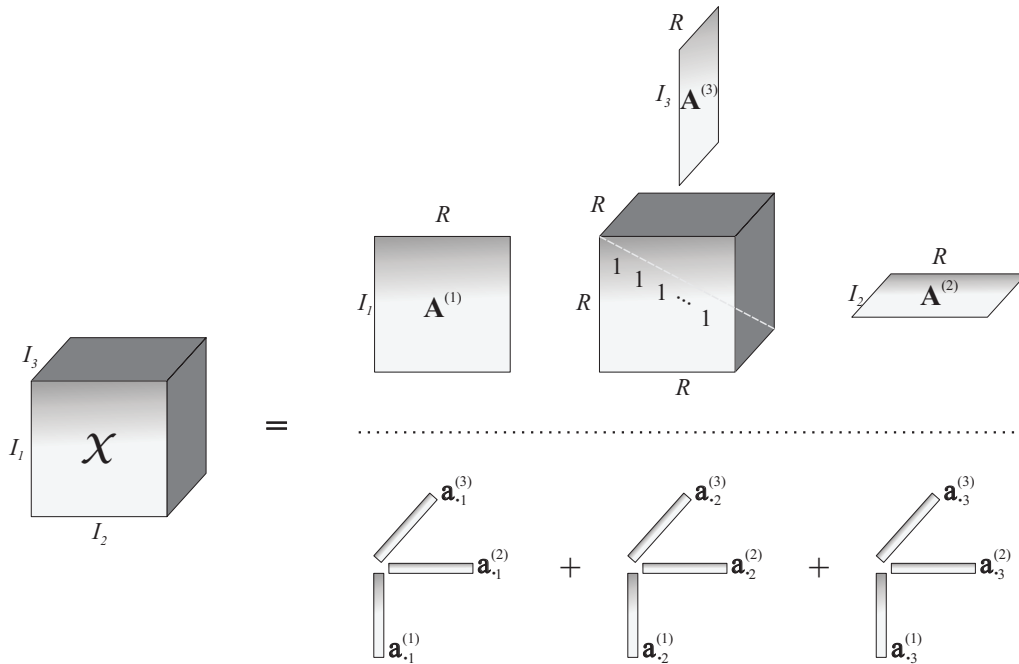
$$\begin{aligned} \bar{\mathcal{X}}_{I_2 I_1 \times I_3 \times I_4} &= \bar{\mathcal{T}}^{(2)} \times_1 \bar{\mathbf{T}}_{I_2 I_1 \times R_2}^{(1)} \\ &= (\mathcal{T}^{(2)} \times_1 \Delta^{-1}) \times_1 (\mathbf{T}_{I_2 I_1 \times R_3}^{(1)} \Delta) \\ &= \mathcal{T}^{(2)} \times_1 (\mathbf{T}_{I_2 I_1 \times R_3}^{(1)} \Delta \Delta^{-1}) \\ &= \mathcal{T}^{(2)} \times_1 \mathbf{T}_{I_2 I_1 \times R_2}^{(1)} \\ &= \mathcal{X}_{I_2 I_1 \times I_3 \times I_4}. \end{aligned} \quad (2.42)$$

This identity implies that the contracted form  $\mathcal{X}_{I_2 I_1 \times I_3 \times I_4}$  is not unique, since  $\bar{\mathcal{T}}^{(1)} *_3^1 \bar{\mathcal{T}}^{(2)} = \mathcal{T}^{(1)} *_3^1 \mathcal{T}^{(2)}$ . In other words, it is not possible to uniquely decompose  $\mathcal{X}$  into the components  $\mathcal{T}^{(1)}$  and  $\mathcal{T}^{(2)}$ , since the contraction  $\mathcal{T}^{(1)} *_3^1 \mathcal{T}^{(2)}$  is not unique. Consequently, the matrix factors of the NTD of  $\mathcal{X}$  are not unique. The authors of [34] present a brief discussion on the uniqueness properties of the NTD model, but it has not been proven. In this thesis, we present a deeper discussion about the uniqueness of NTD models in the next chapter.

#### 2.2.4 PARAFAC decomposition

The PARAFAC decomposition, also known as CANDECOMP (CANonical DECOM-Position) or CP (Canonical Polyadic), was introduced in 1970 by R. Harshman [61] and Carroll & Chang [80]. This decomposition factorizes a tensor into a sum of polyads (i.e., rank-one tensors). The main feature of the PARAFAC model is its intrinsic uniqueness. Indeed, the PARAFAC decomposition of higher-order tensors is essentially unique, i.e., the factors can be estimated up to scaling and permutation ambiguities.

Figure 9 – Block-diagram of a PARAFAC decomposition for a third-order tensor (i) as a special case of the Tucker decomposition and (ii) as a sum of triads.



The PARAFAC decomposition of a given  $N$ -th order tensor  $\mathcal{X} \in \mathbb{C}^{I_1 \times \dots \times I_N}$  is expressed in terms of the outer product (Definition 8) as

$$\mathcal{X} = \sum_{r=1}^R \mathbf{a}_r^{(1)} \circ \mathbf{a}_r^{(2)} \circ \dots \circ \mathbf{a}_r^{(N)}, \quad (2.43)$$

where  $\mathbf{a}_r^{(n)} \in \mathbb{C}^{I_n}$  are column vectors (also called factor loadings) of the matrix factors  $\mathbf{A}^{(n)} \in \mathbb{C}^{I_n \times R}$ , for  $n = 1, \dots, N$ . The PARAFAC model has the following scalar form

$$x_{i_1, \dots, i_N} = \sum_{r=1}^R \prod_{n=1}^N a_{i_n, r}^{(n)}. \quad (2.44)$$

It is worth to note that  $R$  represents the rank of  $\mathcal{X}$ . Indeed,  $R$  denotes the number of columns of the factor matrices and, consequently, the amount of elements to be added in the summations in (2.43) or (2.44) (see Definition 10).

The PARAFAC decomposition can also be interpreted as a special case of a Tucker decomposition with an identity core tensor, as introduced in Definition 12, which yields the following formulation in terms of the mode- $n$  product

$$\mathcal{X} = \mathcal{I}_R^{(N)} \times_1 \mathbf{A}^{(1)} \times_2 \mathbf{A}^{(2)} \dots \times_N \mathbf{A}^{(N)}. \quad (2.45)$$

Figure 9 illustrates both formulations for a PARAFAC decomposition of a third-order tensor. By using (2.8), we can define the following generic formulation for a tall mode- $n$  unfolding of a

PARAFAC model

$$\mathbf{X}_{I_{n+1} \cdots I_N I_1 \cdots I_{n-1} \times I_n} = (\mathbf{A}^{(n+1)} \diamond \cdots \diamond \mathbf{A}^{(N)} \diamond \mathbf{A}^{(1)} \diamond \cdots \diamond \mathbf{A}^{(n-1)}) \mathbf{A}^{(n)T}. \quad (2.46)$$

Notice the similarity between the Equations (2.46) and (2.26). The Kronecker product in the unfolding of the Tucker model is replaced by the Khatri-Rao product in the unfolding of the PARAFAC model due the fact that the matrix factors have the same number of columns, while the core tensor is replaced by the identity tensor.

Let us consider the case where a third-order tensor satisfies the PARAFAC decomposition  $\mathcal{X}=(\mathbf{A},\mathbf{B},\mathbf{C}) \in \mathbb{C}^{I_1 \times I_2 \times I_3}$ , with  $\mathbf{A} \in \mathbb{C}^{I_1 \times R}$ ,  $\mathbf{B} \in \mathbb{C}^{I_2 \times R}$  and  $\mathbf{C} \in \mathbb{C}^{I_3 \times R}$ . Equation (2.43) becomes a sum of triads (triple products) as follows

$$\mathcal{X} = \sum_{r=1}^R \mathbf{a}_{.r} \circ \mathbf{b}_{.r} \circ \mathbf{c}_{.r}. \quad (2.47)$$

By fixing values of the indices  $i_1$ ,  $i_2$  and  $i_3$  in the column vectors  $\mathbf{a}_{.r}$ ,  $\mathbf{b}_{.r}$  and  $\mathbf{c}_{.r}$ , respectively, we can write the following matrix slices

$$\mathbf{X}_{i_1 \cdot \cdot} = \sum_{r=1}^R a_{i_1,r} \mathbf{b}_{.r} \mathbf{c}_{.r}^T = \mathbf{B} \mathbf{diag}_{i_1}(\mathbf{A}) \mathbf{C}^T \in \mathbb{C}^{I_2 \times I_3}, \quad (2.48)$$

$$\mathbf{X}_{\cdot i_2 \cdot} = \sum_{r=1}^R b_{i_2,r} \mathbf{c}_{.r} \mathbf{a}_{.r}^T = \mathbf{C} \mathbf{diag}_{i_2}(\mathbf{B}) \mathbf{A}^T \in \mathbb{C}^{I_3 \times I_1}, \quad (2.49)$$

$$\mathbf{X}_{\cdot \cdot i_3} = \sum_{r=1}^R c_{i_3,r} \mathbf{a}_{.r} \mathbf{b}_{.r}^T = \mathbf{A} \mathbf{diag}_{i_3}(\mathbf{C}) \mathbf{B}^T \in \mathbb{C}^{I_1 \times I_2}, \quad (2.50)$$

for  $i_1 = 1, \dots, I_1$ ,  $i_2 = 1, \dots, I_2$  and  $i_3 = 1, \dots, I_3$ . From the above slices, by stacking them columnwise, we get the three possible tall unfoldings of the tensor  $\mathcal{X}$  in (2.47)

$$\mathbf{X}_{I_1 I_2 \times I_3} = \begin{bmatrix} \mathbf{B} \mathbf{diag}_1(\mathbf{A}) \\ \vdots \\ \mathbf{B} \mathbf{diag}_{I_1}(\mathbf{A}) \end{bmatrix} \mathbf{C}^T = (\mathbf{A} \diamond \mathbf{B}) \mathbf{C}^T, \quad (2.51)$$

$$\mathbf{X}_{I_2 I_3 \times I_1} = \begin{bmatrix} \mathbf{C} \mathbf{diag}_1(\mathbf{B}) \\ \vdots \\ \mathbf{C} \mathbf{diag}_{I_2}(\mathbf{B}) \end{bmatrix} \mathbf{A}^T = (\mathbf{B} \diamond \mathbf{C}) \mathbf{A}^T, \quad (2.52)$$

$$\mathbf{X}_{I_3 I_1 \times I_2} = \begin{bmatrix} \mathbf{A} \mathbf{diag}_1(\mathbf{C}) \\ \vdots \\ \mathbf{A} \mathbf{diag}_{I_3}(\mathbf{C}) \end{bmatrix} \mathbf{B}^T = (\mathbf{C} \diamond \mathbf{A}) \mathbf{B}^T. \quad (2.53)$$

### Uniqueness

The uniqueness of PARAFAC model was discussed in several works as [47, 52, 76, 81–85], among others, but the most well-known result is attributed to Kruskal [82]. Kruskal derived conditions for essential uniqueness of third-order PARAFAC models and Sidiropoulos *et al.* [47, 81] extended the results for an  $N$ -th order tensor.

The PARAFAC decomposition, unlike models based on the Tucker decomposition, is essentially unique, i.e., the tensor  $\mathcal{X}$  in (2.43) can be decomposed into the matrices  $\mathbf{A}^{(n)}$  in a unique way, although they suffer effects of permutation and scaling ambiguities over its columns. This uniqueness property is true if the following sufficient condition is satisfied

$$\sum_{n=1}^N k_{\mathbf{A}^{(n)}} \geq 2R + (N - 1), \quad (2.54)$$

where  $k_{\mathbf{A}^{(n)}}$  is the  $k$ -rank of the the matrix factors  $\mathbf{A}^{(n)} \in \mathbb{C}^{I_n \times R}$ . Since any arbitrary tensor can be written as a PARAFAC decomposition (sum of a finite number of rank-one tensors), the following theorem is valid for any tensor that satisfies the referred condition.

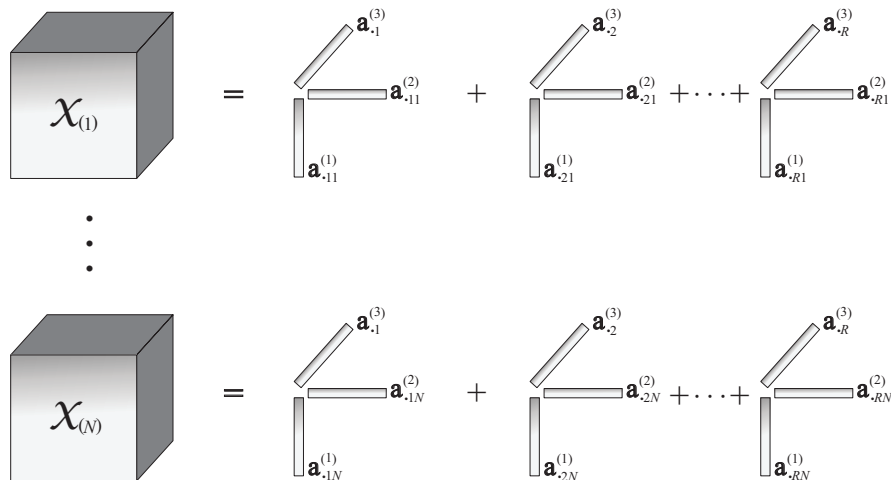
**Theorem 3.** *Consider the a  $N$ -th order tensor  $\mathcal{X} \in \mathbb{C}^{I_1 \times \dots \times I_N}$  that satisfies a PARAFAC decomposition. If the sufficient condition (2.54) is satisfied, the matrix factors  $\mathbf{A}^{(n)} \in \mathbb{C}^{I_n \times R}$ , for  $n = 1, \dots, N$ , are unique up to permutation and scaling ambiguities, such that  $\bar{\mathbf{A}}^{(n)} = \mathbf{A}^{(n)} \mathbf{\Pi} \mathbf{\Delta}_n$ , where  $\mathbf{\Pi} \in \mathbb{C}^{R \times R}$  is a permutation matrix and  $\mathbf{\Delta}_n \in \mathbb{C}^{R \times R}$  are diagonal scaling matrices, with  $\prod_{n=1}^N \mathbf{\Delta}_n = \mathbf{1}$ .*

The proof of this theorem is based on the  $k$ -rank of Khatri-Rao products and rewrite a  $N$ -th order PARAFAC model as another PARAFAC model of third order by concatenating  $N - 2$  factor matrices in only one matrix [81].

#### 2.2.5 Coupled PARAFAC decomposition

Coupled tensor decompositions have been recently proposed in [62, 86–88] for PARAFAC models and they are an emerging tool to analyse multiple datasets in signal processing and statistics. A set of tensor decompositions is said to be “coupled” when at least one of the involved factors is common to all the decompositions. For instance, let us consider the fourth-order tensor  $\mathcal{X} \in \mathbb{C}^{I_1 \times I_2 \times I_3 \times N}$  such that, for each value of  $n$ , with  $n \in [1, N]$  for  $N \geq 2$ ,

Figure 10 – Block-diagram of a coupled PARAFAC decomposition for a fourth-order tensor



we have a tensor  $\mathcal{X}_{(n)} \in \mathbb{C}^{I_1 \times I_2 \times I_3}$  satisfying third-order PARAFAC model. We say that the collection of tensors  $\{\mathcal{X}_{(1)}, \dots, \mathcal{X}_{(N)}\}$  satisfies a coupled PARAFAC decomposition if each  $\mathcal{X}_{(n)}$ , for  $n = 1, \dots, N$ , is given by

$$\mathcal{X}_{(n)} = \sum_{r=1}^R \mathbf{a}_{.rn}^{(1)} \circ \mathbf{a}_{.rn}^{(2)} \circ \mathbf{a}_{.r}^{(3)}, \quad (2.55)$$

where the column fibers  $\mathbf{a}_{.rn}^{(1)} \in \mathbb{C}^{I_1}$ ,  $\mathbf{a}_{.rn}^{(2)} \in \mathbb{C}^{I_2}$  and  $\mathbf{a}_{.r}^{(3)} \in \mathbb{C}^{I_3}$  compose the factor matrices  $\mathbf{A}_{(n)}^{(1)} = [\mathbf{a}_{.1n}^{(1)} \dots \mathbf{a}_{.Rn}^{(1)}] \in \mathbb{C}^{I_1 \times R}$ ,  $\mathbf{A}_{(n)}^{(2)} = [\mathbf{a}_{.1n}^{(2)} \dots \mathbf{a}_{.Rn}^{(2)}] \in \mathbb{C}^{I_2 \times R}$  and  $\mathbf{A}^{(3)} = [\mathbf{a}_{.1}^{(3)} \dots \mathbf{a}_{.R}^{(3)}] \in \mathbb{C}^{I_3 \times R}$ . Notice that the matrix factor  $\mathbf{A}^{(3)}$  is independent of the index  $n$ , being common to all the  $N$  tensors. Figure 10 illustrates a block-diagram for this coupled decomposition. The uniqueness properties of coupled PARAFAC decompositions of third-order tensors was discussed in [86] and the presented results show that the uniqueness conditions can be improved taking into account the coupling between a set of tensor decompositions.

### 2.3 Bibliographic review on tensor decompositions applied to wireless communication systems

In this section, we provide a survey of works found in the literature that address tensor models applied to wireless communication systems. Within this area, there are many works with different applications. We focus on those that deal with systems and applications that, in some way, are related to the main theme of this thesis (tensor decompositions, MIMO/coope-

rative systems and blind signal and channel estimation) or can provide premises for something addressed here. An overview on fundamental tensor models and applications for several MIMO and cooperative systems can be found in [48].

The interest on the use of tensor models as a signal processing tool applied to wireless communication systems started with the pioneer work of Sidiropoulos *et al.* in 2000 [47]. The authors have proposed a blind multiuser separation-equalization-detection for a direct-sequence code-division multiple access (DS-CDMA) systems by using a PARAFAC-based modeling that provides performances close to a non-blind minimum mean-squared error (MMSE) receiver. However, blind receivers provide spectral efficiency gains by using a smaller number of pilot symbols, in contrast to other receivers that assume the use of training sequences for channel estimation [20, 21, 65, 66] or the perfect knowledge of the CSI at destination [29, 67–69].

Also in [47], the authors show an interesting feature of the PARAFAC model that is the fact that the PARAFAC-based receiver does not require knowledge of spreading codes and of channel coefficients or statistic independence to recover the transmitted signals. Moreover, the identifiability of the signals and propagation parameters with a tensor approach is ensured under conditions more relaxed than those based on conventional matrix approaches [6, 45, 47, 81]. In addition, tensor-based approaches in the context of wireless communications allows the benefit from multiple (more than two) forms of signal diversity to perform jointly and blindly multiuser signal separation/equalization and channel estimation under mild conditions.

The authors of [89] propose a PARAFAC-based approach that aims to unify the received signal model of three types of multiuser wireless communication systems, which consider multiple antennas at destination and frequency-selective multipath fading. The proposed modeling is exploited to design a blind receiver that perform user signal separation and equalization iteratively. The simulation results show that the proposed algorithm has a performance close to the MMSE solution, which considers the perfect knowledge of propagation parameters.

Another advantage of tensor approaches applied to wireless systems is the possibility of designing tensor codings to encode the information to be transmitted. A TSTC for MIMO systems was proposed in [35], allowing to spread and multiplex the transmitted symbols, belonging to  $R$  data streams, in space and time domains. This tensor coding is defined as a third-order tensor, whose the modes corresponding to the transmit antenna, data stream and chip, and two matrices that allocate the transmit antennas and data streams at each time-block. This configuration leads the signals received at destination to form a fourth-order tensor that satisfies

a PARATUCK-(2, 4) decomposition. Finally, a blind receiver based on an iterative algorithm is proposed for joint symbols and channel estimation.

In [39], the authors propose a generalized fourth-order PARATUCK2 tensor model applied to a MIMO system with a STF coding. In this model, the core tensor of the fourth-order PARATUCK2 decomposition is a spatial coding matrix combined with two third-order tensor that control the allocation of the data streams and transmit antennas at each time-frequency resource. A receiver based on a Levenberg-Marquardt (LM) algorithm is proposed for blind joint estimation of the information symbols, channels and coding.

In [40], a new tensor space-time-frequency (TSTF) coding structure has been proposed for a MIMO OFDM-CDMA wireless communication system. Two new constrained tensor models called generalized PARATUCK-( $N_1, N$ ) and generalized Tucker-( $N_1, N$ ) models, with high-order tensors as decomposition factors, are introduced. By exploiting these models, two semi-blind receivers for jointly estimating the unfolding of the channel tensor and the symbol matrix are proposed. The first one is based on a two-step alternating least squares (ALS) algorithm, while the second one is a closed-form and low-complexity solution based on the least square (LS) estimation of Kronecker products.

Most recently, the work [37] proposes a new closed-form tensor-based receiver for channel estimation in a MIMO system. The proposed receiver exploits the received signal modeling, which satisfies a fourth-order PARATUCK-(2, 4) tensor model, and performs channel estimation by combining Khatri-Rao and Kronecker factorizations. The authors still propose a modified space-time coding scheme that incorporates a formatting filter.

In the context of cooperative systems, individual channel estimation is a fundamental problem. The CSI of all links between source, relays and destination plays an important role for decision-making that optimizes MIMO relay systems in terms of power allocation, decoding and adaptive relaying protocols that allow to know when a cooperation is feasible and to select a suitable relay [63, 64]. Thus, the reliability of systems with cooperative diversity strongly depends on the accuracy of CSI associated with each hop.

For example, the authors in [19] propose tensor-based receivers for uplink multiuser systems with cooperative diversity, which consider AF and DF relaying protocols. In this case, it is assumed that the CSI is not available and, then, blind receivers using the LM algorithm are proposed to jointly estimate the transmitted symbols and the channels. For this, the authors propose a tensor formulation of the received signal that unify all the considered relaying protocols

in a PARAFAC-based model.

A two-hop AF relay system, with the source using a simplified Khatri-Rao space-time (KRST) coding to encode the signals to be transmitted was introduced in [30]. The used matrix coding induces the signals received at destination to be a third-order tensor, which satisfies a PARAFAC decomposition when considered the direct link (source-destination) and a PARATUCK2 decomposition when considered the relay-assisted link (source-relay-destination). Thus, three receivers that combine these two models are proposed for a joint and semi-blind estimation of transmitted symbols and channels of both hops.

In order to represent high-order tensor in a compact way, the authors of [34] have derived the model NTD, already presented in Subsection 2.2.3, from the idea of multiple Tucker models in a train decomposition format. The presented model is then applied in a one-way two-hop half-duplex MIMO relay system with the source and the relay using a TSTC to encode the symbol matrix. The tensor modeling for the signals received at destination satisfies a fourth-order NTD, or NTD(4). Unfoldings for the proposed NTD(4) were developed to design four receivers (two semi-blind and two supervised) for symbols and channels joint estimation.

In cooperative networks, the existence of relaying antennas between the source and destination lead to a decrease of the signal fading. Consequently, in a multi-hop scenario, when the number of relays is increased we get smaller path-loss of each hop, yielding performance gains and allowing an extension of the coverage area. However, we can not yet find many works that address multi-hop systems.

In [32], a three-hop relaying scenario is addressed, considering a AF relaying protocol. The received signal tensor is modeled by combining PARAFAC and Tucker tensor models and a joint channel estimator based on ALS method is proposed. When compared to conventional matrix-based channel estimators, the proposed estimator can operate under more flexible antenna configurations, improving channel estimation accuracy.

Recently, a one-way multi-hop AF relay system that assumes a KRST coding at each relay was addressed in [18]. The system with  $K$  relays is modeled by means of  $K + 1$  third-order PARAFAC models. A closed-form semi-blind receiver based on a Khatri-Rao factorization was derived to jointly estimate the symbols and the individual channels. Simulation results show performance gains with an increase of the number relays.

For frequency-selective wireless channels, a multicarrier modulation associated to cooperative networks can overcome the rate limitation imposed by multipath and help to mitigate

the deep fading on some spectral bands and the intersymbol interference. In [90], the authors addressed the blind signal recovery for two-hop AF OFDM relaying systems. The signals received at the destination form a third-order tensor (receive antenna, transmitting symbol and subcarriers) and this model is exploited to propose a PARAFAC-based blind algorithm. The exploitation of OFDM systems with cooperative diversity under tensor approaches is still scarce.

### 3 ORIGINAL CONTRIBUTIONS ON TENSOR DECOMPOSITIONS

In this chapter, the first original contributions of this work are presented. In particular, the new tensor decompositions proposed in this thesis are described in the sequel. In the first part, we generalize the NTD model, initially exploited for a fourth-order tensor [34], to higher order tensors. We propose a generic theorem for the uniqueness of this decomposition that fills the lack of discussion on the literature about the NTD uniqueness. In the following, we introduce a new tensor decomposition, which associate the concepts of nested and coupled decompositions. Theorems involving their uniqueness conditions are also provided. The theoretical contributions presented in this chapter will be used directly in the modeling of the cooperative MIMO communication systems in the next chapters, which serves as motivation for the development of the new tensor decompositions addressed here. These new models will also be exploited to derive receiver algorithms and identifiability conditions in order to estimate unknown parameters.

#### 3.1 High-order nested Tucker decomposition – HONTD

This section addresses the high-order nested Tucker decomposition (HONTD), which is a generalization of NTD(4), introduced in [34] and recalled in Subsection 2.2.3, to high-order tensors. It is worthing to remember that, in the case of NTD(4), the nesting takes place by sharing a common factor between two Tucker-(2, 3) models or, equivalently, by contracting a Tucker-(1, 3) decomposition with a Tucker-(2, 3) one.

For a given integer  $N > 0$ , let us consider the following third-order tensor models:

- a tensor  $\mathcal{T}^{(0)} \in \mathbb{C}^{P_1 \times J_0 \times K}$  that satisfies a Tucker-(2, 3) decomposition defined by

$$\mathcal{T}^{(0)} = \mathcal{G}^{(0)} \times_1 \mathbf{B}^{(0)} \times_3 \mathbf{C}; \quad (3.1)$$

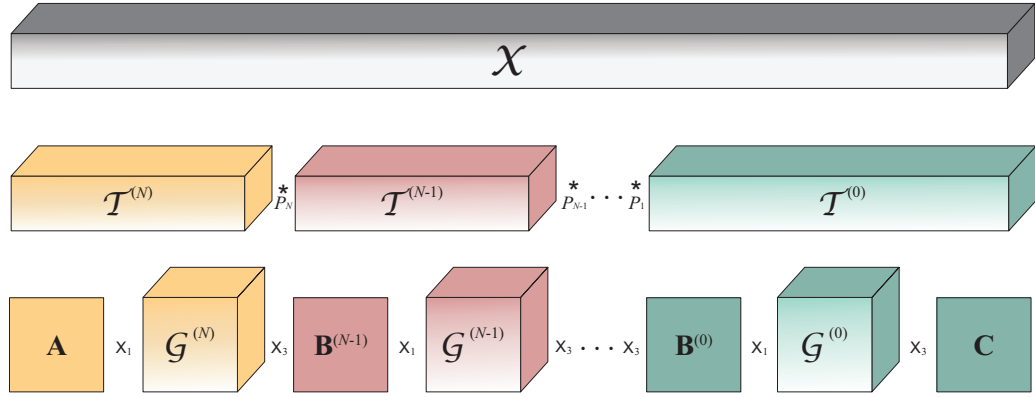
- a set of tensors  $\mathcal{T}^{(n)} \in \mathbb{C}^{P_{n+1} \times J_n \times P_n}$ , for  $n = 1, \dots, N - 1$ , that satisfy Tucker-(1, 3) decompositions defined by

$$\mathcal{T}^{(n)} = \mathcal{G}^{(n)} \times_1 \mathbf{B}^{(n)}; \quad (3.2)$$

- a tensor  $\mathcal{T}^{(N)} \in \mathbb{C}^{I \times J_N \times P_N}$  that satisfies a Tucker-(1, 3) decomposition defined by

$$\mathcal{T}^{(N)} = \mathcal{G}^{(N)} \times_1 \mathbf{A}, \quad (3.3)$$

with the core tensors  $\mathcal{G}^{(n)} \in \mathbb{C}^{R_n \times J_n \times P_n}$ , for  $n = 0, \dots, N$ , and the matrix factors  $\mathbf{A} \in \mathbb{C}^{I \times R_N}$ ,  $\mathbf{C} \in \mathbb{C}^{K \times P_0}$  and  $\mathbf{B}^{(n)} \in \mathbb{C}^{P_{n+1} \times R_n}$ , for  $n = 0, \dots, N - 1$ .

Figure 11 – Block-diagram of a HONTD for a  $(N + 3)$ -order tensor

Given a  $(N + 3)$ -th order tensor  $\mathcal{X} \in \mathbb{C}^{I \times J_N \times \dots \times J_0 \times K}$ , we define the HONTD of  $\mathcal{X}$ , denoted by  $\mathcal{X} = (\mathbf{A}, \mathcal{G}^{(N)}, \mathbf{B}^{(N-1)}, \mathcal{G}^{(N-1)}, \dots, \mathbf{B}^{(0)}, \mathcal{G}^{(0)}, \mathbf{C})$ , as

$$\mathcal{X} = \mathcal{T}^{(N)} *_3^1 \mathcal{T}^{(N-1)} *_3^1 \dots *_3^1 \mathcal{T}^{(1)} *_3^1 \mathcal{T}^{(0)}, \quad (3.4)$$

or equivalently

$$\mathcal{X} = (\mathcal{G}^{(N)} \times_1 \mathbf{A}) *_3^1 (\mathcal{G}^{(N-1)} \times_1 \mathbf{B}^{(N-1)}) *_3^1 \dots *_3^1 (\mathcal{G}^{(1)} \times_1 \mathbf{B}^{(1)}) *_3^1 (\mathcal{G}^{(0)} \times_1 \mathbf{B}^{(0)} \times_3 \mathbf{C}). \quad (3.5)$$

Figure 11 illustrates a block-diagram for this decomposition model. It can be viewed as a nesting of Tucker-(2, 3) models  $(\mathcal{G}^{(n)}, \mathbf{B}^{(n)}, \mathbf{B}^{(n-1)})$ , where two successive models (for  $n$  and  $n + 1$ ) share the factor matrix  $\mathbf{B}^{(n)}$ , for  $n = 0, \dots, N - 1$ . At the middle level of Figure 11, the HONTD is represented as the contraction of the Tucker-(2, 3) model  $\mathcal{T}^{(0)}$  defined in (3.1) with the Tucker-(1, 3) models  $\mathcal{T}^{(n)}$  defined in (3.2)-(3.3), as in (3.4). The HONTD is written in scalar form as

$$x_{i, j_N, \dots, j_0, k} = \sum_{r_N=1}^{R_N} \sum_{p_N=1}^{P_N} \dots \sum_{r_0=1}^{R_0} \sum_{p_0=1}^{P_0} a_{i, r_N} g_{r_N, j_N, p_N}^{(N)} b_{p_N, r_{N-1}}^{(N-1)} \dots b_{p_1, r_0}^{(0)} g_{r_0, j_0, p_0}^{(0)} c_{k, p_0}. \quad (3.6)$$

Note that, due to the consecutive contractions between the tensors  $\mathcal{T}^{(n)}$ , only the end factors ( $\mathbf{A}$  and  $\mathbf{C}$ ) and the core tensors  $(\mathcal{G}^{(n)})$  contribute to the dimensions of the modes of the tensor  $\mathcal{X}$ . This means that the dimensions of the modes of the intermediate factors  $\mathbf{B}^{(n)}$  do not contribute to the dimensions of the resulting tensor. The contraction operations are performed among the modes of  $\mathbf{B}^{(n)}$ . For this reason, the end factors  $\mathbf{A}$  and  $\mathbf{C}$  are denoted by letters different from the other factor matrices. The application of this model for a communication system, exploited in the next chapter, justifies the choice of the notation presented here, where,

given a integer value  $N$ , we describe a  $(N + 3)$ -th order tensor as successive contractions of  $N + 1$  tensors. We will comment on this later.

The simplest case for this decomposition is obtained when  $N = 1$ . In this case, the tensor  $\mathcal{X} \in \mathbb{C}^{I \times J_1 \times J_0 \times K}$  assumes the decomposition  $\mathcal{X} = (\mathbf{A}, \mathcal{G}^{(1)}, \mathbf{B}^{(0)}, \mathcal{G}^{(0)}, \mathbf{C})$ , with  $\mathcal{G}^{(n)} \in \mathbb{C}^{R_n \times J_n \times P_n}$ , for  $n = \{0, 1\}$ ,  $\mathbf{A} \in \mathbb{C}^{I \times R_1}$ ,  $\mathbf{B}^{(0)} \in \mathbb{C}^{P_1 \times R_0}$  and  $\mathbf{C} \in \mathbb{C}^{K \times P_0}$ , yielding the tensor components  $\mathcal{T}^{(1)} \in \mathbb{C}^{I \times J_1 \times P_1}$  and  $\mathcal{T}^{(0)} \in \mathbb{C}^{P_1 \times J_0 \times K}$ . In this case, Equation (3.4) becomes

$$\begin{aligned} \mathcal{X} &= \mathcal{T}^{(1)} *_3^1 \mathcal{T}^{(0)} \\ &= (\mathcal{G}^{(1)} \times_1 \mathbf{A}) *_3^1 (\mathcal{G}^{(0)} \times_1 \mathbf{B}^{(0)} \times_3 \mathbf{C}), \end{aligned} \quad (3.7)$$

and it can be written in scalar form as

$$x_{i,j_1,j_0,k} = \sum_{r_1=1}^{R_1} \sum_{p_1=1}^{P_1} \sum_{r_0=1}^{R_0} \sum_{p_0=1}^{P_0} a_{i,r_1} g_{r_1,j_1,p_1}^{(1)} b_{p_1,r_0}^{(0)} g_{r_0,j_0,p_0}^{(0)} c_{k,p_0}, \quad (3.8)$$

which is equivalent to the NTD(4) in (2.36). Thus, the model presented in (3.4) generalizes the NTD(4) model [34] given in (3.8), in order to represent high-order tensors (higher than four) as a cascade of multiple Tucker models nested by sharing a common matrix factor.

The HONTD can also be viewed as a specific case of a tensor-train (TT) decomposition [79], which consists of a concatenation of third-order tensors, instead of a nesting of Tucker models, and two matrix factors at the extremities, representing a  $N$ -th order tensor as

$$x_{i,j_N,\dots,j_0,k} = \sum_{r_N=1}^{R_N} \sum_{p_N=1}^{P_N} \cdots \sum_{r_1=1}^{R_1} \sum_{p_0=1}^{P_0} a_{i,r_N} g_{r_N,j_N,p_N}^{(N)} g_{p_N,j_{N-1},p_{N-1}}^{(N-1)} \cdots g_{p_2,j_1,r_1}^{(1)} g_{r_1,j_0,p_0}^{(0)} c_{k,p_0}. \quad (3.9)$$

The above model differs from the one given in (3.6) because it does not consider matrix factors between the tensors  $\mathcal{G}^{(n)}$  and  $\mathcal{G}^{(n-1)}$ , for  $n = 1, \dots, N$ .

### 3.1.1 Uniqueness analysis

In this subsection, we discuss the uniqueness of the HONTD. Firstly, note that the non-uniqueness of tensor components in a contraction operation, as discussed in Subsection 2.2.3, can be extended to multiple contractions, i.e., tensors that are written by successive contractions are also not unique. Then, we conclude that the HONTD is also not essentially unique. However, in the following theorem, we demonstrate that, under certain conditions, the HONTD is unique up to scaling ambiguities.

**Theorem 4.** *Consider the  $(N + 3)$ -order tensor  $\mathcal{X} \in \mathbb{C}^{I \times J_N \times \dots \times J_0 \times K}$  that satisfies a HONTD, as defined in (3.4). When the core tensors  $\mathcal{G}^{(n)} \in \mathbb{C}^{R_n \times J_n \times P_n}$ , for  $n = 0, \dots, N$ , are known,*

the factors  $\mathbf{A} \in \mathbb{C}^{I \times R_N}$ ,  $\mathbf{C} \in \mathbb{C}^{K \times P_0}$  and  $\mathbf{B}^{(n)} \in \mathbb{C}^{P_{n+1} \times R_n}$ , for  $n = 0, \dots, N-1$ , are unique up to the following ambiguities:  $\bar{\mathbf{A}} = \mathbf{A} \Delta_{\mathbf{A}}$ ,  $\bar{\mathbf{C}} = \mathbf{C} \Delta_{\mathbf{C}}$  and  $\bar{\mathbf{B}}^{(n)} = \mathbf{B}^{(n)} \Delta_{\mathbf{B}^{(n)}}$ , such that  $\Delta_{\mathbf{A}} = \delta_{\mathbf{A}} \mathbf{I}_{R_N}$ ,  $\Delta_{\mathbf{C}} = \delta_{\mathbf{C}} \mathbf{I}_{P_0}$  and  $\Delta_{\mathbf{B}^{(n)}} = \delta_{\mathbf{B}^{(n)}} \mathbf{I}_{R_n}$ , with  $\delta_{\mathbf{A}} \delta_{\mathbf{C}} \prod_{n=0}^{N-1} \delta_{\mathbf{B}^{(n)}} = 1$ .

*Proof.* Let us consider the following formulation for the HONTD (3.4)

$$\mathcal{X} = \mathcal{T}^{(N)} *_3^1 \mathcal{X}^{(N)}, \quad (3.10)$$

where  $\mathcal{X}^{(N)} \in \mathbb{C}^{P_N \times J_{N-1} \times \dots \times J_0 \times K}$  is a  $(N+2)$ -th order tensor that satisfies a HONTD defined recursively as follows

$$\mathcal{X}^{(\eta+1)} = \mathcal{T}^{(\eta)} *_3^1 \mathcal{X}^{(\eta)}, \quad (3.11)$$

with  $\mathcal{X}^{(\eta)} \in \mathbb{C}^{P_{\eta} \times J_{\eta-1} \times \dots \times J_0 \times K}$ , for  $\eta = 1, \dots, N$ ,  $\mathcal{X}^{(N+1)} = \mathcal{X}$  and  $\mathcal{X}^{(1)} = \mathcal{T}^{(0)}$ .

By taking a mode-1 unfolding of  $\mathcal{X}^{(\eta)}$ , we can rewrite the contraction in (3.11) as the following mode-3 product deduced from (2.20)

$$\mathcal{X}_{P_{\eta+1} \times J_{\eta} \times J_{\eta-1} \dots J_0 K}^{(\eta+1)} = \mathcal{T}^{(\eta)} \times_3 \mathbf{X}_{J_{\eta-1} \dots J_0 K \times P_{\eta}}^{(\eta)}. \quad (3.12)$$

Equation (3.12) represents a Tucker model, where we can assume  $\bar{\mathcal{T}}^{(\eta)} = \mathcal{T}^{(\eta)} \times_3 \Delta^{-1}$  and  $\bar{\mathbf{X}}_{J_{\eta-1} \dots J_0 K \times P_{\eta}}^{(\eta)} = \mathbf{X}_{J_{\eta-1} \dots J_0 K \times P_{\eta}}^{(\eta)} \Delta$  as alternative solutions, with  $\Delta \in \mathbb{C}^{P_{\eta} \times P_{\eta}}$  being a nonsingular ambiguity matrix. However, as it can be viewed in (3.2),  $\mathcal{T}^{(\eta)}$  only has a decomposition factor in first mode, which means that the decomposition factor of third mode is known and equal to identity matrix  $\mathbf{I}_{P_{\eta}}$ . Then, we conclude that  $\Delta = \delta_* \mathbf{I}_{P_{\eta}}$ , where  $\delta_*$  is the scaling factor associated to the ambiguity of a contraction operation, which leads to  $\bar{\mathcal{T}}^{(\eta)} = \delta_*^{-1} \mathcal{T}^{(\eta)}$  and  $\bar{\mathbf{X}}_{J_{\eta-1} \dots J_0 K \times P_{\eta}}^{(\eta)} = \delta_* \mathbf{X}_{J_{\eta-1} \dots J_0 K \times P_{\eta}}^{(\eta)}$ . This means that  $\mathcal{T}^{(\eta)}$  and  $\mathbf{X}_{J_{\eta-1} \dots J_0 K \times P_{\eta}}^{(\eta)}$  can be estimated from  $\mathcal{X}_{P_{\eta+1} \times J_{\eta} \times J_{\eta-1} \dots J_0 K}^{(\eta+1)}$  with a scalar ambiguity, for  $\eta = 1, \dots, N$ .

Moreover, it has been demonstrated that the matrix factors of a Tucker decomposition are unique, up to scalar ambiguities, when the core tensor is known (Theorem 1, Subsection 2.2.1). As  $\mathcal{T}^{(\eta)}$ , for  $\eta = 1, \dots, N$ , is a Tucker model, once we assume that the core tensors  $\mathcal{G}^{(\eta)}$  are known, the matrix factors  $\mathbf{A}$ ,  $\mathbf{B}^{(n)}$  and  $\mathbf{C}$  are unique and admit the scaling ambiguities  $\bar{\mathbf{A}} = \delta_{\mathbf{A}} \mathbf{A}$ ,  $\bar{\mathbf{B}}^{(n)} = \delta_{\mathbf{B}^{(n)}} \mathbf{B}^{(n)}$  and  $\bar{\mathbf{C}} = \delta_{\mathbf{C}} \mathbf{C}$ . In order to prove the relation between the scalar ambiguities, we rewrite (3.12) for  $n = N$  as

$$\mathcal{X}_{I \times J_N \times J_{N-1} \dots J_0 K} = \delta_*^{-1} (\mathcal{G}^{(N)} \times_1 \bar{\mathbf{A}}) \times_3 \bar{\mathbf{X}}_{J_{N-1} \dots J_0 K \times P_N}^{(N)}, \quad (3.13)$$

which yields the following tall unfolding

$$\begin{aligned}
\mathbf{X}_{IJ_{N-1}\dots J_0 K \times J_N} &= \delta_*^{-1} (\bar{\mathbf{A}} \otimes \bar{\mathbf{X}}_{J_{N-1}\dots J_0 K \times P_N}^{(N)}) \mathbf{G}_{R_N P_N \times J_N}^{(N)} \\
&= \delta_*^{-1} (\delta_{\mathbf{A}} \mathbf{A} \otimes \delta_{\mathbf{X}^{(N)}} \mathbf{X}_{J_{N-1}\dots J_0 K \times P_N}^{(N)}) \mathbf{G}_{R_N P_N \times J_N}^{(N)} \\
&= \delta_*^{-1} \delta_{\mathbf{A}} \delta_{\mathbf{X}^{(N)}} (\mathbf{A} \otimes \mathbf{X}_{J_{N-1}\dots J_0 K \times P_N}^{(N)}) \mathbf{G}_{R_N P_N \times J_N}^{(N)}, \tag{3.14}
\end{aligned}$$

where  $\delta_{\mathbf{X}^{(N)}}$  represents a generic scalar that comprise the ambiguities of the decomposition factors included in  $\mathcal{X}^{(N)}$ .

By using the recurrent relation in (3.11) and following the steps in (3.12)-(3.14), we get to show that  $\delta_{\mathbf{X}^{(N)}} = \delta_* \left( \prod_{n=0}^{N-1} \delta_{\mathbf{B}^{(n)}} \right) \delta_{\mathbf{C}}$ . Then (3.14) becomes

$$\mathbf{X}_{IJ_{N-1}\dots J_0 K \times J_N} = \delta_{\mathbf{A}} \left( \prod_{n=0}^{N-1} \delta_{\mathbf{B}^{(n)}} \right) \delta_{\mathbf{C}} (\mathbf{A} \otimes \mathbf{X}_{J_{N-1}\dots J_0 K \times P_N}^{(N)}) \mathbf{G}_{R_N P_N \times J_N}^{(N)}. \tag{3.15}$$

Note that the scaling ambiguity  $\delta_*$  was eliminated in (3.15). Thus, the factors  $\mathbf{A}$ ,  $\mathbf{B}^{(n)}$ , for  $n = 0, \dots, N - 1$ , and  $\mathbf{C}$  are unique with the scalar ambiguities satisfying

$$\delta_{\mathbf{A}} \left( \prod_{n=0}^{N-1} \delta_{\mathbf{B}^{(n)}} \right) \delta_{\mathbf{C}} = 1. \tag{3.16}$$

□

The uniqueness of NTD under the knowledge of the core tensors was not proved in [34]. However, one can note that the above discussion on the HONTD uniqueness remain valid if  $N = 1$ , which corresponds to a NTD. In other words, the uniqueness properties discussed here are also valid for the NTD model.

### 3.2 Coupled nested Tucker decomposition – CNTD

In this section, we introduce a new tensor decomposition that can be viewed as a coupling of multiple NTD [34] models that share common factors. This decomposition is called a coupled nested Tucker decomposition (CNTD) and, in this thesis, it is defined for fifth-order tensors, although it may be applied to higher order tensors. This new tensor model combines the ideas of the models recalled in Subsections 2.2.3 and 2.2.5, generalizing the NTD by assuming tensor factors and extending the coupling concept, initially defined for PARAFAC models, to Tucker-based decompositions. The application of the CNTD model in this thesis represents the first application of such coupled tensor models in the context of wireless communications. Indeed, up to now, the coupled decompositions based on PARAFAC models [62, 86, 88] have

not found applications in telecommunications. As explained in Subsection 2.2.5, the concept of coupled tensor decompositions is related to the existence of one or more components of each decomposition that are shared by all the decompositions.

Consider a set of  $I_5$  tensors  $\mathcal{X}_{(i_5)} \in \mathbb{C}^{I_1 \times I_2 \times I_3 \times I_4}$ , for  $i_5 = 1, \dots, I_5$ , which satisfy NTD models as follows

$$\mathcal{X}_{(i_5)} = \mathcal{T}_{(i_5)}^{(1)} *_3^1 \mathcal{T}^{(2)}, \quad (3.17)$$

where  $\mathcal{T}_{(i_5)}^{(1)} \in \mathbb{C}^{I_1 \times I_2 \times R_3}$  and  $\mathcal{T}^{(2)} \in \mathbb{C}^{R_3 \times I_3 \times I_4}$  are third-order tensors that satisfy Tucker decompositions. Note that, in (3.17), the tensor  $\mathcal{T}^{(2)}$  is independent of the index  $i_5$ , being common to all  $I_5$  decompositions. Thus, we say that the collection of tensors  $\{\mathcal{X}_{(1)}, \dots, \mathcal{X}_{(I_5)}\}$  form a coupling of NTDs by sharing the common tensor  $\mathcal{T}^{(2)}$ .

Let us consider, as a useful example, that the tensors  $\mathcal{T}_{(i_5)}^{(1)}$  and  $\mathcal{T}^{(2)}$  satisfy the following Tucker-(2, 3) and Tucker-(1, 3) models, respectively, assuming that the core tensor and the matrix factors of  $\mathcal{T}_{(i_5)}^{(1)}$  also vary with the index  $i_5$

$$\mathcal{T}_{(i_5)}^{(1)} = \mathcal{G}_{(i_5)}^{(1)} \times_1 \mathbf{A}_{(i_5)}^{(1)} \times_3 \mathbf{A}_{(i_5)}^{(2)T}, \quad (3.18)$$

$$\mathcal{T}^{(2)} = \mathcal{G}^{(2)} \times_3 \mathbf{A}^{(3)}, \quad (3.19)$$

with  $\mathcal{G}_{(i_5)}^{(1)} \in \mathbb{C}^{R_1 \times I_2 \times R_2}$ ,  $\mathcal{G}^{(2)} \in \mathbb{C}^{R_3 \times I_3 \times R_4}$ ,  $\mathbf{A}_{(i_5)}^{(1)} \in \mathbb{C}^{I_1 \times R_1}$ ,  $\mathbf{A}_{(i_5)}^{(2)} \in \mathbb{C}^{R_2 \times R_3}$  and  $\mathbf{A}^{(3)} \in \mathbb{C}^{I_4 \times R_4}$ . Taking into account the coupling of the  $I_5$  NTDs, we define a fifth-order CNTD of a tensor  $\mathcal{X} \in \mathbb{C}^{I_1 \times I_2 \times I_3 \times I_4 \times I_5}$  as the following contraction operation

$$\mathcal{X} = \mathcal{T}^{(1)} *_3^1 \mathcal{T}^{(2)}, \quad (3.20)$$

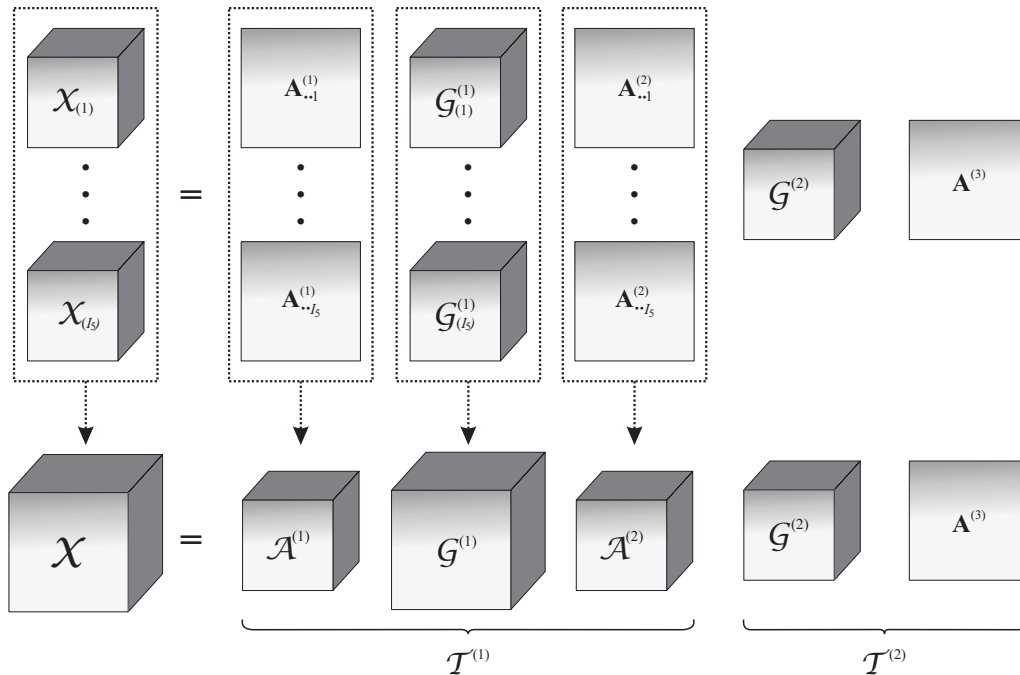
where the  $I_5$  tensors  $\mathcal{T}_{(i_5)}^{(1)} \in \mathbb{C}^{I_1 \times I_2 \times R_3}$  are stacked to form a single fourth-order tensor  $\mathcal{T}^{(1)} \in \mathbb{C}^{I_1 \times I_2 \times R_3 \times I_5}$ , satisfying the following generalized Tucker-(2, 4) decomposition

$$\mathcal{T}^{(1)} = \mathcal{G}^{(1)} \times_1 \mathcal{A}^{(1)} \times_3 \mathcal{A}^{(2)'}, \quad (3.21)$$

where  $\mathcal{A}^{(1)} \in \mathbb{C}^{I_1 \times R_1 \times I_5}$  and  $\mathcal{A}^{(2)} \in \mathbb{C}^{R_2 \times R_3 \times I_5}$ , with the tensor  $\mathcal{A}^{(2)'} \in \mathbb{C}^{R_3 \times R_2 \times I_5}$  obtained by permuting the first two modes of  $\mathcal{A}^{(2)}$ , i.e.,  $\mathbf{A}_{(i_5)}^{(2)'} = \mathbf{A}_{(i_5)}^{(2)T} \in \mathbb{C}^{R_2 \times R_3}$ . The above coupling operation can be given as a concatenation (Definition 17) of the  $I_5$  tensors  $\mathcal{T}_{(i_5)}^{(1)}$  along the fourth mode

$$\mathcal{T}^{(1)} = \mathcal{T}_{(1)}^{(1)} \sqcup_4 \mathcal{T}_{(2)}^{(1)} \dots \sqcup_4 \mathcal{T}_{(I_5)}^{(1)}, \quad (3.22)$$

Figure 12 – Block-diagram of a CNTD for a fifth-order tensor



with

$$\mathcal{G}^{(1)} = \mathcal{G}_{(1)}^{(1)} \sqcup_4 \mathcal{G}_{(2)}^{(1)} \cdots \sqcup_4 \mathcal{G}_{(I_5)}^{(1)}, \quad (3.23)$$

$$\mathcal{A}^{(1)} = \mathbf{A}_{(1)}^{(1)} \sqcup_3 \mathbf{A}_{(2)}^{(1)} \cdots \sqcup_3 \mathbf{A}_{(I_5)}^{(1)}, \quad (3.24)$$

$$\mathcal{A}^{(2)'} = \mathbf{A}_{(1)}^{(2)T} \sqcup_3 \mathbf{A}_{(2)}^{(2)T} \cdots \sqcup_3 \mathbf{A}_{(I_5)}^{(2)T}. \quad (3.25)$$

A block-diagram for this tensor decomposition is shown in Figure 12. The first level of the figure illustrates the multiple NTDs given in (3.17) and the second one represents the CNTD defined in (3.20). From the figure, it is easy to note that the coupling of  $I_5$  branches leads to a compact tensor structure, which replaces the matrix factors by tensor factors. Thus, in the case of a fifth-order tensor, CNTD generalizes NTD by coupling  $I_5$  NTDs or, equivalently, by contracting a generalized Tucker–(2, 4) model with a Tucker–(1, 3) one. In a scalar form, we can write this CNTD as

$$x_{i_1, i_2, i_3, i_4, i_5} = \sum_{r_3=1}^{R_3} t_{i_1, i_2, r_3, i_5}^{(1)} t_{r_3, i_3, i_4}^{(2)}, \quad (3.26)$$

with

$$t_{i_1, i_2, r_3, i_5}^{(1)} = \sum_{r_1=1}^{R_1} \sum_{r_2=1}^{R_2} g_{r_1, i_2, r_3, i_5}^{(1)} a_{i_1, r_1, i_5}^{(1)} a_{r_2, r_3, i_5}^{(2)}, \quad (3.27)$$

$$t_{r_3, i_3, i_4}^{(2)} = \sum_{r_4=1}^{R_4} g_{r_3, i_3, r_4}^{(2)} a_{i_4, r_4}^{(3)}. \quad (3.28)$$

### 3.2.1 Uniqueness analysis

Note that the CNTD model, defined in (3.20), is given as contraction between two tensors. From the discussion in Subsection 2.2.3, we can then conclude that the CNTD is not essentially unique, which means that alternative solutions  $\bar{\mathcal{T}}^{(1)}$  and  $\bar{\mathcal{T}}^{(2)}$  for the tensor components of the contraction in (3.20) leads to the same model, i.e.,  $\bar{\mathcal{T}}^{(1)} *_3^1 \bar{\mathcal{T}}^{(2)} = \mathcal{T}^{(1)} *_3^1 \mathcal{T}^{(2)}$ .

However, like all Tucker-based presented here, the knowledge of the core tensors can ensure that the decomposition factors are unique up to scaling ambiguities. In the following theorem, we provide conditions for the uniqueness of the CNTD model.

**Theorem 5.** Consider the fifth-order tensor  $\mathcal{X} \in \mathbb{C}^{I_1 \times I_2 \times I_3 \times I_4 \times I_5}$  expressed by means of a CNTD, as in (38), by contracting the tensors  $\mathcal{T}^{(1)} \in \mathbb{C}^{I_1 \times I_2 \times R_3 \times I_5}$  and  $\mathcal{T}^{(2)} \in \mathbb{C}^{R_3 \times I_3 \times I_4}$  over their common mode ( $r_3$ ). When the core tensors  $\mathcal{G}^{(1)} \in \mathbb{C}^{R_1 \times I_2 \times R_2 \times I_5}$  and  $\mathcal{G}^{(2)} \in \mathbb{C}^{R_3 \times I_3 \times R_4}$  are known, the factors  $\mathcal{A}^{(1)} \in \mathbb{C}^{I_1 \times R_1 \times I_5}$ ,  $\mathcal{A}^{(2)} \in \mathbb{C}^{R_2 \times R_3 \times I_5}$  and  $\mathbf{A}^{(3)} \in \mathbb{C}^{I_4 \times R_4}$  are unique up to the following ambiguities:  $\bar{\mathbf{A}}_{\cdot i_5}^{(1)} = \mathbf{A}_{\cdot i_5}^{(1)} \mathbf{D}_{\cdot i_5}^{(1)}$ ,  $\bar{\mathbf{A}}_{\cdot i_5}^{(2)T} = \mathbf{A}_{\cdot i_5}^{(2)T} \mathbf{D}_{\cdot i_5}^{(2)}$  and  $\bar{\mathbf{A}}^{(3)} = \mathbf{A}^{(3)} \mathbf{D}^{(3)}$ , such that  $\mathbf{D}_{\cdot i_5}^{(1)} = \delta_{i_5}^{(1)} \mathbf{I}_{R_1}$ ,  $\mathbf{D}_{\cdot i_5}^{(2)} = \delta_{i_5}^{(2)} \mathbf{I}_{R_2}$  and  $\mathbf{D}^{(3)} = \delta^{(3)} \mathbf{I}_{R_4}$ , with  $\delta_{i_5}^{(1)} \delta_{i_5}^{(2)} \delta^{(3)} = 1$ ,  $\forall i_5 \in [1, I_5]$ .

*Proof.* Let us rewrite the contraction in (3.20) as the following mode-1 product

$$\mathcal{X}_{I_2 I_5 I_1 \times I_3 \times I_4} = \mathcal{T}^{(2)} \times_1 \mathbf{T}_{I_2 I_5 I_1 \times R_3}^{(1)}, \quad (3.29)$$

where  $\mathbf{T}_{I_2 I_5 I_1 \times R_3}^{(1)}$  is a tall mode-3 unfolding of  $\mathcal{T}^{(1)}$  and  $\mathcal{X}_{I_2 I_5 I_1 \times I_3 \times I_4}$  is a third-order contracted form of  $\mathcal{X}$  obtained by combining the first, second and fifth modes.

Assuming that  $\mathcal{T}^{(2)}$  and  $\mathbf{T}_{I_2 I_5 I_1 \times R_3}^{(1)}$  can be replaced by the alternatives  $\bar{\mathcal{T}}^{(2)} = \mathcal{T}^{(2)} \times_1 \Delta^{-1}$  and  $\bar{\mathbf{T}}_{I_2 I_5 I_1 \times R_3}^{(1)} = \mathbf{T}_{I_2 I_5 I_1 \times R_3}^{(1)} \Delta$ , we can also conclude that  $\Delta = \delta_* \mathbf{I}_{R_3}$ , where  $\delta_*$  is the scaling ambiguity associated to the contraction in (3.20), since  $\mathcal{T}^{(2)}$  (3.19) only has a factor in third mode. However, as showed in (3.15), the factor  $\delta_*$  is eliminated by the properties of a mode- $n$  product. Therefore, the contraction in (3.20) is unique and the uniqueness of the decomposition factors depends on the uniqueness of tensor components  $\mathcal{T}^{(1)}$  and  $\mathcal{T}^{(2)}$ . As  $\mathcal{T}^{(1)}$

is a generalized Tucker decomposition, the factors  $\mathcal{A}^{(1)}$  and  $\mathcal{A}^{(2)}$  admit the ambiguities  $\bar{\mathbf{A}}_{\cdot i_5}^{(1)} = \delta_{i_5}^{(1)} \mathbf{A}_{\cdot i_5}^{(1)}$ ,  $\bar{\mathbf{A}}_{\cdot i_5}^{(2)T} = \delta_{i_5}^{(2)} \mathbf{A}_{\cdot i_5}^{(2)T}$ , for  $i_5 = 1, \dots, I_5$ , as shown in Subsection 2.2.2. On the other hand,  $\mathcal{T}^{(2)}$  is a Tucker decomposition and the factor  $\mathbf{A}^{(3)}$  admits the ambiguity  $\bar{\mathbf{A}}^{(3)} = \delta^{(3)} \mathbf{A}^{(3)}$ .

Now we prove the relation between the scalar ambiguities  $\delta_{i_5}^{(1)}$ ,  $\delta_{i_5}^{(2)}$  and  $\delta^{(3)}$  of the decomposition factors. By fixing the index  $i_5$  in (3.29), we have

$$[\mathcal{X}_{I_2 I_1 \times I_3 \times I_4}]_{(i_5)} = \mathcal{T}^{(2)} \times_1 [\mathbf{T}_{I_2 I_1 \times R_3}^{(1)}]_{(i_5)}, \quad (3.30)$$

where  $[\mathbf{T}_{I_2 I_1 \times R_3}^{(1)}]_{(i_5)}$  is deduced from (2.32) as

$$[\mathbf{T}_{I_2 I_1 \times R_3}^{(1)}]_{(i_5)} = \left( \mathbf{I}_{I_2} \otimes \mathbf{A}_{\cdot i_5}^{(1)} \right) [\mathbf{G}_{I_2 R_1 \times R_2}]_{(i_5)} \mathbf{A}_{\cdot i_5}^{(2)}. \quad (3.31)$$

Replacing the tensors  $\mathcal{T}^{(2)}$  and  $[\mathbf{T}_{I_2 I_1 \times R_3}^{(1)}]_{(i_5)}$  by their respective definitions in (3.32), and the factors  $\mathbf{A}_{\cdot i_5}^{(1)}$ ,  $\mathbf{A}_{\cdot i_5}^{(2)}$  and  $\mathbf{A}^{(3)}$  by the ambiguities  $\delta_{i_5}^{(1)} \mathbf{A}_{\cdot i_5}^{(1)}$ ,  $\delta_{i_5}^{(2)} \mathbf{A}_{\cdot i_5}^{(2)}$  and  $\delta^{(3)} \mathbf{A}^{(3)}$ , gives

$$[\bar{\mathcal{X}}_{I_2 I_1 \times I_3 \times I_4}]_{(i_5)} = (\mathcal{G}^{(2)} \times_3 \delta^{(3)} \mathbf{A}^{(3)}) \times_1 \left( \left( \mathbf{I}_{I_2} \otimes \delta_{i_5}^{(1)} \mathbf{A}_{\cdot i_5}^{(1)} \right) [\mathbf{G}_{I_2 R_1 \times R_2}]_{(i_5)} \delta_{i_5}^{(2)} \mathbf{A}_{\cdot i_5}^{(2)} \right), \quad (3.32)$$

which yields the following tall unfolding

$$\begin{aligned} [\bar{\mathcal{X}}_{I_4 I_2 I_1 \times I_3}]_{(i_5)} &= \left[ \left( \left( \mathbf{I}_{I_2} \otimes \delta_{i_5}^{(1)} \mathbf{A}_{\cdot i_5}^{(1)} \right) [\mathbf{G}_{I_2 R_1 \times R_2}]_{(i_5)} \delta_{i_5}^{(2)} \mathbf{A}_{\cdot i_5}^{(2)} \right) \otimes \delta^{(3)} \mathbf{A}^{(3)} \right] \mathbf{G}_{R_4 R_3 \times I_3}^{(2)}, \\ &= \delta_{i_5}^{(1)} \delta_{i_5}^{(2)} \delta^{(3)} \left[ \left( \left( \mathbf{I}_{I_2} \otimes \mathbf{A}_{\cdot i_5}^{(1)} \right) [\mathbf{G}_{I_2 R_1 \times R_2}]_{(i_5)} \mathbf{A}_{\cdot i_5}^{(2)} \right) \otimes \mathbf{A}^{(3)} \right] \mathbf{G}_{R_4 R_3 \times I_3}^{(2)}. \end{aligned} \quad (3.33)$$

Thus, the factors  $\mathcal{A}^{(1)}$ ,  $\mathcal{A}^{(2)}$  and  $\mathbf{A}^{(3)}$  are unique if the condition  $\delta_{i_5}^{(1)} \delta_{i_5}^{(2)} \delta^{(3)} = 1$  is satisfied.  $\square$

### 3.2.2 Alternative structure for the CNTD model

In this subsection, we present an alternative structure for the proposed CNTD model, which will be useful in Chapter 6 in an application to wireless communication systems. The CNTD model introduced in previous sections can be expressed as a contraction between a generalized Tucker model and a Tucker one.

In the sequel, we propose a CNTD a little different from the one above mentioned. Indeed, in (3.17)-(3.20), the decomposition model is characterized as a contraction between a generalized Tucker-(2, 4) model and a Tucker-(1, 3) one, while the CNTD of the present subsection is a contraction between a Tucker-(2, 3) model and a generalized Tucker-(1, 4) one.

Let us consider a set of  $I_5$  tensors  $\mathcal{Y}_{(i_5)} \in \mathbb{C}^{I_1 \times I_2 \times I_3 \times I_4}$ , for  $i_5 = 1, \dots, I_5$ , which satisfy NTD models as follows

$$\mathcal{Y}_{(i_5)} = \mathcal{T}^{(3)} *_3^1 \mathcal{T}_{(i_5)}^{(4)}, \quad (3.34)$$

with  $\mathcal{T}^{(3)} \in \mathbb{C}^{I_1 \times I_2 \times R_3}$  and  $\mathcal{T}_{(i_5)}^{(4)} \in \mathbb{C}^{R_3 \times I_3 \times I_4}$  satisfying Tucker decompositions. Since the tensor  $\mathcal{T}^{(3)}$  is independent of the index  $i_5$  and common to all  $I_5$  decompositions, the collection of tensors  $\{\mathcal{Y}_{(1)}, \dots, \mathcal{Y}_{(I_5)}\}$  form a coupling of NTDs by sharing the common tensor  $\mathcal{T}^{(3)}$ .

Now, let us define the tensors  $\mathcal{T}^{(3)}$  and  $\mathcal{T}_{(i_5)}^{(4)}$  as the following Tucker-(2, 3) model and Tucker-(1, 3) one

$$\mathcal{T}^{(3)} = \mathcal{G}^{(3)} \times_1 \mathbf{B}^{(1)} \times_3 \mathbf{B}^{(2)T}, \quad (3.35)$$

$$\mathcal{T}_{(i_5)}^{(4)} = \mathcal{G}_{(i_5)}^{(4)} \times_3 \mathbf{B}_{(i_5)}^{(3)}, \quad (3.36)$$

with  $\mathcal{G}^{(3)} \in \mathbb{C}^{R_1 \times I_2 \times R_2}$ ,  $\mathcal{G}_{(i_5)}^{(4)} \in \mathbb{C}^{R_3 \times I_3 \times R_4}$ ,  $\mathbf{B}^{(1)} \in \mathbb{C}^{I_1 \times R_1}$ ,  $\mathbf{B}^{(2)} \in \mathbb{C}^{R_2 \times R_3}$  and  $\mathbf{B}_{(i_5)}^{(3)} \in \mathbb{C}^{I_4 \times R_4}$ .

By coupling the  $I_5$  decompositions, we get a fifth-order CNTD of the tensor  $\mathcal{Y} \in \mathbb{C}^{I_1 \times I_2 \times I_3 \times I_4 \times I_5}$  as follows

$$\mathcal{Y} = \mathcal{T}^{(3)} *_3^1 \mathcal{T}^{(4)}. \quad (3.37)$$

The tensors  $\mathcal{T}_{(i_5)}^{(4)}$ , for  $i_5 = 1, \dots, I_5$ , are stacked in such a way that yields the fourth-order tensor  $\mathcal{T}^{(4)} \in \mathbb{C}^{R_3 \times I_3 \times I_4 \times I_5}$ , which satisfies the following generalized Tucker-(1, 4) decomposition

$$\mathcal{T}^{(4)} = \mathcal{G}^{(4)} \times_3 \mathcal{B}^{(3)}, \quad (3.38)$$

with

$$\mathcal{T}^{(4)} = \mathcal{T}_{(1)}^{(4)} \sqcup_4 \mathcal{T}_{(2)}^{(4)} \dots \sqcup_4 \mathcal{T}_{(I_5)}^{(4)} \in \mathbb{C}^{R_3 \times I_3 \times I_4 \times I_5}, \quad (3.39)$$

$$\mathcal{G}^{(4)} = \mathcal{G}_{(1)}^{(4)} \sqcup_4 \mathcal{G}_{(2)}^{(4)} \dots \sqcup_4 \mathcal{G}_{(I_5)}^{(4)} \in \mathbb{C}^{R_3 \times I_3 \times R_4 \times I_5}, \quad (3.40)$$

$$\mathcal{B}^{(3)} = \mathbf{B}_{(1)}^{(3)} \sqcup_3 \mathbf{B}_{(2)}^{(3)} \dots \sqcup_3 \mathbf{B}_{(I_5)}^{(3)} \in \mathbb{C}^{I_4 \times R_4 \times I_5}. \quad (3.41)$$

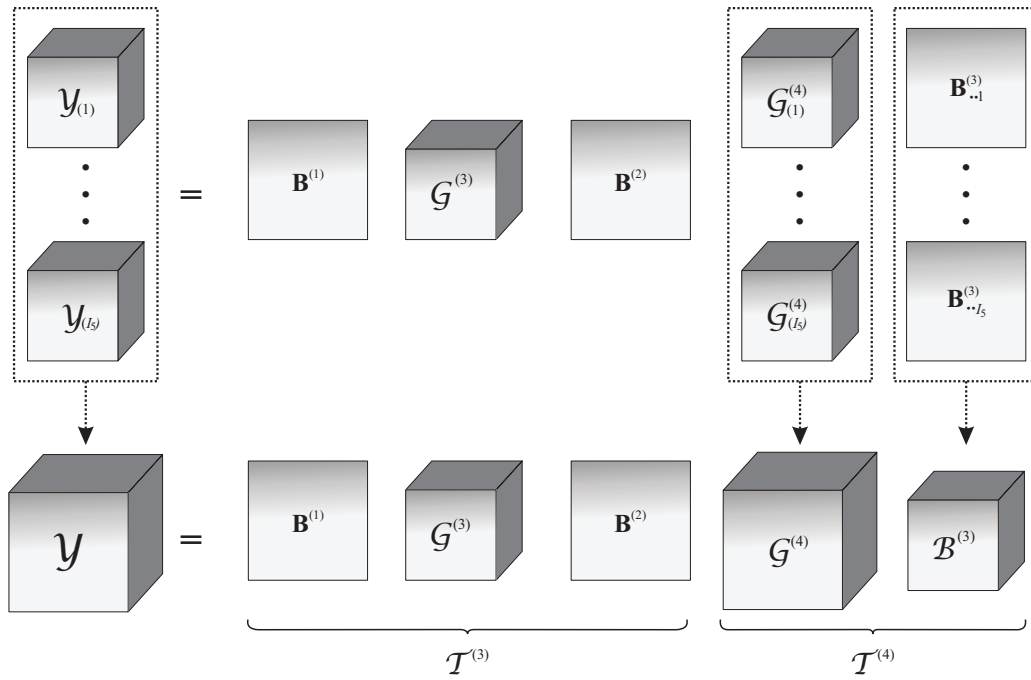
A block-diagram for this model is shown in Figure 13. The CNTD model in (3.37) has the following scalar notation

$$y_{i_1, i_2, i_3, i_4, i_5} = \sum_{r_1=1}^{R_1} \sum_{r_2=1}^{R_2} \sum_{r_3=1}^{R_3} \sum_{r_4=1}^{R_4} b_{i_1, r_1}^{(1)} g_{r_1, i_2, r_2}^{(3)} b_{r_2, r_3}^{(2)} g_{r_3, i_3, r_4, i_5}^{(4)} b_{i_4, r_4, i_5}^{(3)}. \quad (3.42)$$

Note that, in a general way, the decomposition (3.37) for the tensor  $\mathcal{Y}$  is equivalent to the one introduced in (3.20) for the tensor  $\mathcal{X}$ , being the difference due to the structure of the tensor components  $\mathcal{T}^{(1)}$ ,  $\mathcal{T}^{(2)}$ ,  $\mathcal{T}^{(3)}$  and  $\mathcal{T}^{(4)}$ . Hence, we can assume that the same uniqueness properties remain valid.

In the next three chapters, we propose some applications of the new tensor models introduced in this chapter for the context of cooperative MIMO systems. The presented tensor

Figure 13 – Block-diagram of the alternative CNTD model



structures are used to describe the signals received at destination in a multi-hop MIMO relay system, a two-hop MIMO multi-relay system and a two-hop OFDM MIMO relay system, respectively.

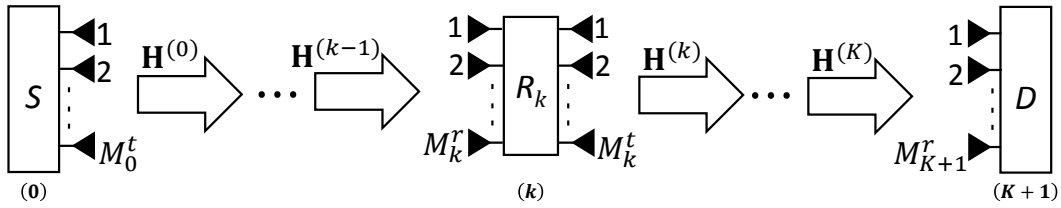
## 4 MULTI-HOP MIMO RELAY SYSTEM WITH TSTC BASED ON HONTD

In this chapter, we present a new one-way multi-hop AF MIMO relaying system composed of  $K$  relays, where the source and the relays use a third-order TSTC [35] to encode the signals to be transmitted. This system can be viewed as a generalization of recently proposed systems [18, 24, 34, 42] to the multi-hop case using tensor coding, leading to the description of a high-order tensor model in a compact way. The signals received at destination satisfy a HONTD of order  $(K + 3)$ , as introduced in Section 3.1. For a case with two relays ( $K = 2$ ), for instance, the signals yield a fifth-order HONTD. This modeling is then exploited to propose new semi-blind receivers to jointly estimate the symbols and the individual channels. In this chapter, we also provide Monte Carlo simulation results to illustrate the impact of design parameters on the system performance and the behavior of the proposed receivers in terms of symbol-error-rate (SER), normalized mean square error (NMSE) of the estimated channels and speed of convergence.

### 4.1 System model

Let us consider the multi-hop MIMO relaying system illustrated in Figure 14, composed of a source ( $S$ ),  $K$  relays ( $R_1, \dots, R_K$ ) and a destination ( $D$ ). The numbers of transmit and receive antennas at node  $k$  are denoted by  $M_k^t$  and  $M_k^r$ , respectively, with  $k \in \{0, \dots, K + 1\}$ . The nodes indexed by 0 and  $K + 1$  correspond to the source and the destination, respectively. The transmission consists of  $K + 1$  steps via  $K$  relays. The source and the relays encode the signals to be transmitted by means of a TSTC and the relays operate in half-duplex mode, using the AF protocol, i.e., retransmitting the received signals without decoding. Synchronization is assumed at the symbol level and the channels undergo frequency-flat fading, with  $\mathbf{H}^{(k)} \in \mathbb{C}^{M_{k+1}^r \times M_k^t}$  being the channel matrix between the nodes  $k$  and  $k + 1$ , for  $k = 0, \dots, K$ .

The symbol matrix encoded by the source is denoted by  $\mathbf{S} \in \mathbb{C}^{N \times R}$ ,  $R$  being the number of data streams transmitted during each symbol period and  $N$  being the number of data symbols per data stream. The TSTC used by the source and the  $k$ -th relay are represented respectively by the tensors  $\mathcal{C}^{(0)} \in \mathbb{C}^{M_0^t \times P_0 \times R}$  and  $\mathcal{C}^{(k)} \in \mathbb{C}^{M_k^t \times P_k \times M_k^r}$ , for  $k = 1, \dots, K$ , where  $P_k$ , for  $k \in \{0, \dots, K\}$ , is the time spreading length of the TSTC used by the node  $k$ .

Figure 14 – Multi-hop MIMO relaying system with  $K$  relays

#### 4.1.1 Case with two relays

In this subsection, we consider the particular case with two relays ( $K = 2$ ). In the next subsection, we generalize the modeling to an arbitrary number  $K$  of relays. The coded signals transmitted by the source towards the relay  $R_1$  forms the tensor  $\mathcal{Y}^{(0)} \in \mathbb{C}^{M_0^t \times P_0 \times N}$  defined as the following mode-3 product

$$\mathcal{Y}^{(0)} = \mathcal{C}^{(0)} \times_3 \mathbf{S} \iff y_{m_0^t, p_0, n}^{(0)} = \sum_{r=1}^R c_{m_0^t, p_0, r}^{(0)} s_{n, r}. \quad (4.1)$$

After transmission through the channel  $\mathbf{H}^{(0)}$ ,  $R_1$  receives the following signal tensor

$$\begin{aligned} \tilde{\mathcal{X}}^{(1)} &= \mathcal{X}^{(1)} + \mathcal{N}^{(1)} \\ &= \mathcal{Y}^{(0)} \times_1 \mathbf{H}^{(0)} + \mathcal{N}^{(1)} \\ &= \mathcal{C}^{(0)} \times_1 \mathbf{H}^{(0)} \times_3 \mathbf{S} + \mathcal{N}^{(1)} \in \mathbb{C}^{M_1^r \times P_0 \times N}, \end{aligned} \quad (4.2)$$

which satisfies a Tucker-(2, 3) model. The tensor  $\tilde{\mathcal{X}}^{(1)}$  represents the noisy version of the signal tensor  $\mathcal{X}^{(1)}$ , with  $\mathcal{N}^{(1)} \in \mathbb{C}^{M_1^r \times P_0 \times N}$  being the additive white Gaussian noise (AWGN) tensor at the relay  $R_1$ .

The relays re-encode the received signals by means of the coding tensor  $\mathcal{C}^{(k)}$ , for  $k \in \{1, 2\}$ . The signals coded at the relay  $R_1$  yield the tensor  $\mathcal{Y}^{(1)} \in \mathbb{C}^{M_1^t \times P_1 \times P_0 \times N}$ , which is given by the following contraction operation

$$\mathcal{Y}^{(1)} = \mathcal{C}^{(1)} *_3^1 \tilde{\mathcal{X}}^{(1)} \iff y_{m_1^t, p_1, p_0, n}^{(1)} = \sum_{m_1^r=1}^{M_1^r} c_{m_1^t, p_1, m_1^r}^{(1)} \tilde{x}_{m_1^r, p_0, n}^{(1)}. \quad (4.3)$$

The coded signal  $\mathcal{Y}^{(1)}$  is then transmitted to the relay  $R_2$  through the channel  $\mathbf{H}^{(1)}$ . The signals received by  $R_2$  can be written as follows

$$\begin{aligned} \tilde{\mathcal{X}}^{(2)} &= \mathcal{Y}^{(1)} \times_1 \mathbf{H}^{(1)} + \mathcal{N}^{(2)} \\ &= (\mathcal{C}^{(1)} *_3^1 \tilde{\mathcal{X}}^{(1)}) \times_1 \mathbf{H}^{(1)} + \mathcal{N}^{(2)} \in \mathbb{C}^{M_2^r \times P_1 \times P_0 \times N}, \end{aligned} \quad (4.4)$$

where  $\mathcal{N}^{(2)} \in \mathbb{C}^{M_2^r \times P_1 \times P_0 \times N}$  is the AWGN tensor at the relay  $R_2$ . Since the above contraction over the mode  $m_1^r$  is an operation in the third mode of the tensor  $\mathcal{C}^{(1)}$ , the tensor (4.4) can also be rewritten as

$$\tilde{\mathcal{X}}^{(2)} = (\mathcal{C}^{(1)} \times_1 \mathbf{H}^{(1)}) *_3^1 \tilde{\mathcal{X}}^{(1)} + \mathcal{N}^{(2)}, \quad (4.5)$$

from which we define the Tucker-(1, 3) model  $\mathcal{T}^{(1)} = \mathcal{C}^{(1)} \times_1 \mathbf{H}^{(1)} \in \mathbb{C}^{M_2^r \times P_1 \times M_1^r}$  and, then, the noiseless signals  $\mathcal{X}^{(2)}$  received by  $R_2$  can be written as

$$\begin{aligned} \mathcal{X}^{(2)} &= \mathcal{T}^{(1)} *_3^1 \mathcal{X}^{(1)} \\ &= (\mathcal{C}^{(1)} \times_1 \mathbf{H}^{(1)}) *_3^1 (\mathcal{C}^{(0)} \times_1 \mathbf{H}^{(0)} \times_3 \mathbf{S}), \end{aligned} \quad (4.6)$$

with the following scalar notation

$$x_{m_2^r, p_1, p_0, n}^{(2)} = \sum_{m_1^r=1}^{M_1^r} \sum_{m_1^t=1}^{M_1^t} \sum_{m_0^t=1}^{M_0^t} \sum_{r=1}^R h_{m_2^r, m_1^t}^{(1)} c_{m_1^t, p_1, m_1^r}^{(1)} h_{m_1^r, m_0^t}^{(0)} c_{m_0^t, p_0, r}^{(0)} s_{n, r}. \quad (4.7)$$

The model defined in (4.6)-(4.7) satisfies a NTD(4) [34] – Equations (3.7)-(3.8) – with the correspondences  $(\mathbf{A}, \mathcal{G}^{(1)}, \mathbf{B}^{(0)}, \mathcal{G}^{(0)}, \mathbf{C}) \iff (\mathbf{H}^{(1)}, \mathcal{C}^{(1)}, \mathbf{H}^{(0)}, \mathcal{C}^{(0)}, \mathbf{S})$ .

Finally, in the third hop,  $R_2$  re-encodes  $\tilde{\mathcal{X}}^{(2)}$  and forwards the coded signals to the destination through the channel  $\mathbf{H}^{(2)}$ , yielding analogously the following model for the received signals

$$\begin{aligned} \tilde{\mathcal{X}}^{(3)} &= (\mathcal{C}^{(2)} \times_1 \mathbf{H}^{(2)}) *_3^1 \tilde{\mathcal{X}}^{(2)} + \mathcal{N}^{(3)} \\ &= \mathcal{T}^{(2)} *_3^1 \tilde{\mathcal{X}}^{(2)} + \mathcal{N}^{(3)} \in \mathbb{C}^{M_3^r \times P_2 \times P_1 \times P_0 \times N}, \end{aligned} \quad (4.8)$$

with  $\mathcal{N}^{(3)} \in \mathbb{C}^{M_3^r \times P_2 \times P_1 \times P_0 \times N}$  being the AWGN tensor at destination and  $\mathcal{T}^{(2)} = \mathcal{C}^{(2)} \times_1 \mathbf{H}^{(2)} \in \mathbb{C}^{M_3^r \times P_2 \times M_2^r}$ . Thus, the noiseless received signals tensor  $\mathcal{X}^{(3)}$  follows the generic tensor structure introduced in Section 3.1 and given as

$$\begin{aligned} \mathcal{X}^{(3)} &= \mathcal{T}^{(2)} *_3^1 \mathcal{T}^{(1)} *_3^1 \mathcal{X}^{(1)} \\ &= (\mathcal{C}^{(2)} \times_1 \mathbf{H}^{(2)}) *_3^1 (\mathcal{C}^{(1)} \times_1 \mathbf{H}^{(1)}) *_3^1 (\mathcal{C}^{(0)} \times_1 \mathbf{H}^{(0)} \times_3 \mathbf{S}), \end{aligned} \quad (4.9)$$

which satisfies a fifth-order HONTD – Equations (3.4)-(3.5), for  $N = 2$  – with the following correspondences  $(\mathbf{A}, \mathcal{G}^{(2)}, \mathbf{B}^{(1)}, \mathcal{G}^{(1)}, \mathbf{B}^{(0)}, \mathcal{G}^{(0)}, \mathbf{C}) \iff (\mathbf{H}^{(2)}, \mathcal{C}^{(2)}, \mathbf{H}^{(1)}, \mathcal{C}^{(1)}, \mathbf{H}^{(0)}, \mathcal{C}^{(0)}, \mathbf{S})$ . Then, we can rewrite the noisy received signals tensor  $\tilde{\mathcal{X}}^{(3)}$  in (4.8) as

$$\tilde{\mathcal{X}}^{(3)} = \mathcal{X}^{(3)} + \tilde{\mathcal{N}}^{(3)}, \quad (4.10)$$

where the tensor  $\bar{\mathcal{N}}^{(3)}$  represents the global noise at destination and given by

$$\bar{\mathcal{N}}^{(3)} = \mathcal{N}^{(3)} + \mathcal{T}^{(2)} *_3^1 (\mathcal{N}^{(2)} + \mathcal{T}^{(1)} *_3^1 \mathcal{N}^{(1)}). \quad (4.11)$$

#### 4.1.2 General case – $K$ relays

Let us now consider the general case with  $K \geq 2$  relays. The signal received at the relay  $R_1$  is the same as defined in (4.2). Similarly as in (4.5) and (4.8), we can derive the expressions for the signals received at the subsequent nodes, assuming that each relay  $R_k$ , for  $k = 1, \dots, K$ , re-encodes the received signals  $\tilde{\mathcal{X}}^{(k)} \in \mathbb{C}^{M_k^r \times P_{k-1} \times \dots \times P_0 \times N}$  by means of a coding tensor  $\mathcal{C}^{(k)}$  resulting in the coded signals  $\mathcal{Y}^{(k)} = \mathcal{C}^{(k)} *_3^1 \tilde{\mathcal{X}}^{(k)} \in \mathbb{C}^{M_k^t \times P_k \times \dots \times P_0 \times N}$  to be transmitted. After transmission via channel  $\mathbf{H}^{(k)}$ , the signals received at the node  $k + 1$  form a  $(k + 3)$ -th order tensor given by

$$\begin{aligned} \tilde{\mathcal{X}}^{(k+1)} &= \mathcal{Y}^{(k)} \times_1 \mathbf{H}^{(k)} + \mathcal{N}^{(k+1)} \\ &= \mathcal{T}^{(k)} *_3^1 \tilde{\mathcal{X}}^{(k)} + \mathcal{N}^{(k+1)} \in \mathbb{C}^{M_{k+1}^r \times P_k \times \dots \times P_0 \times N}, \end{aligned} \quad (4.12)$$

where  $\mathcal{N}^{(k+1)} \in \mathbb{C}^{M_{k+1}^r \times P_k \times \dots \times P_0 \times N}$  is the AWGN tensor at the node  $k + 1$  and  $\mathcal{T}^{(k)}$ , representing the effective channel of each hop, is defined as

$$\mathcal{T}^{(k)} = \mathcal{C}^{(k)} \times_1 \mathbf{H}^{(k)} \in \mathbb{C}^{M_{k+1}^r \times P_k \times M_k^r}. \quad (4.13)$$

Thus, from the recurrent relation (4.12), we can deduce the following formulation for the signals received at the node  $k + 1$

$$\tilde{\mathcal{X}}^{(k+1)} = \mathcal{X}^{(k+1)} + \bar{\mathcal{N}}^{(k+1)}, \quad (4.14)$$

where the noiseless received signal  $\mathcal{X}^{(k+1)}$  and the global noise  $\bar{\mathcal{N}}^{(k+1)}$  are given respectively as

$$\mathcal{X}^{(k+1)} = \mathcal{T}^{(k)} *_3^1 \mathcal{X}^{(k)} \quad (4.15)$$

$$\bar{\mathcal{N}}^{(k+1)} = \mathcal{N}^{(k+1)} + \mathcal{T}^{(k)} *_3^1 \bar{\mathcal{N}}^{(k)}. \quad (4.16)$$

The tensor in (4.15) can then be rewritten in the following Tucker train format

$$\mathcal{X}^{(k+1)} = \mathcal{T}^{(k)} *_3^1 \mathcal{T}^{(k-1)} *_3^1 \dots *_3^1 \mathcal{T}^{(1)} *_3^1 \mathcal{X}^{(1)}, \quad (4.17)$$

from which we derive the noiseless signal tensor received at destination,  $(K + 1)$ -th node, as

$$\mathcal{X}^{(K+1)} = \mathcal{T}^{(K)} *_3^1 \mathcal{T}^{(K-1)} *_3^1 \dots *_3^1 \mathcal{T}^{(1)} *_3^1 \mathcal{X}^{(1)} \in \mathbb{C}^{M_{K+1}^r \times P_K \times \dots \times P_0 \times N}. \quad (4.18)$$

The tensor (4.18) satisfies a  $(K+3)$ -th order HONTD – Equations (3.4)-(3.5) – with the following correspondences

$$(\mathbf{A}, \mathcal{G}^{(N)}, \mathbf{B}^{(N-1)}, \mathcal{G}^{(N-1)}, \dots, \mathbf{B}^{(0)}, \mathcal{G}^{(0)}, \mathbf{C}) \Leftrightarrow (\mathbf{H}^{(K)}, \mathcal{C}^{(K)}, \mathbf{H}^{(K-1)}, \mathcal{C}^{(K-1)}, \dots, \mathbf{H}^{(0)}, \mathcal{C}^{(0)}, \mathbf{S}). \quad (4.19)$$

Note that for the node  $k = 0$ , since the tensor  $\mathcal{T}^{(k)}$  is defined for  $k = 1, \dots, K$ , the signal model in (4.17) becomes the received signal  $\mathcal{X}^{(1)}$  defined in (4.2) for the first hop.

## 4.2 Semi-blind receivers

In this section, we exploit the tensor model of the multi-hop MIMO relaying system presented in Section 4.1 to develop two new semi-blind receivers to jointly estimate the symbols and the channel matrices. The first one is an iterative algorithm based on ALS method, while the second one is a closed-form solution based on LS estimation of Kronecker products (KP), denoted by LSKP.

The estimation of the unknown parameters in a unique way is related to the uniqueness properties of the involved tensor models. A HONTD-based model is unique up to scaling ambiguities when the core tensors are known (see Theorem 4, Subsection 3.1.1). Thus, we assume that the tensor codings used by the source and the relays, corresponding to the core tensors of the Tucker models in (4.17), are known at destination. In the sequel, for the sake of simplicity, the equations are derived for the noiseless case.

### 4.2.1 ALS Receiver

In the sequel, we establish matrix unfoldings of the tensor  $\mathcal{X}^{(K+1)}$  of signals received at destination that will be used to derive the LS cost functions of the ALS-based algorithm for estimating the unknown matrices  $\mathbf{S}$  and  $\mathbf{H}^{(k)}$ , for  $k = 0, \dots, K$ . For that, we rewrite the signal tensor received at destination, using (4.15) and (4.18), in  $K + 1$  different ways (with respect to each hop), as follows

$$\text{for } k = 0, \quad \mathcal{X}^{(K+1)} = \mathcal{A}^{(0)} *_3^1 \mathcal{X}^{(1)}, \quad (4.20)$$

$$\begin{aligned} \text{for } k = 1, \dots, K-1, \quad \mathcal{X}^{(K+1)} &= \mathcal{A}^{(k)} *_3^1 \mathcal{X}^{(k+1)} \\ &= \mathcal{A}^{(k)} *_3^1 \mathcal{T}^{(k)} *_3^1 \mathcal{X}^{(k)} \end{aligned} \quad (4.21)$$

$$\text{for } k = K, \quad \mathcal{X}^{(K+1)} = \mathcal{T}^{(K)} *_3^1 \mathcal{X}^{(K)}, \quad (4.22)$$

with  $\mathcal{X}^{(k)}$  being defined in (4.17) and the auxiliary tensor  $\mathcal{A}^{(k)} \in \mathbb{C}^{M_{K+1}^r \times P_K \times \dots \times P_{k+1} \times M_{k+1}^r}$  accumulating the factors on the left of  $\mathcal{T}^{(k)}$  as follows

$$\mathcal{A}^{(k)} = \mathcal{T}^{(K)} *_3^1 \dots *_3^1 \mathcal{T}^{(k+1)}, \quad \text{if } k \in \{0, \dots, K-1\}. \quad (4.23)$$

Note that the tensors  $\mathcal{A}^{(k)}$  is not defined for  $k = K$  and  $\mathcal{T}^{(k)}$  is not defined for  $k = 0$ .

Firstly, let us analyse the case  $k = K$ . Since the auxiliary tensor  $\mathcal{A}^{(K)}$  is not defined, we get the  $K$ -th contracted tensor from (4.22) as

$$\mathcal{X}_K^{(K+1)} = \mathcal{C}^{(K)} \times_1 \mathbf{H}^{(K)} \times_3 \mathbf{X}_{P_{K-1} \dots P_0 N \times M_K^r}^{(K)}. \quad (4.24)$$

Since the tensor in (4.24) satisfies a Tucker-(2, 3) decomposition, by using the matricization defined in (2.26), we can obtain the following matrix unfolding

$$\mathbf{X}_{P_K \dots P_0 N \times M_{K+1}^r}^{(K+1)} = \left( \mathbf{I}_{P_K} \otimes \mathbf{X}_{P_{K-1} \dots P_0 N \times M_K^r}^{(K)} \right) \mathbf{C}_{P_K M_K^r \times M_K^t}^{(K)} \mathbf{H}^{(K)T}, \quad (4.25)$$

where  $\mathbf{X}_{P_{K-1} \dots P_0 N \times M_K^r}^{(K)}$  is obtained by combining some modes of the tensor  $\mathcal{X}^{(K)}$ . This unfolded matrix will be useful to estimate the channel matrix  $\mathbf{H}^{(K)}$ .

By combining some modes of the tensors  $\mathcal{A}^{(k)}$  and  $\mathcal{X}^{(k)}$ , we can get the tall matrix unfoldings  $\mathbf{A}_{M_{K+1}^r P_K \dots P_{k+1} \times M_{k+1}^r}^{(k)}$  and  $\mathbf{X}_{P_{k-1} \dots P_0 N \times M_k^r}^{(k)}$ , from which we can rewrite the tensor  $\mathcal{X}^{(K+1)}$  in (4.21) as a  $k$ -th contracted tensor  $\mathcal{X}_k^{(K+1)} \in \mathbb{C}^{M_{K+1}^r P_K \dots P_{k+1} \times P_k \times P_{k-1} \dots P_0 N}$  given as

$$\begin{aligned} \mathcal{X}_k^{(K+1)} &= \mathcal{T}^{(k)} \times_1 \mathbf{A}_{M_{K+1}^r P_K \dots P_{k+1} \times M_{k+1}^r}^{(k)} \times_3 \mathbf{X}_{P_{k-1} \dots P_0 N \times M_k^r}^{(k)} \\ &= \mathcal{C}^{(k)} \times_1 \mathbf{A}_{M_{K+1}^r P_K \dots P_{k+1} \times M_{k+1}^r}^{(k)} \mathbf{H}^{(k)} \times_3 \mathbf{X}_{P_{k-1} \dots P_0 N \times M_k^r}^{(k)}. \end{aligned} \quad (4.26)$$

The unfoldings  $\mathbf{A}_{M_{K+1}^r P_K \dots P_{k+1} \times M_{k+1}^r}^{(k)}$  and  $\mathbf{X}_{P_{k-1} \dots P_0 N \times M_k^r}^{(k)}$  can be obtained from Definition 6. The contracted tensor (4.26) satisfies a Tucker-(2, 3) decomposition and can be exploited to derive LS cost functions useful for estimating the channel matrices  $\mathbf{H}^{(k)}$ , for  $k = 1, \dots, K-1$ . Thus, (4.26) gives the following matrix representation for the tensor  $\mathcal{X}^{(K+1)}$  of received signals

$$\mathbf{X}_{P_k \dots P_0 N \times M_{K+1}^r P_K \dots P_{k+1}}^{(K+1)} = \left( \mathbf{I}_{P_k} \otimes \mathbf{X}_{P_{k-1} \dots P_0 N \times M_k^r}^{(k)} \right) \mathbf{C}_{P_k M_k^r \times M_k^t}^{(k)} \left( \mathbf{A}_{M_{K+1}^r P_K \dots P_{k+1} \times M_{k+1}^r}^{(k)} \mathbf{H}^{(k)} \right)^T. \quad (4.27)$$

By applying the Property 1, we can easily get a vectorized form of the matrix in (4.27)

$$\begin{aligned} \mathbf{x}_k^{(K+1)} &= \text{vec} \left( \mathbf{X}_{P_k \dots P_0 N \times M_{K+1}^r P_K \dots P_{k+1}}^{(K+1)} \right) \in \mathbb{C}^{M_{K+1}^r P_K \dots P_0 N} \\ &= \left[ \mathbf{A}_{M_{K+1}^r P_K \dots P_{k+1} \times M_{k+1}^r}^{(k)} \otimes \left( \mathbf{I}_{P_k} \otimes \mathbf{X}_{P_{k-1} \dots P_0 N \times M_k^r}^{(k)} \right) \mathbf{C}_{P_k M_k^r \times M_k^t}^{(k)} \right] \text{vec} \left( \mathbf{H}^{(k)T} \right). \end{aligned} \quad (4.28)$$

This vector will be useful to estimate the channel matrices  $\mathbf{H}^{(k)}$ , for  $k = 1, \dots, K-1$ .

Finally, for  $k = 0$ , since the tensor  $\mathcal{T}^{(0)}$  is not defined, the tensor  $\mathcal{X}^{(K+1)}$  can be rewritten from the first line of (4.20) as

$$\mathcal{X}^{(K+1)} = \mathcal{A}^{(0)} *_{K+2}^1 \mathcal{X}^{(1)}. \quad (4.29)$$

By combining some modes of  $\mathcal{A}^{(0)}$ , we define the following contracted tensor

$$\begin{aligned} \mathcal{X}_0^{(K+1)} &= \mathcal{X}^{(1)} \times_1 \mathbf{A}_{M_{K+1}^r P_K \dots P_1 \times M_1^r}^{(0)} \\ &= \mathcal{C}^{(0)} \times_1 \mathbf{A}_{M_{K+1}^r P_K \dots P_1 \times M_1^r}^{(0)} \mathbf{H}^{(0)} \times_3 \mathbf{S} \in \mathbb{C}^{M_{K+1}^r P_K \dots P_1 \times P_0 \times N}, \end{aligned} \quad (4.30)$$

from which are obtained the following unfolded matrices

$$\mathbf{X}_{M_{K+1}^r P_K \dots P_0 \times N}^{(K+1)} = \left( \mathbf{A}_{M_{K+1}^r P_K \dots P_1 \times M_1^r}^{(0)} \mathbf{H}^{(0)} \otimes \mathbf{I}_{P_0} \right) \mathbf{C}_{M_0^t P_0 \times R}^{(0)} \mathbf{S}^T \quad (4.31)$$

$$\mathbf{X}_{P_0 N \times M_{K+1}^r P_K \dots P_1}^{(K+1)} = \left( \mathbf{I}_{P_0} \otimes \mathbf{S} \right) \mathbf{C}_{P_0 R \times M_0^t}^{(0)} \left( \mathbf{A}_{M_{K+1}^r P_K \dots P_1 \times M_1^r}^{(0)} \mathbf{H}^{(0)} \right)^T. \quad (4.32)$$

The unfolding (4.31) will be useful to estimate the symbol matrix  $\mathbf{S}$ , while the unfolding (4.32) will be useful to estimate the channel matrix  $\mathbf{H}^{(0)}$  under its vectorized form. By applying the Property 1, we get

$$\begin{aligned} \mathbf{x}_0^{(K+1)} &= \text{vec} \left( \mathbf{X}_{P_0 N \times M_{K+1}^r P_K \dots P_1}^{(K+1)} \right) \in \mathbb{C}^{M_{K+1}^r P_K \dots P_0 N} \\ &= \left[ \mathbf{A}_{M_{K+1}^r P_K \dots P_1 \times M_1^r}^{(0)} \otimes \left( \mathbf{I}_{P_0} \otimes \mathbf{S} \right) \mathbf{C}_{P_0 R \times M_0^t}^{(0)} \right] \text{vec} \left( \mathbf{H}^{(0)T} \right). \end{aligned} \quad (4.33)$$

Note that the vectorizations in (4.33) and (4.28) are different ways of writing the same unfolding of  $\mathcal{X}^{(K+1)}$ .

From the unfoldings (4.25), (4.28), (4.31) and (4.33), we deduce the following LS cost functions that will be minimized (in an alternate and iterative way) with respect to  $\mathbf{H}^{(K)}$ ,  $\mathbf{H}^{(k)}$ ,  $\mathbf{S}$  and  $\mathbf{H}^{(0)}$ , respectively, performing a  $(K+2)$ -step ALS-based algorithm

$$\begin{aligned} \hat{\mathbf{H}}^{(K)} &= \arg \min_{\mathbf{H}^{(K)}} \left\| \mathbf{X}_{P_K \dots P_0 N \times M_{K+1}^r}^{(K+1)} - \left( \mathbf{I}_{P_K} \otimes \right. \right. \\ &\quad \left. \left. \mathbf{X}_{P_{K-1} \dots P_0 N \times M_K^r}^{(K)} \right) \mathbf{C}_{P_K M_K^r \times M_K^t}^{(K)} \mathbf{H}^{(K)T} \right\|_F^2 \end{aligned} \quad (4.34)$$

$$\begin{aligned} \hat{\mathbf{H}}^{(k)} &= \arg \min_{\mathbf{H}^{(k)}} \left\| \mathbf{x}^{(K+1)} - \left[ \mathbf{A}_{M_{K+1}^r P_K \dots P_{k+1} \times M_{k+1}^r}^{(k)} \otimes \right. \right. \\ &\quad \left. \left( \mathbf{I}_{P_k} \otimes \mathbf{X}_{P_{k-1} \dots P_0 N \times M_k^r}^{(k)} \right) \mathbf{C}_{P_k M_k^r \times M_k^t}^{(k)} \right] \text{vec} \left( \mathbf{H}^{(k)T} \right) \right\|_F^2 \end{aligned} \quad (4.35)$$

$$\begin{aligned} \hat{\mathbf{S}} &= \arg \min_{\mathbf{S}} \left\| \mathbf{X}_{M_{K+1}^r P_K \dots P_0 \times N}^{(K+1)} - \left( \mathbf{A}_{M_{K+1}^r P_K \dots P_1 \times M_1^r}^{(0)} \mathbf{H}^{(0)} \otimes \right. \right. \\ &\quad \left. \left. \mathbf{I}_{P_0} \right) \mathbf{C}_{M_0^t P_0 \times R}^{(0)} \mathbf{S}^T \right\|_F^2 \end{aligned} \quad (4.36)$$

$$\begin{aligned} \hat{\mathbf{H}}^{(0)} &= \arg \min_{\mathbf{H}^{(0)}} \left\| \mathbf{x}^{(K+1)} - \left[ \mathbf{A}_{M_{K+1}^r P_K \dots P_1 \times M_1^r}^{(0)} \otimes \right. \right. \\ &\quad \left. \left( \mathbf{I}_{P_0} \otimes \mathbf{S} \right) \mathbf{C}_{P_0 R \times M_0^t}^{(0)} \right] \text{vec} \left( \mathbf{H}^{(0)T} \right) \right\|_F^2. \end{aligned} \quad (4.37)$$

Table 1 – ALS receiver for multi-hop MIMO relay system

---

1. Randomly initialize  $\widehat{\mathbf{S}}_{it=0}$  and  $\widehat{\mathbf{H}}_{it=0}^{(k)}$ , for  $k = 0, \dots, K - 1$
2. Update the tensor  $\widehat{\mathcal{X}}_{it}^{(K)}$
3.  $it \leftarrow it + 1$
4. Calculate the LS estimate of  $\mathbf{H}^{(K)}$ :
 
$$\widehat{\mathbf{H}}_{it}^{(K)T} = \left[ \left( \mathbf{I}_{P_K} \otimes \left( \widehat{\mathbf{X}}_{P_{K-1} \dots P_0 N \times M_K^r} \right)_{it-1} \right) \mathbf{C}_{P_K M_K^r \times M_K^t}^{(K)} \right]^\dagger \widehat{\mathbf{X}}_{P_K \dots P_0 N \times M_{K+1}^r}^{(K+1)}$$
5. Calculate the LS estimate of  $\mathbf{H}^{(k)}$ :
 

for  $k = K - 1 : 1$

update the tensors  $\widehat{\mathcal{X}}_{it}^{(k)}$  and  $\widehat{\mathcal{A}}_{it}^{(k)}$   

$$\text{vec} \left( \widehat{\mathbf{H}}_{it}^{(k)T} \right) = \left[ \left( \widehat{\mathbf{A}}_{M_{K+1}^r P_K \dots P_{k+1} \times M_{k+1}^r} \right)_{it} \otimes \left( \mathbf{I}_{P_k} \otimes \left( \widehat{\mathbf{X}}_{P_{k-1} \dots P_0 N \times M_k^r} \right)_{it} \right) \mathbf{C}_{P_k M_k^r \times M_k^t}^{(k)} \right]^\dagger \widehat{\mathbf{X}}^{(K+1)}$$

end
6. Update the tensor  $\widehat{\mathcal{A}}_{it}^{(0)}$  and calculate the LS estimate of  $\mathbf{S}$ :
 
$$\widehat{\mathbf{S}}_{it}^T = \left[ \left( \left( \widehat{\mathbf{A}}_{M_{K+1}^r P_K \dots P_1 \times M_1^r} \right)_{it} \widehat{\mathbf{H}}_{it-1}^{(0)} \otimes \mathbf{I}_{P_0} \right) \mathbf{C}_{M_0^t P_0 \times R}^{(0)} \right]^\dagger \widehat{\mathbf{X}}_{M_{K+1}^r P_K \dots P_0 \times N}^{(K+1)}$$
7. Calculate the LS estimate of  $\mathbf{H}^{(0)}$ :
 
$$\text{vec} \left( \widehat{\mathbf{H}}_{it}^{(0)T} \right) = \left[ \left( \widehat{\mathbf{A}}_{M_{K+1}^r P_K \dots P_1 \times M_1^r} \right)_{it} \otimes \left( \mathbf{I}_{P_0} \otimes \widehat{\mathbf{S}}_{it} \right) \mathbf{C}_{P_0 R \times M_0^t}^{(0)} \right]^\dagger \widehat{\mathbf{X}}^{(K+1)}$$
8. Return to step 2 until convergence.
9. Eliminate the scaling ambiguities using (4.40) and project the estimated symbols onto the symbol alphabet.

---

The ALS receiver derived from the LS cost functions (4.34)-(4.37) is summarized in Table 1. It is worth to note that all unknown parameters are estimated from the noisy signal tensor received at destination, avoiding error propagation.

#### *Identifiability conditions and ambiguity relations*

For computing the pseudo-inverses in the steps 4 to 7 of the Table 1, some conditions are required to ensure the uniqueness of LS solutions. Their arguments must be left-invertible, i.e., they must be full column rank. The analysis of the necessary conditions that ensure its uniqueness depends on the number  $K$  of relays and must be carried out by considering the Properties 3 and 4 (Section 2.1). For the case  $K = 2$ , the following necessary conditions are required

$$\begin{aligned}
 P_0 &\geq \max \left( \frac{M_0^t}{R}, \frac{R}{M_0^t}, \frac{M_1^r}{N} \right), & P_1 &\geq \max \left( \frac{M_1^r}{M_2^r}, \frac{M_2^r}{M_1^r} \right), \\
 P_2 &\geq \max (M_2^r/M_3^r), & M_1^r &\geq M_0^t, & N &\geq R.
 \end{aligned} \tag{4.38}$$

From the Theorem 4, the unknown parameters are affected by the following scaling ambiguities:  $\widehat{\mathbf{S}} = \delta_{\mathbf{S}} \mathbf{S}$  and  $\widehat{\mathbf{H}}^{(k)} = \delta_{\mathbf{H}^{(k)}} \mathbf{H}^{(k)}$ , for  $k = 0, \dots, K$ , such that

$$\delta_{\mathbf{S}} \left( \prod_{k=0}^K \delta_{\mathbf{H}^{(k)}} \right) = 1. \tag{4.39}$$

The scaling ambiguity of  $\widehat{\mathbf{S}}$  can be removed by assuming the a priori knowledge of one pilot symbol ( $s_{1,1}$ ). Concerning the scaling ambiguity of  $\widehat{\mathbf{H}}^{(k)}$ , in order to plot the simulation results, we assumed that one coefficient ( $h_{1,1}^{(k)}$ ) of each channel is known at destination. This assumption has already been adopted in other works [18, 20, 21, 24, 34, 42] in the context of relaying systems. In practice, such a priori information could be obtained by a simple LS estimation using a pilot-symbol generated by the relays [24]. If the use of a pilot-symbol isn't possible, the channel matrices  $\widehat{\mathbf{H}}^{(k)}$  are estimated up to a scalar constant. However, this ambiguity would not affect the symbol estimation neither the design of precoding schemes with CSI. Thus, to eliminate the scaling ambiguities on the estimated parameters, we use the following equations

$$\begin{aligned}\widehat{\mathbf{S}} &\leftarrow (\delta_{\mathbf{S}})^{-1} \widehat{\mathbf{S}} \\ \widehat{\mathbf{H}}^{(k)} &\leftarrow (\delta_{\mathbf{H}^{(k)}})^{-1} \widehat{\mathbf{H}}^{(k)},\end{aligned}\quad (4.40)$$

with  $\delta_{\mathbf{S}} = \widehat{s}_{1,1}/s_{1,1}$  and  $\delta_{\mathbf{H}^{(k)}} = \widehat{h}_{1,1}^{(k)}/h_{1,1}^{(k)}$ .

#### 4.2.2 LSKP Receiver

The LSKP receiver, unlike the ALS-based algorithm, is a closed-form (non-iterative) solution based on LS estimation of factors that compose Kronecker products, by applying a SVD-based low-rank approximation algorithm, introduced in [91] and proposed for the first time in [40] for point-to-point systems. Appendix C shows the procedure of estimation of the matrix factors of a Kronecker product by low-rank approximation.

Starting from (4.15), we can get a contracted tensor similar to (4.24) for the noiseless signal tensor  $\mathcal{X}^{(k+1)}$  received by the node  $k+1$ , for  $k = 1, \dots, K$ . Thus, by combining the last  $k+1$  modes, the following contracted tensor satisfies a Tucker-(2, 3) model

$$\mathcal{X}_k^{(k+1)} = \mathcal{C}^{(k)} \times_1 \mathbf{H}^{(k)} \times_3 \mathbf{X}_{P_{k-1} \dots P_0 N \times M_k^r}^{(k)} \in \mathbb{C}^{M_{k+1}^r \times P_k \times P_{k-1} \dots P_0 N}. \quad (4.41)$$

A tall mode-2 unfolding of the above model is given by

$$\mathbf{X}_{M_{k+1}^r P_{k-1} \dots P_0 N \times P_k}^{(k+1)} = \left( \mathbf{H}^{(k)} \otimes \mathbf{X}_{P_{k-1} \dots P_0 N \times M_k^r}^{(k)} \right) \mathbf{C}_{M_k^t M_k^r \times P_k}^{(k)}. \quad (4.42)$$

Let us now define the KP  $\Omega^{(k)} = \mathbf{H}^{(k)} \otimes \mathbf{X}_{P_{k-1} \dots P_0 N \times M_k^r}^{(k)} \in \mathbb{C}^{M_{k+1}^r P_{k-1} \dots P_0 N \times M_k^t M_k^r}$ , such that we can derive the LS estimation of  $\Omega^{(k)}$  as

$$\widehat{\Omega}^{(k)} = \mathbf{X}_{M_{k+1}^r P_{k-1} \dots P_0 N \times P_k}^{(k+1)} \left( \mathbf{C}_{M_k^t M_k^r \times P_k}^{(k)} \right)^\dagger. \quad (4.43)$$

The main idea of the proposed receiver is to estimate recursively the channel matrix  $\mathbf{H}^{(k)}$  and the matrix unfolding  $\mathbf{X}_{P_{k-1}\dots P_0 N \times M_k^r}^{(k)}$ , from  $k = K$  to  $k = 1$ , by using the LS estimate (4.43) of  $\Omega^{(k)}$  and applying the low-rank approximation algorithm.

In order to avoid error propagation effects, the symbol matrix  $\mathbf{S}$  is directly estimated using the tensor of signals received at destination, as detailed below. From the contracted tensor in (4.30), we define the matrix  $\mathbf{B} = \mathbf{A}_{M_{K+1}^r P_K \dots P_1 \times M_1^r}^{(0)} \mathbf{H}^{(0)}$  and take a tall mode-2 unfolding, obtaining

$$\mathbf{X}_{M_{K+1}^r P_K \dots P_1 N \times P_0}^{(K+1)} = (\mathbf{B} \otimes \mathbf{S}) \mathbf{C}_{M_0^s R \times P_0}^{(0)}. \quad (4.44)$$

Thus, defining  $\Omega^{(0)} = \mathbf{B} \otimes \mathbf{S}$ , we get the following LS estimate for  $\Omega^{(0)}$

$$\widehat{\Omega}^{(0)} = \mathbf{X}_{M_{K+1}^r P_K \dots P_1 N \times P_0}^{(K+1)} \left( \mathbf{C}_{M_0^s R \times P_0}^{(0)} \right)^\dagger. \quad (4.45)$$

Once  $\widehat{\Omega}^{(0)}$  estimated using the signals received at destination, the SVD-based low-rank approximation algorithm allows us to estimate the Kronecker factors  $\mathbf{B}$  and  $\mathbf{S}$  directly from the signals  $\mathcal{X}^{(K+1)}$  received at destination. The LS estimate of the channel matrix  $\mathbf{H}^{(0)}$  is then given by

$$\widehat{\mathbf{H}}^{(0)} = \left( \widehat{\mathbf{A}}_{M_{K+1}^r P_K \dots P_1 \times M_1^r}^{(0)} \right)^\dagger \widehat{\mathbf{B}}. \quad (4.46)$$

The estimated matrix  $\widehat{\mathbf{A}}_{M_{K+1}^r P_K \dots P_1 \times M_1^r}^{(0)}$  is obtained from (4.23) with the channel matrices replaced by their estimates  $\widehat{\mathbf{H}}^{(k)}$ , for  $k = 1, \dots, K$ , obtained in previous steps of the algorithm. The LSKP receiver derived from the LS estimates (4.43), (4.45) and (4.46) is summarized in Table 2.

The LSKP algorithm has the interesting advantage of benefiting from the choice of a coding designed from a unitary (or orthogonal in the real case) matrix. This comes from the fact that the LSKP technique uses only one matrix unfolding of each coding tensor. The ‘‘unitary coding’’ consists of a tensor chosen in such a way that one of its unfoldings is a truncated unitary matrix, leading the unfolded coding to be row-orthonormal. Since a row-orthonormal matrix  $\mathbf{C}$  has its Hermitian transpose equal to its inverse (i.e.  $\mathbf{C}^H \mathbf{C} = \mathbf{I}$ ), the computation of the pseudo-inverses in (4.43) and (4.45) are simplified. Although the term ‘‘unitary’’ is related to a square matrix, we will use throughout this thesis the term ‘‘unitary coding’’ for the row-orthonormal unfolded matrices, whether square or not.

In addition, unitary transformations are isometric (i.e. preserve the norm), leading the LSKP algorithm to benefit of exploit the following property [92].

Table 2 – LSKP receiver for multi-hop MIMO relay system

---

**Stage 1: estimation of the channel matrices  $\mathbf{H}^{(k)}$ , for  $k = 1, \dots, K$**

1.  $\widehat{\mathbf{X}}_{M_{K+1}^r P_{K-1} \dots P_0 N \times P_K}^{(K+1)} = \widetilde{\mathbf{X}}_{M_{K+1}^r P_{K-1} \dots P_0 N \times P_K}^{(K+1)}$ .
2. Calculate the estimates of  $\mathbf{H}^{(k)}$  and  $\mathbf{X}_{P_{k-1} \dots P_0 N \times M_k^r}^{(k)}$  from  $\boldsymbol{\Omega}^{(k)} = \mathbf{H}^{(k)} \otimes \mathbf{X}_{P_{k-1} \dots P_0 N \times M_k^r}^{(k)}$ :  
for  $k = K : 1$ 

$\widehat{\boldsymbol{\Omega}}^{(k)} = \widehat{\mathbf{X}}_{M_{k+1}^r P_{k-1} \dots P_0 N \times P_k}^{(k+1)} \left( \mathbf{C}_{M_k^t M_k^r \times P_k}^{(k)} \right)^\dagger$ Apply the low-rank approximation algorithm in Appendix C to obtain $\widehat{\mathbf{H}}^{(k)}$ and $\widehat{\mathbf{X}}_{P_{k-1} \dots P_0 N \times M_k^r}^{(k)}$ $\widehat{\mathbf{X}}_{M_k^r P_{k-2} \dots P_0 N \times P_{k-1}}^{(k)} \leftarrow \text{reshape} \left( \widehat{\mathbf{X}}_{P_{k-1} \dots P_0 N \times M_k^r}^{(k)} \right)$
---

end

**Stage 2: estimation of the channel  $\mathbf{H}^{(0)}$  and symbol  $\mathbf{S}$  matrices**

3. Calculate the estimates of  $\mathbf{B}$  and  $\mathbf{S}$  from  $\boldsymbol{\Omega}^{(0)} = \mathbf{B} \otimes \mathbf{S}$ :

$$\widehat{\boldsymbol{\Omega}}^{(0)} = \mathbf{X}_{M_{K+1}^r P_K \dots P_1 N \times P_0}^{(K+1)} \left( \mathbf{C}_{M_0^t R \times P_0}^{(0)} \right)^\dagger.$$

Apply the low-rank approximation algorithm in Appendix C to obtain  $\widehat{\mathbf{B}}$  and  $\widehat{\mathbf{S}}$

4. Build  $\widehat{\mathbf{A}}^{(0)}$  from (4.23), with  $\widehat{\mathcal{T}}^{(k)}$  composed by  $\widehat{\mathbf{H}}^{(k)}$  estimated in Stage 1
5. Calculate the LS estimate of  $\mathbf{H}^{(0)}$  using:

$$\widehat{\mathbf{H}}^{(0)} = \left( \widehat{\mathbf{A}}_{M_{K+1}^r P_K \dots P_1 \times M_1^r}^{(0)} \right)^\dagger \widehat{\mathbf{B}}.$$

6. Eliminate the scaling ambiguities using (4.40) and project the estimated symbols onto the symbol alphabet.
- 

**Property 6.** Let  $H_1$  and  $H_2$  be two Hermitian spaces of the same finite dimension. A transformation  $\mathbf{T} : H_1 \rightarrow H_2$  is a unitary transformation, or a linear isometry, if it is linear and

$$\|\mathbf{T}\mathbf{x}\| = \|\mathbf{x}\|, \quad (4.47)$$

for all  $\mathbf{x} \in H_1$ .

*Proof.* Since the norm of a vector  $\mathbf{x}$  is given by

$$\|\mathbf{x}\| = \sqrt{\langle \mathbf{x}, \mathbf{x} \rangle} = \sqrt{\mathbf{x}^H \mathbf{x}},$$

we have

$$\|\mathbf{T}\mathbf{x}\| = \sqrt{(\mathbf{T}\mathbf{x})^H \mathbf{T}\mathbf{x}} = \sqrt{\mathbf{x}^H \mathbf{T}^H \mathbf{T}\mathbf{x}}.$$

As  $\mathbf{T}^H \mathbf{T} = \mathbf{I}$ , then  $\|\mathbf{T}\mathbf{x}\| = \sqrt{\mathbf{x}^H \mathbf{x}} = \|\mathbf{x}\|$ . □

Thus, by allowing the exploitation of unitary coding, the LSKP receiver avoids noise enhancement by conserving the energy of the received signals.

*Identifiability conditions and ambiguity relations*

The parameter identifiability is linked to the uniqueness of the LS estimates (4.43) and (4.45), which require the unfoldings  $\mathbf{C}_{M_k^t M_k^r \times P_k}^{(k)}$  and  $\mathbf{C}_{M_0^t R \times P_0}^{(0)}$  to be full row rank to compute their right inverse. That leads to the necessary identifiability conditions  $P_k \geq M_k^t M_k^r$  and  $P_0 \geq M_0^t R$ . Regarding (4.46), the unfolding  $\widehat{\mathbf{A}}_{M_{K+1}^r P_K \cdots P_1 \times M_1^t}^{(0)}$  must be left-invertible, which leads to the condition  $M_{K+1}^r P_K \cdots P_1 \geq M_1^t$ .

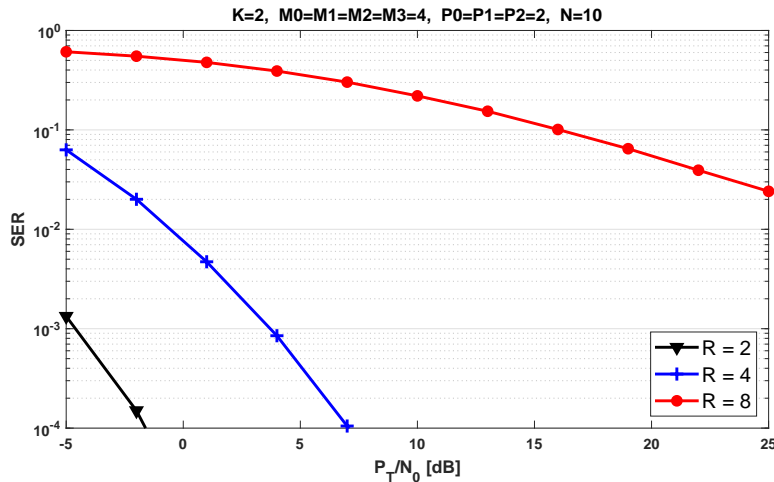
Moreover, the factors of a KP can only be estimated up to scalar ambiguities, as shown in Appendix C. As the steps of the proposed receiver perform the factorization of the KP matrix  $\mathbf{\Omega}^{(k)}$ , the estimated factors have the ambiguities  $\widehat{\mathbf{H}}^{(k)} = \delta_{\mathbf{H}^{(k)}} \mathbf{H}^{(k)}$  and  $\widehat{\mathbf{S}} = \delta_{\mathbf{S}} \mathbf{S}$ . Similarly to the ALS receiver in the previous subsection, these ambiguities are eliminated by assuming a priori knowledge of one pilot symbol ( $s_{1,1}$ ) and one channel coefficient ( $h_{1,1}^{(k)}$ ) of each channel  $\mathbf{H}^{(k)}$ , for  $k = 1, \dots, K$ . The ambiguities are then cancelled as given in (4.40). By comparison, the receiver of [18] based on the estimation of the factors of Khatri-Rao products needs the knowledge of one row of each factor matrix.

### 4.3 Simulation results

In this section, we provide simulation results to illustrate the efficiency of the proposed receivers. The results were averaged over  $5 \times 10^4$  Monte Carlo runs. The SER and channel NMSE are plotted as function of the transmission power to noise spectral density ratio ( $P_T/N_0$ ). White Gaussian noises were added at each receiving node with the same noise variance  $N_0$ . At each run,  $N_0$  was fixed according to the desired  $P_T/N_0$  value. The transmitted symbols were randomly generated from a unit energy 4-QAM alphabet. We assume flat-fading channels, with i.i.d. (independent and identically distributed) complex Gaussian entries. The variance of the channel coefficients follows an exponential path-loss model given by  $\sigma_{\mathbf{H}}^2 = 1/d^4$ , where  $d = D/(K+1)$  is the distance between two relays, and  $D$  is the distance between the source and destination arbitrarily chosen equal to 1. We assume the relays are uniformly distributed between the source and the destination. For all the simulations, we have considered a same number of receive and transmit antennas at the relays, i.e.,  $M_k^r = M_k^t$ . The design parameter values used in the simulations are indicated above each figure.

In Subsections 4.3.1 and 4.3.2, the elements of the coding tensors have unit amplitude and random phase drawn from a uniform distribution between 0 and  $2\pi$ . Each tensor  $\mathcal{C}^{(k)}$  was multiplied by a fixed scalar gain so that the mean power at each transmitting antenna of each node is kept constant. Thus, the coding tensors become  $\mathcal{C}^{(k)} \leftarrow \sqrt{\beta^{(k)}} \mathcal{C}^{(k)}$ , for  $k \in \{0, \dots, K\}$ ,

Figure 15 – ZF receiver performance for different numbers of data stream



with  $\beta^{(k)}$  given by

$$\beta^{(0)} = P_T / R M_0^t \quad (4.48)$$

$$\beta^{(k)} = P_T / (M_k^r M_k^t (P_T \sigma_{\mathbf{H}}^2 + N_0)), \text{ for } k = 1, \dots, K. \quad (4.49)$$

The total transmission power at each node is given as  $P_T = P_{total} / (K + 1)$ , where  $K + 1$  is the number of hops and  $P_{total}$  is the power fixed for the system and arbitrarily chosen equal to 1.

#### 4.3.1 Zero-forcing receiver with perfect channel knowledge

In this subsection, the impact of the choice of the design parameters was evaluated (regardless of the influence of algorithm) in the case of perfect channel knowledge using a zero-forcing (ZF) receiver, which is derived from step 6 of the algorithm in Table 1 and given by

$$\hat{\mathbf{S}}^T = \left[ \left( \mathbf{A}_{M_{K+1}^r P_K \dots P_1 \times M_1^t}^{(0)} \mathbf{H}^{(0)} \otimes \mathbf{I}_{P_0} \right) \mathbf{C}_{M_0^t P_0 \times R}^{(0)} \right]^\dagger \tilde{\mathbf{X}}_{M_{K+1}^r P_K \dots P_0 \times N}^{(K+1)}. \quad (4.50)$$

In the first results, we consider a three-hop system, with two relays ( $K = 2$ ). In the following, we show the impact of the number  $R$  of data streams on symbol estimation performance with the ZF receiver. Figure 15 shows the SER versus  $P_T/N_0$  for  $R \in \{2, 4, 8\}$ . As expected, one can note an increase of the SER when the value of  $R$  is increased. However, a greater number of data streams improves the spectral efficiency by sending more symbols in the same time block.

Figure 16 shows the SER versus  $P_T/N_0$  for different time-spreading lengths  $P_0$ ,  $P_1$  and  $P_2$  of the coding tensors. The significant gain of the configuration  $(P_0, P_1, P_2) = (4, 2, 2)$  with respect to the others shows that it is more efficient to have higher time-spreading at the

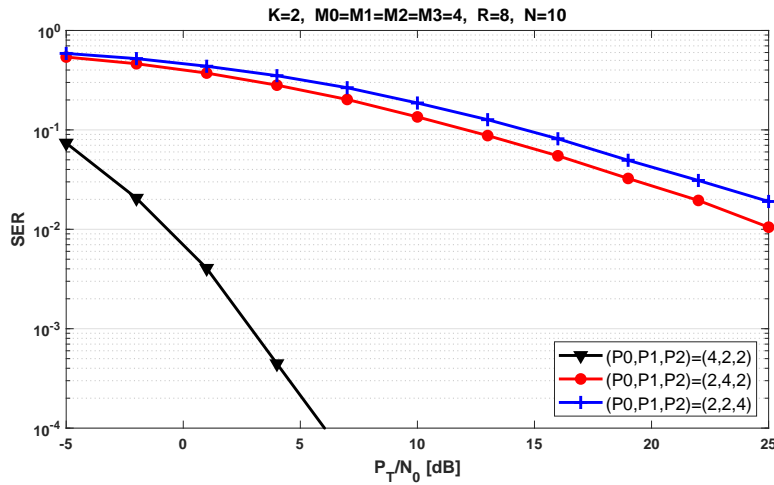
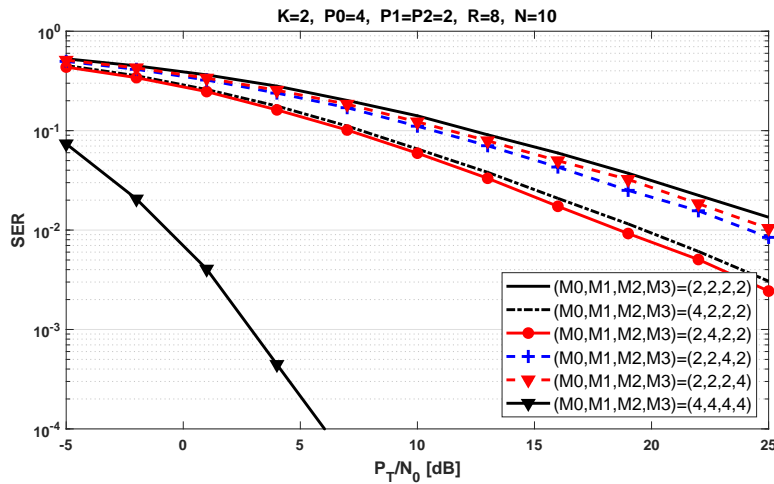
Figure 16 – ZF receiver performance for different values of  $P_0$ ,  $P_1$  and  $P_2$ 

Figure 17 – ZF receiver performance for different numbers of antennas

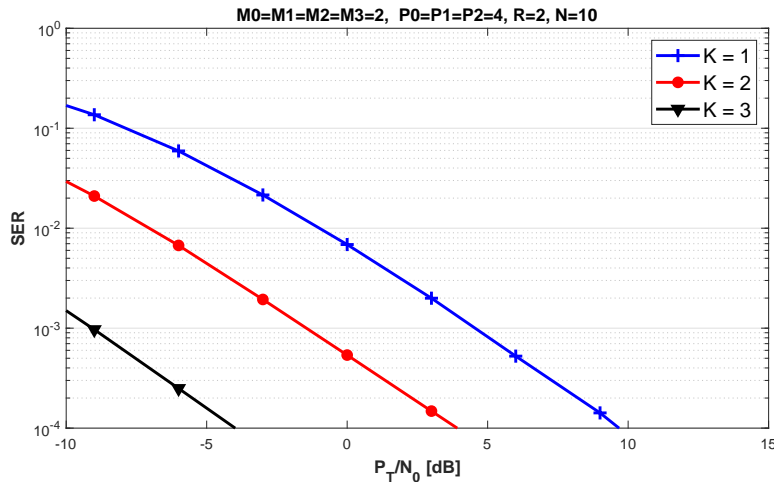


nodes closest to the source. This result comes from the fact that the time-spreading at these nodes is repeated by all the subsequent nodes, increasing even more the number of transmission blocks.

Figure 17 shows the SER versus  $P_T/N_0$  for different numbers of antennas. One can note better results when increasing the number of antennas at the first two hops. These results corroborate the conclusions obtained in [34] concerning a greater efficiency in the exploitation of the spatial diversity at the first hops and can be explained by the dependence of the tensor coding with respect to the number of antennas, which generates redundancy of symbols with less noise and fading in the nodes closer to the source. As expected, the case  $(4, 4, 4, 4)$  yields better performance than all the other cases, due to a greater number of antennas globally used at the source, the relays and the destination, while the case  $(2, 2, 2, 2)$  provides the biggest SER among the tested configurations.

Figure 18 shows the SER versus  $P_T/N_0$  for different numbers of relays,  $K \in$

Figure 18 – ZF receiver performance for different numbers of relays



$\{1, 2, 3\}$ , in order to evaluate the impact of an increase in the number of hops. The case with a single relay ( $K = 1$ ) is equivalent to the two-hop MIMO relay system based on a fourth-order NTD proposed in [34]. We can see that when the number of relays is increased, the SER performance is clearly improved. This result can be explained by the smaller path-loss between nodes and the higher diversity (due to the multiple spreading implemented by the relays) when the number of relays is increased.

#### 4.3.2 ALS receiver performance

The next results evaluate the performance of the proposed semi-blind ALS receiver. For the sake of comparison, we also consider an equivalent one-hop system, corresponding to the case when the direct link is available, where the signals are sent directly from the source to the destination through the channel  $\mathbf{H}^{(0 \rightarrow 3)} \in \mathbb{C}^{M_3^r \times M_0^t}$ . For this case, (4.31) and (4.32) becomes

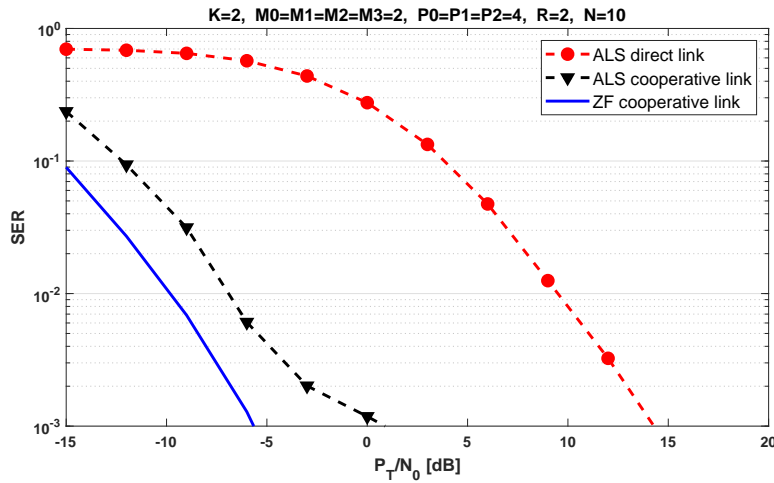
$$\mathbf{X}_{M_3^r P_0 \times N}^{(0 \rightarrow 3)} = (\mathbf{H}^{(0 \rightarrow 3)} \otimes \mathbf{I}_{P_0}) \mathbf{C}_{M_0^t P_0 \times R}^{(0)} \mathbf{S}^T \quad (4.51)$$

$$\mathbf{X}_{P_0 N \times M_3^r}^{(0 \rightarrow 3)} = (\mathbf{I}_{P_0} \otimes \mathbf{S}) \mathbf{C}_{P_0 R \times M_0^t}^{(0)} (\mathbf{H}^{(0 \rightarrow 3)})^T, \quad (4.52)$$

from which we can derive the LS cost functions to estimate the matrices  $\mathbf{H}^{(0 \rightarrow 3)}$  and  $\mathbf{S}$ . The ALS receiver for the single-hop system can be derived from Table 1, excluding the steps 2, 4 and 5 and replacing the steps 6 and 7 by the LS estimates based on (4.51) and (4.52).

For both the cases, the convergence criterion of the iterative algorithms is based on the reconstruction of the received signal tensor ( $\mathcal{X}_{rec}^{(\cdot)}$ ) performed from the estimated parameters. The difference between the Frobenius norm of the current estimation error and the Frobenius norm of the previous estimation error was calculated at each iteration. We have assumed that

Figure 19 – SER performance for the proposed ALS receiver



the convergence is achieved when this difference is less than  $1.0 \times 10^{-5}$ . This procedure is represented below

$$\left( \|\tilde{\mathcal{X}}^{(\cdot)} - \mathcal{X}_{rec}^{(\cdot)}\|_F^2 \right)_{it} - \left( \|\tilde{\mathcal{X}}^{(\cdot)} - \mathcal{X}_{rec}^{(\cdot)}\|_F^2 \right)_{it-1} \leq 1.0 \times 10^{-5}. \quad (4.53)$$

Figure 19 shows the SER versus  $P_T/N_0$  for the ALS receiver with the three-hop (cooperative link) and the one-hop (direct link) scenarios. One can conclude that the proposed three-hop system provides a significant gain over the estimation with the one-hop link. That comes from the multiple TST coding and from the fact that for the three-hop system the path-loss of each hop is smaller than the one of the single-hop system, due to the proportionality of the path-loss to  $d^4$ . For a fixed SER value ( $10^{-3}$ ), it can be observed that the  $P_T/N_0$  gap is around 5 dB and 20 dB for the ALS receivers of the three-hop and one-hop systems, respectively, when compared with the ZF receiver. Despite this degradation, the proposed semi-blind ALS receiver has for advantages on the ZF receiver not to require the a priori knowledge of CSI and also to allow a joint estimation of the symbols and the channels.

Figure 20 shows the number of iterations needed to achieve the convergence by the iterative receivers versus  $P_T/N_0$ . One can note the fastest convergence of the three-hop link for low  $P_T/N_0$  values, showing the advantage of the cooperative network in an adverse situation. However, for high  $P_T/N_0$  values, the smaller number of parameters to be estimated in the direct link increases the speed of convergence, overcoming the one obtained with the relay-assisted link.

In order to evaluate the estimation of the individual channels, Figure 21 shows the channel NMSE versus  $P_T/N_0$  for all the hops of the relay system. The NMSE has been computed

Figure 20 – Convergence of the proposed ALS receiver

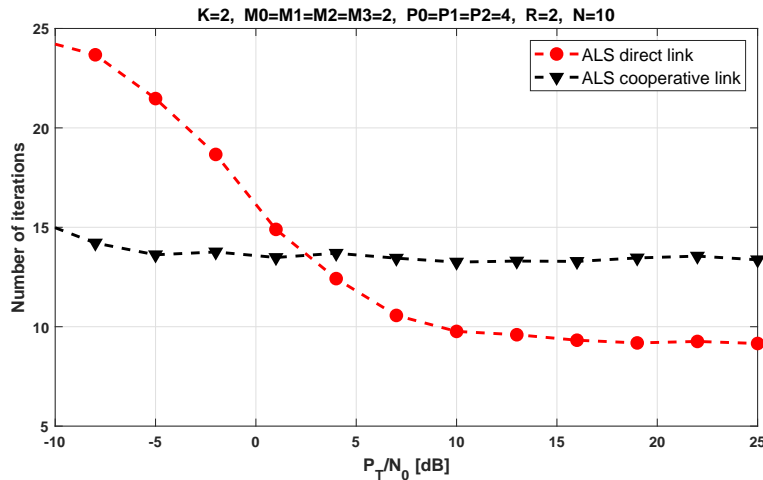
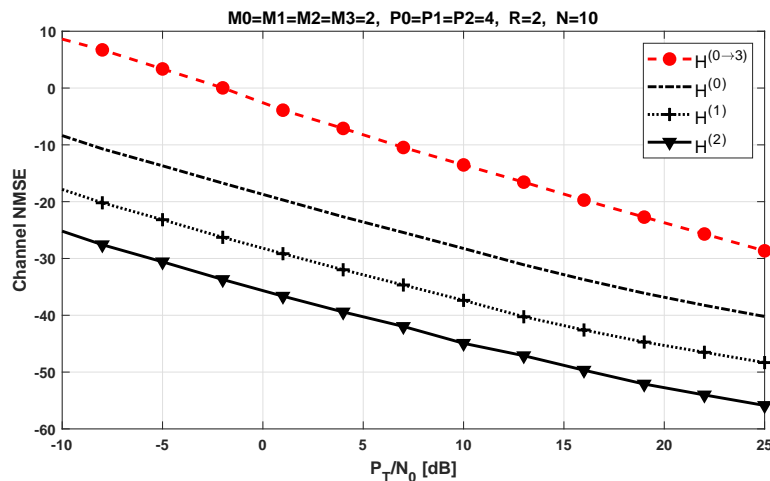


Figure 21 – Channel NMSE for the proposed ALS receiver



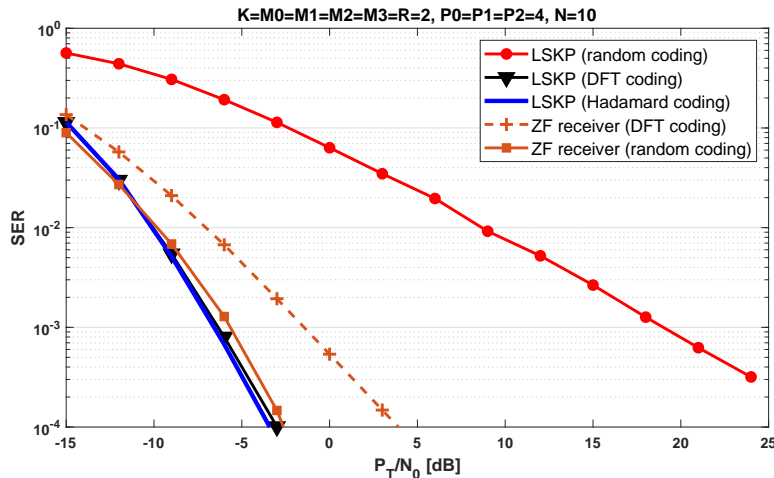
as

$$NMSE = \frac{1}{MC} \sum_{mc} \left( \|\mathbf{H}_{mc} - \hat{\mathbf{H}}_{mc}\|_F^2 \right) / \left( \|\mathbf{H}_{mc}\|_F^2 \right), \quad (4.54)$$

with  $mc = 1, \dots, MC$ ,  $MC$  corresponding to the number of Monte Carlo runs, and  $\mathbf{H}_{mc}$  and  $\hat{\mathbf{H}}_{mc}$  being respectively the real channel and the estimated channel in the  $mc$ -th run. One can note that the channel estimation is improved for the nodes closest to the destination. That comes from the noise enhancement with each new coding applied by the relays. Moreover, we can conclude that the channel estimation is better with the cooperative link than with the direct link.

### 4.3.3 LSKP receiver performance

Now, we evaluate the performance of the proposed LSKP receiver. In this case, three different choices for the coding tensors are considered: i) tensors with elements of unit magnitude

Figure 22 – SER performance comparison with LSKP receiver for  $K = 2$ 

and phase randomly drawn from a uniform distribution between 0 and  $2\pi$ ; ii) tensors such that the unfolding  $\mathbf{C}_{M_0^t R \times P_0}^{(0)}$  (resp.  $\mathbf{C}_{M_k^t M_k^r \times P_k}^{(k)}$ ) is a truncated discrete Fourier transform (DFT) matrix, i.e., composed of the first  $M_0^t R$  (resp.  $M_k^t M_k^r$ ) rows of the DFT matrix of dimension  $P_0 \times P_0$  (resp.  $P_k \times P_k$ ); iii) tensors such that the unfolding  $\mathbf{C}_{M_0^t R \times P_0}^{(0)}$  (resp.  $\mathbf{C}_{M_k^t M_k^r \times P_k}^{(k)}$ ) is a truncated Hadamard matrix, i.e., composed of the first  $M_0^t R$  (resp.  $M_k^t M_k^r$ ) rows of the Hadamard matrix of dimension  $P_0 \times P_0$  (resp.  $P_k \times P_k$ ).

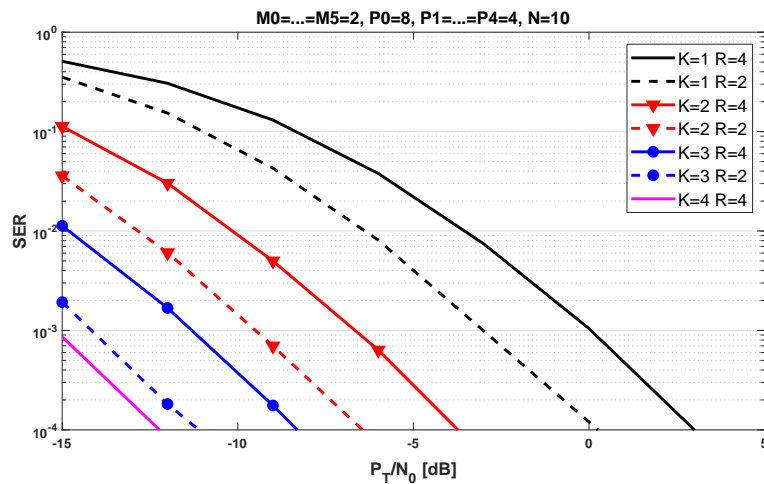
Figure 22 compares the SER versus  $P_T/N_0$  obtained with the proposed LSKP receiver for three different coding tensors and two relays ( $K = 2$ ). We also plot the performance of the ZF receiver introduced in Subsection 4.3.1. The DFT and Hadamard codings with the LSKP receiver give significant SER improvements, overcoming the performance obtained in the other cases. That comes from the fact that in (4.43) and (4.45) – Steps 2 and 3 of the Table 2 – the coding unfolded matrices are unitary, which avoids noise enhancement, since orthogonal transformations preserve the norm and therefore the noise power.

The above conclusion is reached by analyzing the condition number of the pseudo-inverses in (4.45) used by the LSKP receiver for estimating the symbols, as the condition number measures how sensitive a solution is with respect to perturbations in the observed data. It is well known that unitary (isometric) transformations have condition number equal to 1. We have calculated, by means of simulation, the condition number of the pseudo-inverse for each choice of the coding (Hadamard, DFT and random). They are shown in Table 3. The bad conditioning of the pseudo-inverse in (4.45) with the random coding justifies the great degradation of the performance with this coding type. We can also see the similar performances provided by the DFT and Hadamard codings, illustrating the advantage in exploiting the orthogonality property

Table 3 – Condition number of the LSKP and ZF receivers with different codings

Receiver	Coding type	Condition number	
		(mean)	(standard deviation)
LSKP	Hadamard	1	0
	DFT	1	0
	Random	10.32	13.84
ZF	DFT	2.48	1.17
	Random	1.73	0.51

Figure 23 – SER performance with the LSKP receiver for different numbers of relays



regardless of the kind of the used unitary matrix.

It is worth mentioning that a coding with unitary unfoldings is feasible for the LSKP receiver, due to the use of only one matrix unfolding of each coding tensor. This orthogonality property can not be exploited with the ZF receiver, which explains the performance degradation of this receiver. This becomes clear when we observe the conditioning of the pseudo-inverse in (4.50). Table 3 also shows the condition number of this pseudo-inverse for the scenario considered in Figure 22. The non-orthogonality of the pseudo-inverse in (4.50) leads to weaker conditioning, which may cause noise enhancement. From the values in Table 3, we can also conclude that the ZF receiver get a better conditioning with random coding.

Figures 23 and 24 show the SER versus  $P_T/N_0$  for different system configurations, using the DFT coding. In Figure 23, we evaluate the impact of an increase of the number of relays,  $K \in \{1, 2, 3, 4\}$ , for two different values of the number  $R$  of data streams. The multiple time-spreading generated by the TSTC, along with the smaller path-loss of each hop when the number of relays is increased, lead to a performance gain that corroborates the effectiveness of

Figure 24 – SER performance with the LSKP receiver for different values of  $R$  and  $P_0$

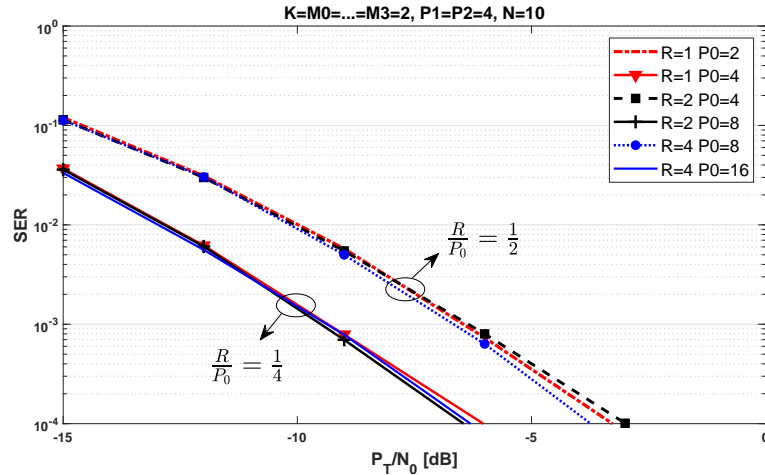
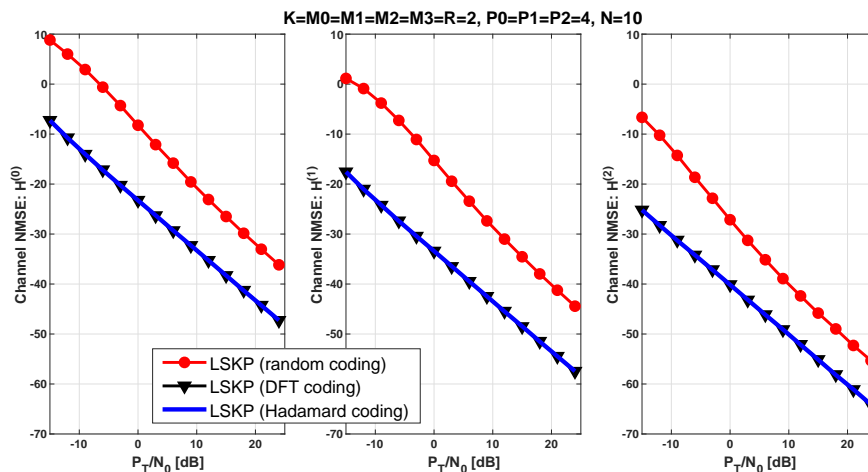


Figure 25 – NMSE of the individual channel estimates with LSKP receiver for  $K = 2$



the multi-hop scenario. One can also note a SER degradation with an increase of  $R$ , due to the larger amount of symbols to be estimated.

Figure 24 shows the impact of the number  $R$  of transmitted data streams and of the time spreading length  $P_0$  at the source. These two parameters are crucial to the transmission rate of the proposed system. For the case with  $K = 2$ , the transmission rate is proportional to  $R/P_0(1 + P_1 + P_1P_2)$ . From this figure, one can conclude that increasing  $P_0$ , with  $R$  fixed, improves the SER, due to a higher time-diversity at the source, at the cost of a smaller transmission rate. On the other hand, increasing  $R$  with  $P_0$  fixed leads to higher SERs, due to a larger number of symbols to be estimated. Note that a same value of  $R/P_0$  implies the same transmission rate, with similar SERs.

Figure 25 shows the channel NMSE versus  $P_T/N_0$  for the individual channels. We

compare the NMSE obtained with the random, DFT and Hadamard codings for the proposed receiver. The results corroborate with the advantage of the system with unitary (DFT and Hadamard) codings, when compared with a random coding. Moreover, the results show a channel estimation improvement for the hops closest to destination. That comes from the recurrent channel estimation that begins with the last hop and ends with the first hop, leading to an error propagation from the nodes closest to destination to the others.

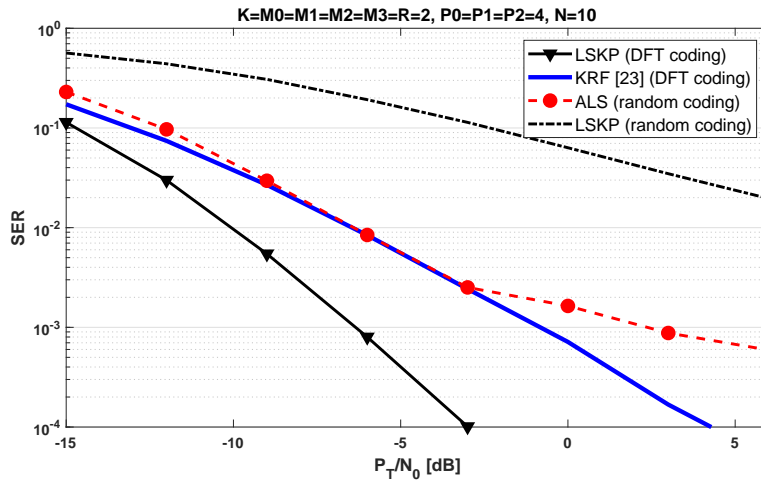
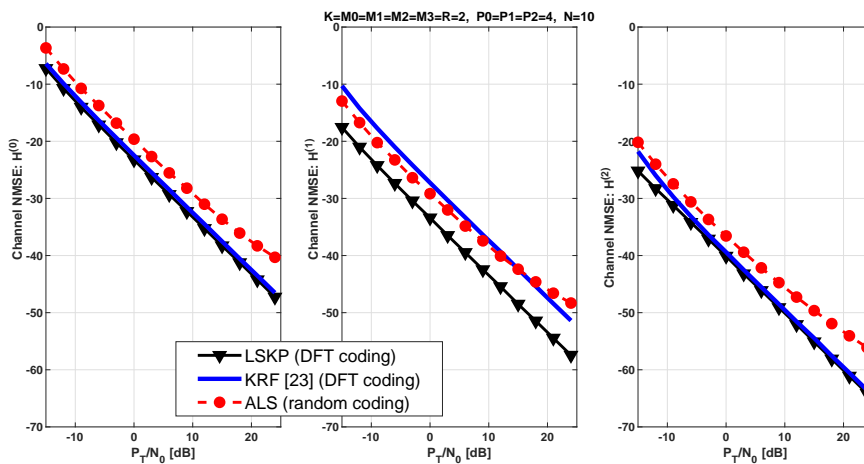
#### 4.3.4 Performance comparison of the proposed receivers

In this subsection, we provide a performance comparison of the proposed semi-blind receivers. We also show the SER performance of receiver based on a Khatri-Rao factorization (KRF) algorithm proposed in [18], which exploits a generalized nested PARAFAC model for a multi-hop relaying system that uses a simplified KRST coding. To plot the curves, the parameters were chosen to ensure roughly the same transmission rate for all the systems. For the proposed system, the transmission rate is proportional to  $R/P_0(1 + P_1 + P_1P_2)$ , while for the system of [18], it is proportional to  $M_0^t/P_0(1 + P_1 + P_1P_2)$ .

For large values of  $N$ , the computational complexities of the LSKP, KRF and ZF receivers are respectively given by  $\mathcal{O}(M^3P^{K+1}N)$ ,  $\mathcal{O}(M^2P^{K+1}N)$  and  $\mathcal{O}(MP^{K+1}N)$ . This shows that the proposed algorithm is a little more complex than the other two techniques, which can be explained by the fact that the KRF uses a tensor coding simpler than the one of the proposed receiver. Moreover, the ZF receiver assumes the perfect knowledge of all the channel matrices, which greatly simplifies the estimation of the information symbols.

From Figure 26, one can note that the ALS performance is better than the one obtained with the LSKP receiver when a random coding is considered. This gain can be explained by the refinement provided by the ALS technique until to achieve the convergence criterion. Despite that, the exploitation of the orthogonality of the coding tensors with the LSKP receiver yields a significant gain over the iterative receiver. We can also conclude from Figure 26 that the proposed LSKP receiver gives a better performance than the receiver of [18] due to the use of TSTC, which exploits spatial transmit diversity at the source and relay nodes.

Figure 27 shows the channel NMSE versus  $P_T/N_0$  for the individual channels. We compare the NMSE obtained with the random and DFT codings for the proposed ALS and LSKP receivers, respectively, and the KRF receiver [18]. The results illustrate the advantage of the system with DFT coding, compared with random coding and with the system [18], in most of

Figure 26 – SER performance comparison for  $K = 2$ Figure 27 – NMSE of the individual channel estimates for  $K = 2$ 

the cases.

#### 4.4 Summary

In this chapter, we have proposed a multi-hop AF MIMO relay system with TSTC at the source and the relays. We have showed that the signals received at destination form a  $(K + 3)$ -th order tensor ( $K$  is the number of relays) that satisfies a HONTD. The contributions in this chapter extends previous works in different ways, either by using a more general relay coding, by extending these works to the multi-hop case and/or by using a different estimation algorithm.

By exploiting the proposed tensor modeling, we have derived two semi-blind receivers, called ALS and LSKP receivers. The receivers allow to jointly estimate the individual channels and the information symbols by exploiting an iterative method, in the case of the ALS

receiver, and by exploiting a closed-form solution, in the case of LSKP receiver. In addition, a ZF receiver was considered to evaluate the impact of some design parameters on the performance of the system.

Simulation results have shown that the performance of the proposed multi-hop system is better than the one obtained by using a direct (source-destination) link, i.e., an increase of  $K$  improve significantly the performance in terms of SER and channel NMSE. Among the different receivers, when considered the use of random coding, the iterative nature of the ALS algorithm provides a refinement of the channels estimation, yielding a better SER than the closed-form LSKP receiver. However, the LSKP receiver allow to exploit a tensor coding with a unitary unfolding, which overcomes the results obtained with the ZF receiver and the ALS one. We also showed that the multi-hop system with TSTC at the source and the relays has performance that overcomes the one obtained with the simpler KRST coding (system in [18]).

For the above reasons, for purposes of application and simulation in the following chapters, we will consider the LSKP method with unitary unfoldings.

## 5 TWO-HOP MIMO MULTIRELAY SYSTEM WITH TSTC BASED ON CNTD

In this chapter, we present a two-hop MIMO multi-relay system with TSTC at the source and the relays. In this system, the multiple relays use orthogonal channels (parallel relaying) to increase the diversity order, assuming that all the relays can communicate directly with the destination. The proposed communication system generalizes the system model of [34] by introducing an additional diversity to the system: the cooperative diversity, obtained through the use of multiple relays in a parallel way. This system can also be viewed as an extension of previous works [24, 30, 35] in different ways, either by proposing a more general tensor decomposition, by using a more general relay coding, by extending these works to the multi-relay case and/or by using a different estimation algorithm.

We show that the signals received at destination form a fifth-order tensor, where each mode is linked with a different signal dimension (space, source code, relay code, time and number of relays), satisfying a CNTD model, as introduced in Subsection 3.2.

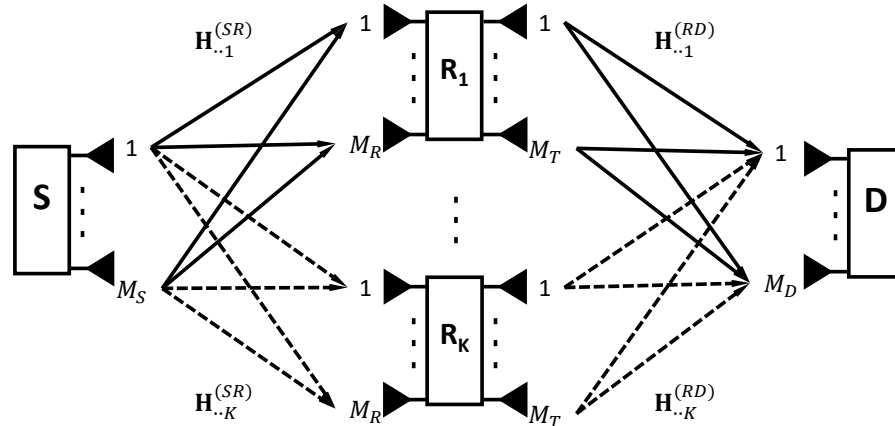
The tensor approach presented in this chapter is used to develop a receiver algorithm based on LSKP technique for jointly estimating the symbol matrix and the individual channels with a global processing of all dataset received from multiple relays. Monte Carlo simulations are provided to illustrate the effectiveness of the cooperative diversity exploitation and to compare the performances of the proposed receiver with other existing ones.

### 5.1 System model

Let us consider the cooperative communication system shown in Figure 28, which is composed of a source ( $S$ ) sending data to the destination through multiple relays ( $R_1, \dots, R_K$ ), where  $K$  is the number of relays. The source-relay and relay-destination channels are assumed to be flat fading and quasi-static. All nodes of the system employ multiple antennas and the relays operate in half-duplex mode.

The following key assumptions are made: (i) the direct link between the source and destination nodes is not available, corresponding to a link with deep fading; (ii) the code tensors are known at the destination; (iii) the relays use the AF protocol; (iv) the relays are synchronized at symbol level and they transmit in orthogonal channels in different time slots.

The global transmission is composed of  $K + 1$  steps, the first step corresponding to the transmission from the source to the relays and the remaining  $K$  steps corresponding to the

Figure 28 – Two-hop MIMO relaying system with  $K$  relays

sequential transmission from the  $K$  relays to the destination. While a relay is transmitting to the destination, the other relays remain silent.

Regarding the use of multiple relays operating in orthogonal channels, also known as parallel relaying, we can find many works in the literature that use this kind of approach [19–21, 93]. However, these works use more simple channel models. Indeed, [20, 93] consider single-antenna nodes, [19, 21] use conventional matrix coding and [19, 21, 93] perform the channel estimation with the use of training sequences.

In this sequel, for the sake of simplicity, we consider the noiseless case for describing the system model. In the first hop of transmission, the symbol matrix  $\mathbf{S} \in \mathbb{C}^{N \times R}$ , with  $R$  data streams composed of  $N$  symbols each, is transmitted by  $M_S$  antennas at the source. TSTC at the source using the coding tensor  $\mathcal{C}^{(S)} \in \mathbb{C}^{M_S \times P \times R}$  provides temporal spreading with length  $P$ , leading to the following tensor of coded signals to be transmitted

$$\mathcal{X}^{(S)} = \mathcal{C}^{(S)} \times_3 \mathbf{S} \in \mathbb{C}^{M_S \times P \times N} \iff x_{m_S, p, n}^{(S)} = \sum_{r=1}^R c_{m_S, p, r}^{(S)} s_{n, r}, \quad (5.1)$$

with  $m_S = 1, \dots, M_S$ ,  $p = 1, \dots, P$  and  $n = 1, \dots, N$ . After transmission through the channel  $\mathbf{H}_{\cdot \cdot k}^{(SR)} \in \mathbb{C}^{M_R \times M_S}$ , the signals received by  $M_R$  antennas at the  $k$ -th relay, during the  $n$ -th symbol period of the  $p$ -th transmission block form a fourth-order tensor given by

$$x_{m_R, p, n, k}^{(R)} = \sum_{m_S=1}^{M_S} h_{m_R, m_S, k}^{(SR)} x_{m_S, p, n}^{(S)} = \sum_{m_S=1}^{M_S} \sum_{r=1}^R h_{m_R, m_S, k}^{(SR)} c_{m_S, p, r}^{(S)} s_{n, r}, \quad (5.2)$$

with  $m_R = 1, \dots, M_R$  and  $k = 1, \dots, K$ . The signals (5.2) received at the relaying node define the fourth-order tensor  $\mathcal{X}^{(R)} \in \mathbb{C}^{M_R \times P \times N \times K}$  given as the following generalized Tucker-(2, 4) decomposition

$$\mathcal{X}^{(R)} = \mathcal{X}^{(S)} \times_1 \mathcal{H}^{(SR)} = \mathcal{C}^{(S)} \times_1 \mathcal{H}^{(SR)} \times_3 \mathbf{S}, \quad (5.3)$$

with  $\mathcal{H}^{(SR)} \in \mathbb{C}^{M_R \times M_S \times K}$ .

Each relay  $k$  re-encodes the received signals, using also a TSTC  $\mathcal{C}_{(k)}^{(R)} \in \mathbb{C}^{M_T \times J \times M_R}$  with length  $J$ , before transmitting the coded signals to destination. The signals transmitted by  $M_T$  antennas at the  $k$ -th relay, through the channel  $\mathbf{H}_{\cdot k}^{(RD)} \in \mathbb{C}^{M_D \times M_T}$ , associated with the  $n$ -th symbol period of the  $p$ -th transmission block at the source and the  $j$ -th transmission block at the relay are given by

$$\mathcal{X}^{(T)} = \mathcal{C}^{(R)} *_3^1 \mathcal{X}^{(R)} \in \mathbb{C}^{M_T \times J \times P \times N \times K} \iff x_{m_T, j, p, n, k}^{(T)} = \sum_{m_R=1}^{M_R} c_{m_T, j, m_R, k}^{(R)} x_{m_R, p, n, k}^{(R)}, \quad (5.4)$$

with  $m_T = 1, \dots, M_T$  and  $j = 1, \dots, J$ . Finally, after transmission from the  $k$ -th relay, the noiseless tensor of signals received by  $M_D$  antennas at the destination is given by

$$x_{m_D, j, p, n, k}^{(SRD)} = \sum_{m_T=1}^{M_T} h_{m_D, m_T, k}^{(RD)} x_{m_T, j, p, n, k}^{(T)}, \quad (5.5)$$

with  $m_D = 1, \dots, M_D$ . Replacing  $x_{m_T, j, p, n, k}^{(T)}$  by its expression deduced from (5.4) and (5.2) gives

$$x_{m_D, j, p, n, k}^{(SRD)} = \sum_{m_T=1}^{M_T} \sum_{m_R=1}^{M_R} \sum_{m_S=1}^{M_S} \sum_{r=1}^R h_{m_D, m_T, k}^{(RD)} c_{m_T, j, m_R, k}^{(R)} h_{m_R, m_S, k}^{(SR)} c_{m_S, p, r}^{(S)} s_{n, r}. \quad (5.6)$$

Thus, the signals received at destination form a fifth-order tensor  $\mathcal{X}^{(SRD)} \in \mathbb{C}^{M_D \times J \times P \times N \times K}$ , whose modes are associated with space, coding (at source and relays), time and cooperative diversities. Note that the tensor in (5.6) satisfies a CNTD model – Equations (3.26)-(3.26) – with the correspondences  $(\mathcal{A}^{(1)}, \mathcal{G}^{(1)}, \mathcal{A}^{(2)}, \mathcal{G}^{(2)}, \mathbf{A}^{(3)}) \iff (\mathcal{H}^{(RD)}, \mathcal{C}^{(R)}, \mathcal{H}^{(SR)}, \mathcal{C}^{(S)}, \mathbf{S})$ .

From (5.6), let us define the following generalized Tucker-(2, 4) model

$$h_{m_D, j, m_S, k}^{(SRD)} = \sum_{m_T=1}^{M_T} \sum_{m_R=1}^{M_R} c_{m_T, j, m_R, k}^{(R)} h_{m_D, m_T, k}^{(RD)} h_{m_R, m_S, k}^{(SR)}, \quad (5.7)$$

which can be expressed in tensor form as

$$\mathcal{H}^{(SRD)} = \mathcal{C}^{(R)} \times_1 \mathcal{H}^{(RD)} \times_3 \mathcal{H}^{(SR)'} \in \mathbb{C}^{M_D \times J \times M_S \times K}, \quad (5.8)$$

where the tensor  $\mathcal{H}^{(SR)'} \in \mathbb{C}^{M_S \times M_R \times K}$  is formed by permuting the first two modes of  $\mathcal{H}^{(SR)} \in \mathbb{C}^{M_R \times M_S \times K}$ , i.e.  $\mathbf{H}_{\cdot k}^{(SR)'} = \mathbf{H}_{\cdot k}^{(SR)T} \in \mathbb{C}^{M_S \times M_R}$ . The tensor  $\mathcal{H}^{(SRD)}$  can be viewed as the effective channel between the source and the destination.

Thus, we can write the received signal model (5.6) as follows

$$x_{m_D, j, p, n, k}^{(SRD)} = \sum_{m_S=1}^{M_S} h_{m_D, j, m_S, k}^{(SRD)} x_{m_S, p, n}^{(S)}, \quad (5.9)$$

which yields the following contraction between the tensors  $\mathcal{H}^{(SRD)}$ , defined in (5.8), and  $\mathcal{X}^{(S)}$ , defined in (5.1),

$$\mathcal{X}^{(SRD)} = \mathcal{H}^{(SRD)} *_3^1 \mathcal{X}^{(S)} \in \mathbb{C}^{M_D \times J \times P \times N \times K}. \quad (5.10)$$

Fixing the index  $k$  in (5.8), the generalized Tucker-(2, 4) model  $\mathcal{H}^{(SRD)}$  can be viewed as  $K$  Tucker-(2, 3) models  $\mathcal{H}_{(k)}^{(SRD)} \in \mathbb{C}^{M_D \times J \times M_S}$ , leading to the following modeling for the tensor of signals received at destination from the  $k$ -th relay

$$\mathcal{X}_{(k)}^{(SRD)} = \mathcal{H}_{(k)}^{(SRD)} *_3^1 \mathcal{X}^{(S)} \in \mathbb{C}^{M_D \times J \times P \times N}. \quad (5.11)$$

Note that the effective channel  $\mathcal{H}^{(SRD)}$  is formed by the concatenation of the individual channels of each relay as given below

$$\mathcal{H}^{(SRD)} = \mathcal{H}_{(1)}^{(SRD)} \sqcup_4 \mathcal{H}_{(2)}^{(SRD)} \dots \sqcup_4 \mathcal{H}_{(K)}^{(SRD)}. \quad (5.12)$$

The tensor (5.11) satisfies a fourth-order NTD, as introduced in [34] and recalled in Subsection 2.2.3, which leads us to write the tensor  $\mathcal{X}^{(SRD)}$  in (5.10) as a coupling of  $K$  tensors  $\mathcal{X}_{(k)}^{(SRD)}$ , satisfying a fifth-order CNTD, as introduced in Section 3.2. Indeed, the tensors (5.1), (5.8), (5.10) and (5.11) correspond to the tensors (3.19), (3.21), (3.20) and (3.17), respectively, resulting in the following correspondences between the models

$$(\mathcal{T}^{(1)}, \mathcal{T}^{(2)}, \mathcal{A}^{(1)}, \mathcal{G}^{(1)}, \mathcal{A}^{(2)}, \mathcal{G}^{(2)}, \mathbf{A}^{(3)}) \iff (\mathcal{H}^{(SRD)}, \mathcal{X}^{(S)}, \mathcal{H}^{(RD)}, \mathcal{C}^{(R)}, \mathcal{H}^{(SR)}, \mathcal{C}^{(S)}, \mathbf{S}). \quad (5.13)$$

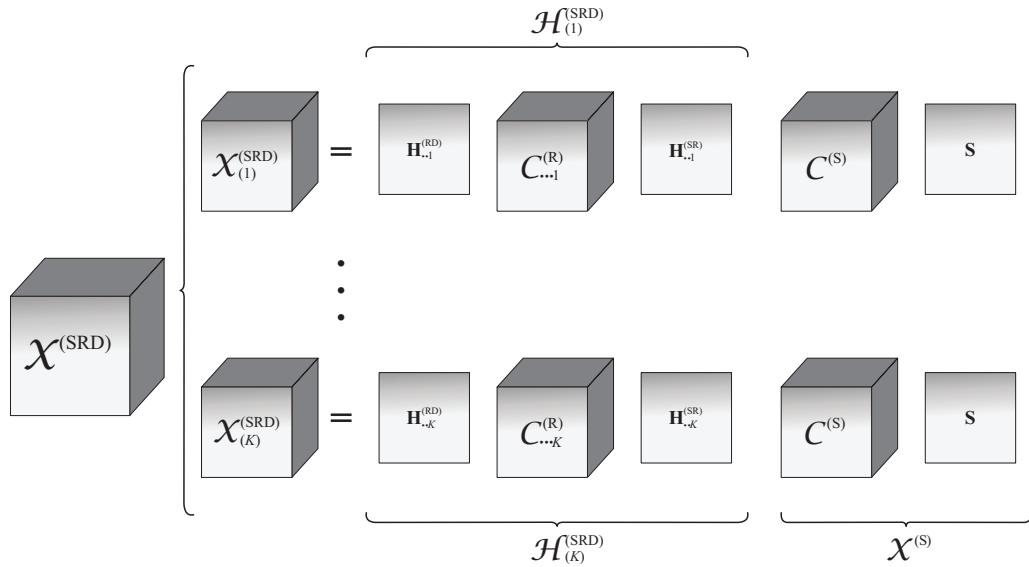
Figure 29 shows a block-diagram of the tensor of received signals  $\mathcal{X}^{(SRD)}$  decomposed into  $K$  branches, illustrating that the tensor of coded signals at the source  $\mathcal{X}^{(S)}$  is transmitted to the destination via  $K$  relays. Each branch corresponds to a NTD that shares the same tensor  $\mathcal{X}^{(S)}$  with the other branches, characterizing a coupling of  $K$  NTD models. Hence, the aim is to jointly estimate the transmitted information symbols and the channels from this dataset using a semi-blind receiver.

It is worth mentioning that the case with a single relay ( $K = 1$ ), the system model proposed in the present chapter is equivalent to the one discussed in Chapter 4.

## 5.2 Semi-blind receiver

By exploiting the CNTD modeling of the proposed MIMO relaying system, we propose a semi-blind receiver for jointly estimating the symbol matrix and the channel tensors.

Figure 29 – Tensor model of noiseless received signals



The receiver is based on a LSKP algorithm, as already used in previous chapter in a different system model. In this section we derive the LSKP for the CNTD model above presented. We assume that the coding tensors  $\mathcal{C}^{(S)}$  and  $\mathcal{C}^{(R)}$ , corresponding to the core tensors of the models (5.1) and (5.8), are known by the receiver. Thus, we have the channel tensors  $\mathcal{H}^{(SR)}$  and  $\mathcal{H}^{(RD)}$  and the symbol matrix  $\mathbf{S}$  as unknown factors to be estimated. The knowledge of the coding tensors ensures that these factors are unique up to scaling ambiguities (see Theorem 5).

By using the correspondences (6.11), the ambiguity relations given in Theorem 5 become  $\delta_k^{(RD)} \delta_k^{(SR)} \delta^{(S)} = 1$ , where  $\delta_k^{(RD)}$ ,  $\delta_k^{(SR)}$  and  $\delta^{(S)}$  are the scalar ambiguity factors of  $\mathcal{H}^{(RD)}$ ,  $\mathcal{H}^{(SR)}$  and  $\mathbf{S}$ , respectively. Note that the ambiguities on  $\mathcal{H}^{(RD)}$  and  $\mathcal{H}^{(SR)}$  depend on the relay.

To derive the LSKP receiver, let us define LS estimations of Kronecker products based on a low-rank approximation algorithm. Applying (2.20) to the tensor  $\mathcal{X}^{(SRD)}$  in (5.10), we get the following mode-3 product

$$\mathcal{X}_{M_D \times J \times P_N \times K}^{(SRD)} = \mathcal{H}^{(SRD)} \times_3 \mathbf{X}_{P_N \times M_S}^{(S)}, \quad (5.14)$$

where  $\mathbf{X}_{P_N \times M_S}^{(S)}$  is mode-1 unfolding of (5.1). By replacing  $\mathcal{H}^{(SRD)}$  and using the Property 5, the tensor  $\mathcal{X}_{M_D \times J \times P_N \times K}^{(SRD)}$  becomes

$$\mathcal{X}_{M_D \times J \times P_N \times K}^{(SRD)} = \mathcal{C}^{(R)} \times_1 \mathcal{H}^{(RD)} \times_3 \left( \mathcal{H}^{(SR)'} \times_1 \mathbf{X}_{P_N \times M_S}^{(S)} \right). \quad (5.15)$$

Defining  $\mathcal{V} = \mathcal{H}^{(SR)'} \times_1 \mathbf{X}_{P_N \times M_S}^{(S)} \in \mathbb{C}^{P_N \times M_R \times K}$ , the above model is a generalized Tucker-(2, 4)

decomposition, which allows us to write, from (2.33), the following unfolding

$$\mathbf{X}_{M_D P N \times K J}^{(SRD)} = \left( \mathbf{H}_{M_D \times K M_T}^{(RD)} \bowtie \mathbf{V}_{P N \times K M_R} \right) \mathbf{C}_{K M_T M_R \times K J}^{(R)}, \quad (5.16)$$

where

$$\mathbf{V}_{P N \times K M_R} = \mathbf{X}_{P N \times M_S}^{(S)} \mathbf{H}_{M_S \times K M_R}^{(SR)} = (\mathbf{I}_P \otimes \mathbf{S}) \mathbf{C}_{P R \times M_S}^{(S)} \mathbf{H}_{M_S \times K M_R}^{(SR)}. \quad (5.17)$$

On the other hand, applying (2.21) to (5.10) and replacing  $\mathcal{X}^{(S)}$  by (5.10), we can deduce the following mode-1 product

$$\begin{aligned} \mathcal{X}_{J K M_D \times P \times N}^{(SRD)} &= \mathcal{X}^{(S)} \times_1 \mathbf{H}_{J K M_D \times M_S}^{(SRD)} \\ &= \mathcal{C}^{(S)} \times_1 \mathbf{H}_{J K M_D \times M_S}^{(SRD)} \times_3 \mathbf{S}. \end{aligned} \quad (5.18)$$

The above model is a Tucker-(2, 3) decomposition, from which we can write the following tall unfolding

$$\mathbf{X}_{N J K M_D \times P}^{(SRD)} = \left( \mathbf{S} \otimes \mathbf{H}_{J K M_D \times M_S}^{(SRD)} \right) \mathbf{C}_{R M_S \times P}^{(S)}, \quad (5.19)$$

where the matrix  $\mathbf{H}_{J K M_D \times M_S}^{(SRD)}$  is the following tall mode-3 unfolding of  $\mathcal{H}^{(SRD)}$  deduced from (2.33) as

$$\mathbf{H}_{J K M_D \times M_S}^{(SRD)} = \left[ \mathbf{I}_J \otimes \text{bdiag} \left( \mathbf{H}_{\cdot \cdot k}^{(RD)} \right) \right] \mathbf{C}_{J K M_T \times K M_R}^{(R)} \mathbf{H}_{K M_R \times M_S}^{(SR)} \quad (5.20)$$

Defining the matrices  $\Phi = \mathbf{H}_{M_D \times K M_T}^{(RD)} \bowtie \mathbf{V}_{P N \times K M_R} \in \mathbb{C}^{M_D P N \times K M_T M_R}$  and  $\Omega = \mathbf{S} \otimes \mathbf{H}_{J K M_D \times M_S}^{(SRD)} \in \mathbb{C}^{N J K M_D \times R M_S}$ , we deduce the following LS estimates of KP from (5.16) and (5.19)

$$\hat{\Phi} = \mathbf{X}_{M_D P N \times K J}^{(SRD)} \left( \mathbf{C}_{K M_T M_R \times K J}^{(R)} \right)^\dagger, \quad (5.21)$$

$$\hat{\Omega} = \mathbf{X}_{N J K M_D \times P}^{(SRD)} \left( \mathbf{C}_{R M_S \times P}^{(S)} \right)^\dagger. \quad (5.22)$$

Thus, the LSKP receiver estimates the matrices  $\mathbf{H}_{M_D \times K M_T}^{(RD)}$ ,  $\mathbf{V}_{P N \times K M_R}$ ,  $\mathbf{S}$  and  $\mathbf{H}_{J K M_D \times M_S}^{(SRD)}$  as factors of a balanced block KP and of a KP, by applying the low-rank approximation algorithm proposed in [91] and recalled in Appendix C, using the LS estimates  $\hat{\Phi}$  and  $\hat{\Omega}$  in (5.21) and (5.22), respectively. For the case of (5.21), which is related to the factorization of a block Kronecker product, a straightforward extension of the method in [91] was needed. The discussion on this extension to block Kronecker products is also presented in Appendix C. Once  $\hat{\mathbf{V}}_{P N \times K M_R}$  and  $\hat{\mathbf{H}}_{J K M_D \times M_S}^{(SRD)}$  are estimated, the unfolding  $\mathbf{H}_{K M_R \times M_S}^{(SR)}$  can be estimated

Table 4 – LSKP receiver for two-hop MIMO multirelay system

- 
1. Calculate the LS estimate of the block Kronecker product  $\Phi = \mathbf{H}_{M_D \times KM_T}^{(RD)} \bowtie \mathbf{V}_{PN \times KM_R}$ :  

$$\hat{\Phi} = \tilde{\mathbf{X}}_{M_D PN \times KJ}^{(SRD)} \left( \mathbf{C}_{KM_T M_R \times KJ}^{(R)} \right)^\dagger.$$
  2. Apply the SVD-based low-rank approximation algorithm in Appendix C to estimate the matrices  $\hat{\mathbf{H}}_{M_D \times KM_T}^{(RD)}$  and  $\hat{\mathbf{V}}_{PN \times KM_R}$  from  $\hat{\Phi}$  calculated in step 1.
  3. Calculate the LS estimate of the Kronecker product  $\Omega = \mathbf{S} \otimes \mathbf{H}_{JKM_D \times M_S}^{(SRD)}$ :  

$$\hat{\Omega} = \tilde{\mathbf{X}}_{NJKM_D \times P}^{(SRD)} \left( \mathbf{C}_{RM_S \times P}^{(S)} \right)^\dagger.$$
  4. Apply the SVD-based low-rank approximation algorithm in Appendix C to estimate the matrices  $\hat{\mathbf{S}}$  and  $\hat{\mathbf{H}}_{JKM_D \times M_S}^{(SRD)}$  from  $\hat{\Omega}$  calculated in step 3.
  5. Eliminate the scaling ambiguities using (5.23).
  6. Estimate the channel  $\mathcal{H}^{(SR)}$ , from (5.17), using  

$$\hat{\mathbf{H}}_{M_S \times KM_R}^{(SR)} = \left[ \left( \mathbf{I}_P \otimes \hat{\mathbf{S}} \right) \mathbf{C}_{PR \times M_S}^{(S)} \right]^\dagger \hat{\mathbf{V}}_{PN \times KM_R},$$
or from (5.20), using  

$$\hat{\mathbf{H}}_{KM_R \times M_S}^{(SR)} = \left[ \left( \mathbf{I}_J \otimes \text{bdiag} \left( \hat{\mathbf{H}}_{\cdot \cdot k}^{(RD)} \right) \right) \mathbf{C}_{JKM_T \times KM_R}^{(R)} \right]^\dagger \hat{\mathbf{H}}_{JKM_D \times M_S}^{(SRD)}.$$
  7. Project the estimated symbols onto the symbol alphabet.
- 

from (5.17) or (5.20). The LSKP receiver derived from the above LS estimates is summarized in Table 4.

#### Identifiability conditions and ambiguity relations

Note that for computing the pseudo-inverses in (5.21) and (5.22), as well as for computing  $\hat{\mathbf{H}}_{KM_R \times M_S}^{(SR)}$ , some conditions are required to ensure the uniqueness of LS solutions. The unfoldings  $\mathbf{C}_{KM_T M_R \times KJ}^{(R)}$  and  $\mathbf{C}_{RM_S \times P}^{(S)}$  must be full row rank and then the conditions  $J \geq M_T M_R$  and  $P \geq RM_S$  are necessary. For the LS estimate of  $\mathbf{H}_{KM_R \times M_S}^{(SR)}$  from (5.17) or (5.20), we must have  $PR \geq M_S$  and  $N \geq R$  or  $JM_T \geq M_R$  and  $M_D \geq M_T$ .

For eliminating the scaling ambiguities on the estimates, we assume the knowledge of one pilot symbol ( $s_{1,1}$ ). In order to plot the simulation results, we assumed the a priori knowledge of one coefficient of  $\mathcal{H}^{(RD)}$  for each relay ( $h_{1,1,k}^{(RD)}$ ) such that we get the following ambiguity relations

$$\begin{aligned}
 \hat{\mathbf{H}}_{\cdot \cdot k}^{(RD)} &\leftarrow \left( \delta_k^{(RD)} \right)^{-1} \hat{\mathbf{H}}_{\cdot \cdot k}^{(RD)} \\
 \hat{\mathbf{V}}_{\cdot \cdot k} &\leftarrow \delta_k^{(RD)} \hat{\mathbf{V}}_{\cdot \cdot k} \\
 \hat{\mathbf{S}} &\leftarrow \left( \delta^{(S)} \right)^{-1} \hat{\mathbf{S}} \\
 \hat{\mathbf{H}}_{JKM_D \times M_S}^{(SRD)} &\leftarrow \delta_k^{(S)} \hat{\mathbf{H}}_{JKM_D \times M_S}^{(SRD)},
 \end{aligned} \tag{5.23}$$

with  $\delta_k^{(RD)} = \hat{h}_{1,1,k}^{(RD)} / h_{1,1,k}^{(RD)}$  and  $\delta^{(S)} = \hat{s}_{1,1} / s_{1,1}$ . The computational complexity of the proposed receiver is  $\mathcal{O}((NKPJM_D)(KM_R M_T + RM_S))$ . Assuming  $R = M_D = M_R = M_T = M_S = M$

and  $P = J$ , it becomes  $\mathcal{O}(NKP^2M^3(K+1))$ .

### 5.3 Simulation results

In this section, we provide Monte Carlo simulation results to illustrate the effectiveness of the proposed two-hop MIMO multi-relay system. In order to evaluate the impact of the choice of the design parameters on the system behavior (regardless of the influence of algorithm), we consider a ZF receiver, which is obtained by assuming a perfect knowledge of the channel tensors at destination. The ZF receiver is defined from an unfolding of (5.18) as

$$\mathbf{S}^T = \left( \left( \mathbf{I}_P \otimes \left[ \left( \mathbf{I}_J \otimes \text{bdiag} \left( \mathbf{H}_{\cdot\cdot k}^{(RD)} \right) \right) \mathbf{C}_{JKM_T \times KM_R}^{(R)} \mathbf{H}_{KM_R \times M_S}^{(SR)} \right] \right) \mathbf{C}_{PM_S \times R}^{(S)} \right)^\dagger \mathbf{X}_{PJKM_D \times N}^{(SRD)}. \quad (5.24)$$

Then, the performance of the proposed LSKP receivers is evaluated.

The receiver performance were averaged over  $5 \times 10^4$  Monte Carlo runs for various system configurations. The SER and the NMSE of the channels were plotted as function of the transmission power to noise spectral density ratio ( $P_T/N_0$ ). The transmitted symbols were randomly generated from a unit energy 4-QAM alphabet. Several system configurations were tested for the proposed system. The design parameter values used in the simulations are indicated above each figure. In all the simulations we consider the same number of receiving and transmitting antennas at the relays ( $M_R = M_T$ ).

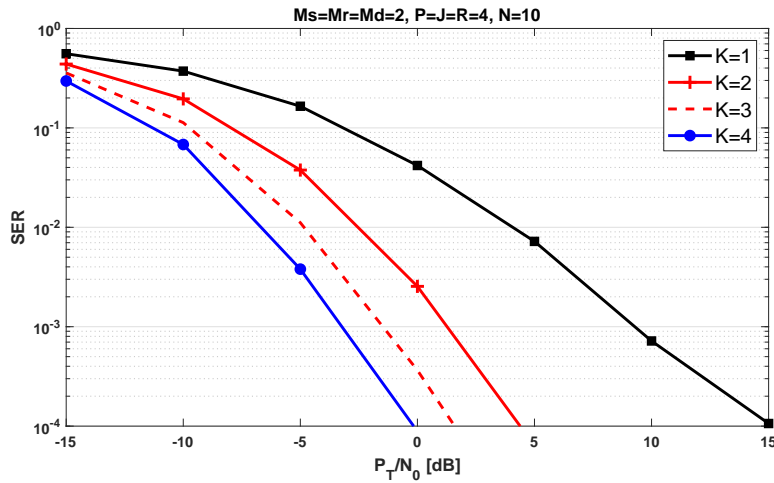
The channel tensors  $\mathcal{H}^{(SR)}$  and  $\mathcal{H}^{(RD)}$  are assumed to be Rayleigh flat-fading and quasi-static, composed of i.i.d. complex Gaussian entries with zero-mean and unit variance. The channel powers were adjusted taking into account the same exponential path-loss model given by  $\sigma_{\mathbf{H}}^2 = 1/d^4$ , where  $d$  is the distance of each hop. The distance  $d$  of each hop was considered the same and equal to  $D_0/2$ , where  $D_0$  is the source-destination distance, arbitrarily chosen equal to 1.

AWGN were added at each receiving node with the same noise variance  $N_0$ . In the noisy model, we consider the global noise tensor  $\mathcal{N}^{(SRD)} \in \mathbb{C}^{M_D \times J \times P \times N \times K}$  given by

$$n_{m_D, j, p, n, k}^{(SRD)} = \sqrt{N_0} n_{m_D, j, p, n, k}^{(D)} + \sum_{m_T=1}^{M_T} \sum_{m_R=1}^{M_R} h_{m_D, m_T, k}^{(RD)} c_{m_T, j, m_R, k}^{(R)} \left( \sqrt{N_0} n_{m_R, p, n, k}^{(R)} \right), \quad (5.25)$$

where  $n_{m_D, j, p, n, k}^{(D)}$  and  $n_{m_R, p, n, k}^{(R)}$  are entries of the tensors  $\mathcal{N}^{(D)} \in \mathbb{C}^{M_D \times J \times P \times N \times K}$  and  $\mathcal{N}^{(R)} \in \mathbb{C}^{M_R \times P \times N \times K}$  that represent the noise at the destination and at the relays, respectively. At each run,  $N_0$  was fixed according to the desired  $P_T/N_0$  value.

Figure 30 – ZF receiver performance for different numbers of relays



For the simulations with the ZF receiver, the coding tensors  $\mathcal{C}^{(S)}$  and  $\mathcal{C}^{(R)}$  were generated with unit amplitude coefficients and random phase drawn from a uniform distribution between 0 and  $2\pi$ . For the LSKP receiver, as discussed in the previous chapter, the coding tensors were chosen in such a way that the unfolding used in the algorithm is a row-orthonormal matrix (unitary coding – truncated DFT matrix). In both cases, each coding tensor was multiplied by a fixed scalar gain so that all the transmission nodes have the same mean power and the total transmission power is kept constant, regardless of the number of relays and antennas. Thus, the coding tensors become  $\mathcal{C}^{(S)} \leftarrow \sqrt{\beta^{(S)}} \mathcal{C}^{(S)}$  and  $\mathcal{C}^{(R)} \leftarrow \sqrt{\beta^{(R)}} \mathcal{C}^{(R)}$ , with

$$\beta^{(S)} = P_T/M_S R \quad (5.26)$$

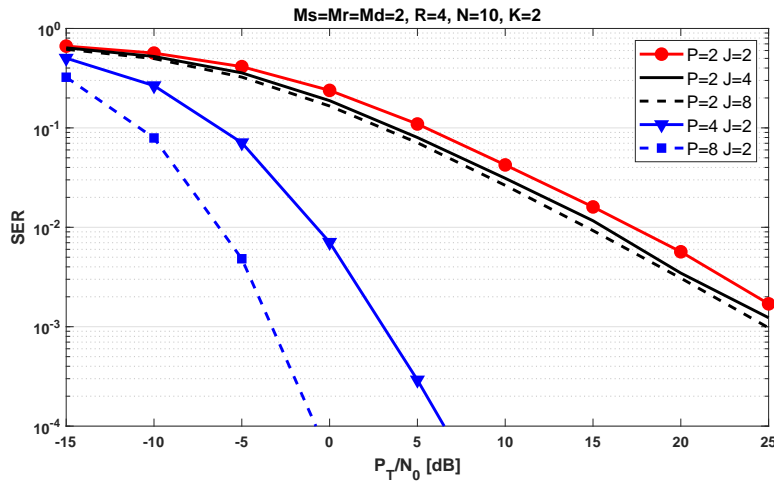
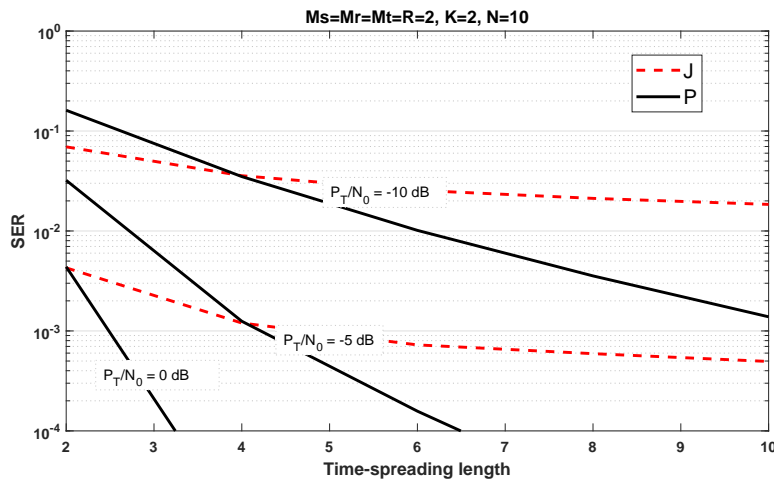
$$\beta^{(R)} = P_T/(M_T M_R (P_T \sigma_{\mathbf{H}}^2 + N_0)), \quad (5.27)$$

where  $P_T = P_{total}/(K + 1)$ , with  $P_{total}$  being the total system power arbitrarily chosen equal to 1.

### 5.3.1 ZF performance with perfect channel knowledge

Now, we present some simulation results concerning the use of the ZF receiver in order to study the behavior of the proposed system when some parameters are modified. Although some parameter settings used in this subsection do not satisfy the identifiability conditions given in Subsection 5.2 for the LSKP receiver, the presented results aim to evaluate the impact of the choice of these parameters on the system performance, regardless of the estimation algorithm.

Figure 30 shows the SER provided by the ZF receiver versus  $P_T/N_0$  for  $K \in \{1, 2, 3, 4\}$  in order to evaluate the impact of an increase in the number of relays on the system

Figure 31 – ZF receiver performance for different time-spreading lengths  $P$  and  $J$ Figure 32 – Trade-off for the time-spreading lengths  $P$  and  $J$ 

performance. The case with a single relay ( $K = 1$ ) is equivalent to the two-hop MIMO relay system proposed in [34], as well as to the system model presented in Chapter 4 when  $K = 1$ . A more reasonable comparison between the two systems will be discussed in more details later. For the ZF receiver, the SER performance is clearly improved when the number of relays is increased. This result shows the gain provided by the cooperative diversity. Unless otherwise defined, the next results are obtained with two relays ( $K = 2$ ).

In Figures 31 and 32, we evaluate the impact of the time-spreading lengths  $P$  and  $J$  on the system performance. Figure 31 shows the SER versus  $P_T/N_0$  for the combinations  $(P, J) = (2, 2), (2, 4), (2, 8), (4, 2)$  and  $(8, 2)$ . We can note that any increase of  $P$  or  $J$  yields a performance improvement. However, an increase of  $P$  clearly provides a greater gain than an increase of  $J$ . That is evidenced by the difference between the curves with  $(P, J) = (4, 2)$  and  $(8, 2)$ , and the ones with  $(P, J) = (2, 4)$  and  $(2, 8)$ . It can also be justified by the correlation of the relay noise (5.25) with the temporal spreading  $J$ , via relay coding. In order to clarify the

Figure 33 – ZF receiver performance for different numbers of data streams

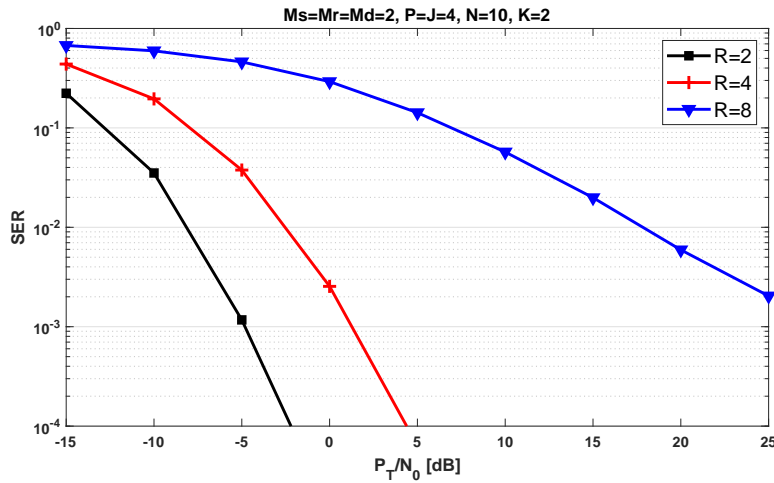
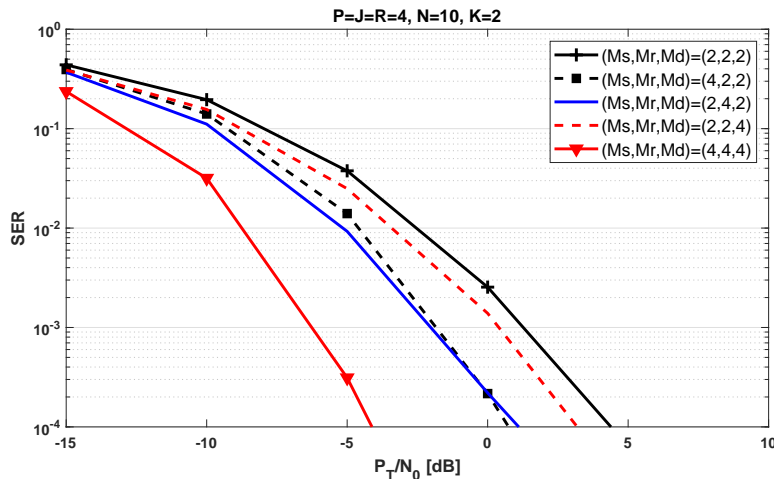


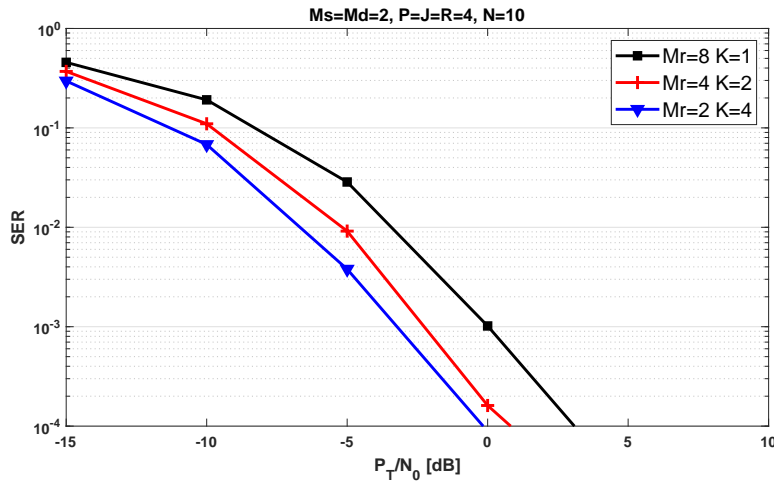
Figure 34 – ZF receiver performance for different numbers of antennas



dependence of the SER with respect to the time-spreading lengths  $J$  and  $P$ , Figure 32 shows, for fixed levels of  $P_T/N_0$ , SER curves as functions of  $P$  or  $J$ . In this figure, only one of the time-spreading lengths varies at each time, the other one is kept constant. When  $P$  varies, we set  $J = 4$ , and when  $J$  varies, we have  $P = 4$ . From the slope of the curves, we can clearly see that an increase of  $P$  leads to greater SER gains, as the spread signal at the source is subject to a new spreading at relay node. One can also note a SER floor when  $J$  is increased, in scenarios with low  $P_T/N_0$  values, establishing then a trade-off between the performance gain and transmission rate degradation due to an increasing in the time-spreading at the relays.

Figure 33 shows the SER versus  $P_T/N_0$  for  $R \in \{2, 4, 8\}$ . The results show, as expected, the SER degradation by increasing the number of data streams sent by the source. A higher value of  $R$  implies more information to be estimated at destination with the same resources. Note that the dimensions of the received signals tensor does not depend on  $R$ .

In the sequel, we evaluate the impact of the number of antennas at the source, relays

Figure 35 – ZF receiver performance for  $KM_R$  constant

and destination. Figure 34 shows the SER versus  $P_T/N_0$  for the combinations  $(M_S, M_R, M_D) = (2, 2, 2), (4, 2, 2), (2, 4, 2), (2, 2, 4)$  and  $(4, 4, 4)$ . The performance obtained with  $(4, 4, 4)$ , when compared with the one obtained with  $(2, 2, 2)$ , shows the expected improvement by increasing the number of antennas in the MIMO system. From the curves with  $(4, 2, 2), (2, 4, 2), (2, 2, 4)$ , we also observe that increasing  $M_S$  or  $M_R$  leads to a more pronounced improvement than increasing  $M_D$ . That can be explained by the dependence of the tensor codings  $\mathcal{C}^{(S)}$  and  $\mathcal{C}^{(R)}$  with  $M_S$  and  $M_R$ . Due to the multiple TSTC, a better performance is expected with an increase of  $M_S$ . However, the similar performance between the curves  $(4, 2, 2)$  and  $(2, 4, 2)$  can be explained from the fact that an increase in the value of  $M_R$  implies a greater addition of antennas, since, globally, the number of relaying antennas depends on the number of relays, i.e.  $KM_R$ .

In Figure 35, the curves show the SER versus  $P_T/N_0$  for different configurations that keep  $KM_R$  constant. From this figure, we can conclude that exploiting the cooperative diversity (increasing  $K$ ) is more effective than an increase of the number of antennas at the relays ( $M_R$ ). This comes from the fact that an increase in  $K$  yields more diversity, since the size of the received signals tensor – Equation 5.9 – depends on the number of relays and does not depend on the number of antennas  $M_R$ .

In order to evaluate configurations with the same size of the received signal tensor (i.e. same amount of signals received at destination), Figure 36 shows the SER versus  $P_T/N_0$  when  $KM_D$  constant. From the figure, we can see that the exploitation of the cooperative diversity is still more effective than exploiting the spatial diversity at destination (increasing  $M_D$ ). This comes from the fact that the multiple relays use orthogonal channels, i.e. the relays do not interfere with each other, while multiple antennas interfere each other.

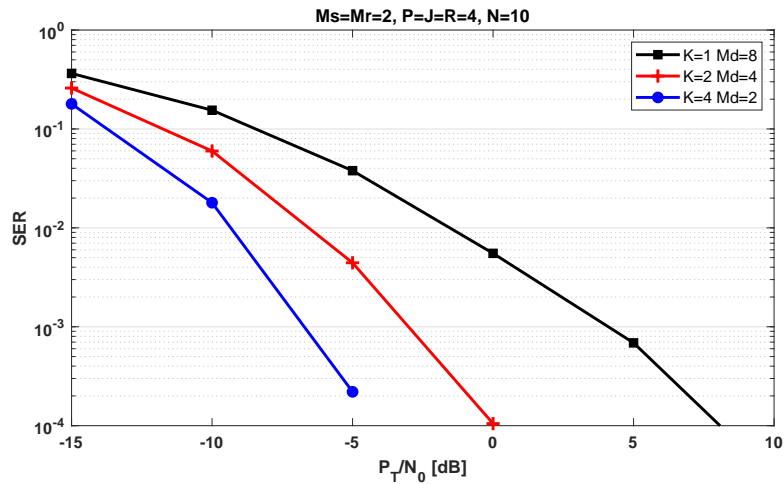
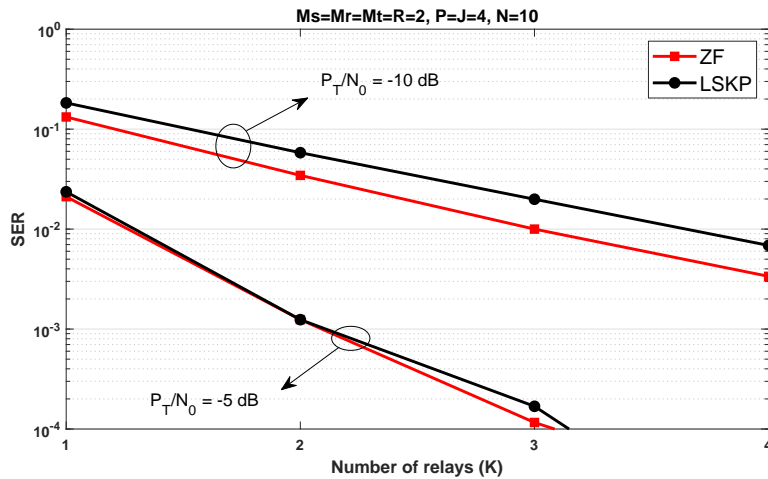
Figure 36 – ZF receiver performance for  $KM_D$  constant

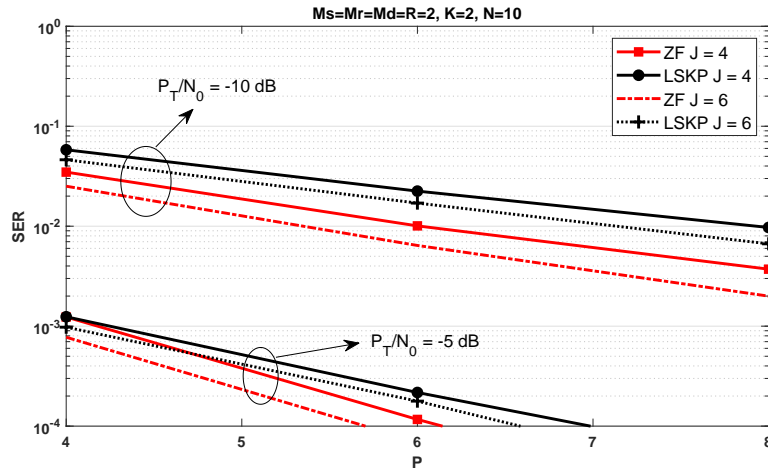
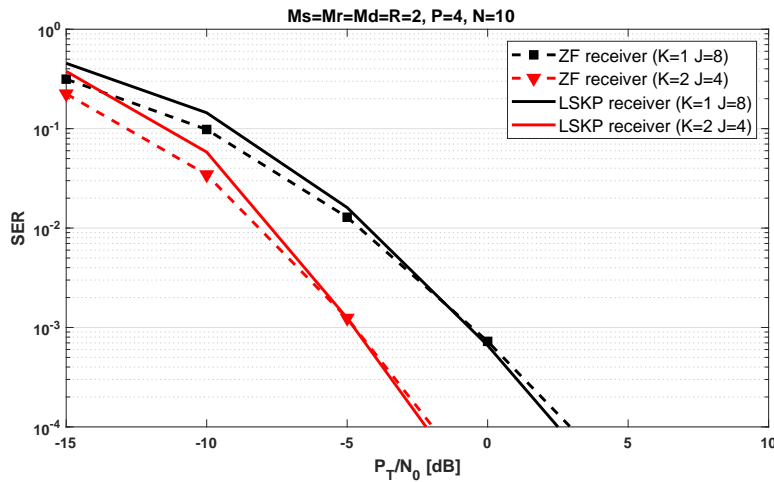
Figure 37 – Impact of the number of relays on the SER performance



### 5.3.2 LSKP receiver performance

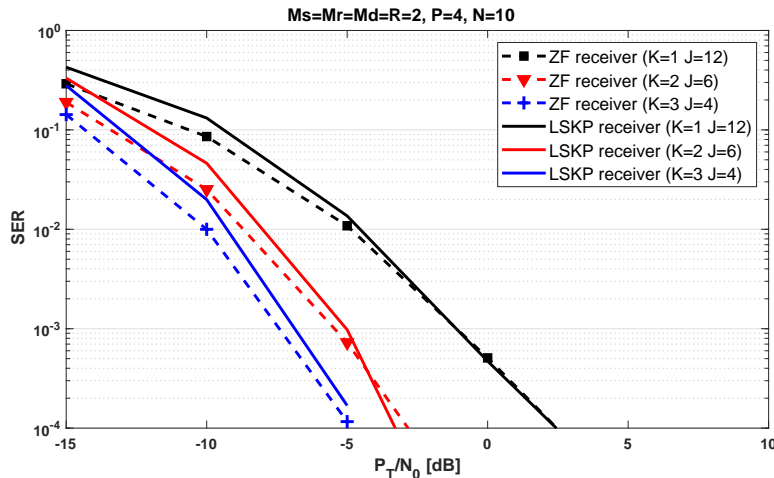
In the next experiments, we evaluate the performance of the proposed LSKP receiver for the proposed MIMO multi-relay system. Firstly, we study the behavior of the proposed semi-blind receiver by changing the number of relays and in the time-spreading lengths, for fixed  $P_T/N_0$  values. Figure 37 shows the SER versus  $K$  (number of relays) for the LSKP receiver in comparison with the ZF method. This figure shows that the number of relays has a great impact on the SER, illustrating the benefits of the cooperative diversity in the network. Moreover, it is possible to see that the proposed receiver provides a SER performance very close to the one of the ZF method, especially for a low SNR. Figure 38 shows the SER versus  $P$  for two values of  $J$  and  $P_T/N_0$ . This figure shows that the proposed receiver is able to efficiently exploit the time-spreading at the source and relay in order to improve the SER. Once again, it can be viewed that the LSKP and the ZF receivers provide close SER curves.

Figure 38 – Impact of the time-spreading length on the SER performance

Figure 39 – SER performance for the LSKP receiver with  $JK = 8$ 

Figures 39 and 40 show the SER obtained by the LSKP versus  $P_T/N_0$ , for several values of  $K$  and  $J$ , considering the cases (a)  $JK = 8$  and (b)  $JK = 12$ . When  $K = 1$ , the proposed system is equivalent to the NTD-based MIMO single-relay system introduced in [34]. For a fair comparison between the systems, we plot curves with configurations that preserve the same transmission rate. The transmission rate of the proposed multi-relay system is proportional to  $R/P(JK + 1)$ . For the single-relay system of [34] (case  $K = 1$ ), the transmission rate is proportional to  $R/P(J + 1)$ . In other words, to keep the same transmission rate for both systems, we use the same values of  $R$  and  $P$ , and the same value of the product  $JK$ .

In both cases, one can note significant gains in the SER performance with an increase in the number of relays, for a fixed value of  $JK$ . The cooperative diversity exploited by the CNTD-based system allows to improve the symbol estimation in comparison with the NTD-based system. The single-relay system does not exploit cooperative diversity, inducing an increase of  $J$  to obtain the same transmission rate. The simulation results show that the cooperative diversity

Figure 40 – SER performance for the LSKP receiver with  $JK = 12$ 

gain is more advantageous than the gain provided by time-spreading. Once again, the LSKP receiver gives performances close to the one obtained with the ZF receiver.

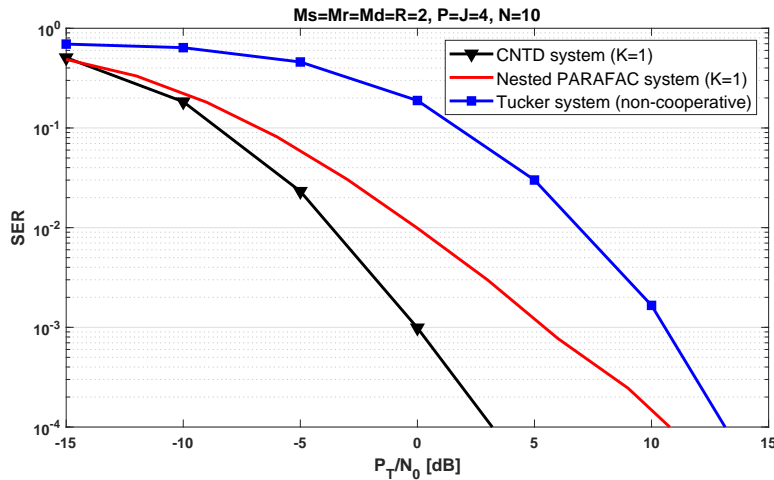
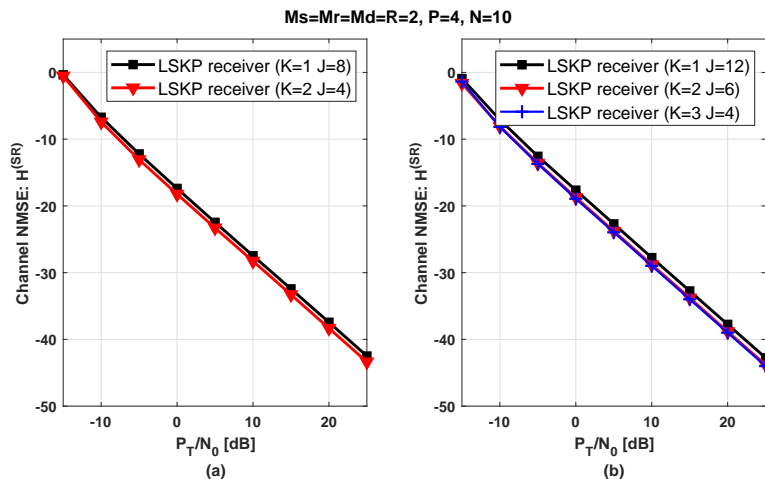
In Figures 37 to 40, we can note that the LSKP overcomes the ZF performance in some cases. This degradation can be explained by the orthogonality property of the matrices  $\mathbf{C}_{KM_T M_R \times KJ}^{(R)}$  and  $\mathbf{C}_{RM_S \times P}^{(S)}$ , discussed in Property 6, which cannot be exploited by the ZF receiver. As discussed in Chapter 4, the pseudo-inverse in (5.24), used by the ZF receiver, has a weaker conditioning when compared to the pseudo-inverse in (5.22) used by the LSKP receiver, which may cause noise enhancement. By means of simulation, we have calculated the condition number of the pseudo-inverse in (5.24). It has an average value of 1.62, with a standard deviation of 0.43, for the considered scenario.

Aiming to illustrate the advantages of the CNTD-based system over other tensor-based approaches, in Figure 41, we provide a SER comparison between the proposed LSKP receiver and two existing systems that consider space-time coding structures. The first one is a receiver based on a Khatri-Rao factorization (KRF) algorithm proposed in [18] for a nested PARAFAC based multi-hop relaying system that uses a simplified KRST coding. The second one is a non-cooperative system using a TSTC at the source, equivalent to the one proposed in Chapter 4 (Subsection 4.3.2), which is equivalent to the one proposed in this chapter when relays are absent. For the sake of comparison, we propose a LSKP-based solution for this system, which is based on the following relationship

$$\mathbf{S} \otimes \mathbf{H}^{(SD)} = \mathbf{X}_{NM_D \times P}^{(SD)} \left( \mathbf{C}_{RM_S \times P}^{(S)} \right)^\dagger, \quad (5.28)$$

where  $\mathbf{H}^{(SD)} \in \mathbb{C}^{M_D \times M_S}$  is the channel matrix between the source and destination and  $\mathbf{X}_{NM_D \times P}^{(SD)}$  is the tall mode-3 unfolding of the received signal tensor  $\mathcal{X}^{(SD)} \in \mathbb{C}^{M_D \times P \times N}$  that satisfies a

Figure 41 – SER performance comparison for several receivers

Figure 42 – NMSE of  $\mathcal{H}^{(SR)}$  for the LSKP receiver with (a)  $JK = 8$  and (b)  $JK = 12$ 

third-order Tucker decomposition. In order to have a fair comparison, we simulated the proposed LSKP with  $K = 1$ .

From Figure 41, we can conclude that the use of TSTC leads the proposed receiver to give better performance than the one of [18], due to a more efficient exploitation of the spatial transmit diversity at the source and relay nodes by this coding. When compared to the non-cooperative system, as expected, one can conclude that the proposed relay system provides a remarkable gain in the symbol estimation, which can be explained by the smaller path-loss experienced by each hop in a cooperative system, leading to a less severe channel attenuation. The new TSTC applied by the relay, inserting more diversity, also justify this outperforming.

Figures 42 and 44 give the NMSE of the estimated channels computed as given in 4.54. Figures 42 (a) and 43 (a) show respectively the NMSE of  $\mathcal{H}^{(SR)}$  and  $\mathcal{H}^{(RD)}$  versus  $P_T/N_0$  for  $JK = 8$  and Figures 42 (b) and 43 (b) show respectively the NMSE of  $\mathcal{H}^{(SR)}$  and

Figure 43 – NMSE of  $\mathcal{H}^{(RD)}$  for the LSKP receiver with (a)  $JK = 8$  and (b)  $JK = 12$

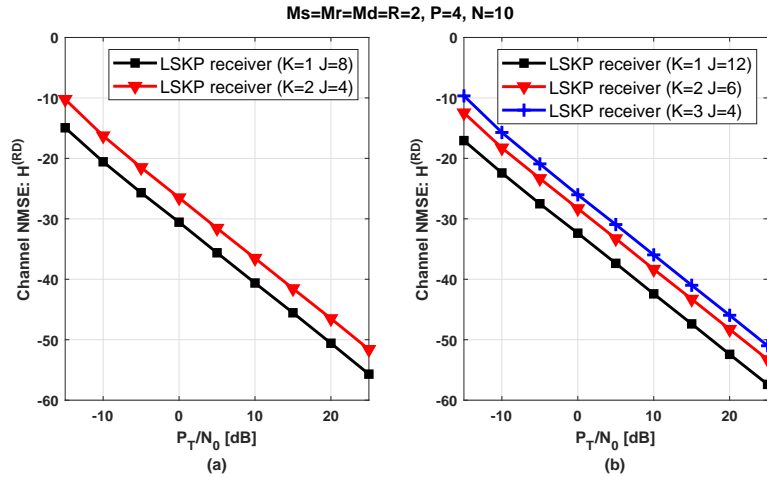
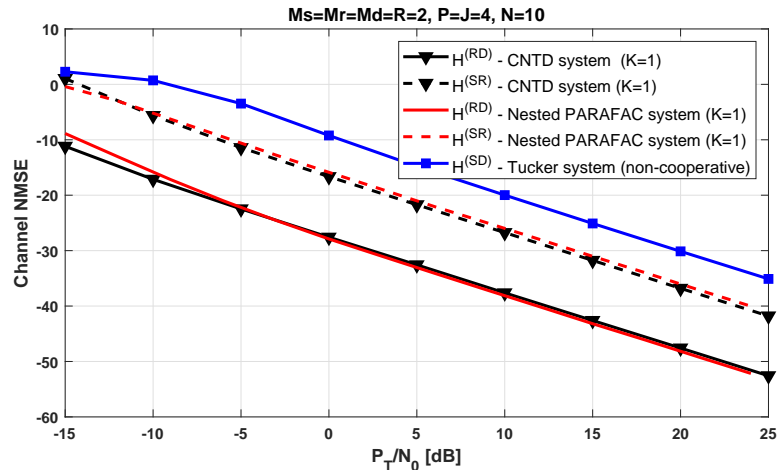


Figure 44 – Channel NMSE comparison for several receivers



$\mathcal{H}^{(RD)}$  versus  $P_T/N_0$  for  $JK = 12$ . It can be noted in Figures 42 (a) and 42 (b) that the NMSEs of  $\mathcal{H}^{(SR)}$  are similar for all the tested configurations, including the two different values of the product  $JK$ . However, for the NMSE of  $\mathcal{H}^{(RD)}$ , one can note in Figures 43 (a) and 43 (b) a degradation in the estimate of the channels when the number of relays is increased. That comes from the fact that, with more relays, there are more channel coefficients to be estimated by the receiver with the same number of received signals. Note that when we fix  $JK$ , the system has the same quantity of data arriving at destination.

Figure 44 compares the NMSE of  $\mathcal{H}^{(SR)}$  and  $\mathcal{H}^{(RD)}$  provided by the proposed receiver with the ones provided by the technique of [18] and by the non-cooperative approach based on (5.28). Once again, in order to have a fair comparison, we simulated the proposed LSKP with  $K = 1$ . From this figure, we can conclude that the non-cooperative approach provides NMSE much worse than the other methods. Moreover, the proposed receiver and the method of [18]

provided roughly similar NMSE curves.

## 5.4 Summary

In this chapter, a two-hop MIMO multi-relay system using TSTC at the source and the relay nodes has been proposed. The signals received at destination define a fifth-order tensor, which satisfies a CNTD model. This CNTD is characterized by a contraction between a generalized Tucker decomposition and a Tucker one. Assuming the core tensors known, essential uniqueness of a fifth-order CNTD has been established.

By exploiting this tensor modeling, a semi-blind receiver has been derived for the proposed system, which exploits the cooperative diversity induced by  $K$  relays operating in a sequential way. The performance of the proposed receiver has been evaluated by means of extensive Monte Carlo simulations. The simulation results show the effectiveness of exploiting the cooperative diversity by increasing the number of relays. In comparison with the NTD-based single-relay system [34], the proposed CNTD-based system allows to improve the SER performance, keeping the same transmission rate. It is also shown that the CNTD-based system with TSTC at the source and the relays outperform the cooperative system of [18] and the non-cooperative system of Chapter 4, which are based on other tensor approaches.

## 6 TWO-HOP OFDM MIMO RELAY SYSTEM WITH TSTC BASED ON CNTD

In this chapter, we present a two-hop OFDM MIMO relay system with tensor codings at the source and the relay. The transmission scheme is composed of two steps. In the first one, the source sends a data tensor using a TSTC with multiplexing of the symbols across space (antennas), time (blocks) and frequency (subcarriers) domains. In the second one, the AF relay re-encodes the received signals by using a new TSTC before forwarding them to the destination. The signals received at destination form a fifth-order tensor that satisfies a CNTD, as introduced in Subsection 3.2.2.

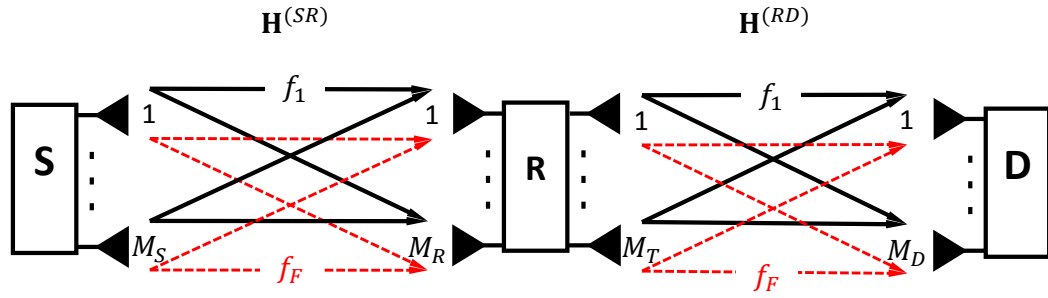
The system proposed in this chapter exploits a little different structure for the CNTD model in relation to Chapter 5. Indeed, in the previous chapter, the received signal tensor is written as a fifth-order CNTD, characterized as a contraction between a generalized Tucker–(2, 4) model and a Tucker–(1, 3) one, while the CNTD of the present chapter is given as a contraction between a Tucker–(2, 3) model and a generalized Tucker–(1, 4) one.

By exploiting matrix unfoldings of the signal tensor model, we derive a closed-form semi-blind receiver, based on the LSKP technique, for jointly estimating the symbols and channels. Monte Carlo simulation results are provided to evaluate the behavior of the system and to illustrate the effectiveness of the proposed receiver.

### 6.1 System Model

Let us consider a two-hop OFDM MIMO relay system as given in Figure 45, composed of a source (S), a relay (R) and a destination (D), with a transmission scheme in two steps. In the first one, the source sends symbols multiplexed in space, time and frequency to the relay. The information symbols constitute a tensor  $\mathcal{S} \in \mathbb{C}^{N \times R \times F}$  that is encoded by the TSTC  $\mathcal{C}_{(f)}^{(S)} \in \mathbb{C}^{M_S \times P \times R}$ , which provide multiplexing of the symbols across the space, time and frequency domains, with  $f = 1, \dots, F$ , where  $N$ ,  $R$ ,  $F$ ,  $P$  and  $M_S$  are respectively the numbers of symbol periods, data streams, subcarriers, transmission blocks and transmit antennas. The subcarriers used by the source are assumed neighbors in such a way that the channel coefficients are invariant across the subcarriers. Due to this assumption, the number  $F$  of subcarriers must not be very high. The coded signals to be transmitted by the  $m_S$ -th antenna of the source, during  $n$ -th symbol period of the  $p$ -th transmission block, associated with the  $f$ -th subcarrier, are given

Figure 45 – Two-hop OFDM MIMO relaying system



by

$$x_{m_S,p,n,f}^{(S)} = \sum_{r=1}^R c_{m_S,p,r,f}^{(S)} s_{n,r,f}. \quad (6.1)$$

The above equation shows that, at each symbol period  $n$  of the  $p$ -th block, the source transmits a linear combination of  $R$  data streams, using a certain transmit antenna and subcarrier. The signals are sent to the  $M_R$  receive antennas at the relay node through the channels with coefficients  $h_{m_R,m_S}^{(SR)}$ , for  $1 \leq m_R \leq M_R$  and  $1 \leq m_S \leq M_S$ , that attenuate in the same way over all the subcarriers. The signals received by the relay are given as

$$x_{m_R,p,n,f}^{(SR)} = \sum_{m_S=1}^{M_S} \sum_{r=1}^R h_{m_R,m_S}^{(SR)} c_{m_S,p,r,f}^{(S)} s_{n,r,f}. \quad (6.2)$$

For the sake of simplicity, the noise was omitted in the description of the received signals.

In the second step, the relay re-encodes the received signals before forwarding them to the destination through the channels with coefficients  $h_{m_D,m_T}^{(RD)}$ , for  $1 \leq m_D \leq M_D$  and  $1 \leq m_T \leq M_T$ , where  $M_D$  and  $M_T$  are respectively the numbers of receive antennas at destination and transmit antennas at the relay. The relay uses the TSTC  $\mathcal{C}^{(R)} \in \mathbb{C}^{M_T \times J \times M_R}$ , where  $J$  is the number of transmission blocks, which gives the following signals received at destination

$$x_{m_D,j,p,n,f}^{(SRD)} = \sum_{m_T=1}^{M_T} \sum_{m_R=1}^{M_R} \sum_{m_S=1}^{M_S} \sum_{r=1}^R h_{m_D,m_T}^{(RD)} c_{m_T,j,m_R}^{(R)} h_{m_R,m_S}^{(SR)} c_{m_S,p,r,f}^{(S)} s_{n,r,f}. \quad (6.3)$$

Note that the tensor in (6.3) satisfies the CNTD model given in (3.42), with the correspondences  $(\mathbf{B}^{(1)}, \mathcal{G}^{(3)}, \mathbf{B}^{(2)}, \mathcal{G}^{(4)}, \mathcal{B}^{(3)}) \iff (\mathbf{H}^{(RD)}, \mathcal{C}^{(R)}, \mathbf{H}^{(SR)}, \mathcal{C}^{(S)}, \mathcal{S})$ .

The coded transmitted signals defined in (6.1) satisfy a generalized Tucker-(1, 4) model with the following tensor representation

$$\mathcal{X}^{(S)} = \mathcal{C}^{(S)} \times_3 \mathcal{S} \in \mathbb{C}^{M_S \times P \times N \times F}. \quad (6.4)$$

From the received signal model (6.3), we can define the effective channel between the source and the destination as

$$h_{m_D, j, m_S}^{(SRD)} = \sum_{m_T=1}^{M_T} \sum_{m_R=1}^{M_R} h_{m_D, m_T}^{(RD)} c_{m_T, j, m_R}^{(R)} h_{m_R, m_S}^{(SR)} \quad (6.5)$$

which has the following tensor notation

$$\mathcal{H}^{(SRD)} = \mathcal{C}^{(R)} \times_1 \mathbf{H}^{(RD)} \times_3 \mathbf{H}^{(SR)T} \in \mathbb{C}^{M_D \times J \times M_S}, \quad (6.6)$$

corresponding to a Tucker-(2, 3) model. The received signals in (6.3) are then written as the following summation

$$x_{m_D, j, p, n, f}^{(SRD)} = \sum_{m_S=1}^{M_S} h_{m_D, j, m_S}^{(SRD)} x_{m_S, p, n, f}^{(S)} \quad (6.7)$$

which represents the contraction between the tensors  $\mathcal{H}^{(SRD)}$  and  $\mathcal{X}^{(S)}$  over the common mode ( $m_S$ ).

By fixing the index  $f$  in (6.4), we get the tensor  $\mathcal{X}_{(f)}^{(S)} = \mathcal{C}_{(f)}^{(S)} \times_3 \mathbf{S}_{(f)} \in \mathbb{C}^{M_S \times P \times N}$  that represents the coded signals transmitted by the subcarrier  $f$ . Thus, we can write the signals received by the destination with the subcarrier  $f$  as the following contraction between the tensors  $\mathcal{H}^{(SRD)}$  and  $\mathcal{X}_{(f)}^{(S)}$  over the common mode  $m_S$

$$\mathcal{X}_{(f)}^{(SRD)} = \mathcal{H}^{(SRD)} *_3^1 \mathcal{X}_{(f)}^{(S)} \in \mathbb{C}^{M_D \times J \times P \times N}. \quad (6.8)$$

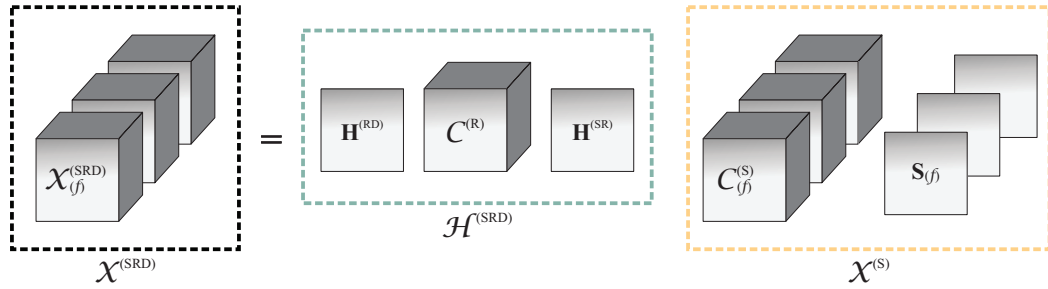
The tensor (6.8) represents the signals received at destination of the system of Figure 45 when a single subcarrier ( $f$ ) is considered and satisfies a fourth-order NTD [34]. For the multicarrier case, the collection of tensors  $\{\mathcal{X}_{(1)}^{(SRD)}, \dots, \mathcal{X}_{(F)}^{(SRD)}\}$  forms a coupling of NTDs by sharing the common tensor  $\mathcal{H}^{(SRD)}$ . Note that the tensor  $\mathcal{H}^{(SRD)}$  is independent of the index  $f$ , being common to all  $F$  decompositions. Thus, the tensor of received signals (6.3) can be viewed as a coupling of tensors  $\mathcal{X}_{(f)}^{(SRD)}$ , for  $f = 1, \dots, F$ , and, then, it is rewritten as the following CNTD

$$\mathcal{X}^{(SRD)} = \mathcal{H}^{(SRD)} *_3^1 \mathcal{X}^{(S)} \in \mathbb{C}^{M_D \times J \times P \times N \times F}. \quad (6.9)$$

Note that the symbol tensor  $\mathcal{X}^{(S)}$  is given by concatenating the slices  $\mathcal{X}_{(f)}^{(S)}$  along the fourth mode as follows

$$\mathcal{X}^{(S)} = \mathcal{X}_{(1)}^{(S)} \sqcup_4 \mathcal{X}_{(2)}^{(S)} \dots \sqcup_4 \mathcal{X}_{(F)}^{(S)}. \quad (6.10)$$

Figure 46 – Block diagram for the CNTD-based signal model



The tensors (6.4), (6.6), (6.8) and (6.9) correspond to the tensors (3.38), (3.35), (3.34) and (3.37), respectively, with the following correspondences between the models

$$(\mathcal{T}^{(3)}, \mathcal{T}^{(4)}, \mathbf{B}^{(1)}, \mathcal{G}^{(3)}, \mathbf{B}^{(2)}, \mathcal{G}^{(4)}, \mathcal{B}^{(3)}) \iff (\mathcal{H}^{(SRD)}, \mathcal{X}^{(S)}, \mathbf{H}^{(RD)}, \mathcal{C}^{(R)}, \mathbf{H}^{(SR)}, \mathcal{C}^{(S)}, \mathcal{S}). \quad (6.11)$$

Figure 46 shows a block diagram to illustrate this modeling for the signals in (6.9) based on a CNTD. As discussed in Subsection 3.2.2, the tensor model exploited here is another application of CNTD, different from the one exploited in Chapter 5, by considering a contraction between a Tucker-(2, 3) model and a generalized Tucker-(1, 4) one, instead of a generalized Tucker-(2, 4) model and a Tucker-(1, 3) one.

In the noisy model

$$\tilde{\mathcal{X}}^{(SRD)} = \mathcal{X}^{(SRD)} + \mathcal{N}^{(SRD)}, \quad (6.12)$$

we consider the global noise tensor \$\mathcal{N}^{(SRD)} \in \mathbb{C}^{M\_D \times J \times P \times N \times F}\$ given by

$$\mathcal{N}^{(SRD)} = \mathcal{N}^{(D)} + (\mathcal{C}^{(R)} \times_1 \mathbf{H}^{(RD)}) *_3^1 \mathcal{N}^{(R)}, \quad (6.13)$$

which has the following scalar notation

$$n_{m_D, j, p, n, f}^{(SRD)} = n_{m_D, j, p, n, f}^{(D)} + \sum_{m_T=1}^{M_T} \sum_{m_R=1}^{M_R} h_{m_D, m_T}^{(RD)} c_{m_T, j, m_R}^{(R)} n_{m_R, p, n, f}^{(R)}, \quad (6.14)$$

where \$n\_{m\_D, j, p, n, f}^{(D)}\$ and \$n\_{m\_R, p, n, f}^{(R)}\$ are entries of the tensors \$\mathcal{N}^{(D)} \in \mathbb{C}^{M\_D \times J \times P \times N \times F}\$ and \$\mathcal{N}^{(R)} \in \mathbb{C}^{M\_R \times P \times N \times F}\$ that represent the noise at the destination and at the relay, respectively.

## 6.2 Semi-blind receiver

In this section, we develop a closed-form semi-blind receiver to estimate the symbols and the channel matrices. The receiver follows the LSKP approach used in previous chapter.

By combining the first two modes of (6.9), we define the following contracted form of  $\mathcal{X}^{(SRD)}$ , which satisfies a generalized Tucker-(2, 4) model,

$$\begin{aligned}\mathcal{X}_{M_D J \times P \times N \times F}^{(SRD)} &= \mathcal{X}^{(S)} \times_1 \mathbf{H}_{M_D J \times M_S}^{(SRD)} \\ &= \mathcal{C}^{(S)} \times_1 \mathbf{H}_{M_D J \times M_S}^{(SRD)} \times_3 \mathcal{S},\end{aligned}\quad (6.15)$$

from which we can get the following unfolded matrix

$$\mathbf{X}_{NM_D J \times FP}^{(SRD)} = \left( \mathbf{S}_{N \times FR} \otimes \mathbf{H}_{M_D J \times M_S}^{(SRD)} \right) \mathbf{C}_{FRM_S \times FP}^{(S)}, \quad (6.16)$$

where  $\mathbf{H}_{M_D J \times M_S}^{(SRD)}$  represents a mode-3 unfolding of the effective channel (6.6) and it is given by

$$\mathbf{H}_{M_D J \times M_S}^{(SRD)} = \left( \mathbf{H}^{(RD)} \otimes \mathbf{I}_J \right) \mathbf{C}_{M_T J \times M_R}^{(R)} \mathbf{H}^{(SR)}. \quad (6.17)$$

To define the unfoldings in (6.17) and (6.16), we used the matrices  $\mathbf{C}_{M_T J \times M_R}^{(R)}$  and  $\mathbf{C}_{FRM_S \times FP}^{(S)}$ , respectively, which represent unfoldings of the coding tensors  $\mathcal{C}^{(R)}$  and  $\mathcal{C}^{(S)}$ . Note that the unfolding  $\mathbf{C}_{FRM_S \times FP}^{(S)}$  is defined as a block matrix given by  $\text{bdiag} \left[ \mathbf{C}_{\cdot \cdot 1f}^{(S)} \cdots \mathbf{C}_{\cdot \cdot Rf}^{(S)} \right]$ .

From (6.16), we define the KP  $\mathbf{\Omega} = \mathbf{S}_{N \times FR} \otimes \mathbf{H}_{M_D J \times M_S}^{(SRD)} \in \mathbb{C}^{NM_D J \times FRM_S}$ . Thus, we derive the LS estimate of  $\mathbf{\Omega}$  as

$$\widehat{\mathbf{\Omega}} = \mathbf{X}_{NM_D J \times FP}^{(SRD)} \left( \mathbf{C}_{FRM_S \times FP}^{(S)} \right)^\dagger. \quad (6.18)$$

From the LS estimate (6.18), we obtain the estimates of the symbols and the effective channel  $\widehat{\mathbf{S}}_{N \times FR}$  and  $\widehat{\mathbf{H}}_{M_D J \times M_S}^{(SRD)}$  by applying the low-rank approximation algorithm.

In order to estimate the individual channel matrices  $\mathbf{H}^{(SR)}$  and  $\mathbf{H}^{(RD)}$ , we consider a reshaped form of  $\widehat{\mathbf{H}}_{M_D J \times M_S}^{(SRD)}$  defined as follows

$$\widehat{\mathbf{H}}_{M_D M_S \times J}^{(SRD)} = \left( \mathbf{H}^{(RD)} \otimes \mathbf{H}^{(SR)T} \right) \mathbf{C}_{M_T M_R \times J}^{(R)}. \quad (6.19)$$

Defining the KP  $\mathbf{\Gamma} = \mathbf{H}^{(RD)} \otimes \mathbf{H}^{(SR)T} \in \mathbb{C}^{M_D M_S \times M_T M_R}$ , the LS estimate of  $\mathbf{\Gamma}$  is given by

$$\widehat{\mathbf{\Gamma}} = \widehat{\mathbf{H}}_{M_D M_S \times J}^{(SRD)} \left( \mathbf{C}_{M_T M_R \times J}^{(R)} \right)^\dagger. \quad (6.20)$$

Once  $\widehat{\mathbf{\Gamma}}$  is estimated using  $\widehat{\mathbf{H}}_{M_D M_S \times J}^{(SRD)}$ , obtained previously by the algorithm, we apply again the low-rank approximation algorithm to estimate  $\widehat{\mathbf{H}}^{(SR)}$  and  $\widehat{\mathbf{H}}^{(RD)}$ . The LSKP receiver is summarized in Table 5, where  $\tilde{\mathbf{X}}_{NM_D J \times FP}^{(SRD)}$  is the noisy version of the unfolding  $\mathbf{X}_{NM_D J \times FP}^{(SRD)}$ .

### Identifiability Conditions

Table 5 – LSKP receiver for two-hop OFDM MIMO relay system

- 
1. Compute the LS estimate of the KP  $\mathbf{\Omega} = \mathbf{S}_{N \times FR} \otimes \mathbf{H}_{M_D J \times M_S}^{(SRD)}$ :  

$$\hat{\mathbf{\Omega}} = \tilde{\mathbf{X}}_{NM_D J \times FP}^{(SRD)} \left( \mathbf{C}_{FR M_S \times FP}^{(S)} \right)^\dagger.$$
  2. Estimate the matrix unfoldings  $\hat{\mathbf{S}}_{N \times FR}$  and  $\hat{\mathbf{H}}_{M_D J \times M_S}^{(SRD)}$  by applying the low-rank approximation algorithm in Appendix C.
  3.  $\hat{\mathbf{H}}_{M_D M_S \times J}^{(SRD)} \leftarrow \text{reshape} \left( \hat{\mathbf{H}}_{M_D J \times M_S}^{(SRD)} \right).$
  4. Compute the LS estimate of the KP  $\mathbf{\Gamma} = \mathbf{H}^{(RD)} \otimes \mathbf{H}^{(SR)T}$ :  

$$\hat{\mathbf{\Gamma}} = \hat{\mathbf{H}}_{M_D M_S \times J}^{(SRD)} \left( \mathbf{C}_{M_T M_R \times J}^{(R)} \right)^\dagger.$$
  5. Estimate the matrices  $\hat{\mathbf{H}}^{(RD)}$  and  $\hat{\mathbf{H}}^{(SR)}$  by applying the low-rank approximation algorithm in Appendix C.
  6. Eliminate the scaling ambiguities using (6.21) and project the estimated symbols onto the alphabet.
- 

To compute the LS estimates in (6.18) and (6.20), the unfoldings of the known tensor codings  $\mathbf{C}_{FR M_S \times FP}^{(S)}$  and  $\mathbf{C}_{M_T M_R \times J}^{(R)}$  must be right-invertible, which leads to the necessary identifiability conditions  $P \geq R M_S$  and  $J \geq M_T M_R$ . As already discussed in previous chapters, the factors of a KP can only be estimated up to scalar ambiguities, as shown in Appendix C. Thus, the factorization of the KPs  $\hat{\mathbf{\Omega}}$  and  $\hat{\mathbf{\Gamma}}$  leads to estimated factors with the ambiguities  $\hat{\mathbf{S}}_{N \times FR} = \alpha_{\mathbf{S}} \mathbf{S}_{N \times FR}$  and  $\hat{\mathbf{H}}^{(\cdot)} = \alpha_{\mathbf{H}^{(\cdot)}} \mathbf{H}^{(\cdot)}$ , where  $\alpha_{\mathbf{S}}$  and  $\alpha_{\mathbf{H}^{(\cdot)}}$  are the scaling ambiguities. These ambiguities can be removed by assuming the a priori knowledge of one pilot symbol ( $s_{1,1,1}$ ) and one coefficient of one channel matrix ( $h_{1,1}^{(RD)}$ ) in such a way that we can make  $\alpha_{\mathbf{S}} = \hat{s}_{1,1,1}/s_{1,1,1}$  and  $\alpha_{\mathbf{H}^{(RD)}} = \hat{h}_{1,1}^{(RD)}/h_{1,1}^{(RD)}$ . The ambiguities are then cancelled as follows

$$\begin{aligned}
 \hat{\mathbf{S}}_{N \times FR} &\leftarrow \alpha_{\mathbf{S}}^{-1} \hat{\mathbf{S}}_{N \times FR} \\
 \hat{\mathbf{H}}^{(RD)} &\leftarrow \alpha_{\mathbf{H}^{(RD)}}^{-1} \hat{\mathbf{H}}^{(RD)} \\
 \hat{\mathbf{H}}^{(SR)} &\leftarrow \alpha_{\mathbf{H}^{(RD)}} \hat{\mathbf{H}}^{(SR)}.
 \end{aligned} \tag{6.21}$$

### 6.3 Simulation Results

In this section, simulation results are provided to illustrate the efficiency of the proposed receiver for the two-hop OFDM MIMO relay system. The results were averaged over  $5 \times 10^4$  Monte Carlo runs and are given in terms of SER and channel NMSE, which are plotted as function of the total transmission power to noise spectral density ratio ( $P_T/N_0$ ).

The transmitted symbols were randomly generated from a unit energy 4-QAM alphabet and white Gaussian noises with variance  $N_0$  were added at each receiving node. At each run,  $N_0$  was fixed according to the desired  $P_T/N_0$  value. The channels are assumed to be flat-fading, with i.i.d. complex Gaussian entries. An exponential path-loss model is assumed to

simulate the variance of the channel coefficients, i.e.  $\sigma_{\mathbf{H}}^2 = 1/d^4$ , where  $d$  is the distance of each hop.

The coding tensors  $\mathbf{C}_{FRM_S \times FP}^{(S)}$  and  $\mathbf{C}_{M_T M_R \times J}^{(R)}$  were chosen as a truncated discrete Fourier transform (DFT) matrix in order to avoid the noise enhancement, as discussed previously. The coding tensors are normalized by using (5.26)-(5.27) in order to control the transmission power at each node. The total system power  $P_T$  is kept constant and arbitrarily chosen equal to 1. The other parameters used in the simulations are indicated above each figure.

In some results, we provide a comparison with a non-coupled estimation of the symbol and channel matrices, in order to illustrate the advantage of the proposed receiver based on a coupled tensor model. The non-coupled estimation is done by considering separately the signals of each subcarrier, which is equivalent to  $F$  independent estimations of a single-carrier system. In other words, the non-coupled receiver is simply the application of the proposed LSKP method with  $F = 1$ , which is equivalent to the NTD-based receiver of [34].

Since the information symbols are multiplexed across the multiple carriers, each non-coupled estimate yields a slice  $\mathbf{S}_{..f} \in \mathbb{C}^{N \times R}$  of the symbol tensor. However, to compute the SER performance in the non-coupled case, the entire estimated symbol tensor is taken into account.

We also provide the performance for the case of perfect channel knowledge using a ZF receiver, which can be derived from (6.15) as

$$\mathbf{S}_{N \times FR}^T = \left[ \left( \mathbf{I}_{FP} \otimes \mathbf{H}_{M_D J \times M_S}^{(SRD)} \right) \mathbf{C}_{FPM_S \times FR}^{(S)} \right]^\dagger \tilde{\mathbf{X}}_{FPM_D J \times N}^{(SRD)}. \quad (6.22)$$

### 6.3.1 ZF and LSKP performance

Figure 47 shows the SER versus  $P_T/N_0$  for different numbers of subcarriers,  $F \in \{1, 2, 4\}$ . One can note that the SER performance is not significantly changed when  $F$  is increased. That leads to the conclusion that, compared to the single-carrier two-hop MIMO relay system (case  $F = 1$ ), the multi-carrier system allows to increase the number of information symbols without degrading the SER performance due to a simultaneous increase of received signals. However, it is worth noting that the spectral efficiency of the system, given by  $R/P(J + 1)$ , does not depend on the number  $F$  of subcarriers. Compared to the non-coupled estimation, we also conclude that the symbols estimation is not significantly changed, regardless the number of subcarriers.

Figure 48 shows the SER versus  $F$  for fixed  $P_T/N_0$  values with the ZF and LSKP

Figure 47 – SER performance for different numbers of subcarriers

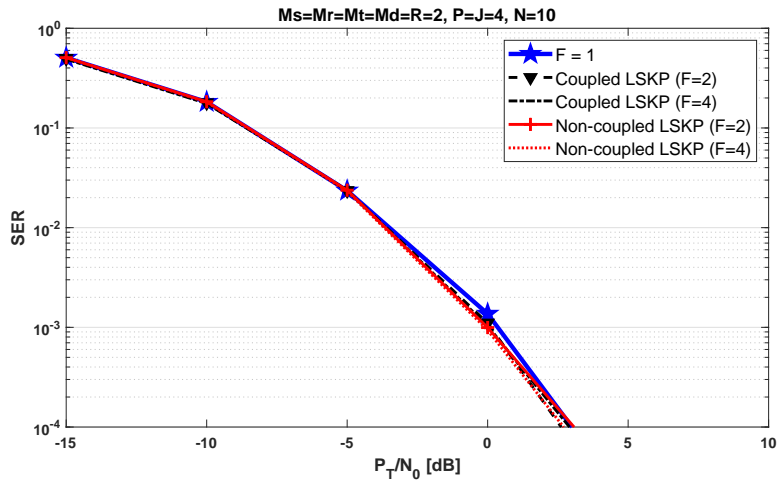


Figure 48 – Influence of the number of subcarriers on the SER performance

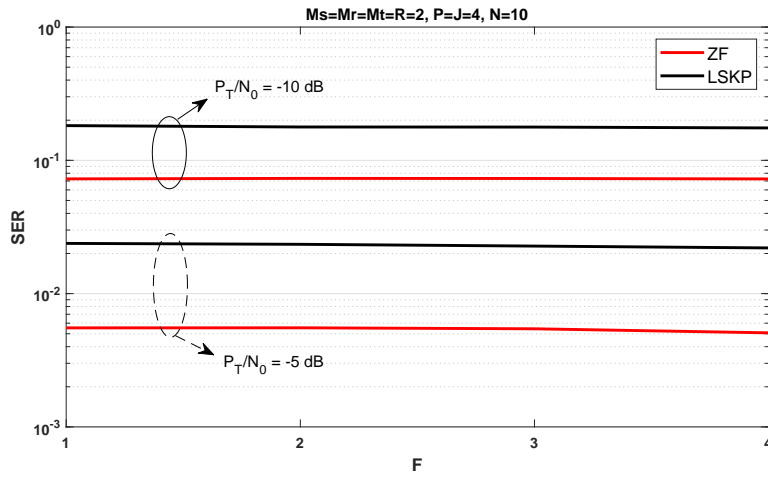
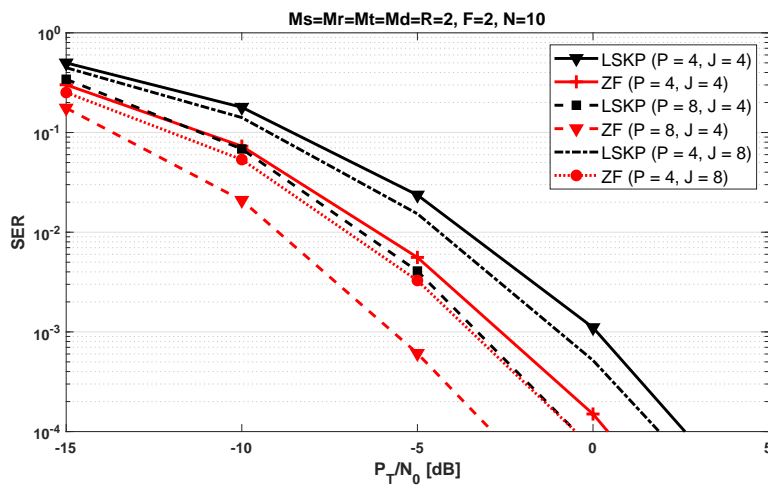


Figure 49 – Performance comparison with ZF receiver for different values of  $P$  and  $J$



receivers, in order to illustrate more clearly how sensitive is the system to an increase in  $F$ . From this result, one can really note the low impact of the number of subcarriers on the system performance in relation to symbol estimation, regardless the receiver algorithm.

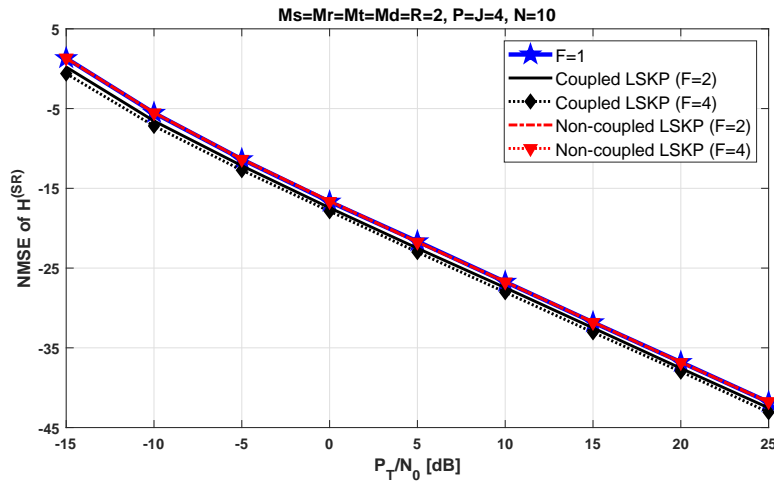
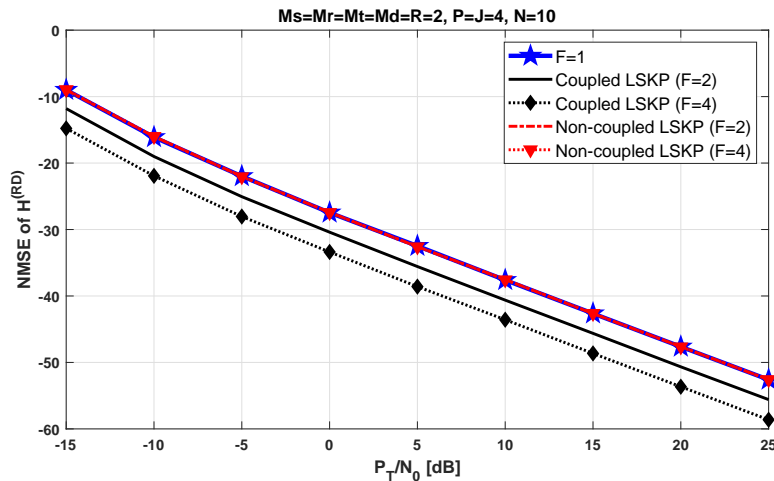
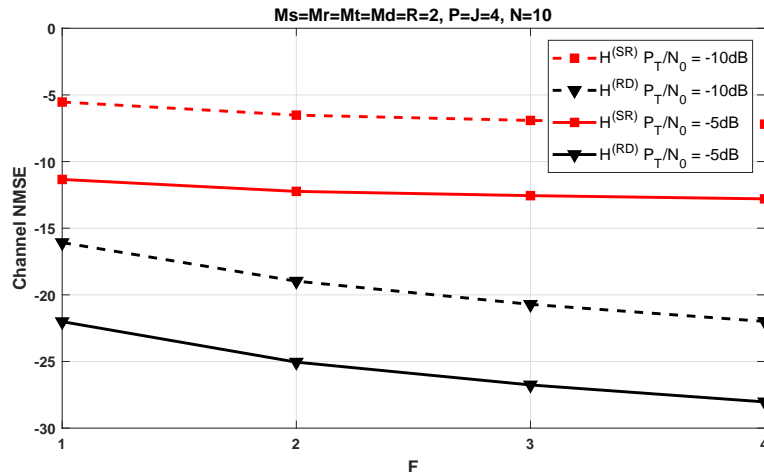
Figure 50 – NMSE of  $\mathbf{H}^{(SR)}$  for coupled and non-coupled estimationFigure 51 – NMSE of  $\mathbf{H}^{(RD)}$  for coupled and non-coupled estimation

Figure 49 compares the SER versus  $P_T/N_0$  provided by the proposed system for different values of the time spreading lengths  $P$  and  $J$ . As expected, an increase of  $P$  and  $J$  yields a performance improvement, with an increase of  $P$  providing a more pronounced gain than an increase of  $J$ . We can note a SER degradation when the proposed receiver is compared to the ZF one. For a target SER of  $10^{-3}$ , the ZF receiver provides a gain of around 2 dB over the proposed one. However, the proposed semi-blind LSKP receiver has for advantage over the ZF one the fact that it does not assume the channel knowledge, allowing a joint estimation of the symbols and the channels.

Concerning the channel estimation, Figure 50 and 51 show the NMSE of the estimated channels versus  $P_T/N_0$  for the same cases addressed in Figure 47. We can note that, for both  $\mathbf{H}^{(SR)}$  and  $\mathbf{H}^{(RD)}$  matrices, the non-coupled channel estimation keeps the same performance when the number of subcarriers is increased. These results are equivalent to the case  $F = 1$ .

Figure 52 – Impact of the number of subcarriers on the channel NMSE



For the coupled-based receiver, we can note some improvement in the channel estimation when  $F$  is increased, being more significant for the relay-destination channel ( $\mathbf{H}^{(RD)}$ ). For a fixed NMSE value, the coupled LSKP gives gains of 1 dB for  $\mathbf{H}^{(SR)}$  and approximately 6 dB for  $\mathbf{H}^{(RD)}$  with  $F = 4$ . The channel estimation gain of the coupled-based receiver is due to the fact that the channel matrices compose the coupled factor  $\mathcal{H}^{(SRD)}$ , common to all subcarriers, leading the destination to have a greater amount of resources (received signals) to be jointly processed.

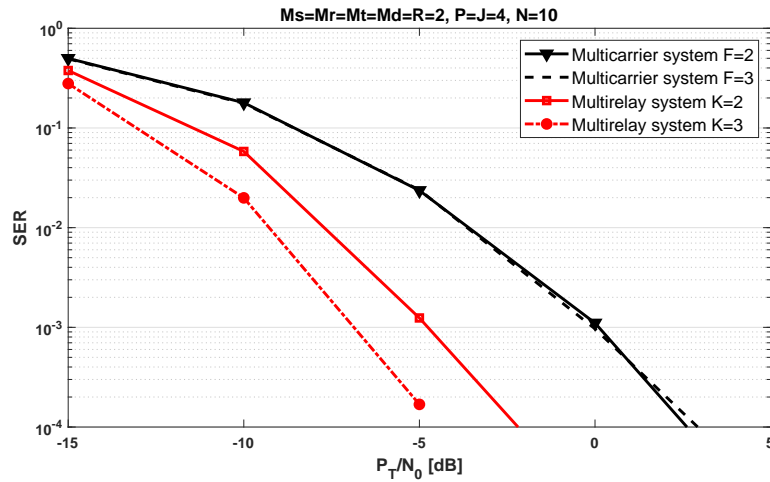
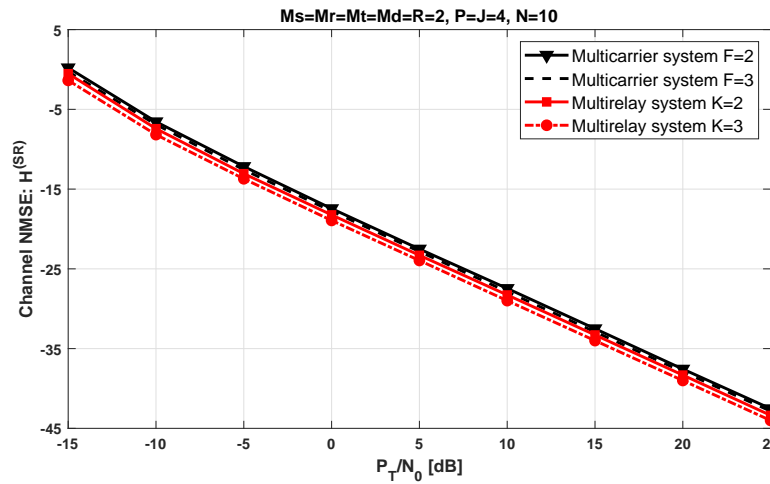
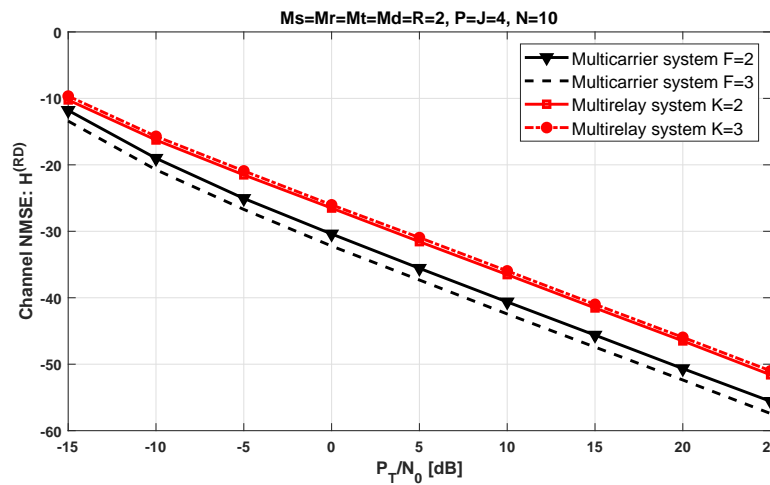
Figure 52 shows the NMSE of the estimated channels versus  $F$  for fixed values of  $P_T/N_0$ , corroborating with the above conclusions. From the slope of the curves, one can note a more significant influence of the number of subcarriers on the estimation of  $\mathbf{H}^{(RD)}$ , while we can note a slight gain in the estimation of  $\mathbf{H}^{(SR)}$ .

### 6.3.2 Performance comparison of CNTD-based systems

In this subsection, we provide a comparison between the two CNTD-based systems proposed in this thesis (corresponding to Chapters 5 and 6). Although these chapters deal with different systems – a two-hop MIMO multirelay system in Chapter 5 and a two-hop OFDM MIMO single-relay system in Chapter 6 – we would like to compare the behavior of systems based on coupled tensor decompositions, such as the proposed CNTD model.

It is worth remembering that both systems are modeled by using different tensor structures of the CNTD model. The multirelay system is written in terms of the coupling of  $K$  effective channel tensors  $\mathcal{H}_{(k)}^{(SRD)}$ , where  $K$  is the number of relays and  $k = 1, \dots, K$ , having as common factor the coded symbol tensor  $\mathcal{X}^{(S)}$ . The coupling of the multicarrier system is given

Figure 53 – SER performance for CNTD-based systems

Figure 54 – NMSE of  $\mathbf{H}^{(SR)}$  for CNTD-based systemsFigure 55 – NMSE of  $\mathbf{H}^{(RD)}$  for CNTD-based systems

in terms of  $F$  coded symbol tensors  $\mathcal{X}_{(f)}^{(S)}$ , where  $F$  is the number of subcarriers and  $f = 1, \dots, F$ , having as common factor the effective channel tensors  $\mathcal{H}^{(SRD)}$ .

Figures 53, 54 and 55 show respectively the SER, the NMSE of  $\mathbf{H}^{(SR)}$  and the NMSE of  $\mathbf{H}^{(RD)}$  versus  $P_T/N_0$  for both the systems, considering  $K = \{2, 3\}$  and  $F = 1$  for the multirelay system and  $K = 1$  and  $F = \{2, 3\}$  for the multicarrier system.

One can note in Figure 53 that the addition of relays in the multirelay system improves significantly the estimation of symbols, which is not observed for an increase in the number of subcarriers in the multicarrier system. That is due to the fact that an increase in  $F$  does not add diversity, since the channel attenuation is the same for all subcarriers. On the other hand, from Figures 54 and 55, it is noticeable that a greater number of subcarriers provides some improvement in the channel estimation, which does not happen with an addition of relays in the multirelay system. Note that the estimation gains in each system are given in terms of the common factors.

The common tensors  $\mathcal{X}^{(S)}$  and  $\mathcal{H}^{(SRD)}$  define the coupling of a collection of decompositions in their respective systems, and therefore we call them by coupling factors. The respective non-common factors  $\mathcal{H}_{(k)}^{(SRD)}$  and  $\mathcal{X}_{(f)}^{(S)}$ , for  $k = 1, \dots, K$  and  $f = 1, \dots, F$ , are then coupled so that the destination has more resources to estimate the common parameters, yielding thus some improvement on the receiver performance. The fact that these performance gains occur in terms of the coupling (common) factors can be understood as a good advantage of tensor approaches based on coupled decompositions.

## 6.4 Summary

In this chapter, we have proposed a two-hop OFDM MIMO relay system with a TSTC at the source and the relay. The coded signals transmitted by the source multiplexes symbols in space, time and frequency domains, and the signals received at destination form a fifth-order tensor that satisfies a CNTD, which consists in a contraction between a Tucker-(2, 3) model and a generalized Tucker-(1, 4) one.

The tensor modeling was exploited in order to derive a non-iterative receiver for the proposed system, based on the LSKP method. Monte Carlo simulation results have been provided to illustrate the behavior of the system and evaluate the effectiveness of the proposed joint and semi-blind receiver. Simulation results show that the OFDM MIMO relay system allows to increase the number of information symbols to be transmitted from the source without loss of SER performance and spectral efficiency. The results also show an improvement in the

channel estimation when the number of subcarriers is increased, due to the joint processing of all the subcarriers.

We have also provided a comparison between the two CNTD-based systems proposed in this thesis. The results have shown that systems based on coupled decompositions have interesting advantages in the estimation of some parameters. The common factors, through which the coupling takes place in each case, had gains in their estimates.

## 7 CONCLUSION

This thesis has addressed the study of nested tensor decompositions applied to the signal processing in cooperative MIMO systems. In particular, generalizations of nested decompositions based on Tucker model were proposed in order to model received signals in MIMO relay system with tensor codings at the source and the relays. A performance analysis of each proposed system was provided to illustrate their behavior and effectiveness, evaluating the improvements of the techniques addressed for wireless communication. In the sequel, we provide a brief conclusion of each chapter that have proposed original contributions.

In Chapter 3, we have introduced two new tensor decompositions, called high-order nested Tucker decomposition (HONTD) and coupled nested Tucker decomposition (CNTD). Both the models generalize the NTD introduced in [34] to higher order tensors. HONTD results from the contraction of several Tucker models in a train format, yielding a  $(N + 3)$ -th order tensor, where  $N \geq 1$  is the number of nesting between two consecutive Tucker models. CNTD admits tensor factors, contrarily to NTD and HONTD that assume only matrix factors. The proposed CNTD can be viewed as a coupling of multiple NTDs that share a common factor, and it extends the coupling concept initially defined for PARAFAC models [62, 86, 87] to Tucker-based ones. This model was particularly studied for two cases of a fifth-order tensor. The first one is characterized as a contraction between a generalized Tucker– $(2, 4)$  model and a Tucker– $(1, 3)$  one, while the second is a contraction between a Tucker– $(2, 3)$  model and a generalized Tucker– $(1, 4)$  one. Uniqueness conditions for both models were deeply discussed, showing that, under certain conditions, the decomposition factors are unique up to scaling ambiguities. It was shown that the proposed uniqueness theorem is also valid to the NTD model introduced in [34], filling the lack of discussion on the NTD uniqueness in the literature.

In Chapter 4, we have proposed a multi-hop MIMO relaying system composed of  $K$  AF relays operating with TSTC. This system generalizes existing systems [18, 24, 34, 42] in different ways, either by using a more general relay coding, by extending these works to the multihop case and/or by using a different estimation algorithm. Assuming a third-order TSTC at the source and the relays, we show that the signals received at destination satisfy the new HONTD. Considering the tensor codings known at the destination, we have derived two semi-blind receivers based on a recurrent relations of the received signals for jointly estimating the information symbols and the individual channels. The first one is a iterative solution based on an ALS method. The second one is a closed form solution based on a LSKP technique

that considers a SVD-based low-rank approximation algorithm. Identifiability conditions and ambiguity relations were provided. The LSKP receiver exploits matrix unfoldings of coding tensors under the form of unitary matrices, avoiding noise enhancement. Monte Carlo simulation were provided to evaluate the performance of the proposed receivers and the impact of the number of relays. Simulation results have shown that a tensor coding with a unitary unfolding yields a better performance when compared to random codings. An increase of the number of relays also improve significantly the performance.

In Chapter 5, we have proposed a two-hop MIMO multi-relay system with TSTC at the source and the relays. The multiple relays use orthogonal channels (parallel relaying) to increase the diversity order, assuming that all the relays can communicate directly with the destination. This system can be viewed as a generalization of recently proposed systems [24, 30, 34, 35], aiming to exploit the cooperative diversity provided by the multiple relays in a MIMO system with tensor coding. We show that the signals received at destination form a fifth-order tensor, where each mode is linked with a different signal dimension (space, source code, relay code, time and number of relays). Indeed, the proposed system exploits both the space (antenna) and cooperative diversities, as well as time-spreading at the source and relays. This tensor satisfies the new CNTD. This tensor modeling is used to develop a receiver algorithm for jointly estimating the symbol matrix and the individual channels with a global processing of all datasets received from multiple relays. The proposed algorithm is a closed-form solution that uses the LSKP technique. Monte Carlo simulations are provided to illustrate the effectiveness of the cooperative diversity exploitation and to compare the performances of the proposed receiver with other existing ones. Simulation results show the improvement induced by an increase of the number of relays.

Chapter 6 we have proposed a two-hop OFDM MIMO relaying system with tensor codings at the source and the relay. We assume a TSTC at the source, with data symbols multiplexed across space, time and frequency domains. In the second hop, the AF relay re-encodes the received signals by using a new TSTC before forwarding them to the destination. The signals received at destination form a fifth-order tensor that satisfies a CNTD. However, the CNTD used presented in this chapter is a little different from the one used in Chapter 5. By exploiting matrix unfoldings of the signal tensor model, we have proposed a semi-blind LSKP receiver for jointly estimating the symbols and the channels. Monte Carlo simulation results have been provided to illustrate the behavior of the system and evaluate the effectiveness of

the proposed joint and semi-blind receiver. The results show an improvement in the channel estimation when the number of subcarriers is increased, due to the joint processing of all the subcarriers. CNTD-based OFDM MIMO relay system also allows to increase the number of information symbols to be transmitted from the source without loss of SER performance and spectral efficiency. A comparison between the two CNTD-based systems proposed in this thesis have also provided. The results have shown that systems based on coupled decompositions have interesting advantages in the estimation of coupling parameters.

Globally, from the results presented in Chapters 4, 5 and 6, we can conclude some important features, advantages, concerns and limitations of the proposed cooperative MIMO systems and receivers, which can be highlighted as follows:

- The tensor structure of the TSTC applied to the addressed systems provides an addition of diversity, leading to performance gains in most of the cases;
- As a cost of this performance gain, TSTC provides a degradation in the transmission rate due to the multiple spreading at the source and the relays, undergoing a greater loss in multi-hop cases;
- It is possible to draw a tradeoff between an increase of diversity provided by the time-spreading and a degradation of the transmission rate;
- We can note, in all cases, that the spreading generated by the TSTC is more effectively exploited at the source than at the relay nodes;
- The spatial diversity of antennas is better exploited in the first hops (closer to the source);
- The multiple amplifications of the noise provided by the AF relays become the estimation of the channels of the first hops more difficult. Channels closest to the destination are better estimated;
- A OFDM source sending a data tensor with symbols multiplexed in space, time and frequency domains allows to increase the number of symbols to be transmitted without loss of SER performance and spectral efficiency;
- Due to the iterative nature, ALS-based receivers can work better than closed-form receivers when the coding is randomly chosen. However, if the algorithm allows unitary (orthogonal) coding, the closed-form receiver performance can overcome the one obtained with an iterative algorithm;
- The computational cost may be high for large numbers of symbols, antennas and relays (in the multi-relay cases);

- The proposed tensor-based solutions require that some a priori information is available at destination to ensure their uniqueness and to eliminate the scaling ambiguities;
- These solutions are also related to the LS uniqueness of some pseudo-inverses, which impose necessary conditions for some configuration parameters. Furthermore, these conditions are less restrictive than the ones imposed by conventional matrix approaches.
- Receivers based on coupled tensor decompositions yield gains in the estimation of coupling (common) factors.

## 8 FUTURE WORKS

In view of the presented results and the main conclusions highlighted in the previous chapter, in this chapter, we raise the main perspectives and future works that can be derived from the research developed in this thesis. In the first part, we summarize some partial developments carried out with a new cooperative OFDM MIMO system and a new coupled tensor model, which can be viewed as an extension of the CNTD and of the systems proposed in the Chapters 5 and 6. Finally, we quote some generic perspectives that can be addressed in future researches.

### 8.1 Two-hop OFDM MIMO multi-relay system and doubly coupled tensor decomposition

In this section, we present partial developments carried out with a new cooperative two-hop OFDM MIMO multi-relay system based on a new tensor decomposition called doubly coupled nested Tucker decomposition (D-CNTD). This cooperative network can be viewed as a combination of the systems proposed in Chapters 5 and 6 and is composed by a OFDM source sending a coded symbol tensor with data multiplexed in the space, time and frequency domains,  $K$  AF relays operating in parallel cooperation and a destination. This system generalizes the two-hop MIMO multi-relay system of Chapter 5 by considering multiple carriers at the source to send independent data or, equivalently, it generalizes the two-hop OFDM MIMO relay system of Chapter 6 by considering a case with multiple relays. The purpose of combining multiple relays with multiple carriers is to doubly benefit from the advantages observed in the systems based on coupled decompositions. A scheme for this system is similar to the one in Figure 28.

Aiming to mitigate the limitation related to the low transmission rates, we assume that the relays only forward the signals received from the source, block-by-block, without implement a new spreading. Since the exploitation of the diversity provided by the TSTC is more efficient at the source, the performance will not be so degraded due to the absence of a new spreading at the relays. Moreover, the OFDM source allows to improve the transmission rate by increasing the number of subcarriers, leading to a larger number of symbols to be transmitted without loss of SER performance and spectral efficiency.

In the sequel, we briefly describe the transmission scheme and signal modeling for this system. Let us assume the OFDM source sending the coded data  $\mathcal{X}^{(S)}$  defined in (6.4) as

follows

$$\mathcal{X}^{(S)} = \mathcal{C}^{(S)} \times_3 \mathcal{S} \in \mathbb{C}^{M_S \times P \times N \times F}, \quad (8.1)$$

with  $\mathcal{C}^{(S)} \in \mathbb{C}^{M_S \times P \times R \times F}$  and  $\mathcal{S} \in \mathbb{C}^{N \times R \times F}$ . The signals are transmitted towards the  $K$  relays through the channels  $\mathbf{H}_{..k}^{(SR)} \in \mathbb{C}^{M_R \times M_S}$ , for  $k = 1, \dots, K$ . Analogously to the system of Chapter 6, we assume neighboring subcarriers in such a way that the channel matrices  $\mathbf{H}_{..k}^{(SR)}$  are invariant across the subcarriers. Thus, we can write the signals received at the  $k$ -th relay, associated with the  $f$ -th subcarrier as

$$\mathcal{X}_{..kf}^{(R)} = \mathcal{X}_{(f)}^{(S)} \times_1 \mathbf{H}_{..k}^{(SR)} \in \mathbb{C}^{M_R \times P \times N}. \quad (8.2)$$

The relay  $k$  re-encodes the received signals, using a coding  $\mathcal{C}_{(k)}^{(R)} \in \mathbb{C}^{M_T \times P \times M_R}$ , which does not apply a new spreading of the signals. The tensor  $\mathcal{C}_{(k)}^{(R)}$  only apply a matrix coding  $M_T \times M_R$  for each time-block  $p$  received from the source. Then, the signals transmitted by  $M_T$  antennas of the  $k$ -th relay, associated with the  $f$ -th subcarrier are given by

$$\mathcal{X}_{..kf}^{(T)} = \mathcal{C}_{(k)}^{(R)} *_3 \mathcal{X}_{..kf}^{(R)} \in \mathbb{C}^{M_T \times P \times N}. \quad (8.3)$$

Finally, after transmission through the channel matrices  $\mathbf{H}_{..k}^{(RD)} \in \mathbb{C}^{M_D \times M_T}$ , the tensor of signals received at destination coming from the  $k$ -th relay, associated with the  $f$ -th subcarrier is given by

$$\mathcal{X}_{..kf}^{(SRD)} = \mathcal{X}_{..kf}^{(T)} \times_1 \mathbf{H}_{..k}^{(RD)} \in \mathbb{C}^{M_D \times P \times N}, \quad (8.4)$$

which can be written in the scalar notation as

$$x_{m_D, p, n, k, f}^{(SRD)} = \sum_{m_T=1}^{M_T} \sum_{m_R=1}^{M_R} \sum_{m_S=1}^{M_S} \sum_{r=1}^R h_{m_D, m_T, k}^{(RD)} c_{m_T, p, m_R, k}^{(R)} h_{m_R, m_S, k}^{(SR)} c_{m_S, p, r, f}^{(S)} s_{n, r, f}. \quad (8.5)$$

From the signal modeling given in (8.5), we can define the effective channel tensor  $\mathcal{H}_{(k)}^{(SRD)} \in \mathbb{C}^{M_D \times P \times M_S}$  as

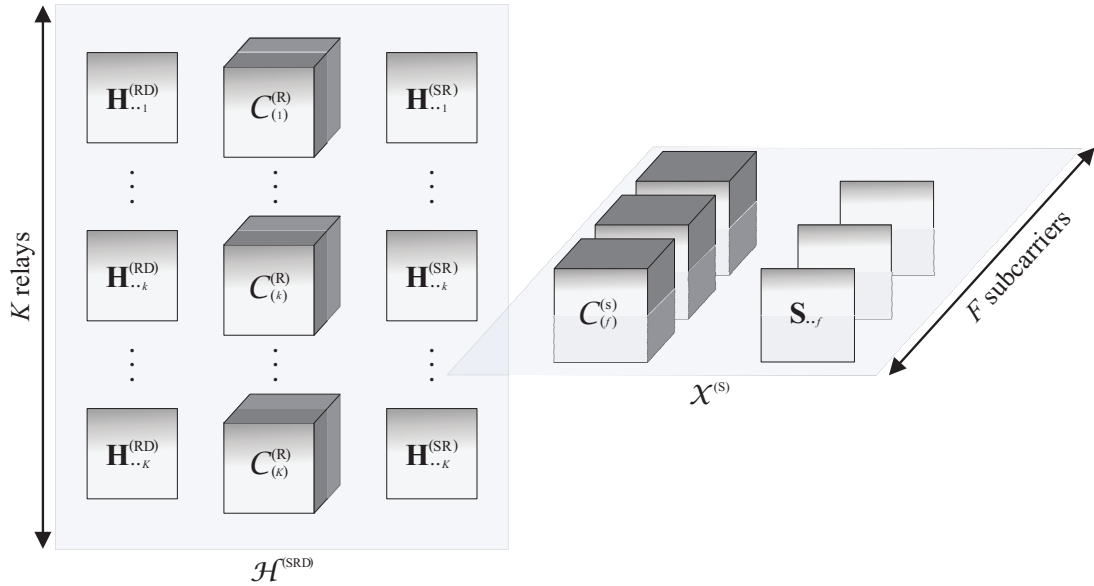
$$\mathcal{H}_{(k)}^{(SRD)} = \mathcal{C}_{(k)}^{(R)} \times_1 \mathbf{H}_{..k}^{(RD)} \times_2 \mathbf{H}_{..k}^{(SR)}, \quad (8.6)$$

and then rewrite the received signal tensor in (8.4) as

$$\mathcal{X}_{..kf}^{(SRD)} = \mathcal{H}_{(k)}^{(SRD)} *_3 \mathcal{X}_{(f)}^{(S)} \in \mathbb{C}^{M_D \times P \times N}. \quad (8.7)$$

Since the tensors  $\mathcal{H}_{(k)}^{(SRD)}$  and  $\mathcal{X}_{(f)}^{(S)}$  satisfy respectively a Tucker-(2, 3) decomposition and a Tucker-(1, 3) one, the tensor in (8.7) corresponds to a fourth-order NTD.

Figure 56 – Block-diagram for a doubly coupled nested Tucker decomposition



This tensor model suggests the existence of a double coupling of the signals, whether due to multiple relays or multiple subcarriers. In other words, we can say that the destination receives the tensor of signals

$$\mathcal{X}_{\dots f}^{(SRD)} = \mathcal{H}^{(SRD)} *_3^1 \mathcal{X}_{(f)}^{(S)} \in \mathbb{C}^{M_D \times P \times N \times K}, \quad (8.8)$$

with the information forwarded by all relays and associated to a subcarrier  $f$  or, otherwise, we can say that the destination receives the tensor of signals

$$\mathcal{X}_{\dots k}^{(SRD)} = \mathcal{H}_{(k)}^{(SRD)} *_3^1 \mathcal{X}^{(S)} \in \mathbb{C}^{M_D \times P \times N \times F}, \quad (8.9)$$

coming from a given relay  $k$  and associated with all subcarriers. The decompositions in (8.8) and (8.10) individually satisfy a CNTD, since each one represent a coupling of  $K$  and  $F$  NTDs, respectively. In this way, we define the received signal tensor  $\mathcal{X}^{(SRD)} \in \mathbb{C}^{M_D \times P \times N \times K \times F}$  as a doubly coupled nested Tucker decomposition (D-CNTD), which is characterized by the following contraction between a generalized Tucker-(2, 4) decomposition and a generalized Tucker-(1, 4) one

$$\mathcal{X}^{(SRD)} = \mathcal{H}^{(SRD)} *_3^1 \mathcal{X}^{(S)}. \quad (8.10)$$

Figure 56 shows a block-diagram for the scheme of the proposed decomposition. Note that for each subcarrier  $f$ , the tensor  $\mathcal{X}_{(f)}^{(S)}$  is common to all relays and, for each relay  $k$ , the tensor  $\mathcal{H}_{(k)}^{(SRD)}$  is common to all subcarriers. The double coupling can be viewed in different ways in order to improve the estimations of all unknown parameters, allowing, for instance, to get performance gains in the channel and symbol estimations simultaneously.

## 8.2 Perspectives

Future developments related to the system and tensor decomposition mentioned in the previous section are still necessary. A deep analysis on the uniqueness of the D-CNTD model is required in order to get necessary conditions to ensure it, as well as the relationship between the ambiguities. The tensor modeling will be exploited aiming to derive semi-blind receivers to jointly estimate the symbols and individual channels. The future studies include the development of optimization algorithms, including supervised techniques, as well as theoretical analyses of the performance and numerical stability of the proposed algorithms.

Other perspectives refer to the study of two-way MIMO relay systems, where the transmission occurs in both directions (downlink and uplink), and cooperative networks that involve relays operating in full-duplex mode, which allow to receive and transmit signals simultaneously. Tensor codings for these systems should be considered. A study on alternative structures for the coding tensor in order to overcome the limitations of the transmission rate imposed by the TSTC is also quoted.

## REFERENCES

- 1 GOLDSMITH, A. **Wireless communications**. [S.l.]: Cambridge university press, 2005.
- 2 PAULRAJ, A.; NABAR, R.; GORE, D. **Introduction to space-time wireless communications**. [S.l.]: Cambridge university press, 2003.
- 3 TSE, D.; VISWANATH, P. **Fundamentals of wireless communication**. [S.l.]: Cambridge university press, 2005.
- 4 RAPPAPORT, T. S. **Wireless communications: principles and practice**. [S.l.]: prentice hall PTR New Jersey, 1996. v. 2.
- 5 GOLDSMITH, A.; JAFAR, S. A.; JINDAL, N.; VISHWANATH, S. Capacity limits of MIMO channels. **IEEE Journal on selected areas in Communications**, v. 21, n. 5, p. 684–702, 2003.
- 6 ALMEIDA, A. L. F. de. **Tensor modeling and signal processing for wireless communication systems**. Nice, France: PhD thesis - Université de Nice Sophia Antipolis, 2007.
- 7 FERNANDES, C. A. R. **Nonlinear MIMO communication systems: Channel estimation and information recovery using volterra models**. Nice, France: PhD thesis - Université de Nice Sophia Antipolis, 2009.
- 8 WINTERS, J. On the capacity of radio communication systems with diversity in a Rayleigh fading environment. **IEEE journal on selected areas in communications**, v. 5, n. 5, p. 871–878, 1987.
- 9 FOSCHINI, G. J.; GANS, M. J. On limits of wireless communications in a fading environment when using multiple antennas. **Wireless personal communications**, v. 6, n. 3, p. 311–335, 1998.
- 10 TELATAR, E. Capacity of multi-antenna Gaussian channels. **European transactions on telecommunications**, v. 10, n. 6, p. 585–595, 1999.
- 11 TAROKH, V.; SESHADRI, N.; CALDERBANK, A. R. Space-time codes for high data rate wireless communication: Performance criterion and code construction. **IEEE transactions on information theory**, v. 44, n. 2, p. 744–765, 1998.
- 12 YAO, H.; WORNELL, G. W. Structured space-time block codes with optimal diversity-multiplexing tradeoff and minimum delay. In: **Global Telecommunications Conference, 2003. GLOBECOM'03. IEEE**. [S.l.: s.n.], 2003. v. 4, p. 1941–1945.
- 13 ZHENG, L.; TSE, D. N. C. Diversity and multiplexing: A fundamental tradeoff in multiple-antenna channels. **IEEE Transactions on information theory**, v. 49, n. 5, p. 1073–1096, 2003.
- 14 JUNGnickel, V.; HAUSTEIN, T.; POHL, V.; HELMOLT, C. von. Link adaptation in a multi-antenna system. In: **Vehicular Technology Conference, 2003. VTC 2003-Spring. The 57th IEEE Semiannual**. [S.l.: s.n.], 2003. v. 2, p. 862–866.
- 15 HEATH, R. W.; LOVE, D. J. Multimode antenna selection for spatial multiplexing systems with linear receivers. **IEEE Transactions on Signal Processing**, v. 53, n. 8, p. 3042–3056, 2005.

- 16 MEULEN, E. C. V. D. Three-terminal communication channels. **Advances in applied Probability**, v. 3, n. 1, p. 120–154, 1971.
- 17 LANEMAN, J. N. Cooperative diversity – models, algorithms, and architectures. In: **Fitzek F.H.P., Katz M.D. (eds) Cooperation in Wireless Networks: Principles and Applications**. [S.l.]: Springer.
- 18 FREITAS JR, W. C.; FAVIER, G.; ALMEIDA, A. L. F. de. Sequential closed-form semiblind receiver for space-time coded multihop relaying systems. **IEEE Signal Processing Letters**, v. 24, n. 12, p. 1773–1777, 2017.
- 19 FERNANDES, C. A. R.; ALMEIDA, A. L. F. de; COSTA, D. B. da. Unified tensor modeling for blind receivers in multiuser uplink cooperative systems. **IEEE Signal Processing Letters**, v. 19, n. 5, p. 247–250, 2012.
- 20 HAN, X.; ALMEIDA, A. L. F. de; YANG, Z. Channel estimation for MIMO multi-relay systems using a tensor approach. **EURASIP Journal on Advances in Signal Processing**, v. 163, n. 1, 2014.
- 21 RONG, Y.; KHANDAKER, M. R. A.; XIANG, Y. Channel estimation of dual-hop MIMO relay system via parallel factor analysis. **IEEE Transactions on Wireless Communications**, v. 11, n. 6, p. 2224–2233, 2012.
- 22 SOFOTASIOS, P. C.; FIKADU, M. K.; MUHAIDAT, S.; FREEAR, S.; KARAGIANNIDIS, G. K.; VALKAMA, M. Relay selection based full-duplex cooperative systems under adaptive transmission. **IEEE Wireless Communications Letters**, v. 6, n. 5, p. 602–605, 2017.
- 23 CHEN, G.; XIAO, P.; KELLY, J. R.; LI, B.; TAFAZOLLI, R. Full-duplex wireless-powered relay in two way cooperative networks. **IEEE Access**, v. 5, p. 1548–1558, 2017.
- 24 XIMENES, L. R.; FAVIER, G.; ALMEIDA, A. L. F. de. Semi-blind receivers for non-regenerative cooperative MIMO communications based on nested PARAFAC modeling. **IEEE transactions on signal processing**, v. 63, n. 18, p. 4985–4998, 2015.
- 25 ALMEIDA, A. L. F. de; FAVIER, G.; MOTA, J. C. M. A constrained factor decomposition with application to MIMO antenna systems. **IEEE Transactions on Signal Processing**, v. 56, n. 6, p. 2429–2442, 2008.
- 26 RANKOV, B.; WITTNEBEN, A. Spectral efficient protocols for half-duplex fading relay channels. **IEEE Journal on Selected Areas in Communications**, v. 25, n. 2, 2007.
- 27 LIU, Y.; LI, S.; MU, X.; ZHANG, J. Tensor-based semi-blind channel estimation for three-hop MIMO relay systems. In: **Wireless Communications & Signal Processing (WCSP), 2015 International Conference on**. [S.l.: s.n.], 2015. p. 1–5.
- 28 TODING, A.; KHANDAKER, M.; RONG, Y. Optimal joint source and relay beamforming for parallel MIMO relay networks. In: **Proceedings of the 6th International Conference on Wireless Communications, Networking and Mobile Computing**. [S.l.: s.n.], 2010.
- 29 TODING, A.; KHANDAKER, M. R. A.; RONG, Y. Joint source and relay optimization for parallel MIMO relay networks. **EURASIP Journal on Advances in Signal Processing**, v. 174, n. 1, 2012.

- 30 XIMENES, L. R.; FAVIER, G.; ALMEIDA, A. L. F. de; SILVA, Y. C. B. PARAFAC-PARATUCK semi-blind receivers for two-hop cooperative MIMO relay systems. **IEEE Transactions on Signal Processing**, v. 62, n. 14, p. 3604–3615, 2014.
- 31 FREITAS JR, W. C.; FAVIER, G.; ALMEIDA, A. L. F. de. Generalized Khatri-Rao and Kronecker space-time coding for MIMO relay systems with closed-form semi-blind receivers. **Signal Processing**, v. 151, p. 19–31, 2018.
- 32 CAVALCANTE, Í. V.; ALMEIDA, A. L. F. de; HAARDT, M. Joint channel estimation for three-hop MIMO relaying systems. **IEEE Signal Processing Letters**, v. 22, n. 12, p. 2430–2434, 2015.
- 33 CHIONG, C. W.; RONG, Y.; XIANG, Y. Channel training algorithms for two-way MIMO relay systems. **IEEE transactions on signal processing**, v. 61, n. 16, p. 3988–3998, 2013.
- 34 FAVIER, G.; FERNANDES, C. A. R.; ALMEIDA, A. L. F. de. Nested Tucker tensor decomposition with application to MIMO relay systems using tensor space-time coding (TSTC). **Signal Processing**, v. 128, p. 318–331, 2016.
- 35 FAVIER, G.; COSTA, M. N.; ALMEIDA, A. L. F. de; ROMANO, J. M. T. Tensor space-time (TST) coding for MIMO wireless communication systems. **Signal Processing**, v. 92, n. 4, p. 1079–1092, 2012.
- 36 KAMMOUN, I.; BELFIORE, J.-C. A new family of Grassmann space-time codes for non-coherent MIMO systems. **IEEE Communications Letters**, v. 7, n. 11, p. 528–530, 2003.
- 37 ARAÚJO, G. T. de; ALMEIDA, A. L. F. de. Closed-Form Channel Estimation for MIMO Space-Time Coded Systems Using a Fourth-Order Tensor-Based Receiver. **Circuits, Systems, and Signal Processing**, v. 37, n. 3, p. 1343–1357, 2017.
- 38 ALMEIDA, A. L. F. de; FAVIER, G.; MOTA, J. C. M. Space-time spreading-multiplexing for MIMO wireless communication systems using the PARATUCK-2 tensor model. **Signal Processing**, v. 89, n. 11, p. 2103–2116, 2009.
- 39 ALMEIDA, A. L. F. de; FAVIER, G.; XIMENES, L. R. Space-time-frequency (STF) MIMO communication systems with blind receiver based on a generalized PARATUCK2 model. **IEEE Transactions on Signal Processing**, v. 61, n. 8, p. 1895–1909, 2013.
- 40 FAVIER, G.; ALMEIDA, A. L. F. de. Tensor space-time-frequency coding with semi-blind receivers for MIMO wireless communication systems. **IEEE Transactions on Signal Processing**, v. 62, n. 22, p. 5987–6002, 2014.
- 41 ALMEIDA, A. L. F. de; FAVIER, G. Double Khatri-Rao space-time-frequency coding using semi-blind PARAFAC based receiver. **IEEE Signal Processing Letters**, v. 20, n. 5, p. 471–474, 2013.
- 42 XIMENES, L. R.; FAVIER, G.; ALMEIDA, A. L. F. de. Closed-form semi-blind receiver for MIMO relay systems using double Khatri-Rao space-time coding. **IEEE Signal Processing Letters**, v. 23, n. 3, p. 316–320, 2016.
- 43 ZHANG, Z.; ZHANG, W.; TELLAMBURA, C. Cooperative OFDM channel estimation in the presence of frequency offsets. **IEEE Transactions on Vehicular Technology**, v. 58, n. 7, p. 3447–3459, 2009.

- 44 MARANHÃO, J. P. A.; COSTA, J. P. C. L. da; FREITAS, E. P. de; MARINHO, M. A. M.; GALDO, G. del. Multi-hop cooperative XIXO transmission scheme for delay tolerant wireless sensor networks. In: **20th International ITG Workshop on Smart Antennas**. [S.l.: s.n.], 2016. p. 1–5.
- 45 KOLDA, T. G.; BADER, B. W. Tensor decompositions and applications. **SIAM review**, v. 51, n. 3, p. 455–500, 2009.
- 46 COMON, P. Tensor decompositions—State of the art and applications. In: **IMA Conf Mathematics in Signal Processing**. Warwick, UK: [s.n.], 2000.
- 47 SIDIROPOULOS, N. D.; GIANNAKIS, G. B.; BRO, R. Blind PARAFAC receivers for DS-CDMA systems. **IEEE Transactions on Signal Processing**, v. 48, n. 3, p. 810–823, 2000.
- 48 ALMEIDA, A. L. F. de; FAVIER, G.; MOTA, J. C. M.; COSTA, J. P. C. L. da. Overview of tensor decompositions with applications to communications. In: **Signals and Images: Advances and Results in Speech, Estimation, Compression, Recognition, Filtering, and Processing**. [S.l.]: CRC-Press, chapter 12, 2016. p. 325–356.
- 49 CICHOCKI, A.; MANDIC, D.; LATHAUWER, L. de; ZHOU, G.; ZHAO, Q.; CAIAFA, C.; PHAN, H. A. Tensor decompositions for signal processing applications: From two-way to multiway component analysis. **IEEE Signal Processing Magazine**, v. 32, n. 2, p. 145–163, 2015.
- 50 HACKBUSCH, W. **Tensor spaces and numerical tensor calculus**. [S.l.]: Springer Science & Business Media, 2012. v. 42.
- 51 CICHOCKI, A.; ZDUNEK, R.; PHAN, A. H.; AMARI, S.-i. **Nonnegative matrix and tensor factorizations: applications to exploratory multi-way data analysis and blind source separation**. [S.l.]: John Wiley & Sons, 2009.
- 52 LIU, X.; SIDIROPOULOS, N. D. Cramér-Rao lower bounds for low-rank decomposition of multidimensional arrays. **IEEE Transactions on Signal Processing**, v. 49, n. 9, p. 2074–2086, 2001.
- 53 XIE, K.; WANG, L.; WANG, X.; XIE, G.; WEN, J.; ZHANG, G.; CAO, J.; ZHANG, D.; XIE, K.; WANG, X. *et al.* Accurate Recovery of Internet Traffic Data: A Sequential Tensor Completion Approach. **IEEE/ACM Transactions on Networking**, v. 26, n. 2, p. 793–806, 2018.
- 54 XIE, K.; PENG, C.; WANG, X.; XIE, G.; WEN, J.; CAO, J.; ZHANG, D.; QIN, Z. Accurate Recovery of Internet Traffic Data Under Variable Rate Measurements. **IEEE/ACM Transactions on Networking**, v. 26, n. 3, p. 1137–1150, 2018.
- 55 XIE, K.; LI, X.; WANG, X.; CAO, J.; XIE, G.; WEN, J.; ZHANG, D.; QIN, Z. On-Line Anomaly Detection With High Accuracy. **IEEE/ACM Transactions on Networking**, v. 26, n. 3, p. 1222–1235, 2018.
- 56 LATHAUWER, L. de; CASTAING, J. Tensor-based techniques for the blind separation of DS-CDMA signals. **Signal Processing**, v. 87, n. 2, p. 322–336, 2007.
- 57 ZHOU, G.; CICHOCKI, A. Fast and unique Tucker decompositions via multiway blind source separation. **Bulletin of the Polish Academy of Sciences: Technical Sciences**, v. 60, n. 3, p. 389–405, 2012.

- 58 ZHOU, G.; CICHOCKI, A. Canonical polyadic decomposition based on a single mode blind source separation. **IEEE Signal Processing Letters**, IEEE, v. 19, n. 8, p. 523–526, 2012.
- 59 SIDIROPOULOS, N. D.; BUDAMPATI, R. S. Khatri-Rao space-time codes. **IEEE Transactions on Signal Processing**, v. 50, n. 10, p. 2396–2407, 2002.
- 60 TUCKER, L. R. Some mathematical notes on three-mode factor analysis. **Psychometrika**, v. 31, n. 3, p. 279–311, 1966.
- 61 HARSHMAN, R. A. Foundations of the PARAFAC procedure: models and conditions for an "explanatory" multimodal factor analysis. **UCLA Working Papers in Phonetics**, v. 16, p. 1–84, 1970.
- 62 SØRENSEN, M.; LATHAUWER, L. de. Coupled tensor decompositions for applications in array signal processing. In: **IEEE 5th International Workshop on Computational Advances in Multi-Sensor Adaptive Processing (CAMSAP)**. [S.l.: s.n.], 2013. p. 228–231.
- 63 IBRAHIM, A. S.; SADEK, A. K.; SU, W.; LIU, K. R. Cooperative communications with relay-selection: when to cooperate and whom to cooperate with? **IEEE Transactions on Wireless Communications**, v. 7, n. 7, 2008.
- 64 SHAH, V. K.; GHARGE, A. P. A review on relay selection techniques in cooperative communication. **International Journal of Engineering and Innovative Technology (IJEIT)**, v. 2, n. 4, p. 65–69, 2012.
- 65 DU, J.; YUAN, C.; ZHANG, J. Low complexity PARAFAC-based channel estimation for non-regenerative MIMO relay systems. **Iet Communications**, v. 8, n. 12, p. 2193–2199, 2014.
- 66 ROEMER, F.; HAARDT, M. Tensor-based channel estimation and iterative refinements for two-way relaying with multiple antennas and spatial reuse. **IEEE Transactions on Signal Processing**, v. 58, n. 11, p. 5720–5735, 2010.
- 67 NG, B. K.; SOUSA, E. S. Multicarrier spread space-spectrum multiple access for the MIMO forward link transmission. In: **Personal, The 13th IEEE International Symposium on Indoor and Mobile Radio Communications**. Lisbon, Portugal: [s.n.], 2002. v. 3, p. 1300–1304.
- 68 RONG, Y.; TANG, X.; HUA, Y. A unified framework for optimizing linear nonregenerative multicarrier MIMO relay communication systems. **IEEE Transactions on Signal Processing**, v. 57, n. 12, p. 4837–4851, 2009.
- 69 YANG, L.-L.; HANZO, L. Broadband MC DS-CDMA using space-time and frequency-domain spreading. In: **IEEE 56th Vehicular Technology Conference**. Vancouver, Canada: [s.n.], 2002. v. 3, p. 1632–1636.
- 70 LATHAUWER, L. de. **Signal processing based on multilinear algebra**. Leuven, Belgium: PhD thesis - Katholieke Universiteit Leuven, 1997.
- 71 TRACY, D. S.; SINGH, R. P. A new matrix product and its applications in partitioned matrix differentiation. **Statistica Neerlandica**, v. 26, n. 4, p. 143–157, 1972.
- 72 TRACY, D. S. Balanced partitioned matrices and their Kronecker products. **Computational Statistics & Data Analysis**, v. 10, n. 3, p. 315–323, 1990.

- 73 LIU, S.; TRENKLER, G. Hadamard, Khatri-Rao, Kronecker and other matrix products. **International Journal of Information and Systems Sciences**, v. 4, n. 1, p. 160–177, 2008.
- 74 HITCHCOCK, F. L. The expression of a tensor or a polyadic as a sum of products. **Journal of Mathematics and Physics**, v. 6, n. 1-4, p. 164–189, 1927.
- 75 CICHOCKI, A. Tensor networks for big data analytics and large-scale optimization problems. **arXiv preprint arXiv:1407.3124**, 2014.
- 76 HARSHMAN, R. A.; LUNDY, M. E. Uniqueness proof for a family of models sharing features of Tucker’s three-mode factor analysis and PARAFAC/CANDECOMP. **Psychometrika**, v. 61, n. 1, p. 133–154, 1996.
- 77 FAVIER, G.; ALMEIDA, A. L. F. de. Overview of constrained PARAFAC models. **EURASIP Journal on Advances in Signal Processing**, v. 62, n. 14, 2014.
- 78 OSELEDETS, I. V.; TYRTYSHNIKOV, E. TT-cross approximation for multidimensional arrays. **Linear Algebra and its Applications**, v. 432, n. 1, p. 70–88, 2010.
- 79 OSELEDETS, I. V. Tensor-train decomposition. **SIAM Journal on Scientific Computing**, v. 33, n. 5, p. 2295–2317, 2011.
- 80 CARROLL, J. D.; CHANG, J.-J. Analysis of individual differences in multidimensional scaling via an N-way generalization of “Eckart-Young” decomposition. **Psychometrika**, v. 35, n. 3, p. 283–319, 1970.
- 81 SIDIROPOULOS, N. D.; BRO, R. On the uniqueness of multilinear decomposition of N-way arrays. **Journal of Chemometrics: A Journal of the Chemometrics Society**, v. 14, n. 3, p. 229–239, 2000.
- 82 KRUSKAL, J. B. Three-way arrays: rank and uniqueness of trilinear decompositions, with application to arithmetic complexity and statistics. **Linear algebra and its applications**, v. 18, n. 2, p. 95–138, 1977.
- 83 KRUSKAL, J. B. Rank, decomposition and uniqueness for 3-way and  $N$ -way arrays. In: COPPI, R.; BOLASCO, S. (Ed.). **Multiway data analysis**. Netherlands: North-Holland, 1989. p. 7–18.
- 84 HARSHMAN, R. A. Determination and proof of minimum uniqueness conditions for PARAFAC1. **UCLA Working Papers in phonetics**, v. 22, n. 111-117, p. 3, 1972.
- 85 LATHAUWER, L. de. A link between the canonical decomposition in multilinear algebra and simultaneous matrix diagonalization. **SIAM journal on Matrix Analysis and Applications**, v. 28, n. 3, p. 642–666, 2006.
- 86 SØRENSEN, M.; LATHAUWER, L. de. Coupled canonical polyadic decompositions and (coupled) decompositions in multilinear rank- $(l_{r,n}, l_{r,n}, 1)$  terms—part i: uniqueness. **SIAM Journal on Matrix Analysis and Applications**, v. 36, n. 2, p. 496–522, 2015.
- 87 SØRENSEN, M.; DOMANOV, I.; LATHAUWER, L. de. Coupled canonical polyadic decompositions and (coupled) decompositions in multilinear rank- $(L_{r,n}, L_{r,n}, 1)$  terms—part II: algorithms. **SIAM Journal on Matrix Analysis and Applications**, v. 36, n. 3, p. 1015–1045, 2015.

- 88 REN, C.; FARIAS, R. C.; AMBLARD, P.-O.; COMON, P. Performance bounds for coupled models. In: **IEEE Sensor Array and Multichannel Signal Processing Workshop (SAM)**. [S.l.: s.n.], 2016. p. 1–5.
- 89 ALMEIDA, A. L. F. de; FAVIER, G.; MOTA, J. C. M. PARAFAC-based unified tensor modeling for wireless communication systems with application to blind multiuser equalization. **Signal Processing**, v. 87, n. 2, p. 337–351, 2007.
- 90 WANG, Z.; WANG, J.; XING, C.; FEI, Z.; KUANG, J. Tensor-based blind signal recovery for multi-carrier amplify-and-forward relay networks. **Science China Information Sciences**, v. 57, n. 10, p. 1–11, 2014.
- 91 LOAN, C. F. V.; PITSIANIS, N. Approximation with Kronecker products. In: **Linear algebra for large scale and real-time applications**. [S.l.: s.n.], 1993. p. 293–314.
- 92 GALLIER, J. Basics of Hermitian Geometry. In: **Geometric Methods and Applications**. [S.l.: s.n.], 2011. p. 321–342.
- 93 GAO, F.; CUI, T.; NALLANATHAN, A. On channel estimation and optimal training design for amplify and forward relay networks. **IEEE Transactions on Wireless Communications**, v. 7, n. 5, 2008.
- 94 ECKART, C.; YOUNG, G. The approximation of one matrix by another of lower rank. **Psychometrika**, v. 1, n. 3, p. 211–218, 1936.

## APPENDIX A – UNIQUENESS PROPERTIES OF TENSOR MODELS

### A.1 - Proof of Theorem 1 for the uniqueness of the Tucker model

Let us consider the following mode- $n$  unfolding of  $\mathcal{X} \in \mathbb{C}^{I_1 \times \dots \times I_N}$  given in (2.26)

$$\mathbf{X}_n = (\mathbf{A}^{(n+1)} \otimes \dots \otimes \mathbf{A}^{(N)} \otimes \mathbf{A}^{(1)} \otimes \dots \otimes \mathbf{A}^{(n-1)}) \mathbf{G}_n \mathbf{A}^{(n)T}. \quad (\text{A.1})$$

We want to demonstrate that, when the core tensor  $\mathcal{G}$  is known, the matrices  $\mathbf{A}^{(n)}$  are unique up to scaling ambiguities  $\delta_n$ , for  $n = 1, \dots, N$ . By vectorizing the mode- $n$  unfolding (A.1), and using the Property 1, we get

$$\text{vec}(\mathbf{X}_n) = (\mathbf{A}^{(n)} \otimes \dots \otimes \mathbf{A}^{(N)} \otimes \mathbf{A}^{(1)} \otimes \dots \otimes \mathbf{A}^{(n-1)}) \text{vec}(\mathbf{G}_n). \quad (\text{A.2})$$

Replacing  $\mathbf{A}^{(n)}$  by the alternative  $\bar{\mathbf{A}}^{(n)}$  and using the Property 2 gives

$$\begin{aligned} \text{vec}(\mathbf{X}_n) &= (\mathbf{A}^{(n)} \Delta_n \otimes \dots \otimes \mathbf{A}^{(N)} \Delta_N \otimes \mathbf{A}^{(1)} \Delta_1 \otimes \dots \otimes \mathbf{A}^{(n-1)} \Delta_{n-1}) \text{vec}(\mathbf{G}_n) \\ &= (\mathbf{A}^{(n)} \otimes \dots \otimes \mathbf{A}^{(N)} \otimes \mathbf{A}^{(1)} \otimes \dots \otimes \mathbf{A}^{(n-1)}) \\ &\quad (\Delta_n \otimes \dots \otimes \Delta_N \otimes \Delta_1 \otimes \dots \otimes \Delta_{n-1}) \text{vec}(\mathbf{G}_n). \end{aligned} \quad (\text{A.3})$$

Comparing (A.3) with (A.1), we can conclude that these models are equivalent if the term  $(\Delta_n \otimes \dots \otimes \Delta_N \otimes \Delta_1 \otimes \dots \otimes \Delta_{n-1})$  is equal to a identity matrix  $I_{\bar{R}}$  of size  $\bar{R} \times \bar{R}$ , with  $\bar{R} = \prod_{n=1}^N R_n$ . This is true if  $\Delta_n = \delta_n \mathbf{I}_{R_n}$ , for  $n = 1, \dots, N$ , and  $\prod_{n=1}^N \delta_n = 1$ .

### A.2 - Proof of Theorem 2 for the uniqueness of the generalized Tucker model

Let us take  $\bar{\mathbf{A}}_{\cdot \cdot i_4}^{(1)} = \mathbf{A}_{\cdot \cdot i_4}^{(1)} \Delta_{\cdot \cdot i_4}^{(1)}$  and  $\bar{\mathbf{A}}_{\cdot \cdot i_4}^{(3)} = \mathbf{A}_{\cdot \cdot i_4}^{(3)} \Delta_{\cdot \cdot i_4}^{(3)}$  as alternative solutions for  $\mathbf{A}_{\cdot \cdot i_4}^{(1)}$  and  $\mathbf{A}_{\cdot \cdot i_4}^{(3)}$  in the unfolding (2.34), and consider the core tensor  $\mathcal{G}$  as known. From (2.35), we get

$$\begin{aligned} [\bar{\mathbf{X}}_{I_1 I_3 \times I_2}]_{(i_4)} &= \left( \mathbf{A}_{\cdot \cdot i_4}^{(1)} \Delta_{\cdot \cdot i_4}^{(1)} \otimes \mathbf{A}_{\cdot \cdot i_4}^{(3)} \Delta_{\cdot \cdot i_4}^{(3)} \right) [\mathbf{G}_{R_1 R_3 \times I_2}]_{(i_4)} \\ &= \left( \mathbf{A}_{\cdot \cdot i_4}^{(1)} \otimes \mathbf{A}_{\cdot \cdot i_4}^{(3)} \right) \left( \Delta_{\cdot \cdot i_4}^{(1)} \otimes \Delta_{\cdot \cdot i_4}^{(3)} \right) [\mathbf{G}_{R_1 R_3 \times I_2}]_{(i_4)}. \end{aligned} \quad (\text{A.4})$$

By comparing (A.4) with (2.34), we can conclude that the tensors  $\mathcal{X}$  and  $\bar{\mathcal{X}}$  are identical if the term  $(\Delta_{\cdot \cdot i_4}^{(1)} \otimes \Delta_{\cdot \cdot i_4}^{(3)})$  is equal to a identity matrix  $\mathbf{I}_{R_1 R_3}$ , which implies  $\Delta_{\cdot \cdot i_4}^{(n)} = \delta_{i_4}^{(n)} \mathbf{I}_{R_n}$ , for  $n = 1, 3$ , with  $\delta_{i_4}^{(1)} \delta_{i_4}^{(3)} = 1, \forall i_4 \in [1, I_4]$ . Each  $\delta_{i_4}^{(n)}$  is the scalar ambiguity for the  $i_4$ -th mode-3 slice of  $\mathcal{A}^{(n)}$ .

## APPENDIX B – MATRIX REPRESENTATION OF A GENERALIZED TUCKER DECOMPOSITION

### B.1 - Proof of the unfolding (2.32)

We want to demonstrate the tall mode-3 unfolding given in (2.32) for the generalized Tucker-(2, 4) decomposition in (2.31). Considering the matricization defined in (2.8) with  $\mathbb{S}_1 = \{2, 4, 1\}$  and  $\mathbb{S}_2 = \{3\}$  for a fourth-order tensor  $\mathcal{X} \in \mathbb{C}^{I_1 \times I_2 \times I_3 \times I_4}$ , the tall mode-3 unfolding is given by

$$\mathbf{X}_{I_2 I_4 I_1 \times I_3} = \sum_{i_1=1}^{I_1} \sum_{i_2=1}^{I_2} \sum_{i_3=1}^{I_3} \sum_{i_4=1}^{I_4} x_{i_1, i_2, i_3, i_4} \left( \mathbf{e}_{i_2}^{(I_2)} \otimes \mathbf{e}_{i_4}^{(I_4)} \otimes \mathbf{e}_{i_1}^{(I_1)} \right) \left( \mathbf{e}_{i_3}^{(I_3)} \right)^T, \quad (\text{B.1})$$

where  $x_{i_1, i_2, i_3, i_4}$  is given in (2.31). From (2.8), it is easy to deduce the following expression for  $g_{r_1, i_2, r_3, i_4}$

$$g_{r_1, i_2, r_3, i_4} = \left( \mathbf{e}_{i_2}^{(I_2)} \otimes \mathbf{e}_{i_4}^{(I_4)} \otimes \mathbf{e}_{r_1}^{(R_1)} \right)^T \mathbf{G}_{I_2 I_4 R_1 \times I_4 R_3} \left( \mathbf{e}_{i_4}^{(I_4)} \otimes \mathbf{e}_{r_3}^{(R_3)} \right). \quad (\text{B.2})$$

Replacing (2.31) and (B.2) into (B.1) gives

$$\begin{aligned} \mathbf{X}_{I_2 I_4 I_1 \times I_3} &= \sum_{i_1=1}^{I_1} \sum_{i_2=1}^{I_2} \sum_{i_3=1}^{I_3} \sum_{i_4=1}^{I_4} \sum_{r_1=1}^{R_1} \sum_{r_3=1}^{R_3} a_{i_1, r_1, i_4}^{(1)} a_{i_3, r_3, i_4}^{(3)} \\ &\quad \left( \mathbf{e}_{i_2}^{(I_2)} \otimes \mathbf{e}_{i_4}^{(I_4)} \otimes \mathbf{e}_{i_1}^{(I_1)} \right) \left( \mathbf{e}_{i_2}^{(I_2)} \otimes \mathbf{e}_{i_4}^{(I_4)} \otimes \mathbf{e}_{r_1}^{(R_1)} \right)^T \\ &\quad \mathbf{G}_{I_2 I_4 R_1 \times I_4 R_3} \left( \mathbf{e}_{i_4}^{(I_4)} \otimes \mathbf{e}_{r_3}^{(R_3)} \right) \left( \mathbf{e}_{i_3}^{(I_3)} \right)^T. \end{aligned} \quad (\text{B.3})$$

By taking the summations with common terms, from Property (2), we get

$$\begin{aligned} &\sum_{i_1=1}^{I_1} \sum_{i_2=1}^{I_2} \sum_{r_1=1}^{R_1} a_{i_1, r_1, i_4}^{(1)} \left( \mathbf{e}_{i_2}^{(I_2)} \otimes \mathbf{e}_{i_4}^{(I_4)} \otimes \mathbf{e}_{i_1}^{(I_1)} \right) \left( \mathbf{e}_{i_2}^{(I_2)} \otimes \mathbf{e}_{i_4}^{(I_4)} \otimes \mathbf{e}_{r_1}^{(R_1)} \right)^T \\ &= \left( \sum_{i_2=1}^{I_2} \mathbf{e}_{i_2}^{(I_2)} \mathbf{e}_{i_2}^{(I_2)T} \right) \otimes \left( \mathbf{e}_{i_4}^{(I_4)} \mathbf{e}_{i_4}^{(I_4)T} \right) \otimes \left( \sum_{i_1=1}^{I_1} \sum_{r_1=1}^{R_1} a_{i_1, r_1, i_4}^{(1)} \mathbf{e}_{i_1}^{(I_1)} \mathbf{e}_{r_1}^{(R_1)T} \right) \\ &= \mathbf{I}_{I_2} \otimes \mathbf{e}_{i_4}^{(I_4)} \mathbf{e}_{i_4}^{(I_4)T} \otimes \mathbf{A}_{\cdot i_4}^{(1)} \end{aligned} \quad (\text{B.4})$$

and

$$\begin{aligned} \sum_{i_3=1}^{I_3} \sum_{r_3=1}^{R_3} a_{i_3, r_3, i_4}^{(3)} \left( \mathbf{e}_{i_4}^{(I_4)} \otimes \mathbf{e}_{r_3}^{(R_3)} \right) \left( \mathbf{e}_{i_3}^{(I_3)} \right)^T &= \mathbf{e}_{i_4}^{(I_4)} \otimes \left( \sum_{i_3=1}^{I_3} \sum_{r_3=1}^{R_3} a_{i_3, r_3, i_4}^{(3)} \mathbf{e}_{r_3}^{(R_3)} \mathbf{e}_{i_3}^{(I_3)T} \right) \\ &= \mathbf{e}_{i_4}^{(I_4)} \otimes \mathbf{A}_{\cdot i_4}^{(3)T}. \end{aligned} \quad (\text{B.5})$$

Replacing (B.4) and (B.5) into (B.3), we get

$$\mathbf{X}_{I_2 I_4 I_1 \times I_3} = \sum_{i_4=1}^{I_4} \left( \mathbf{I}_{I_2} \otimes \mathbf{e}_{i_4}^{(I_4)} \mathbf{e}_{i_4}^{(I_4)T} \otimes \mathbf{A}_{\cdot i_4}^{(1)} \right) \mathbf{G}_{I_2 I_4 R_1 \times I_4 R_3} \left( \mathbf{e}_{i_4}^{(I_4)} \otimes \mathbf{A}_{\cdot i_4}^{(3)T} \right). \quad (\text{B.6})$$

Solving the summation in equation above, we obtain (2.32), q.e.d.

## B.2 - Proof of the unfolding (2.33)

Now, we will demonstrate the unfolding in (2.33) for the same generalized Tucker-(2, 4) decomposition. Let us consider  $\mathbb{S}_1 = \{1, 3\}$  and  $\mathbb{S}_2 = \{4, 2\}$  and, from (2.8), we write the unfolding  $\mathbf{X}_{I_1 I_3 \times I_4 I_2}$  as follows

$$\begin{aligned} \mathbf{X}_{I_1 I_3 \times I_4 I_2} &= \sum_{i_1=1}^{I_1} \sum_{i_2=1}^{I_2} \sum_{i_3=1}^{I_3} \sum_{i_4=1}^{I_4} x_{i_1, i_2, i_3, i_4} \left( \mathbf{e}_{i_1}^{(I_1)} \otimes \mathbf{e}_{i_3}^{(I_3)} \right) \left( \mathbf{e}_{i_4}^{(I_4)} \otimes \mathbf{e}_{i_2}^{(I_2)} \right)^T \\ &= \sum_{i_1=1}^{I_1} \sum_{i_2=1}^{I_2} \sum_{i_3=1}^{I_3} \sum_{i_4=1}^{I_4} \sum_{r_1=1}^{R_1} \sum_{r_3=1}^{R_3} g_{r_1, i_2, r_3, i_4} a_{i_1, r_1, i_4}^{(1)} a_{i_3, r_3, i_4}^{(3)} \left( \mathbf{e}_{i_1}^{(I_1)} \otimes \mathbf{e}_{i_3}^{(I_3)} \right) \left( \mathbf{e}_{i_4}^{(I_4)} \otimes \mathbf{e}_{i_2}^{(I_2)} \right)^T, \end{aligned} \quad (\text{B.7})$$

with  $g_{r_1, i_2, r_3, i_4}$  given by

$$g_{r_1, i_2, r_3, i_4} = \left( \mathbf{e}_{i_4}^{(I_4)} \otimes \mathbf{e}_{r_1}^{(R_1)} \otimes \mathbf{e}_{r_3}^{(R_3)} \right)^T \mathbf{G}_{I_4 R_1 R_3 \times I_4 I_2} \left( \mathbf{e}_{i_4}^{(I_4)} \otimes \mathbf{e}_{i_2}^{(I_2)} \right). \quad (\text{B.8})$$

Replacing (B.8) into (B.7) gives

$$\begin{aligned} \mathbf{X}_{I_1 I_3 \times I_4 I_2} &= \sum_{i_4=1}^{I_4} \sum_{i_3=1}^{I_3} \sum_{i_2=1}^{I_2} \sum_{i_1=1}^{I_1} \sum_{r_1=1}^{R_1} \sum_{r_3=1}^{R_3} a_{i_1, r_1, i_4}^{(1)} a_{i_3, r_3, i_4}^{(3)} \left( \mathbf{e}_{i_1}^{(I_1)} \otimes \mathbf{e}_{i_3}^{(I_3)} \right) \\ &\quad \left( \mathbf{e}_{i_4}^{(I_4)} \otimes \mathbf{e}_{r_1}^{(R_1)} \otimes \mathbf{e}_{r_3}^{(R_3)} \right)^T \mathbf{G}_{I_4 R_1 R_3 \times I_4 I_2} \left( \mathbf{e}_{i_4}^{(I_4)} \otimes \mathbf{e}_{i_2}^{(I_2)} \right) \left( \mathbf{e}_{i_4}^{(I_4)} \otimes \mathbf{e}_{i_2}^{(I_2)} \right)^T \end{aligned} \quad (\text{B.9})$$

By using Property (2) and separating the summations with common terms, we get

$$\begin{aligned} \mathbf{X}_{I_1 I_3 \times I_4 I_2} &= \left[ \sum_{i_4=1}^{I_4} \left( \mathbf{e}_{i_4}^{(I_4)T} \otimes \sum_{i_1=1}^{I_1} \sum_{r_1=1}^{R_1} a_{i_1, r_1, i_4}^{(1)} \left( \mathbf{e}_{i_1}^{(I_1)} \mathbf{e}_{r_1}^{(R_1)T} \right) \otimes \right. \right. \\ &\quad \left. \left. \sum_{i_3=1}^{I_3} \sum_{r_3=1}^{R_3} a_{i_3, r_3, i_4}^{(3)} \left( \mathbf{e}_{i_3}^{(I_3)} \mathbf{e}_{r_3}^{(R_3)T} \right) \right) \right] \\ &\quad \mathbf{G}_{I_4 R_1 R_3 \times I_4 I_2} \left[ \sum_{i_4=1}^{I_4} \mathbf{e}_{i_4}^{(I_4)} \mathbf{e}_{i_4}^{(I_4)T} \otimes \sum_{i_2=1}^{I_2} \mathbf{e}_{i_2}^{(I_2)} \mathbf{e}_{i_2}^{(I_2)T} \right], \end{aligned} \quad (\text{B.10})$$

which simplifies as

$$\begin{aligned} \mathbf{X}_{I_1 I_3 \times I_4 I_2} &= \sum_{i_4=1}^{I_4} \left( \mathbf{e}_{i_4}^{(I_4)T} \otimes \mathbf{A}_{\cdot i_4}^{(1)} \otimes \mathbf{A}_{\cdot i_4}^{(3)} \right) \mathbf{G}_{I_4 R_1 R_3 \times I_4 I_2} \left( \mathbf{I}_{I_4} \otimes \mathbf{I}_{I_2} \right) \\ &= \left[ \mathbf{A}_{\cdot 1}^{(1)} \otimes \mathbf{A}_{\cdot 1}^{(3)} \quad \mathbf{A}_{\cdot 2}^{(1)} \otimes \mathbf{A}_{\cdot 2}^{(3)} \quad \cdots \quad \mathbf{A}_{\cdot I_4}^{(1)} \otimes \mathbf{A}_{\cdot I_4}^{(3)} \right] \mathbf{G}_{I_4 R_1 R_3 \times I_4 I_2}, \end{aligned} \quad (\text{B.11})$$

which corresponds to the unfolding (2.33). The term between parentheses is equivalent to a block Kronecker product as given in Definition 2 (Section 2.1).

## APPENDIX C – LS ESTIMATION OF KRONECKER PRODUCT FACTORS

Let us consider the matrix  $\Phi = \mathbf{A} \otimes \mathbf{B} \in \mathbb{C}^{IM \times JN}$  defined as a Kronecker product between the matrices  $\mathbf{A} \in \mathbb{C}^{I \times J}$  and  $\mathbf{B} \in \mathbb{C}^{M \times N}$ . The estimation of the Kronecker matrices consists in factorizing of the input data  $\Phi$  in order to get the factors  $\mathbf{A}$  and  $\mathbf{B}$ . This factorization can be viewed as the following optimization problem

$$\arg \min_{\widehat{\mathbf{A}}, \widehat{\mathbf{B}}} \|\Phi - \widehat{\mathbf{A}} \otimes \widehat{\mathbf{B}}\|_F^2. \quad (\text{C.1})$$

The minimization of the above LS cost function can be solved by using a low-rank approximation method, which has as goal to find the matrix argument that minimizes (C.1), under the constraint of the rank being less than or equal to a value  $r \in \mathbb{N}$ . The traditional solution for this approximation is obtained by exploiting a truncated SVD of the input data. For that, we recall the Eckart-Young-Mirsky Theorem.

**Theorem 6.** (Eckart-Young-Mirsky Theorem) *Let  $\mathbf{D} = \mathbf{U}\Sigma\mathbf{V}^H$  be the SVD and  $\widehat{\mathbf{D}}$  be an estimate of the matrix  $\mathbf{D} \in \mathbb{C}^{m \times n}$ . The  $m$  columns of  $\mathbf{U} \in \mathbb{C}^{m \times m}$  and the  $n$  columns of  $\mathbf{V} \in \mathbb{C}^{n \times n}$  are the left- and right-singular vectors of  $\mathbf{D}$ , respectively, and  $\Sigma \in \mathbb{C}^{m \times n}$  is a diagonal matrix with non-negative real entries called singular values of  $\mathbf{D}$ . The rank- $r$  matrix  $\widehat{\mathbf{D}}_r$  that minimizes the error  $\|\mathbf{D} - \widehat{\mathbf{D}}\|_F$  is obtained from the truncated SVD  $\widehat{\mathbf{D}}_r = \mathbf{U}_r \Sigma_r \mathbf{V}_r^H$ , where  $\Sigma_r$  is the same matrix  $\Sigma$  except for containing only the  $r$  largest singular values (other singular values are replaced by zero).*

In other words, the minimizer  $\widehat{\mathbf{D}}_r$ , obtained by the rank- $r$  truncated SVD of  $\mathbf{D}$ , is the matrix that best approximates  $\widehat{\mathbf{D}}$  to  $\mathbf{D}$ , i.e.

$$\|\mathbf{D} - \widehat{\mathbf{D}}_r\|_F = \min_{\widehat{\mathbf{D}} | \text{rank}(\widehat{\mathbf{D}}) \leq r} \|\mathbf{D} - \widehat{\mathbf{D}}\|_F, \quad (\text{C.2})$$

with  $r < \text{rank}(\mathbf{D})$ . The proof of this theorem can be found in [94].

Based on the above theorem, we can obtain a rank-1 approximation by computing the largest singular value and its corresponding singular vectors. The rank-one approximation is given by  $\sigma_1 \mathbf{u}_{\cdot 1} \mathbf{v}_{\cdot 1}^H$ , where  $\mathbf{u}_{\cdot 1}$  and  $\mathbf{v}_{\cdot 1}$  are the left- and right-singular vector, respectively, associated to the largest singular value  $\sigma_1$ .

For the problem in (C.1), which is related to the factorization of Kronecker products, we can use the method proposed in [91]. The main idea is to get  $\Omega \leftarrow \text{reshape}(\Phi) \in \mathbb{C}^{NM \times JI}$ , a rearrangement of the elements of  $\Phi \in \mathbb{C}^{IM \times JN}$ , so that  $\|\Phi - \widehat{\mathbf{A}} \otimes \widehat{\mathbf{B}}\|_F^2$  is exactly equal to

$\|\Omega - \text{vec}(\widehat{\mathbf{B}})\text{vec}(\widehat{\mathbf{A}})^T\|_F^2$ . Since  $\text{vec}(\widehat{\mathbf{B}})\text{vec}(\widehat{\mathbf{A}})^T$  generates a rank-1 matrix, we ensure that the truncated matrix  $\Omega_{r=1} = \sigma_1 \mathbf{u}_{.1} \mathbf{v}_{.1}^H = \text{vec}(\widehat{\mathbf{B}})\text{vec}(\widehat{\mathbf{A}})^T$  is the matrix that minimizes the error Frobernius norm. Thus, the estimated matrices  $\widehat{\mathbf{A}}$  and  $\widehat{\mathbf{B}}$  can be obtained under their vectorized forms  $\text{vec}(\widehat{\mathbf{B}}) = \sigma_1 \mathbf{u}_{.1}$  and  $\text{vec}(\widehat{\mathbf{A}}) = \mathbf{v}_{.1}^*$ . The necessary permutation in the elements of  $\Phi$  to obtain  $\Omega$  is described below.

We can write  $\Phi = \mathbf{A} \otimes \mathbf{B} \in \mathbb{C}^{IM \times JN}$  in the following block-form (where each element  $a_{ij}\mathbf{B}$  represents one block)

$$\Phi = \begin{bmatrix} a_{11}\mathbf{B} & a_{12}\mathbf{B} & \cdots & a_{1J}\mathbf{B} \\ a_{21}\mathbf{B} & a_{22}\mathbf{B} & \cdots & a_{2J}\mathbf{B} \\ \vdots & \vdots & \ddots & \vdots \\ a_{I1}\mathbf{B} & a_{I2}\mathbf{B} & \cdots & a_{IJ}\mathbf{B} \end{bmatrix}. \quad (\text{C.3})$$

The permutation of the elements of  $\Phi$  to become  $\Omega$  a rank-1 matrix is given by the following vectorized form, obtained by block-to-block vectorization, represented by the operator  $\text{vec}_b(\cdot)$

$$\begin{aligned} \mathbf{v} &= \text{vec}_b(\Phi) \\ &= [\text{vec}(a_{11}\mathbf{B})^T \cdots \text{vec}(a_{I1}\mathbf{B})^T \cdots \text{vec}(a_{1J}\mathbf{B})^T \cdots \text{vec}(a_{IJ}\mathbf{B})^T]^T \in \mathbb{C}^{JINM}. \end{aligned} \quad (\text{C.4})$$

Note that the vector  $\mathbf{v}$  can be equivalently obtained by the Khatri-Rao product between the vectorizations of the matrices  $\mathbf{A}$  and  $\mathbf{B}$ ,  $\mathbf{v} = \text{vec}(\mathbf{A}) \diamond \text{vec}(\mathbf{B})$ . Now, we take the matrix form of this vector, obtaining the matrix  $\Omega = \text{unvec}(\mathbf{v}) \in \mathbb{C}^{NM \times JI}$ . It is easy to note that the matrix  $\Omega$  can be obtained by  $\text{vec}(\widehat{\mathbf{B}})\text{vec}(\widehat{\mathbf{A}})^T$ .

Due to the properties of matrix products, the scalar  $\sigma_1$ , or even fractions of it, can float between the factors, i.e.  $\text{vec}(\widehat{\mathbf{B}})\text{vec}(\widehat{\mathbf{A}})^T = (\sigma_1 \mathbf{u}_{.1}) \mathbf{v}_{.1}^H = \mathbf{u}_{.1} (\sigma_1 \mathbf{v}_{.1}^H) = (\delta_u \mathbf{u}_{.1}) (\delta_v \mathbf{v}_{.1}^H)$ , with  $\delta_u \delta_v = \sigma_1$ . Thus, the reconstruction of the factors  $\mathbf{A}$  and  $\mathbf{B}$  can be affected by scaling ambiguities  $\widehat{\mathbf{A}} = \delta_{\mathbf{A}} \mathbf{A}$  and  $\widehat{\mathbf{B}} = \delta_{\mathbf{B}} \mathbf{B}$ , so that

$$\begin{aligned} \mathbf{A} \otimes \mathbf{B} &= \widehat{\mathbf{A}} \otimes \widehat{\mathbf{B}} \\ &= (\delta_{\mathbf{A}} \mathbf{A}) \otimes (\delta_{\mathbf{B}} \mathbf{B}) \\ &= \delta_{\mathbf{A}} \delta_{\mathbf{B}} (\mathbf{A} \otimes \mathbf{B}). \end{aligned} \quad (\text{C.5})$$

The above equation is only true if  $\delta_{\mathbf{A}} \delta_{\mathbf{B}} = 1$ . To eliminate these ambiguities, it is enough to know an element of  $\mathbf{A}$  or  $\mathbf{B}$ , or impose it equal to 1, such that  $\delta_{\mathbf{A}} = \widehat{a}_{1,1}/a_{1,1}$  or  $\delta_{\mathbf{B}} = \widehat{b}_{1,1}/b_{1,1}$  and  $\delta_{\mathbf{A}} = \delta_{\mathbf{B}}^{-1}$ .

For the case where the matrices  $\mathbf{A} \in \mathbb{C}^{I \times KJ}$  and  $\mathbf{B} \in \mathbb{C}^{M \times KN}$  are partitioned and  $\Phi$  is defined as an block Kronecker product of  $\mathbf{A}$  with  $\mathbf{B}$  (see Definition 2 - Section 2.1) a straightforward extension is required.

Let us consider the matrix  $\Phi$  given as

$$\Phi = \mathbf{A} \boxtimes \mathbf{B} = \begin{bmatrix} \mathbf{A}_1 \otimes \mathbf{B}_1 & \mathbf{A}_2 \otimes \mathbf{B}_2 & \cdots & \mathbf{A}_K \otimes \mathbf{B}_K \end{bmatrix} \in \mathbb{C}^{IM \times KJN}. \quad (\text{C.6})$$

Defining  $\Phi_k = \mathbf{A}_k \otimes \mathbf{B}_k$ , for  $k = 1, \dots, K$ , such that  $\Phi = [\Phi_1 \ \cdots \ \Phi_K]$ , we can get the reshaped matrix  $\Omega$  as follows

$$\begin{aligned} \Omega &= \begin{bmatrix} \text{unvec}(\text{vec}_b(\Phi_1)) & \cdots & \text{unvec}(\text{vec}_b(\Phi_K)) \end{bmatrix} \\ &= \begin{bmatrix} \text{vec}(\widehat{\mathbf{B}}_1)\text{vec}(\widehat{\mathbf{A}}_1)^T & \cdots & \text{vec}(\widehat{\mathbf{B}}_K)\text{vec}(\widehat{\mathbf{A}}_K)^T \end{bmatrix} \in \mathbb{C}^{NM \times KJI}. \end{aligned} \quad (\text{C.7})$$

In this way, the matrix  $\Omega$  is then composed by  $K$  rank-1 blocks, which can be solved separately in the approximation problem. In other words, we can solve the low rank approximation by computing  $K$  SVDs related to the blocks  $\Omega_k = \text{vec}(\widehat{\mathbf{B}}_k)\text{vec}(\widehat{\mathbf{A}}_k)^T$ . This block-by-block approximation yields a scaling ambiguity for each computed SVD, leading the matrices  $\mathbf{A}$  and  $\mathbf{B}$  to be affected by the following ambiguities  $\widehat{\mathbf{A}}_k = \delta_{\mathbf{A}}^{(k)} \mathbf{A}_k$  and  $\widehat{\mathbf{B}}_k = \delta_{\mathbf{B}}^{(k)} \mathbf{B}_k$ , with  $\delta_{\mathbf{A}}^{(k)} \delta_{\mathbf{B}}^{(k)} = 1$ , for  $k = 1, \dots, K$ .